From Plywood Sheets to Optimized Three-Dimensional Reciprocal Frame Structures:

A generative design approach for minimizing raw material usage

Name	M.J. (Max) de Munnik
Student no.	1343033
Mail	m.j.d.munnik@student.tue.nl maxdemunnik@hotmail.com
Graduation committee	Dr. ir. S.P.G. (Faas) Moonen ir. A.P.H.W. (Arjan) Habraken ir. T.S. (Tom) Godthelp (SIDstudio)
Date	23-05-2023
Course	Graduation project SED (7K45M0)
University	Eindhoven University of Technology
Department	Architecture, building and planning

Preface

Before you lies the Master's thesis "From Plywood Sheets to Optimized Three-Dimensional Reciprocal Frame Structures: A generative design approach for minimizing raw material usage ". This research has been performed to complete the master's program Structural Engineering and Design at Eindhoven University of Technology. This research has been performed between April 2023 and May 2024.

In times of rapid development of computational speed and artificial intelligence, I believe it has become increasingly important to become familiar with computer science and programming, even as a practical structural engineer. Reciprocal frame development has become inherently connected to computer science as determining the exact reciprocal frame geometry is nearly impossible without computers. The combination of computer science and structural engineering lies at the foundation of this research.

Every other week, meetings were conducted with fellow students during their graduation to discuss the progress and ask questions. I was motivated by the great work that was delivered by other students and I have learnt a lot from the work that was performed by others. Additionally, I was challenged to clearly explain the process and challenges during my research to other students. Therefore I would like to thank my fellow students in the RESED group, and in special Arjan Habraken for the guidance and support during my graduation project. Additionally, I would like to thanks Faas Moonen for his feedback during the intermediate colloquium of this project.

Finally, I want to thank my family and friends for the support during this research. It was not always easy to keep my motivation up, but you have helped me to keep motivated at all times. I would also like to thank you, my reader. I hope you enjoy reading this thesis.

Max de Munnik

Tilburg, 23/05/2024



Summary

To reduce environmental impact, structures should be made from environmentally friendly material and minimize the waste of material. Plywood reciprocal frames can potentially offer a solution that combines both the fact that relatively short members are used in reciprocal structures offers the opportunity for sustainable construction because it allows structural elements to be retrieved from smaller standardized products. Prior research on reciprocal structures has not adequately addressed the structural optimization of individual elements in reciprocal structures. Additionally, there has not been any focus on the minimization of waste material. To properly address these two untapped areas of research, the following research question is answered in this research: *What approach can be used to generatively design and digitally fabricate an optimized three-dimensional reciprocal frame structure on a rectangular floor plan minimizing the amount of standard plywood sheets required?*

To answer the research question, a reciprocal frame designer is developed. This reciprocal frame designer tool can generatively design reciprocal frames based on a set of parameters. The reciprocal frames are generatively designed by applying the center-to-center method (controlled by the *scale factor* parameter) on a two-dimensional tessellation. The tessellation mainly decides what the resulting structure looks like and is controlled by a set of parameters (*base dimensions, pattern type, edge size and density gradient*). The resulting two-dimensional reciprocal frame is then inflated to a three-dimensional structure by moving the z-coordinates of the beam nodes. The amount of inflation is controlled by the final geometric parameter; the *eccentricity*. The final geometry is found by mathematically minimizing the geometric 'error' by using the L-BFGS-B algorithm, that performs a directed search for the optimal solution.

The next step is to automatically optimize the individual beam sections, enabling them to be structurally sound under Eurocode loading whilst minimizing their dimensions. Firstly, the element shape to optimally transfer (predominantly) bending moments whilst supporting other elements along the beam is determined by comparing multiple designs. The connection behaviour between the elements is established by parametric FEM calculations. The internal forces in the reciprocal frames can then be determined using a FEM line model. Using the internal forces, the individual sections are iteratively optimized using a custom by-part optimization process.

How the resulting geometry can be obtained as efficiently as possible from the (standard) plywood sheets is determined by (a) bin-packing algorithm(s). As a result, the number of sheets required to produce the structure is known. Therefore, the reciprocal frame designer can be seen as a black-box function with the design parameters as input and the number of sheets as output. This black-box function is used to optimize the initial set of design parameters. Firstly, an initial exploration has been performed to find the areas of interest. The resulting area of interest is often a tessellation edge size where two rows of beam elements can be obtained from one sheet. Within this area of interest, the set of parameters resulting in the least amount of plywood sheets is deemed the optimal reciprocal frame.

For each tessellation pattern, there are multiple layouts that result in the lowest amount of plywood sheets. Generally, the smaller the scale factor, the more optimal the structure. The most optimal tessellation patterns are the triangle pattern and the square pattern. The other patterns are less efficient due to the inconsistent beam lengths or the relatively large beam lengths resulting from the tessellation geometry.

Contents

1. INTRODUCTION 3
1.1 Background and motivation 5
1.2 Research problem and objectives 6
1.3 Research question 7

2. RESEARCH METHOD 8

3. LITERARY REVIEW 11
3.1 Reciprocal frames: Introduction 12
3.2 Reciprocal frames: History 13
3.3 Reciprocal frames: Geometry 15
3.4 Reciprocal frames: Form finding 19
3.5 Reciprocal frames: Structural principles 21
3.6 Reciprocal frames: Detailing 24
3.7 Reciprocal frames: Cladding 25
3.8 Plywood 27
3.9 Digital fabrication techniques for plywood 28
3.10 The bin packing problem 30

4. PRELIMINARY DESIGN 34
4.1 Element shape 35
4.2 Connection behaviour 40
4.3 Cladding 51
4.4 Connection to foundation 55

5. RECIPROCAL FRAME DESIGNER 58
5.1 Workflow 59
5.2 Input plan 59
5.3 Tessellation 59
5.4 2D reciprocal frame 62
5.5 Inflation to 3D structure 65
5.6 Minimizing model error 66
5.7 Conclusion 68

6. STRUCTURAL INTEGRITY AND OPTIMIZATION 69
6.1 Exact beam geometry 70
6.2 FEM modelling 71
6.3 Load determination 73
6.4 Load combinations 75
6.5 Determining point loads 76
6.6 Obtaining FEM forces 77
6.7 Flow of forces 78
6.8 Structural checks 83
6.9 Stress concentration prediction 90
6.10 Section optimization 96
6.11 Structural report 100

7. DIGITAL MANUFACTURING 101
7.1 Digital manufacturing data 102
7.2 Cutting pattern 103
7.3 Construction method 104
7.4 Physical test models 105

8. PARAMETRIC OPTIMIZATION 107
8.1 Optimization goal 108
8.2 Optimization problem 108
8.3 Optimization algorithm 109
8.4 Optimization approach 113

9. RESULTS 115
9.1 Reciprocal frame designer 116
9.2 Parametric optimization results 123

10. CONCLUSIONS 135

11. RECOMMENDATIONS 138

12. LITERATURE 139
12.1 Figures 144

APPENDIX 1: USER MANUAL 147
Reciprocal frame designer 147
Parametric optimization 151

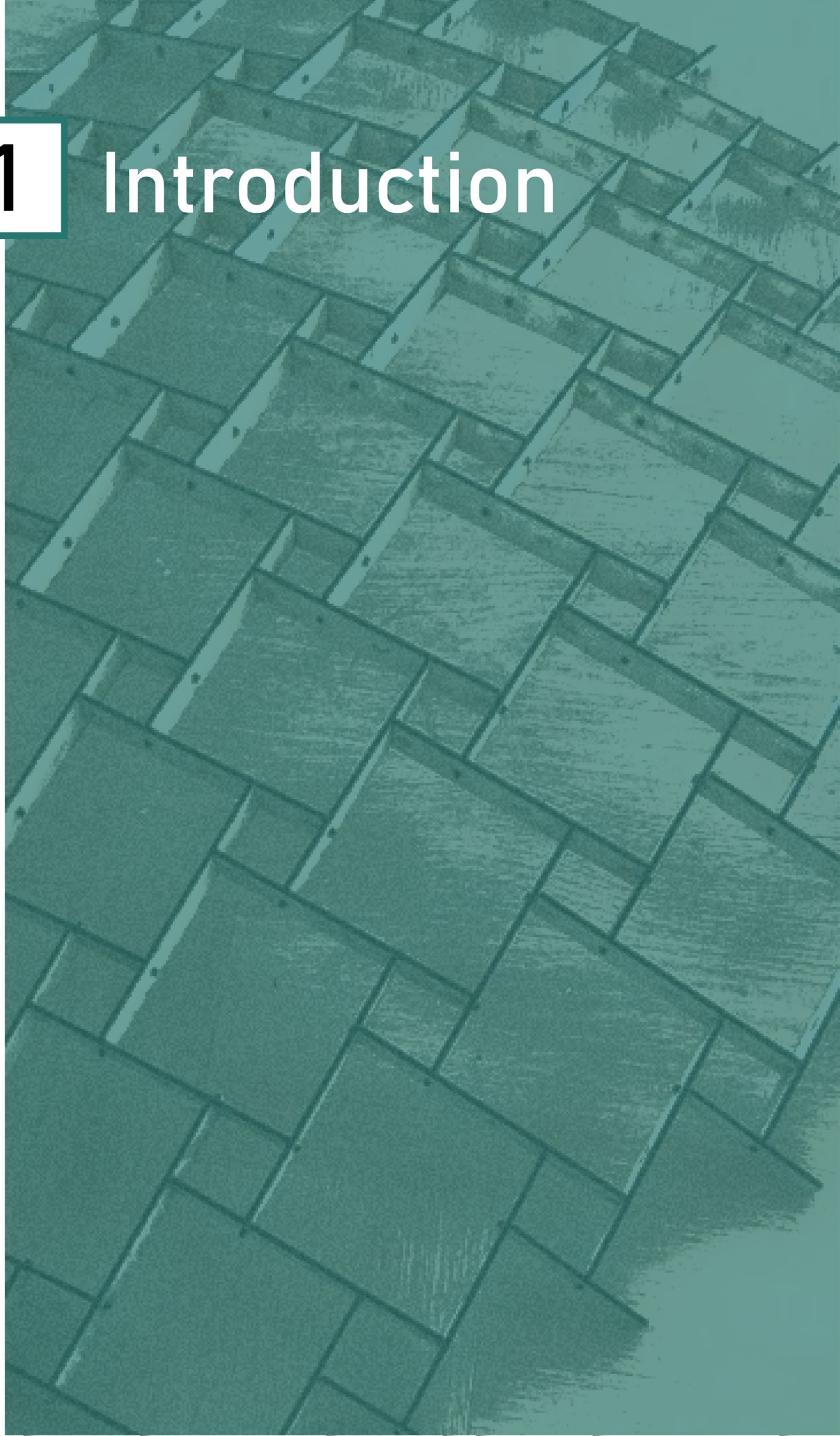
APPENDIX 2: DETAILED STRUCTURAL CALCULATIONS 154

APPENDIX 3: PARAMETRIC OPTIMIZATION OVERVIEWS 165

ANNEX 1: CALCULATION REPORTS 171

ANNEX 2: PLYWOOD CUTTING PATTERNS 172
2.1: Plywood cutting pattern of a non-optimized RF (T = 30mm) 172
2.2: Plywood cutting pattern after optimization: Triangle (T =21mm) 173
2.3: Plywood cutting pattern for example case: Square (T=21mm) 174

ANNEX 3: SCALE MODEL PICTURES 175



1 Introduction

The building industry is becoming increasingly aware of its responsibility towards the environment – even though it has to be pushed by legislation from (inter)national politics. Reciprocity (i.e. cooperation and mutual exchange) is not only a fundamental principle for societies, but also holds a potential for sustainable construction in the form of reciprocal structures. Reciprocal structures are structures where the members cooperate by supporting each other and being supported by each other. This structural layout results in structures consisting of relatively short members with respect to the span. The fact that relatively short members are used in reciprocal structures offers the opportunity for sustainable construction because it allows the structural elements to be retrieved from smaller standardized products. Additionally, it eases the transportation requirements resulting in less emissions during transportation.

The members of reciprocal structures are often heavily loaded by bending moment in one of the beam axes and little in the other beam axis. This enables the opportunity to use plywood sheets as the primary structural material of reciprocal structures. Plywood is almost always produced in the form of sheets meaning that large beam height can only be obtained in one axis.

The use of standard plywood products enables the exploitation of the efficiency of the current plywood production processes, as no custom (and likely less efficient) production processes are required. Additionally, plywood more efficiently uses the timber that is harvested from trees compared to for instance sawn timber. This makes the use of plywood especially resource efficient.

However, selecting a sustainable material for a structure does not directly result in a sustainable structure. Timber is only sustainable when it is harvested sustainably and when waste is minimized. Structures are often designed to minimize the total volume of all structural elements, however a minimum of the structural volume does not necessarily mean a minimum of stock material that is used to produce the structural elements. It thus does not mean that the amount of trees used to create a structure is minimized.

This research thesis focuses on the development of an optimization strategy for reciprocal structures from plywood with the aim of minimizing the amount of plywood sheets used to produce the structural elements, ultimately maximizing the structure's resource efficiency. The study will investigate the impact of various design parameters such as member cross-section, connections, and geometric parameters on the structural behavior and thus efficiency of these systems. Furthermore, the research will explore the use of computational tools and manufacturing techniques to enable the digital fabrication of reciprocal structures.

This research aims to contribute to advancing sustainable construction and promote the use of renewable materials in buildings. Additionally, this research aims to display the advantages of optimizing for stock material instead of for instance structural volume.

1.1 Background and motivation

Researching environmentally friendly building construction is crucial for addressing the current need to reduce the environmental impact of the built environment. The built environment is responsible for 38% of the total CO_2 emissions in the Netherlands (1).

The portion of the structure that contributes to the total emissions of a building depends mainly on the materialization of the structure and other design choices. For utility buildings in the Netherlands for example, the average portion of emissions caused by the structure is 53%. For housing this number is even raised to 61% (2). These percentages are expected to increase as buildings become more energy efficient due to better installations and insulation materials/technologies (3). Given this significant contribution of structures to the overall CO_2 emissions in the Netherlands, it is becoming more and more important for structural designers or engineers to adopt a more environmentally conscious design approach.

Two solutions that are often provided for designing more climate friendly structures are lightweight structures and the use of climate friendly materials. Timber is an example of a lightweight and climate friendly material. Timber, however, can only really be considered climate friendly when it is harvested sustainably and used optimally (i.e. waste is minimized).

When sawn timber is harvested from a tree (or a log), around 50% of the log is considered to be waste material (4). In contrast, for plywood only 25% of the log is considered to be waste material (5). This is a direct result of the way plywood is produced. As visible in Figure 1, plywood is created by peeling a log instead of sawing planks from the log. This thus means that plywood is a more resource efficient material.

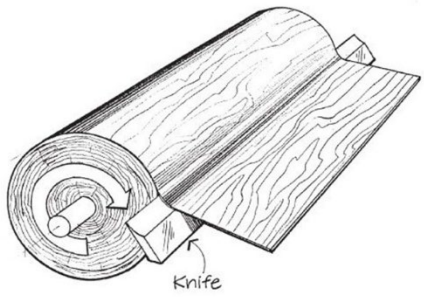


Figure 1: Log peeling to create plywood sheets (6)

Besides using climate friendly materials and designing climate friendly structures, it is also important to motivate society to become more climate-conscious. A study by Kellert et al. (7) concludes that buildings with connections to nature, such as structures constructed from natural materials (e.g. timber) can lead to improved health and well-being. In turn, this may lead to more sustainable behavior. This effect is expected to be enlarged when the building is aesthetically pleasing.

Combining an environmentally friendly and resource efficient material and an aesthetically pleasing structure has resulted in the research topic of plywood reciprocal structures. This research may show that reciprocal structures offer a feasible and aesthetically pleasing alternative to more conventional structures.

1.2 Research problem and objectives

Previous research on reciprocal structures has predominantly focused on their design methods, tools and aesthetics. Some attention has also been given to structural computation and checks according to international codes, such as Eurocode. For example, Godthelp et al. developed a timber reciprocal design tool that incorporated Eurocode 5 checks. (8). This research also includes the automatic digital manufacturing (pre-fabrication) of the separate structural elements. Similarly, Parigi et al. created a form finding method of a reciprocal frame by optimizing the fitness of the structural geometry.

Some researchers have focused more on geometrical optimization. For instance a research by Y. Su et al. (9) where reciprocal structures are optimized by moving the nodes of the elements to minimize the strain energy of the structure. There, the model error must be kept below an acceptable value in order to make sure that the geometry is still in order.

However, prior research has not adequately addressed the material and structural optimization of reciprocal structures. No research has been performed on the optimization of separate cross-sections in combination with geometrical optimization.

Furthermore, the amount of raw material (e.g. number of plywood sheets) required to construct the reciprocal frame is not considered in any previous research. This represents an untapped area for improving the efficiency of reciprocal structures, especially in terms of their structural and material performance.

Performing optimization focused on optimizing the amount of raw material required for producing the structural elements, may result in structures that are not only material and cost effective, but also more environmentally friendly.

1.3 Research question

The previously mentioned untapped area of reciprocal frame optimization results in the following research question that is investigated in this thesis:

*What approach can be used to **generatively design** and **digitally fabricate** an **optimized** three-dimensional reciprocal frame structure on a rectangular floor plan minimizing the amount of **standard plywood sheets** required?*

The research question consists of the following aspects:

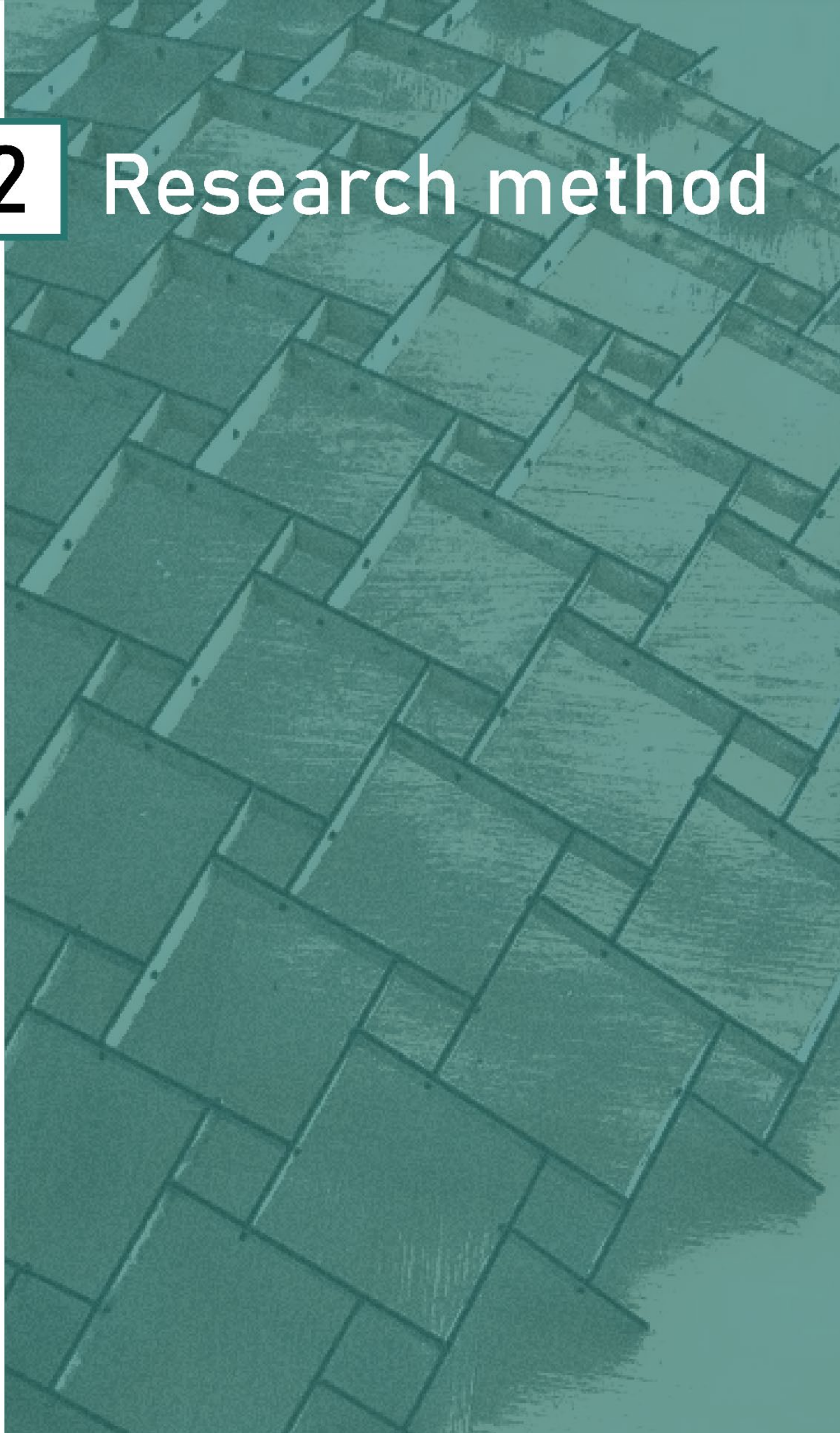
- **Generative design:** a three dimensional reciprocal frame should be designed on a rectangular floor plan purely based on a number of parameters without any user intervention.
- **Digital fabrication:** files for digital fabrication should automatically be generated. That includes an overview of how structural elements should be obtained from the plywood sheets.
- **Optimization:** the optimization should be focused on minimizing the number of plywood sheets required. This optimization is twofold: the optimization of individual cross-sections and optimization of the parameters that make up the generative design.
- **Standard plywood sheets:** the optimization should be performed to generate a solution of beams that can be cut from standard plywood sheets.

Research objectives

Besides answering the research question, there are a few additional objectives for the research. A reciprocal frame designer tool should be developed where a reciprocal frame is designed based on a few design parameters and a rectangular base size. This reciprocal frame designer should be open-source (i.e. freely available and usable without using any paid subscription software). The reciprocal frame designer should automatically optimize the individual cross sections and automatically generate production data.

To make the reciprocal frame designer open-source, the project should be fully programmed in Python. The only time additional software may be used, is for the structural computation of the reciprocal frame. This additional software preferably is also open-source.

2 Research method



The basis of the research is the development of a reciprocal frame designer that digitally designs a reciprocal frame based on a few design parameters and a rectangular floor plan. The reciprocal frame designer should optimize the individual cross sections in the structure. Additionally, the reciprocal frame designer should generate a reciprocal frame consisting of elements that can be obtained/retrieved from plywood sheets with predefined dimensions.

The resulting reciprocal frame designer basically should be a black-box function that returns a structural design based on the design parameters, see Figure 2. Using this black-box function, the design parameters can be optimized using a multivariate optimization algorithm.

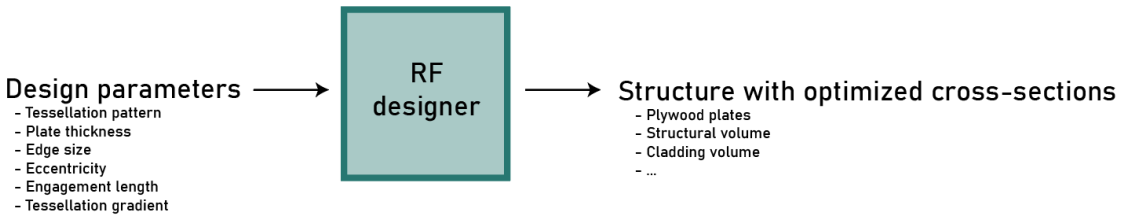


Figure 2: RF designer schematized as a black-box function

The optimization of the design parameters should be focused on finding the structure that can be obtained using the minimum amount of plywood sheets. Additional optimization requirements - for instance the volume of the structural elements or the volume of the cladding - may be included in the optimization.

Structure of the thesis

To create the reciprocal frame designer, firstly a thorough literature review will be conducted. In this literature review, information on existing techniques and methods for reciprocal frame will be gathered. In the literary research information is also gathered on the material that is to be used for the development of the reciprocal frame designer; plywood. This information is not only limited to the production process and structural behaviour. There is additional attention for digital fabrication techniques that can be used for the creation of structural plywood elements. Additionally, methods for efficiently obtaining the structural elements from plywood sheets are explored, addressing the so called 'bin packing problem.'

Before being able to design a reciprocal frame, crucial preliminary design choices have to be made. These preliminary design choices include decisions related the shape of the structural elements, the behaviour of the connections between the elements and the cladding that is used to weatherproof the structure. These choices are discussed in detail in the dedicated chapter ‘4. Preliminary design’.

When all preliminary information is obtained, the development of the reciprocal frame designer can be started. The designer designs a reciprocal frame based on several variable input values (tessellation edge size, scale factor, sheet thickness, eccentricity and the tessellation gradient). The process of how the reciprocal frame designer creates

a structure based on these variables is discussed extensively in chapter ‘5. Reciprocal frame designer’.

During the cross-section optimization that is performed by the reciprocal frame designer, multiple structural calculations are performed. The calculations to obtain internal forces are performed using a FEM model, whilst the unity checks are performed by the reciprocal frame designer. These structural calculations and FE modelling are discussed in chapter ‘6. Structural integrity and optimization’.

The reciprocal frame designer is not only created to design but also to generate digital manufacturing data for robotic manufacturing. The process of creating this production data is explained in chapter 7. Digital manufacturing'. In this chapter, scale model testing and on-site assembly is also discussed.

Finally, using the reciprocal frame designer, the input variables are optimized to find the reciprocal structure that can be created from the least plywood sheets. This optimization process is explained in chapter ’8. Parametric optimization’.

To showcase the effectiveness of the optimization and the resulting structures that can be obtained using the reciprocal frame design tool, some example cases as well as the results of the parametric optimization will be discussed in chapter ‘9. Results’.

Finally the research is concluded conclude the research and summarizing key findings, and provide recommendations for future work. The structure of the research is visualized in Figure 3.

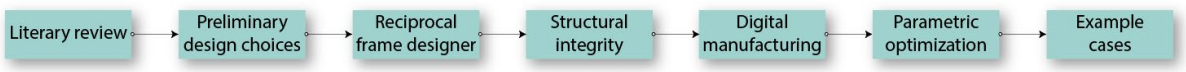
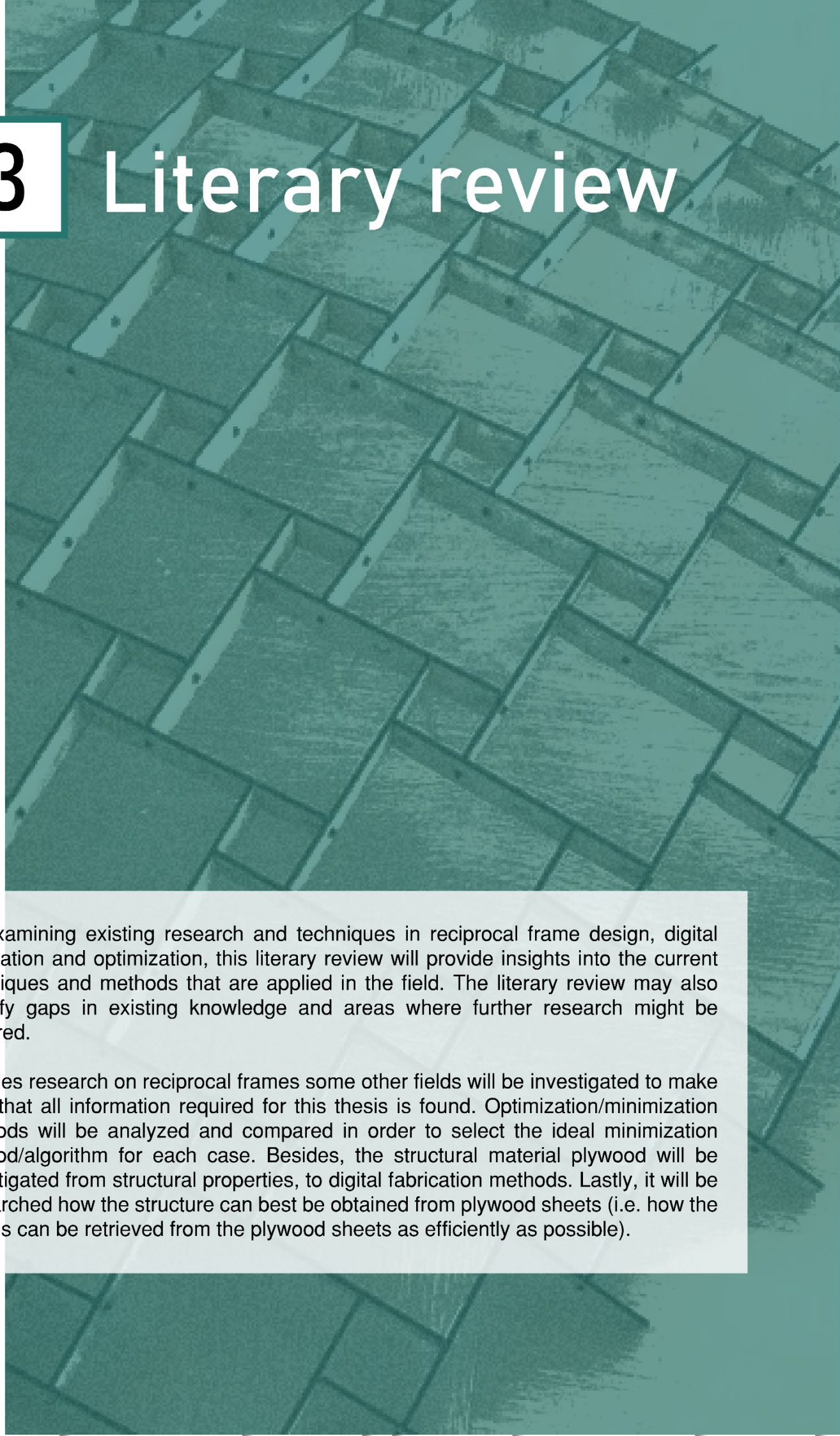


Figure 3: Thesis structure/chapter order



3 Literary review

By examining existing research and techniques in reciprocal frame design, digital fabrication and optimization, this literary review will provide insights into the current techniques and methods that are applied in the field. The literary review may also identify gaps in existing knowledge and areas where further research might be required.

Besides research on reciprocal frames some other fields will be investigated to make sure that all information required for this thesis is found. Optimization/minimization methods will be analyzed and compared in order to select the ideal minimization method/algorithm for each case. Besides, the structural material plywood will be investigated from structural properties, to digital fabrication methods. Lastly, it will be researched how the structure can best be obtained from plywood sheets (i.e. how the beams can be retrieved from the plywood sheets as efficiently as possible).

3.1 Reciprocal frames: Introduction

Reciprocal frames (short: RF's) are structures where the span is larger than the beam length due to their layout. The basic principle behind reciprocal structures is the concept that each beam in the system relies on its neighbors to support it, creating a network of interconnected or interlocking members.

In reciprocal structures, the intermittent supports (beam connections that are not directly supported by a foundation) are almost always not at the beam ends. Instead, beams are often supported along the length of another beam (8).

The origin of the term 'reciprocal frame' can be traced back to its creator, Graham Brown, who developed this innovative structural system in the UK. Brown chose to use the term 'reciprocal' to describe the mutual support that the structural elements provide to each other (10).

Depending on the requirements of the project, reciprocal structures can be created using different materials; e.g. timber, steel and bamboo. In modern reciprocal frame designs, timber is the most used material due to the heigh strength-to-weight ratio of the material.

Figure 5 shows a simple (single unit) reciprocal frame structure. Each member both supports another beam, and is supported by another beam. This interaction is the basis of reciprocal frame structures. Modern day adaptations of reciprocal frames are often based on the repetition of such simple reciprocal structures, or units.



Figure 5: Simple reciprocal structure (11)

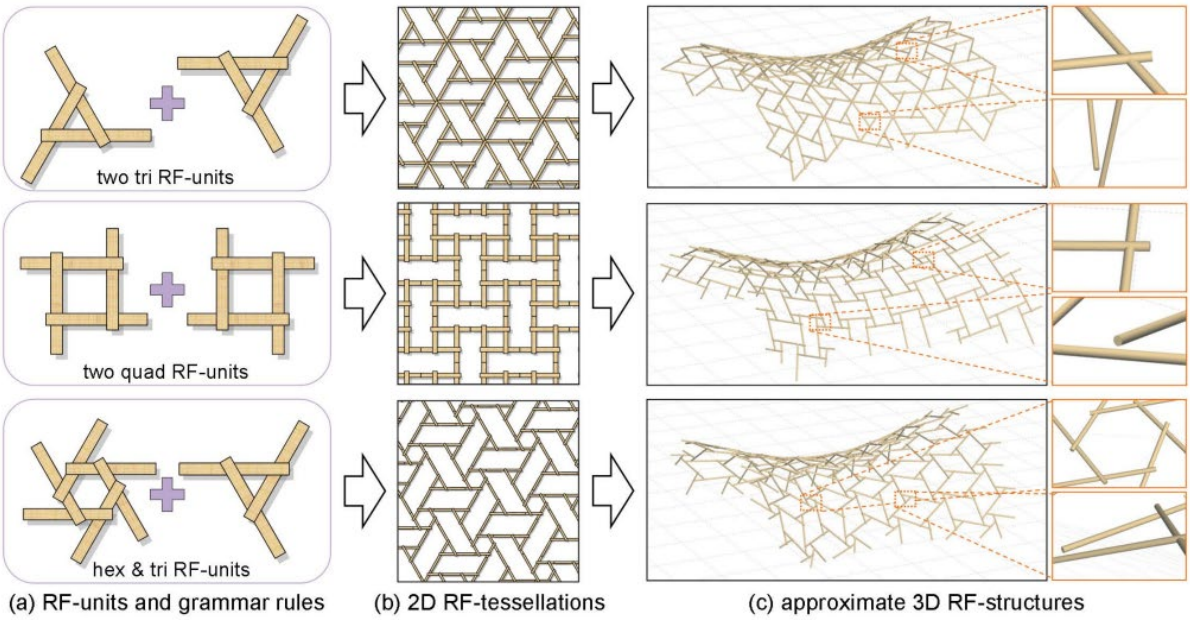


Figure 4: Rf units and resulting tessellations and 3d approximations, derived from Mellado et al. (62)

Figure 4 shows how simple RF-units shape a complex RF structure. This is done by repeating RF-units into a 2d tessellation. Due to inter-member eccentricity, a curved structure can be created using only straight beams.

The connections between these beams can often be simple and low-tech, enabling the structures to be quickly assembled.

However, reciprocal frames, with a large number of elements are often difficult to comprehend. In the past, engineers relied on design methods that are manual and tedious (12). Recently, tools have been developed to design 3D RF-structures.

3.2 Reciprocal frames: History

Origin

In history, multiple civilizations relied on structures that could be described as reciprocal structures. Early examples can be found in the neolithic civilization, where simple RF structures were used in the form of tipi's (8).

The first written documentation of structures closely resembling the current RF form is present in Japan. Historical records suggest that in the late 12th century, Chogen, a Buddhist monk developed a method for spiral layering of wooden beams (13).

In the history of western architecture, most buildings were constructed using timber floors. As buildings became bigger, timber had to be enabled to span larger distances. Often, these great timbers had to be brought from far away. This however was not always possible, so alternative floor designs were investigated. Those circumstances are likely the reason for inventive beam grillage designs, where the spanning distance is larger than the length of the beams. Figure 6 shows a typical medieval beam grillage.

Leonardo Da Vinci, one of the great renaissance thinkers, was interested in structures that look more like the modern RF structures. His sketch in Volume I of the Codex Madrid was very similar to that in Figure 6. He, took this idea a bit further by repeating this grillage pattern in his sketches of the Codex Atlantico (Figure 7)(13).

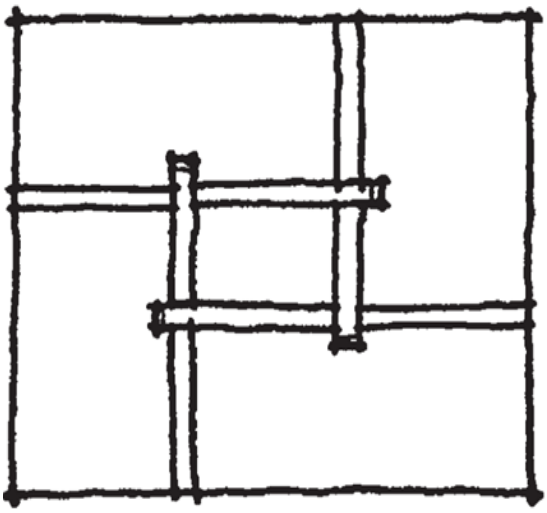


Figure 6: Typical medieval floor grillage configuration (13)

John Wallis made his own RF timber system which was published in 1760. Additionally to the determination of the geometry, he also performed calculations to analyze the stability of the structure (14). The research of Wallis

on reciprocal frame structures represents a significant contribution to the field of construction, particularly in the area of static calculus. With its innovative analytic approach, Wallis' work marked the first instance in which RF structures were subjected to scientific investigation, thereby establishing a foundation for further research and development in the field.

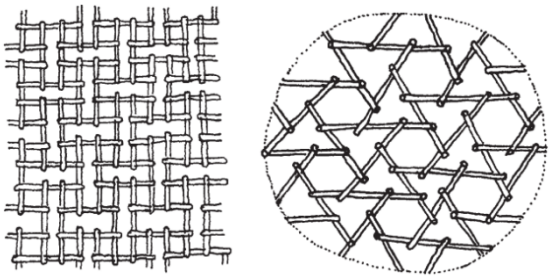


Figure 7: Da Vinci's sketches in the Codex Atlantico, resketched by A. E. Piroozfar (13)

In the 20th century, several three-dimensional grillage structures that are similar to the reciprocal frame were constructed. One of few European examples of a reciprocal structure that was conceived for aesthetical purposes is the Casa Negre, designed by Architect Josep Maria Jujol (Figure 8) (15). The roof structure consists of mutually supporting and spiraling beams.



Figure 8: Casa Negre roof, designed by Josep Maria Jujol, Photo: Jaime Segura (15).

Another example of reciprocal frame structures is the Zollinger roof. The design of the structure has made an impact on the construction industry after World War I. Architect Zollinger invented a roof structure using in plane jointing instead of overlapping jointing which lead to an increase in ease of production and assembly (Figure 9) (16). Zollinger stated that his technique resulted in 60 percent less wood and 40 percent less labor in comparison to standard roof structures for that time (8).

Recent History

In recent decades, the study of reciprocal frames has gained increasing attention among academics, driven in large part by the rapid development of computation speeds and a fascination with their aesthetic appeal.

As a result, numerous form-finding techniques have been developed, many of which have found practical applications in building design and construction.

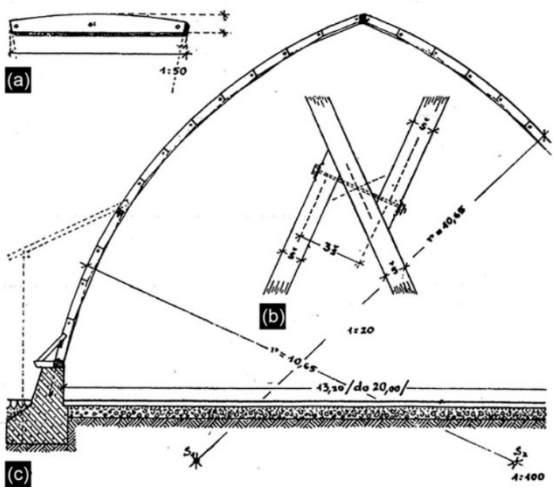


Figure 9: Section and detail of Zollinger lamella roof design (16).

Recent RF projects are mainly pavilions that are resulting from research projects. An example of this is the KREOD pavilion in London (see Figure 10). The design challenge in this structure was the fact that it was made without screws or glue, but with dowels. Due to the constant curvature, the structure could be made from identical prefabricated elements. Li adopted simple manufacturing and wood planks to prevent complex CNC manufacturing (17). In this project, a highly complex geometric optimization method is used.

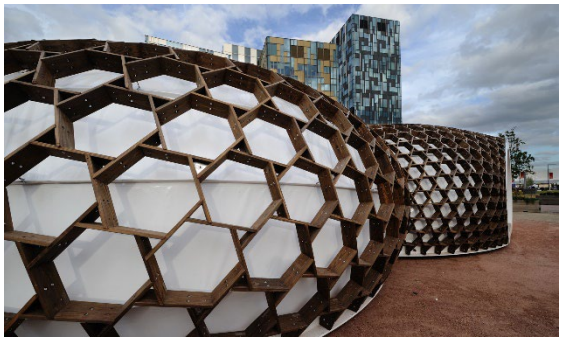


Figure 10: KREOD pavilion in London, designed by Chun Qing Li(17)

Another recent project is the R2 Pavilion, which is made using prefabricated so-called 'shell-nexorade' elements. This project was largely focused on the robotic fabrication of the elements. In the prefabricated elements, panels are used that function as load distributers but also as stabilizing elements.

The Frans Masereel Centrum in Kasterlee, Belgium is a recent example where a reciprocal frame is used in a non-temporary building (see Figure 11) (18). The reciprocal roof structure is supported by concrete walls. In this project, a reciprocal structure is used to enable the usage of sawn timber whilst having a rather large span. In the project, a parametric optimization was performed to minimize the material usage. This project showcases the aesthetical possibilities of using reciprocal frames.



Figure 11: Frans Masereel Centrum roof structure (18)

3.3 Reciprocal frames: Geometry

To comprehend, analyze, and represent structures effectively, designs have to be made easy and well organized. While conventional structures can be designed and illustrated using manual or computer-aided design methods, this is not the case for reciprocal frames. This is particularly evident when dealing with three-dimensional reciprocal grids featuring eccentric joint configurations, as the manual design approach may fall short (8).

An typical design method for standard structures can be established by creating a two- or three-dimensional grid structure that is made from a series of intersecting members where the members meet each other at their extremities.

Four analytical methods exist in literature that transform standard frames (or a polygenic tessellation) to reciprocal frames: the translation method, the rotation method, the extended translation method and the center-to-center method (19–23). These methods are applied to single polygons and then connected later using additional methods.

Single unit design methods

The methods that are found for turning a single convex polygon (= closed polygon where any line segment connecting two points inside the polygon lies completely within the polygon) into a reciprocal frame unit.

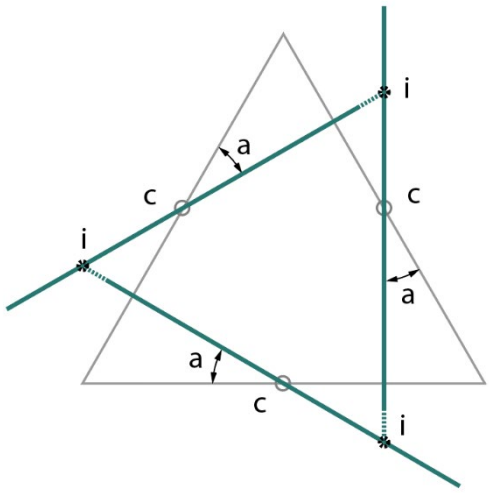


Figure 12: Rotation design method applied to triangular polygon. c = center point, i = intersection point, a = angle of rotation

Rotation method

To create a reciprocal frame unit from any convex polygon, firstly the rotation method can be used. The middle point for each of the side of the polygon needs to be considered. The sides of the polygon are rotated around the center point by a certain angle (a). Finally, the intersection point at every line is joined with the rotated lines. This method is visualized in Figure 12.

Translation method

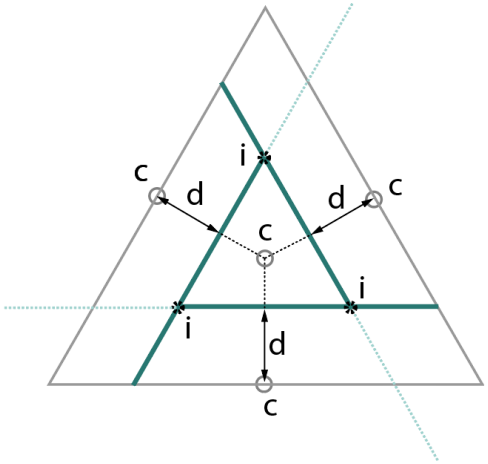


Figure 13: Translation design method applied to triangular polygon. c = center point, i = intersection point and d = translation length

To create a reciprocal frame using the rotation method, each of the sides of the polygon are translated inwards with a prescribed distance. The lines are then cut of at the intersection point. This method is visualized in Figure 13.

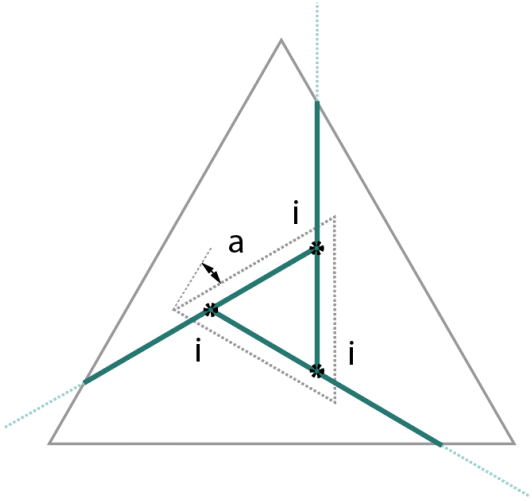


Figure 14: rotation and translation design method applied to triangular polygon. i = intersection point and a = rotation angle

Rotation and translation method

A reciprocal frame unit can also be designed by combining the previous

methods; resulting in the 'rotation and translation method' (see Figure 14). This method however does not add extra freedom of form in designing. Furthermore, the complexity to create a regular grid is increased (8). It proves to be challenging to determine the transitions between several polygons through basic geometric rules. This study seeks to employ relatively simple geometric principles for determining a reciprocal frame. As a result, the combination of rotation and translation is not included further in this research.

Center-to-center method

The final method to create reciprocal structures that is researched is the center-to-center method. To apply this method, first the convex polygon must be scaled down towards its center point. Secondly, the center points of the main polygon and the scaled down polygon are connected with straight lines. After that the lines are extended until they meet at the intersection points. This process is depicted in Figure 15.

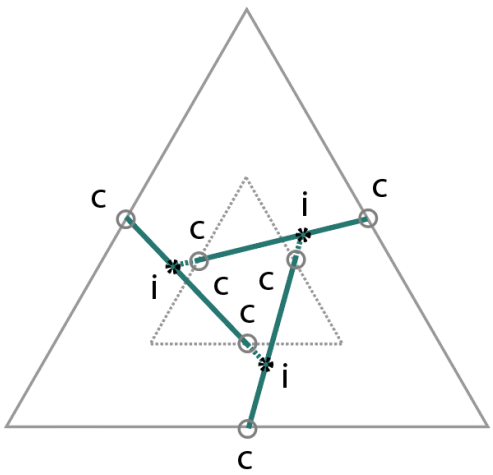


Figure 15: center-to-center method applied to triangular polygon. Where c = center point and i = intersection point.

Combining reciprocal frame units

A reciprocal frame consists of multiple reciprocal frame units. Combining multiple units can often simply be done by applying the design methods to the separate units.

Rotation method

The rotation method works perfectly when combining multiple polygons (see Figure 16). The downside however is the fact that multiple rotation angles need to be used to find a possible reciprocal frame design. This results in a complicated form finding procedure. Furthermore, the support positions are not constant and are dependent on the rotation angle. This makes the resulting structure less predictable.

Additionally, as visualized in Figure 16 the position of the free ends (indicated with red squares) are not ideal. One could extend the free end until the next beam, but that would result in a large unsupported span.

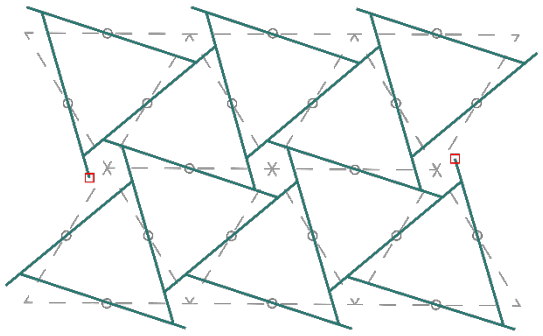


Figure 16: Reciprocal frame designed on triangular polygons using rotation method. Red squares indicate free ends with unfavourable positions

Displacement method

The displacement method creates a reciprocal frame that aligns with the original grid. However, the method also creates some issues when combining multiple reciprocal frame units.

Firstly, the same issues with the positions of the free ends as the rotation method are found. Secondly, in a continuous reciprocal frame, the pattern cannot be continuous. Resulting in aesthetically unpleasing connections as visualized in Figure 17.

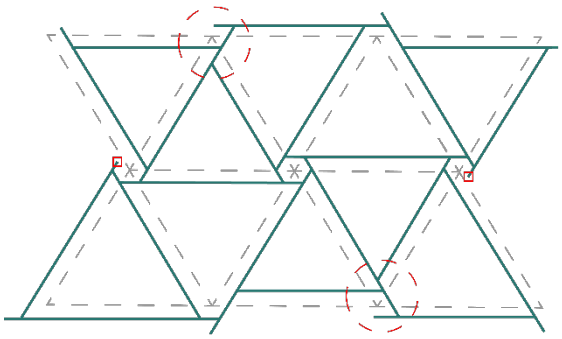


Figure 17: Reciprocal frame designed on triangular polygons using translation method. Red squares indicate free ends with unfavourable positions. Red circles indicate problematic locations

Center-to-center method

The center-to-center method is based on scaling instead of polygon transformations (24). This makes the positions of the free ends more predictable. Furthermore, a consistent pattern is found. Also the intersections between the neighbouring polygons are automatically created. The resulting geometry is visualized in Figure 18.

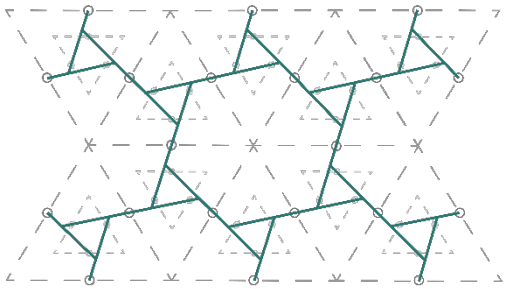


Figure 18: Reciprocal frame designed on triangular polygons using the center-to-center method.

In some inconsistent polygon layouts (e.g. a combination of squares and triangles) kinked members may be created (see dashed lines in Figure 19). These kinked members create difficulties in detailing and may create unfavourable internal forces in the members.

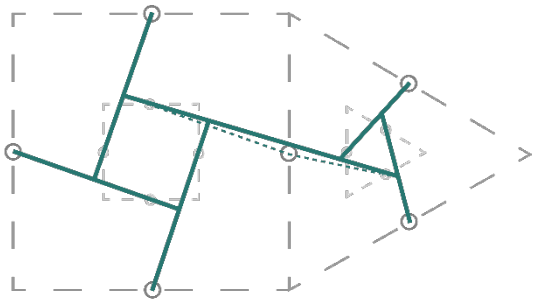


Figure 19: Reciprocal frame between square and triangle, resulting in a kinked member (dashed line)

To solve these issues, the kinked members must be straightened out. This is done by connecting the ends of both elements and ignoring the center point that creates the kink.

Another downside of the center-to-center method is the larger free planes that would have to be spanned by a secondary structure (e.g. cladding).

Comparing design methods

As mentioned before, the rotation and translation method adds additional complexity to the creation of a regular grid, whilst not adding extra freedom of form, therefore this method is not considered.

The center-to-center method naturally creates a regular grid when using basic polygons. The resulting reciprocal frame is found by a single scaling factor. Additionally, intersections with neighboring polygons are automatically created because all elements start on the center of the edge.

For the translation method and the rotation method, two neighboring

reciprocal units will not necessarily share a point, making it more difficult to create large reciprocal frames. Additionally, the unfavorable positions of free ends may create issues.

The translation method also has some issues with repetitive/continuous polygon grids, where strange connections may be found.

Finally, each of the methods have an influence on the aesthetics of the reciprocal frame unit and thus the overall reciprocal frame. This aspect of selecting the method should obviously also be considered.

3.4 Reciprocal frames: Form finding

Transforming a two dimensional reciprocal structure into a three dimensional reciprocal structure requires additional form finding. Form finding is the process of finding a feasible architectural and structural shape for a structure.

Due to the complex layout of three dimensional reciprocal frames, large reciprocal frames cannot be designed by free hand. In recent history, several methods to design three dimensional reciprocal frame structures have been developed. All of these methods are based on a starting with a design that roughly represents what the structure should look like, without complying to actual inter-member interaction requirements. This design then requires an iterative design process to generate a feasible design that does comply with all requirements to realistically simulate the interaction between the members.

The geometric design methods as described in the previous chapter provide a basis for the design of 3d reciprocal structures. These two dimensional frames are turned into three dimensional reciprocal frames using the methods that are elaborated in the following paragraphs.

3D design methods

Trial-and-error

The first reciprocal frame structures were designed before iterative digital computation was available. Therefore most early designs were made using trial and error (13). Many amateur construction projects based on reciprocity nowadays are still designed using trial and error. In these cases, the interaction between the members is not completely relevant as no additional structural (FE) calculations are performed in these cases.

Mapping

A method to transform a 2d reciprocal frame into a 3d structure is the mapping method, where a two-dimensional tessellation is mapped onto a three-dimensional surface. The flat representation of the mapped surface must match the size of the two-dimensional tessellation. Additionally, the tessellation edges should match the edges of the mapped surface. Mapping may result in a non-uniform reciprocal frame density. This can be avoided using non-uniform projection densities.

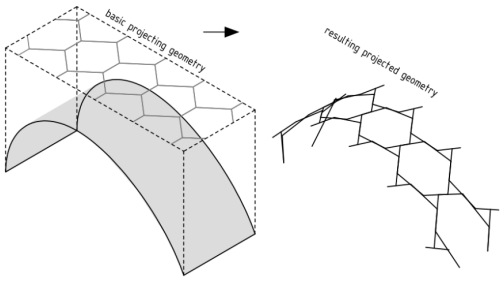


Figure 20: Generating a 3d reciprocal frame by mapping a 2d tessellation onto a 3d surface (8) [edited]

The mapping method will result in a solution that will not satisfy the eccentricity conditions, therefore form finding methods need to be used to satisfy these conditions.

Lift tessellation to 3d

Additionally, a 3d reciprocal frame structure can be made by lifting elements into the 3d shape (25). This method may not always produce coherent reciprocal structures, it however enables large designs that can be interactively explored.

A method to lift the tessellation is to move each element until the eccentricity requirements are roughly satisfied. Similarly to the mapping method, additional computation is required to satisfy all conditions after the transformation.

Form finding methods

As mentioned before, the structural shape resulting from previous design methods does not satisfy all structural requirements. The eccentricity between members should be described by an infinitively stiff element that is orthogonal to both beams. In literature two main form finding methods to achieve a correct structural shape are typically used: a numerical minimization and dynamic relaxation.

Numerical method

With increasing computational speed of computers, iterative solver methods can be used to calculate reciprocal structures.

Iterative solvers determines the best geometric solution of a reciprocal frame by calculating the best fitting value from a range of alternatives. The most optimal solution is found by minimizing an error function (or maximizing a fitness function). For reciprocal frames the problem is defined by finding the ideal eccentricity between members:

$$\min f(error) = sum|e_{act} - e_{req}|$$

The equation above in words can be explained as: minimize the difference between the actual eccentricity and the required eccentricity for all connections.

Several researches have used this design method. Song et al. have used the method to keep the reciprocal frame as close as possible to the basic surface during the optimization procedure (26). Pugnale et al. developed a method to optimize the intersection location (or engagement length) and eccentricity using a genetic algorithm and a gradient based solver (27).

Su et al. have made a more advanced iterative solver, using bar elements, which allows finite element computations (9). In this study, the error function was extended consisting of: length condition, perpendicular condition and colinear condition.

All numerical methods in the aforementioned researches are based on multivariate optimization or minimization algorithms. It is important

to mention that algorithms do not necessarily have to be indeterministic, there are minimization algorithms that solve deterministically. This means that the numerical method can perform a directed search to find the optimal structural shape.

Numerical methods do not allow instant results of the reciprocal frame to be visible, which may be a downside. Iterative design methods however allow a high degree of flexibility and control over the form-finding process.

Dynamic relaxation

The dynamic relaxation method is not completely indeterministic, meaning that the form finding procedure does not involve any randomness.

The dynamic relaxation is performed applying a fictional bending force on an undeformed regular grid structure causing it to transform into a reciprocal frame. The balance in the structure is found through the dissipation of kinetic energy.

Additionally, the geometrical reciprocal frame design methods (as described previously) can be used to determine initial reciprocal frame geometry. Dynamic relaxation can be performed afterwards to optimize for instance the eccentricities (8).

Dynamic relaxation also requires iterations to convert to a solution. The number of required iterations depend on the optimization procedure and the degrees of freedom in the structure

An advantage of dynamic relaxation is that the same structural model can be used for both the form finding and FE (structural) analyses.

3.5 Reciprocal frames: Structural principles

In general, two-dimensional (flat) reciprocal frames transfer loads by bending moment. This means that reciprocal frames can be described as section active structures (8). However, three-dimensional reciprocal structures cannot be described as space structures, where forces are transferred by normal force and all members are connected at their ends.

In reciprocal frame structures, members do not connect at their extremities, but at intermediate locations on the beam. This results in a different flow of forces where forces are transferred by a combination of bi-axial bending and shear instead of normal force. The complex characteristics of reciprocal frame structures make the understanding of the flow of forces less straightforward, and load paths cannot immediately be established.

Forces in a planar reciprocal unit

To create a force equilibrium in a reciprocal frame (unit), a minimum of three elements per unit is required (28).

If there is no eccentricity between the members, and thus the reciprocal unit is planar, the structural scheme is as shown in Figure 21a. In the scheme the loads are assumed to act on the nodes only.

The resulting moments are shown in Figure 21b. In this schematization it is assumed that the cross sections have the same bending stiffness EI. When the stiffnesses of the beams are not equal, the flow of forces is also not equal due to the statical indeterminacy.

When analyzing the internal forces, it is inherent that the connections act as intermediate supports. These intermediate supports are visualized in Figure 21c. From force equilibrium, it can be calculated that the reaction forces at the intermediate supports can be calculated with the following formula:

$$R = \frac{FL^3}{2(L-a)}$$

As mentioned in chapter '3.3 Reciprocal frames: Geometry', the scale factor determines the location of the intermediate support along the beam. This location also influences the maximum bending moment in the beam. When the point loads F are constant, the maximum bending moment is related to the location of the intersection or 'support point' on the beam.

Figure 22 shows the relation of the maximum bending moment in the beam with respect to the location of the intermediate support along the beam. In mathematical terms this relation is described as an 'upward exponential decay'. This behaviour means that the closer the support is at the end of the beam (towards the middle of the span) the larger the bending moment in the beam. This behaviour can also be explained by the fact that the point loads will act closer to the supports.

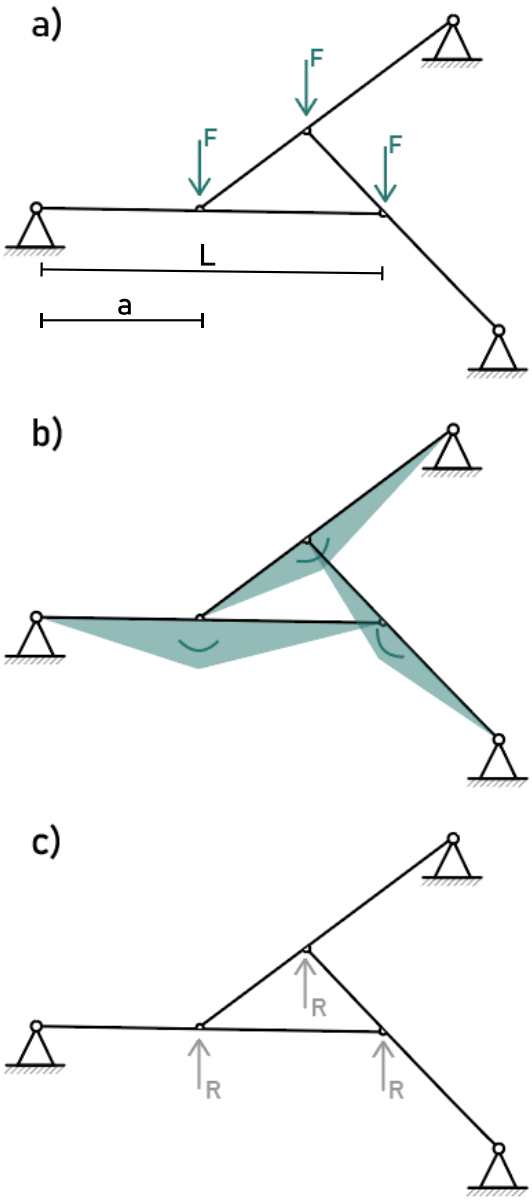


Figure 21: a) Schematization and b) internal forces of a 3-element reciprocal unit. c) Intermediate 'support reactions'

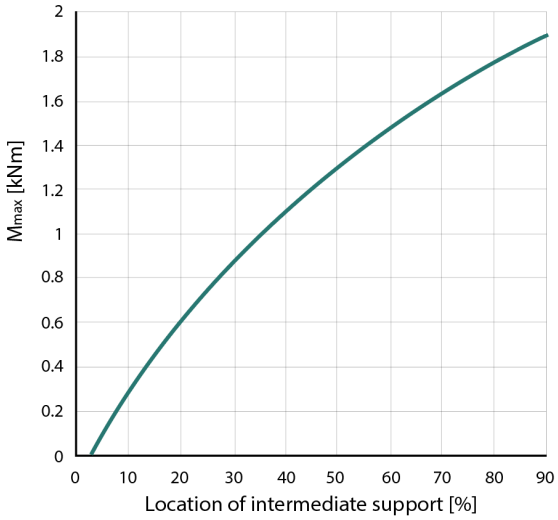


Figure 22: Graph of the maximum bending moment in the beam of a reciprocal unit related to the location of the intermediate support along the beam (location of intermediate support = a/L*100%).

Forces in an eccentric reciprocal unit

When an eccentricity is created between the members in the reciprocal frame, the computation of the internal forces becomes a lot more complicated. Besides the bending moment in downward direction, also a normal force and a bending moment in the other direction of the beam axis is added. Due to this complex combination of forces, it becomes almost inevitable to use FE (computer) analyses to perform structural calculations (29).

To be able to transfer normal forces through the eccentric connections, shear forces must be transferred through the eccentric node. See chapter '3.6 Reciprocal frames: Detailing' for more details about the connections.

The nodal eccentricity is usually modeled by using an infinitely stiff connecting element (8,9,29). Within this connecting element, the required degrees of freedom can be generated by using an intermediate node.

Forces in an eccentric RF

By connecting reciprocal units with an inter-member eccentricity, a curved dome-like reciprocal frame can be created (see for example Figure 23). There are also methods to create this effect without eccentricity, this however is not within the scope of this research.

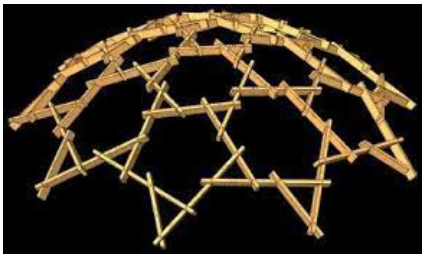


Figure 23: Example of a dome-like reciprocal frame (8)

A dome shape is usually beneficial for structures where the beams meet at the ends. However, for reciprocal frames, curving does not necessarily have to be beneficial due to the different internal flow of forces.

Typically, when comparing a 2d structure to a curved structure, the bending moments are reduced in a curved structure compared to the 2d structure. In return, there is an additional normal force parallel to the surface of the dome. The fact that the beams do not meet at the extremities in reciprocal frames makes this behaviour less straightforward.

The normal forces in the beams (that are generated by curving the structure) are transferred to the other beams by bending in the other beam axis instead of directly transferring the normal force in a structure where the beams meet at the extremities. This means that adding curvature generates an additional bending moment in the elements in the axis parallel to the dome's surface (9).

3.6 Reciprocal frames: Detailing

In reciprocal frame design, the connection between the element is largely determining the shape of the elements and thus the aesthetics of the structure.

As mentioned before, the connections between the beams in a reciprocal frames are quite complex due to the eccentricity between the members and the multiple different angles at which the beam elements connect. By researching the internal forces in the reciprocal frames it was found that the connections need to be able to transfer both normal forces (along the beam axis) and shear forces in all directions so the bending moment and accompanying shear forces can be transferred.

In recent history, several connection methods/types have been applied in reciprocal frame structures. In this chapter the different connection types will be described.

Notching joints

A method that is often used when reciprocal frame structures are made from sheet materials is the notching joint. In this method, the angle at which the beams come together is determined and the beams are be notched accordingly. By doing so, the beams can be interlocked with each other in the direction of the rotation without needing any additional attributes (e.g. screws) (31). To apply this method, the notches need to be applied accurately to make sure the interlocking takes place. See Figure 24 for an example sketch of a notching joint.

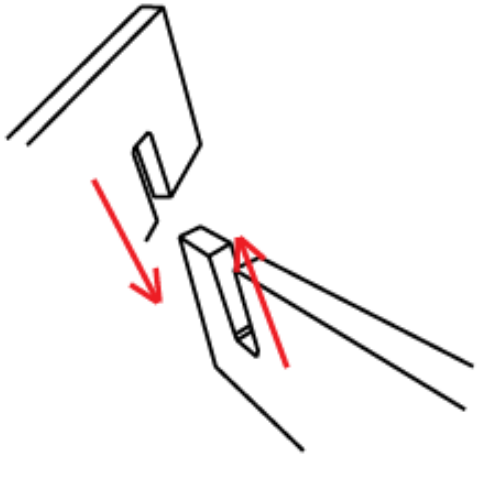


Figure 24: Example sketch of a notching joint between two beams, used in a reciprocal frame designed by N. Melenbrink et al. (30,31).

Friction joint

Another connection method is created by using friction between the members. This method also requires extreme accuracy, especially during manufacturing. The cuts that are made in the beams enable the beams to have grip on each other. The assembly is therefore only stable when the construction is finished (31). See Figure 25 for an example of the friction joint.

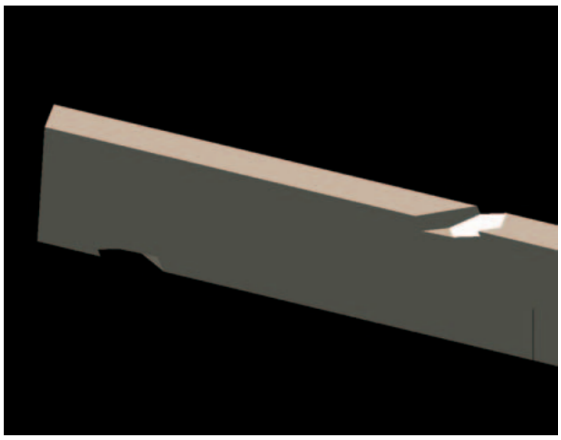


Figure 25: example of a beam cut to allow for a friction joint (13).

Mechanically fastened joint

Previous methods are traditional methods creating connections without

any additional fasteners or attributes. Connections can however also be made using (steel) mechanical fasteners. Several of these methods have been applied before. These methods are advantageous because they give the engineer a more predictable behaviour, making it easier to check if the structure is strong and stable enough.

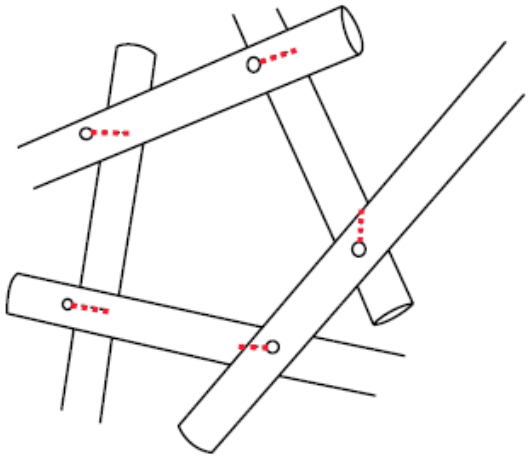


Figure 26: reciprocal beams connected with metal pins (31)

Figure 26 shows a typical joint that can be made using metal pins, but there are obviously many more ways to use mechanical fasteners.

Additionally, sometimes the connections are made by tying rope around the connection. This is especially done when the beams have a circular cross section.

Mortise and tenon joint

Finally, a method that is not used that often is the use of a mortise and tenon kind of joint. This kind of joint was used in a research by E. Corio, see Figure 27.



Figure 27: Mortise and tenon joint, as used in 'Reciprocal-Framed Grid Shell' (32)

In this joint design, the beams are supported at the ends by an extending, more shallow, part that penetrates a 'gap' in the supporting beam. Contrary to the notching joint, the gaps are in the middle (center line) of the beam. This location is more advantageous in terms of internal forces, because the gaps are placed at the locations where the bending stresses are the smallest.

3.7 Reciprocal frames: Cladding

For a reciprocal frame structure to be used as (part of) a building, weatherproofing must be applied. This is done by adding a cladding to the structure and thus filling the gaps between the beams. There are several ways this has been performed in existing reciprocal frame buildings. This chapter will discuss the different methods that have been used before

Timber sheathing

One method of cladding a reciprocal frame is by connecting timber sheets to the structure. These timber sheets will completely cover the structure. Insulating and moisture-/waterproof material can be added if required.

This method has been applied in the Frans Masereel centrum, see Figure 28. For 2d reciprocal frames, this method

can often be used with standard sized plywood sheets (if the reciprocal frame structure is designed correctly)



Figure 28: Sheeting applied to reciprocal structure in Frans Masereel centrum in Belgium (33)

However, if the structure is curved, like in the Frans Masereel centrum. Every free span needs a custom sized plywood sheet, resulting in many uniquely shaped plywood sheets. This requires additional manufacturing to take place, and makes the process of assembling a reciprocal structure a lot more complex.

Weather resistant tensile fabric

To prevent creating multiple unique cladding elements that need to fit precisely on each of the beams of the reciprocal frame, multiple architects/designers have opted to create a weatherproofing based on a weather resistant tensile fabric.

One example where this cladding type is used is the Kreod Pavilion in London (Figure 29). A tensile fabric is connected on the nodes on the inside of the structure. This leaves the reciprocal frame exoskeleton visible from the outside whilst the inside is weatherproofed. In this example, the internal tensile fabric is connected to the structure at several nodes.

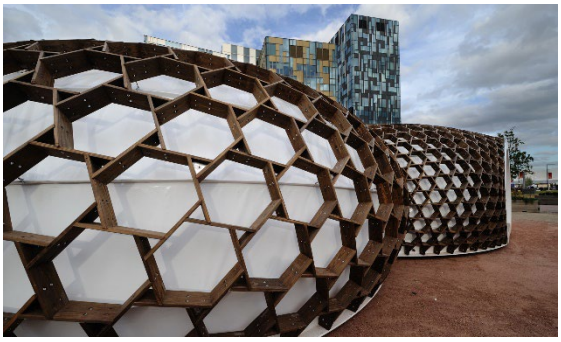


Figure 29: KREOD pavilion in London, designed by Chun Qing Li(17)

Instead of putting the fabric on the inside, it could potentially also be used on the outside of the structure. This would require the fabric to be placed at a certain distance from the structure to make sure the fabric does not come in contact with the structure.

Aluminum panels

Another method of applying the cladding is by making the cladding part of the reciprocal units. This method can be used when the reciprocal frame is designed modularly.

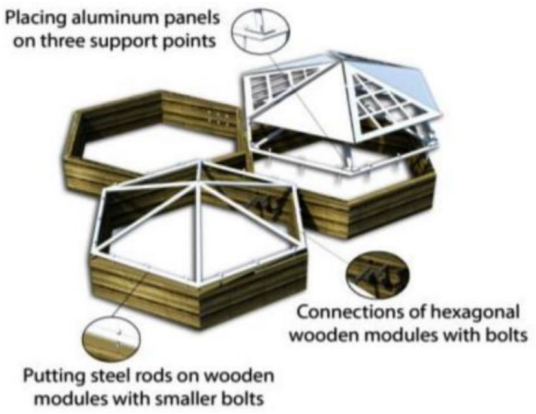


Figure 30: Aluminium panel cladding as used in the work by Z. Tošić et al.(34)

An example of this method is found in the work by Z. Tošić et al. (34). In that design hexagonal wooden modules are prefabricated including the cladding (see Figure 30). The hexagonal units are later connected to create a reciprocal frame.

3.8 Plywood

Besides researching reciprocal structures, it is important to know the properties of the material that is going to be used for the structure. Plywood is often applied for structural purposes, most often the plywood is used as sheeting over beams. This means that plywood is often used for out of plane bending.

Plywood is a material consisting of veneers bonded with an adhesive (35). Each veneer layer (or ply) is usually oriented with its grain running perpendicularly to the adjacent layer to reduce the shrinkage and improve the strength of the finished material.

Manufacturing

The manufacturing process of plywood consists of nine main processes: log storage, log debarking and bucking, heating the logs, peeling the logs into veneers, drying the veneers, gluing the veneers together, pressing the veneers in a hot press, plywood cutting and other finishing processes such as sanding (35).

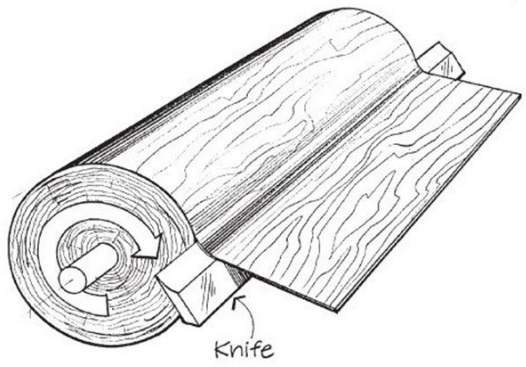


Figure 31: Log peeling to create plywood sheets (6)

The most important takeaway from the manufacturing process is the raw-material efficiency plywood has over e.g. sawn timber. The reason for this is the fact that the log is peeled instead of sawn. This reduces the waste material for a log to 25% compared to 50% for sawn timber (5).

Structural plywood

Plywood can be classified into two main classes, structural plywood and non-structural plywood. Non-structural plywood is intended for e.g. furniture making, whilst structural plywood is suitable for heavy-duty external applications.

To be classified as structural plywood, the sheets need to meet certain standard requirements. An example of these requirements is having an A-bond glue, which is resistant against weakening by environmental causes.

Structural behaviour

Timber is a natural, anisotropic material. In the material many structural defects may occur. Since in plywood each layer is stacked orthogonally, the impact of defects is a lot smaller. In balanced, symmetrical plywood layups, the material may be assumed to be homogeneous and orthotropic (36).

The structural properties of plywood are dependent on multiple factors: timber quality/type, adhesive and layup. The exact material properties of plywood are thus also dependent on the thickness of the plywood sheet. These exact material properties can be determined from classical lamination theory, or experiments.

Plywood (and timber) are viscoelastic materials, especially when heavily loaded for a prolonged time. However,

at low stresses the material can be assumed to be elastic (37). In the Eurocode it is stated that plywood may be assumed to be orthotropic and linear elastic (38). Additional deformations resulting from e.g. the viscoelasticity are considered as creep deformations.

3.9 Digital fabrication techniques for plywood

Typical fabrication techniques for timber sheet (2D) materials are CNC-routing, laser cutting, and waterjet cutting. Laser cutting is often used for sheet material. It however is usually restricted to timber sheets with a thickness of approximately 12mm. This limitation can be problematic for thick structural elements, Therefore laser cutting is not considered in this research.

Waterjet cutting is a cutting method that uses a high-pressure water jet to cut a wide range of materials. Despite being counterintuitive to combine water and timber in production, waterjet cutting can be effectively used with plywood materials (39). Waterjet cutting offers some advantages over CNC-routing, like the absence of heat during cutting. This enables waterjet cutting to achieve highly precise contours.

Regardless of the thickness of plywood, it is necessary to have a 3mm gap between elements to be able to create tabs that prevent parts from moving during cutting. The internal corner radius can be as small as 0.4mm, which is practically negligible for timber elements. When thicker sheets are used however, the internal corner radius is also enlarged significantly.

CNC, short for Computer Numerical Control, uses a computer program to control machine tools. In the case of CNC-routing, a hand-held router serves as the spindle for cutting various materials. Unlike waterjet cutting, the plate thickness affects the thickness of the cutter and the minimum internal radius in CNC-routing applications.

Cutter thickness CNC

The thickness of the CNC cutter plays a significant role in determining the final cutting layout. The cutter thickness is equal to the diameter or width of the cutting tool used in the CNC machine. It influences the accuracy of the cuts, the quality of the finish and the efficiency of the cutting process.

The choice of cutter thickness depends on several factors: the type and hardness of the timber, the desired finish, and the detailedness of the design. Smaller cutter thicknesses are very effective for intricate details and finer finishes. Larger cutter thicknesses are preferable for rough cuts and bulk removal of material.

Another aspect is the feed rate or the speed at which the cutter moves through the timber. The feed rate, combined with the cutter thickness, determines the amount of material that the cutter removes per pass. A larger cutter thickness (combined with a higher feed rate), can remove more material at once. This enables faster cutting, but reduces precision. On the

other hand, a smaller cutter thickness with a slower feed rate allows for more precise cuts but requires more passes to complete the job (40).

Table 1: CNC guidelines acc. Plywood + Panel (41)

Thickness plywood (mm)	CNC Cutter Width (mm)	Min. Internal Radius (mm)	Minimum Gap (mm)
0-6mm	6	3	6
7-15mm	8	4	8
16-19mm	10	5	10
20-30mm	12	6	13**
> 30mm	16/20 mm*	8/10	17/21**

For CNC cutting plywood, the company Plywood + Panel made table with general design parameters for cutting plywood plates with certain thicknesses (see Table 1). These guidelines give a good indication of what values to use for the RF design tool. It may however turn out in practice that these values should be adjusted to this specific design layout.

For thicker plates, the cutter width may depend on the hardness of the plywood (*), and the gap between cut elements is increased with 1mm to allow for a roughing pass (**).

CNC milling tools typically have a cylindrical shape. As a result, they will create a radius when cutting an internal angle. If internal edges with sharp corners are needed, for instance to enable fitting a rectangular part into an equally sized hole, it is recommended to use a shape with undercuts rather than reducing the radius of the internal edges (see Figure 32) Click or tap here to enter text.(42).

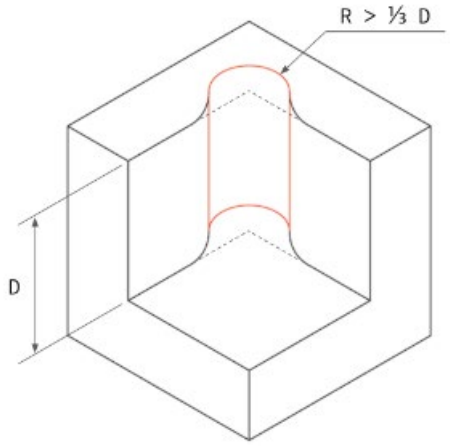


Figure 32: Undercut in corners to be able to fit a rectangular element (42).

Generally, CNC may be more restricting and complicated compared to waterjet cutting. However, CNC is widely applied in the Netherlands and should therefore be an available option for producing the reciprocal frame.

Three dimensional elements

Although it is less common, CNC milling can also be used to create three dimensional cuts/shapes. This requires the CNC milling tool to rotate in three dimensions. This requires specialized CNC milling tools. Waterjet cutting can also be used to create three dimensional shapes from timber. This method is also not very common.

3.10 The bin packing problem

Bin packing algorithms play an important role in reducing material usage and optimizing the efficiency of the manufacturing process, especially when designing a reciprocal frame where the structural elements are made from plywood. Using bin packing algorithms, the individual beams of the reciprocal frame structure can be efficiently packed into the plywood sheets. This will reduce waste and thus the number of sheets required.

Bin packing algorithms work by considering the dimensions and shapes of the beams, as well as the available size of the plywood sheets. The goal of the algorithms is to find the most optimal arrangement of the beam elements on the plywood sheets, minimizing the unused space.

In computational science, the bin packing problem (BPP) is known to be NP-hard (43). This means that there is no algorithm that can solve a problem optimally for all instances (in a reasonable amount of time) (44). Therefore, various approximation algorithms have been developed to find good solutions within a reasonable time. These algorithms aim pack the eminent in a way that is close to the optimal solution, they may however not guarantee an optimal result in all cases.

Several heuristic algorithms that approximate the optimal solution have been developed, each have their (dis-) advantages in terms of spatial efficiency and computational speed (45). The four most commonly applied algorithms are explained and compared in the next paragraphs. For comparing runtime complexity, the 'Big-O Notation' is used (46).

The Big-O notation is a method to describe the (time)efficiency of an algorithm. In simple terms, it measures how efficiently an algorithm scales with larger inputs. The notation is expressed as $O(f(n))$, where $f(n)$ represents the worst-case time complexity or growth rate of the algorithm. If the time complexity of an algorithm is $O(n^2)$, it means that when the number of elements to be sorted (n) increases, the runtime will increase quadratically. In this example, if the number of elements is doubled the running time will thus increase four times.

Shelf algorithms

Shelf algorithms can be considered to be the simplest methods for producing packings (45). A shelf is a sub-rectangle of the bin. During the packing process, the available space within the bin is divided into shelves, starting from the bottom and moving upwards. The rectangles are placed from left to right within each shelf. The shelf that is on top is considered to be the 'open shelf'.

Since the rectangles are packed from the bottom, the space above the open shelf is always free. This particular setup enables the height of the open shelf to be altered each time a rectangle is placed on it

Unlike the open shelf, the shelves below it, known as closed shelves, do not offer the same flexibility. Once items are placed on closed shelves, their height

cannot be adjusted. When packing a rectangle onto the shelf it is decided whether the rectangle is rotated or not.

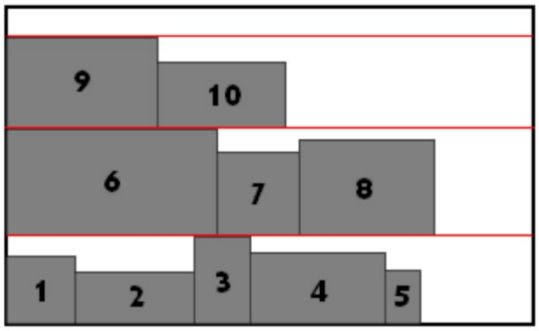


Figure 33: A sample packing using a shelf algorithm

Like the other types of algorithms, there are a lot of sub-variants. These are based on the destination bin determination method, as discussed later. The time complexity of shelf algorithms are: $t = O(n)$.

Guillotine algorithms

The guillotine algorithm is based on the guillotine split placement. This split placement is performed by firstly placing a rectangle to a corner of a free rectangle of the bin. After placing the rectangle, the remaining (L-shaped) free space is split into two separate free rectangles (45).



Figure 34: A sample packing using a guillotine algorithm

The Guillotine algorithm is highly appreciated because it accurately keeps track of the available free space within the bin without overlooking any empty areas, which sets it apart from shelf algorithms. However, one limitation of this algorithm is that it only considers placements where a rectangle completely fits inside a free rectangle. It does not attempt to place a rectangle in a way that the object would cross multiple split lines.

The time complexity of guillotine algorithms are $t = O(n^2)$. Therefore it may run significantly longer than shelf algorithms, especially for large datasets.

Maximal rectangles algorithms

This algorithm is based on an extension of the guillotine split placement. The Maximal Rectangles algorithm stores the free rectangles, representing the free space within the bin (similarly to the guillotine algorithm). Unlike the guillotine algorithm, which chooses one of the two split axes, the Maximal Rectangles algorithm performs an alternative operation that corresponds to picking both squares instantaneously.

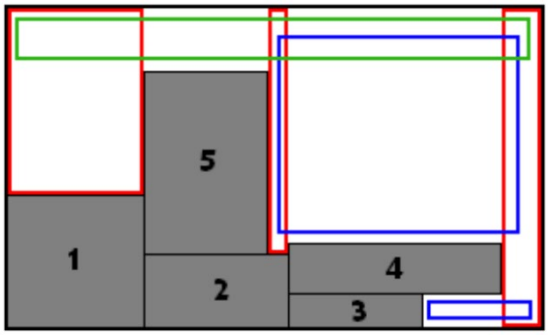


Figure 35: A sample packing using a maximal rectangles algorithm

After packing each rectangle and having intersected it with the elements and produced the set of new potential maximal rectangles. The algorithm loops through each pair of elements to remove the unnecessary free rectangles from the list. This operation is quite

time consuming. In the end, this results in a time complexity of $t = O(|F^2|n)$ for the maximal rectangle algorithm.

To know the actual complexity of the algorithm the growth rate F must be known. According to Jylänki et al., most of the times the growth rate F is linear, but may reach up to n^2 in a worst case scenario. Therefore it can be assumed that the complexity of these algorithms is $t = O(n^3)$ but may reach up to $O(n^5)$.

Skyline algorithms

The Maximal Rectangles algorithm involves another data manipulation to maintain the list of maximal free rectangles. To simplify this process and enable the implementation of the Bottom-Left heuristics, a simplified data structure is proposed.

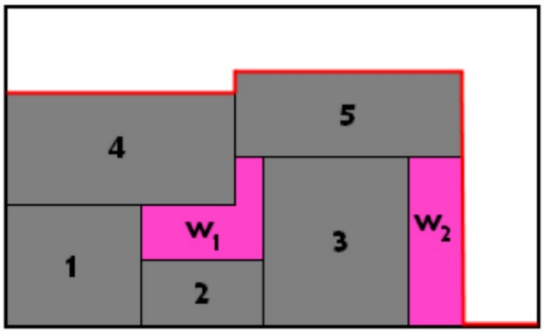


Figure 36: A sample packing using a skyline algorithm

The Skyline algorithm utilizes a "lossy" data structure similarly to the Shelf algorithms. This means the algorithm cannot track the free areas of the bin very accurately. As a result, it may mistakenly mark some unused space as used space. As a trade-off for the reduced area efficiency, the Skyline algorithm offers faster packing results compared to the Maximal Rectangles data structure.

The Skyline algorithm works by storing a list of horizontal – "skyline" – edges, which represent the topmost edges of the rectangles that are already packed. This list grows linearly with the number of packed rectangles. As a result, the time complexity of skyline algorithms is $t = O(n^2)$.

Since it is simple to compute the free rectangles that will be lost when packing a rectangle, the Guillotine data structure can be used to store this space. In this case, the guillotine date is used as a secondary data structure called the 'waste map'. Including a waste map in the packing process does not increase the complexity of the calculation, it however may increase the efficiency of the packing.

Destination bin determination methods

There are a lot of sub-variants of shelf algorithms, based on the way new items are stored in the shelfs. These sub-variants are of the following types:

- Bin next fit (BNF): only one bin (or shelf) is considered opened.
- Bin first fit (BFF): places items in the bins in the order they were opened.
- Bin best fit (BBF): items are packed in the bin that gives the best score for a predefined criterion.
- Bin worst fit (BWF): items are packed in the bin that gives the worst score for a predefined criterion.

For the BBF algorithm, for shelf algorithms, this can mean sorting so that as little width is left in the self after placing the item. Alternatively, as little

height difference between the item and the shelf can be sought, or as little area left after placing the item. The BWF algorithms obviously does the opposite

Shelf algorithms have a basic time complexity of $t = O(n)$. The following time complexity is added due to these determination methods:

- Bin next fit (BNF): 1
- Bin first fit (BFF): $\log n$
- Bin best fit (BBF): n
- Bin best fit (BWF): n

Online or offline bin packing

There are two main types of bin packing problems, online and offline bin packing (47). Online bin packing means that each of the items that need to be packed are received one at the time. Therefore, the items must be placed without knowledge of future items.

In offline bin packing, the whole sequence is known in advance. this enables sorting the items. This adds $t = O(n)$ complexity to the algorithm, but may improve the results drastically.

The sorting may be based on rectangle height or width, the ratio between the sides, the area of the rectangle etc. The most optimal presorting method is dependent on the input data.

4 Preliminary design

Before being able to make a reciprocal frame design and optimization tool, some design choices must be made. These choices consist of the element design and the assumed cladding of the structure. What choices are made, and the influence these choices make on the structural behaviour and design of the reciprocal frames are discussed in this chapter.

4.1 Element shape

The beam elements within a reciprocal structure serve as the fundamental load-bearing components that transfer the forces through the system. Optimizing their morphology involves refining their shape to maximize their capacity while minimizing material usage.

As mentioned before, the beam elements have the function to support other beams along the span and be supported at the ends. The required support (end) conditions of the beam play an important role in the design of the members. The following conditions apply at both ends where the beam is supported:

- **Lateral and Vertical Support**: Displacement in both lateral directions and in the vertical direction must be prevented.
- **Torsional support:** Providing stability against rotation around the local beam axis.

An additional requirement from the aspect of sustainability is the minimization of non-sustainable material. Therefore layouts that use non-timber materials in the connections are filtered out.

The support conditions and sustainability requirements result in four possible designs as visualized in Figure 37. Each design incorporates what can be termed as 'consoles' at the beam ends where the beam is supported by another beam (a cross-section of these supporting beams is visible in the figure). Design 1 and 2, in contrast to designs 3 and 4, situate the console along the upper edge of the beam. The difference between design 3 and design 4 is found in the way the eccentricity is managed within the beam. In design 3, the gaps for the supported beams are placed centrically, and the consoles at the beam ends are placed eccentrically. Conversely, design 4 flips this arrangement, with eccentrically placed gaps and centrally positioned consoles.

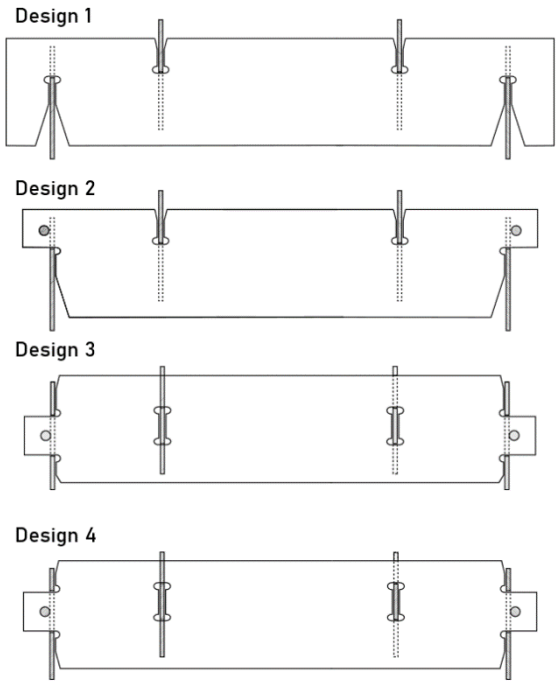


Figure 37: Beam morphology design options

Designs 3 and 4 have vertical support considerations achieved by material placed both above and below the gaps. In design 1 and 2, these conditions do not apply. Therefore, a connector needs to be added to disable upward movement of the supported beams.

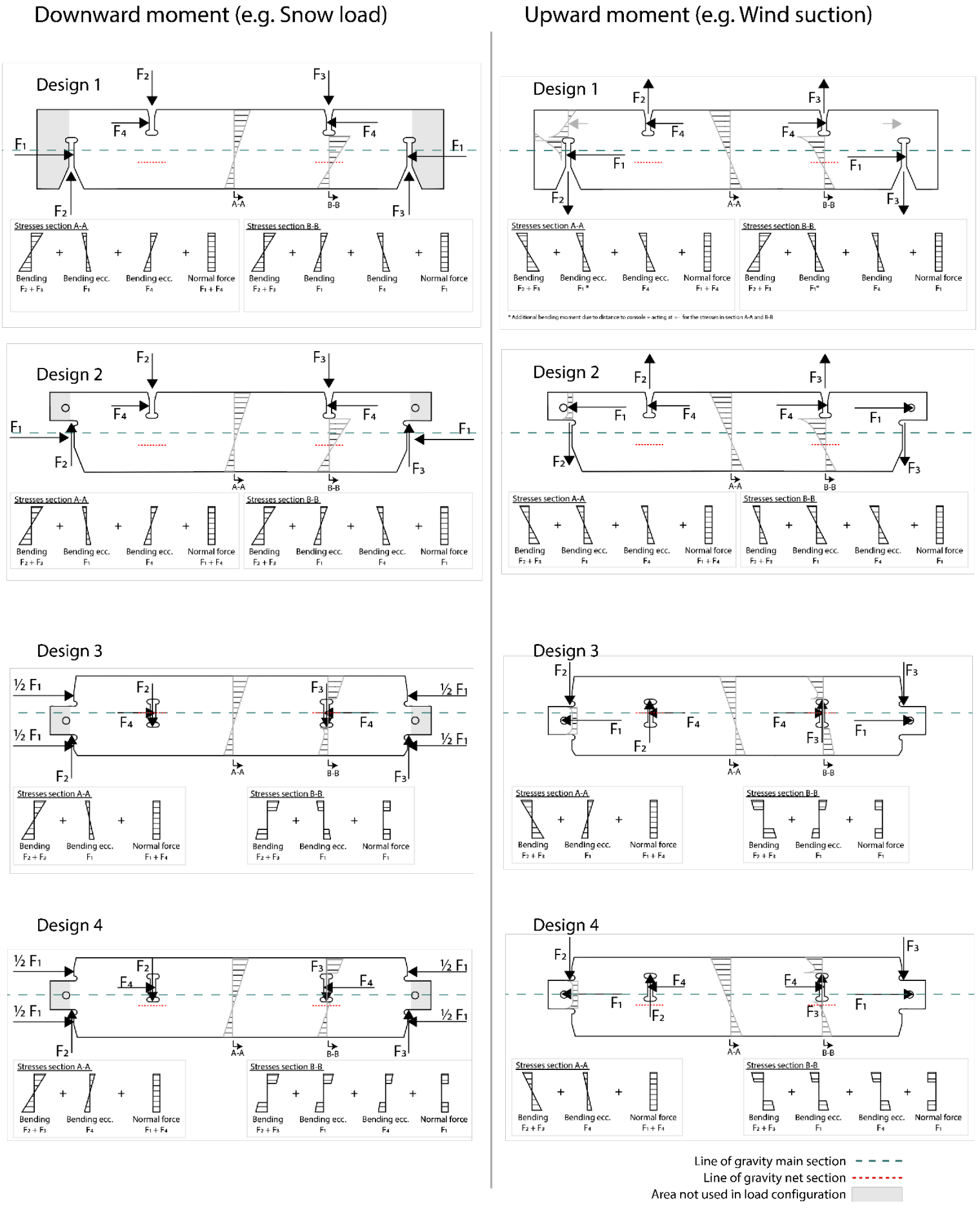


Figure 39: Load positions used to determine dimensions per design. Left column: downward moment. Right column: upward moment

For the beam to transfer tension loads from and to the adjacent members, the support beam needs to be laterally supported from both sides. For design 1 this is achieved by extending the beam beyond the support beam so the tension force can be transferred using contact between the elements. The forces are transferred to the element by tension and bending through the console.

For design 2, 3 and 4, a timber dowel is used to transfer tensile forces through the console. The forces in the console are purely tensile forces, there is no considerable bending in the console.

To compare the design variants, firstly the internal and external forces as schematized in Figure 39 are examined and compared. Note that the stress concentrations in compressive areas are deliberately left out in the figure since they can be disregarded according to the Eurocode (38).

Comparison of internal forces

For design 1, in the case of compression and downward bending, no stress concentrations in tension can be found. The compressive forces F_1 and F_4 work on opposing sides of the line of gravity. In some cases this may result in the forces canceling each other out. However, due to the fact that these loads are positioned relatively far from the line of gravity, this may result in a relatively large additional bending moment due to F_4.

In the case of tension and upward bending in design, large stress concentrations in tension arise. Firstly, at the positions of the gaps, there are stress concentrations at the places where the stresses are largest (in the outer fibers of the section). Additionally, there are stress concentrations due to bending in the consoles. This may result in rather large consoles compared to other design variants.

For design 2, the internal forces are similar compared to design 1. The difference between the designs is the fact that there is no stress concentration due to bending in the console. There is only a stress concentration due to tension in the console. This results in a lower (i.e. smaller) console in most cases compared to design 1. Design 2 offers another issue, when loaded in tension. The beam exerts the tension force with large eccentricity on adjacent members, causing potential instability of the members and disadvantageous internal forces.

Design 3 positions the holes for the supported beams in more advantageous positions, where the internal stresses are lowest; in the middle of the beam. A downside to this design choice is the fact that there is a stress concentration in tension in both load cases with positive and negative bending. These stress concentrations are however less extreme compared to designs 1 and 2. The only additional bending moment in the member is caused by the eccentricity of the member, which is insurmountable. Similar stress concentrations at the consoles also take place in this design.

Design 4 tries to tackle the problem of the stress concentration in the case of

downward bending by placing the holes a bit higher and the consoles along the neutral axis of the beam. This solution however introduces additional bending moment due to F_4 in the reduced section. Additionally, in the case of negative bending and tension, the stress concentrations are larger compared to design 3.

When comparing the internal forces, design 3 is the obvious most advantageous design. The stress concentrations are on the most advantageous positions. And the least additional bending moment due to compressive or tension forces are introduced in the member.

Comparing required ULS sizes

To validate the conclusion drawn by looking at the internal forces, the minimum required sizes for ULS are compared.

To make a realistic comparison, a 6x6m reciprocal structure with a central height of 3m is used. The load conditions of the structure are according to Eurocode regulations, where the structure is placed in Dutch wind area II, in an unbuilt area. The structure is of consequence class 2.

To make a comparison for the all-round behaviour of the structural elements, three locations within the same structure are compared (indicated with the black line in the circle in Figure 41):

1. Extreme bending in M_{zz} direction: most extreme under accumulated snow load
2. Extreme bending in M_{yy} direction: most extreme under distributed snow load
3. Extreme compression N: most extreme under distributed snow loads

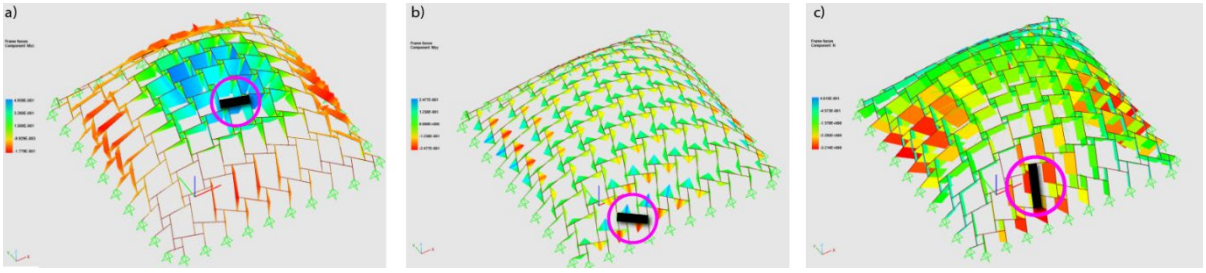


Figure 41: Beam locations for design comparison. a) Heavily loaded in M_{zz} (load displayed is accumulated snow load) b) Heavily loaded in M_{yy} (load displayed is distributed snow load) c) Heavily loaded in N (load displayed is distributed snow load)

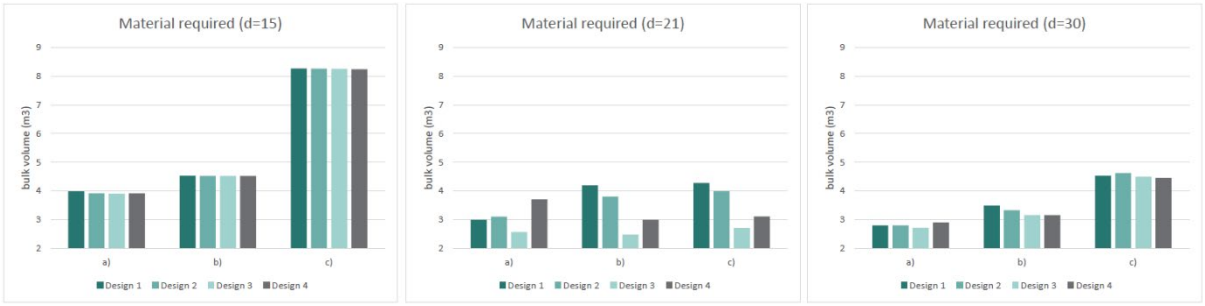


Figure 40: Bulk material volume required for each design variants for each of the locations. Left to right: plate thickness 10mm, 21mm and 30mm

The result of the comparison is displayed in Figure 40, where the optimal layouts are compared for different beam thicknesses. For each layout, the console heights, beam height, corner radii and gap heights are optimized to create the smallest overall section.

Peterson's stress concentration factors are used for the estimation of the stress concentrations (48). These stress concentrations are based on experiments with steel, so the real stress concentrations may be different. However, the stress concentrations determined by Peterson give a good indication of the stress concentrations for a comparison in the preliminary design phase.

For beams with a thickness of 10mm, the size of the beam is governed by (lateral torsional) buckling. Therefore, there are no large differences in material required for each of the designs. However, the results of design 1 and 2 are slightly higher due to the fact that forces F_4 have a large eccentricity, introducing a large bending moment due to compression.

For beams with a thickness of 21mm, the optimal beam sizes variate much more. The reason for this is the fact that the designs are governed by stress concentration in the net section for design 1 and 2, and stresses (non-concentrated) in de net section for design 3 and 4.

For beams with a thickness of 30mm, a combination of governing in the net section and stability occurs. Therefore, the results are a mix between LC1 and LC2. For designs 1 and 2, a thicker beam seems to be more optimal. For the other designs, the volume required is actually increased.

Overall, the consoles are always larger for design 1, which automatically results in a larger beam height and larger gaps in the beams. The reason for the larger console height is depicted in Figure 42. Due to tension force F_t acting eccentrically to the console, bending occurs in both parts of the console. Additionally, tension takes place at the corner radius, resulting in stress concentration.

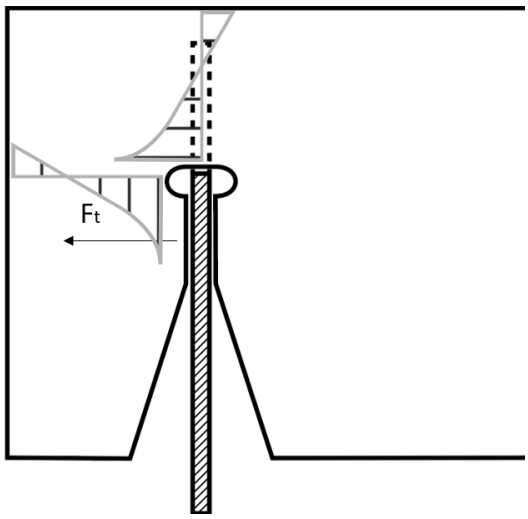


Figure 42: Stress concentration and bending in console of design 1

Design 4 is slightly worse compared to design 3 due to upward bending moment being governing.

To conclude, design 3 is most optimal in almost all load cases and beam thicknesses. There are some exceptions, where for instance combined bending and stability are governing. However, in those cases design 3 is only slightly worse. Therefore, design 3 is picked as final beam design in the reciprocal frame design tool.

4.2 Connection behaviour

A crucial aspect in accurately modeling the reciprocal structure involves specifying the nature of the connection between the beam elements. The structure is stable when all connections are considered as pure hinges. However, the actual design of these connections may lead to a more rigid behavior. This rigidity may lead to a decrease in the bending moment midspan of the beams while introducing a bending moment in the connections.

An important assumption in traditional structural analysis is that joints are treated as either perfectly rigid or perfectly hinged. Consequently, when assessing a structure, joints are typically simplified as being either fully fixed or fully hinged. In reality, structural connections rarely exhibit either perfect rigid or perfect hinge conditions (49).

To determine the actual connection behaviour, the connection stiffness will be evaluated through Finite Element Method (FEM) modeling in Ansys. Since the connection is entirely parametric, it is necessary to examine all potential connection configurations. This assessment will focus on the connection's response to bending in both of the primary directions.

Theoretical background

A rigid joint is defined in basic structural analysis as a joint in which the structural members in the joint do not change orientation with respect to each other. For pinned joints, no moment is transferred through the connection. As a result, the connected structural members are free to rotate with respect to each other. A semi-rigid joint has a behaviour between these two extremes, where there is a transfer of moment in combination with member rotation and thus limited joint rotation. The deformed shape and bending moment in a beam is affected by the rigidity of the connection, as visualized in Figure 43 Click or tap here to enter text.(50).

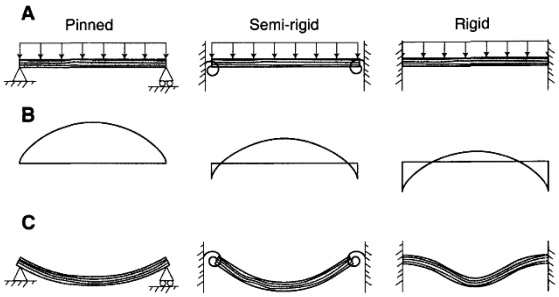


Figure 43: Diagrams of beams having pinned, semi-rigid, and rigid end fixity: (A) loading, (B) qualitative bending shape (50)

McGuire examined the issue of semi-rigid connections in dynamically loaded beams of an unspecified material (49). He developed a function for joint stiffness in relation to the normalized minimum natural frequency (Figure 44). The joint stiffness a_{ij} is defined as:

$$a_{ij} = \frac{kL}{E_b I_b}$$

Where:

- k = rotational connection stiffness
- L = beam length
- E_b = beam modulus of elasticity
- I_b = beam second moment of area

McGuire demonstrated that when $a_{ij} < 1$, pinned behaviour can be assumed because the deformed shape is similar to that of a pinned connection. Additionally, he identified rigid behaviour when $a_{ij} > 100$.

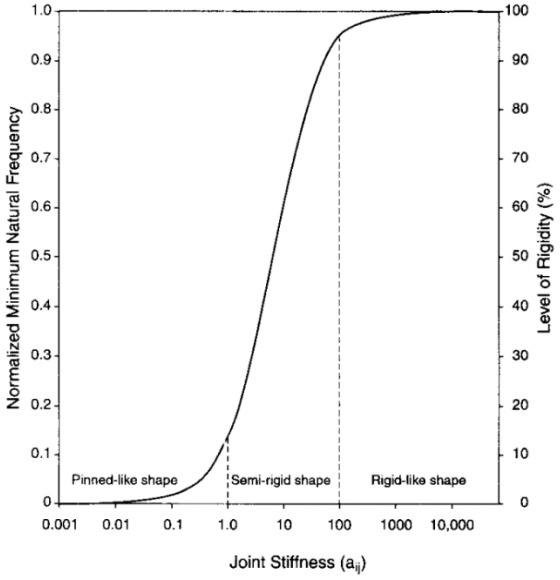


Figure 44: The continuum of joint stiffness versus normalized minimum natural frequency (50)

The Eurocode for timber provides little information about the limits of pinned or rigid connections. The only information written about the rigidity of the connections is written in NEN-EN 1995-1-1 5.4.2 (7): "*Connections may be assumed to be rotationally stiff, if their deformation has no significant effect upon the distribution of member forces and moments. Otherwise, connections may be generally assumed to be rotationally pinned.*"

Research on fixed timber joints has shown that full rigid behaviour of timber connections may be neither possible nor desirable in timber structures (50). Therefore, it may be preferable to be able to consider the connections as pure hinges.

Method

The inter-member joints are designed as visualized in Figure 45, allowing for variations in the heights of the beams and the tenon. Furthermore, the dowel's size may vary. The joint stiffness for the entire range of design possibilities will be examined, considering the following design variables (with their respective variable ranges):

- Dowel size *5 – 20 mm*
- Beam height *88 – 400 mm*
- Beam thickness *10 – 50 mm*
- Eccentricity *0 – 50 mm*

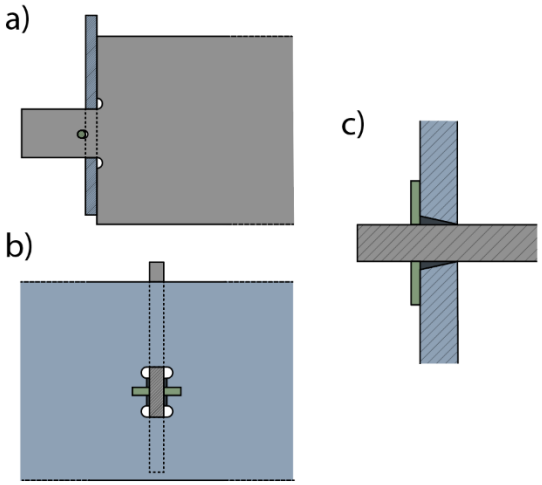


Figure 45: Connection details, where blue = beam 1, grey = beam 2 and green = dowel. a) side view, b) front view and c) top view

To determine the joint behaviour, a FEM model in Ansys is used. The plywood is modelled as a linear elastic orthotropic material. The linear elastic, and yield properties are listed in Table 2. These properties are determined from a research on plywood connections by Wieringa et al. (51). The yield properties are determined from research on the in plane mechanical properties of plywood (52).

Within the FEM model, no post-yielding capacity is taken into account, where the post-yielding tangent modulus is set to 0 MPa. The simplified stress-strain relationship employed in the FEM model is illustrated in Figure 46. The actual behavior, derived from tension and compression tests (52) is plotted in black. As can be observed, the FEM

model slightly underestimates the compressive capacity, particularly in the context of strain hardening for plywood.

Table 2: Linear elastic and yield properties of spruce plywood (51,52)

Linear elastic properties of spruce plywood			
Density	ρ	460	kg/m^3
Young's modulus	E_1	6682	N/mm^2
	E_2	5318	N/mm^2
	E_3	1921	N/mm^2
Shear modulus	G_{12}	350	N/mm^2
	G_{13}	52	N/mm^2
	G_{23}	38	N/mm^2
Poisson's ratio	υ_{12}	0.04	-
	υ_{23}	0.191	-
	υ_{13}	0.248	-
Yield properties of spruce plywood			
Normal yielding	$\sigma_{yd,c,x}$	30	N/mm^2
	$\sigma_{yd,c,y}$	18	N/mm^2
	$\sigma_{yd,c,z}$	24	N/mm^2
Shear yielding	$\tau_{yd,xy}$	12	N/mm^2
	$\tau_{yd,yz}$	8	N/mm^2
	$\tau_{yd,xz}$	12	N/mm^2

The yield criterion used in the FEM model is the Hill yield criterion. The Hill yield criterion closely aligns with the actual yield behaviour but it may slightly overestimate the materials capacity (52).

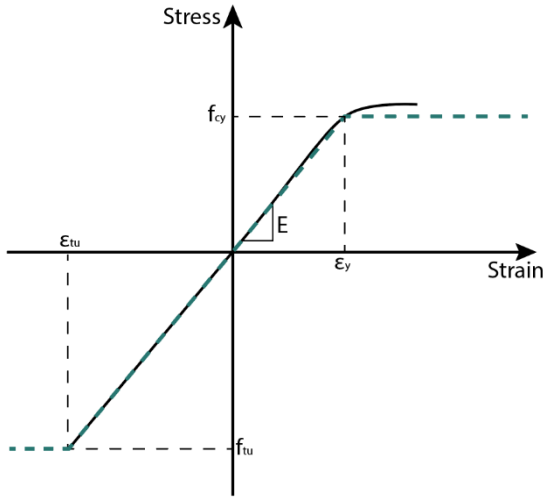


Figure 46: schematization of stress strain behaviour used in the FEM model (green) and the stress strain behaviour from tests (black)(52).

The connection is represented in the model as three distinct volumes, encompassing both beams and the dowel (as illustrated in Figure 48). The interaction between these volumes is established using the Normal Lagrange contact formulation, which is chosen for its minimal penetration tolerance, making it the most realistic option. Both beams adhere to the material properties specified in Table 2, while the dowel is characterized by standard sawn wood (C22) properties, including the corresponding yield behavior.

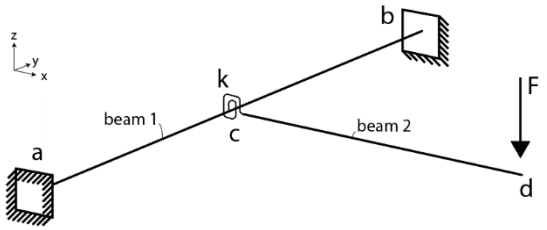


Figure 47: Structural scheme used to determine joint stiffness (for weak direction force F acts in positive y-direction)

To attain the pure joint stiffness behavior, it is necessary to establish the moment-rotation characteristics. This is achieved by employing the structural configuration depicted in Figure 47.

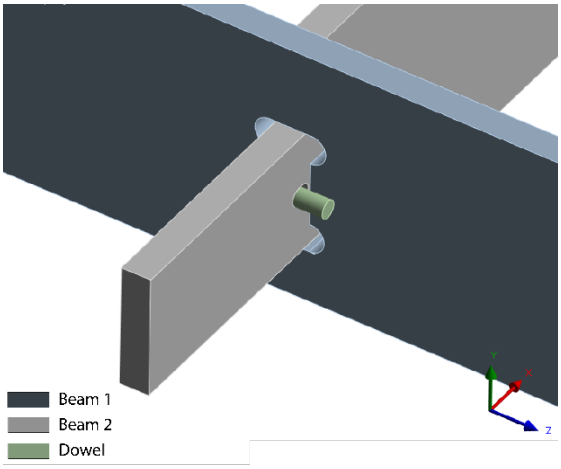


Figure 48: Connection detail volumes

The displacement in node d can be decomposed in the following components for the strong direction (F in negative z-direction):

- Rotation of beam 1
- Bending of beam 2
- Rotation in joint c

For the weak direction (F in positive y-direction) the following components are part of the displacement in d:

- Bending of beam1
- Bending of beam 2
- Rotation in joint c

To isolate only the displacement attributed to the joint, the deformation when $k = \infty$ needs to be subtracted from the total deformation.

Design choices

Before conducting an investigation across the entire design spectrum, a connection of typical size is used to assess whether the connection behaves as anticipated. This phase also serves as an opportunity to make initial design decisions. In this particular connection, both beams have a height of 200mm and a thickness of 20mm. The eccentricity between the beams is 10mm. Additionally, the dowel has a diameter of 10mm, and the tenon has a height of 70mm.

Bending in the strong direction behaves as expected but with a lower stiffness than expected resulting in hinged behaviour. In the weak direction, the connection with the originally designed connection behaves relatively stiff, resulting in semi rigid behaviour, therefore some changes have been made to enable less rotational resistance in the weak direction.

Bending in the weak direction

When subjected to bending in the weak direction (around the y-axis in Figure 48), when the gap surrounds the tenon snugly, the connection will initiate yielding in tension within the beam along the red line in Figure 49.

To ensure that the connection does not fail due to rotation, it is important to obtain the rotational capacity of the joint primarily from dowel bearing/yielding, rather than relying on beam yielding. Moreover, dowel bearing exhibits yielding behavior in compression, which is far less brittle compared to yielding in tension.

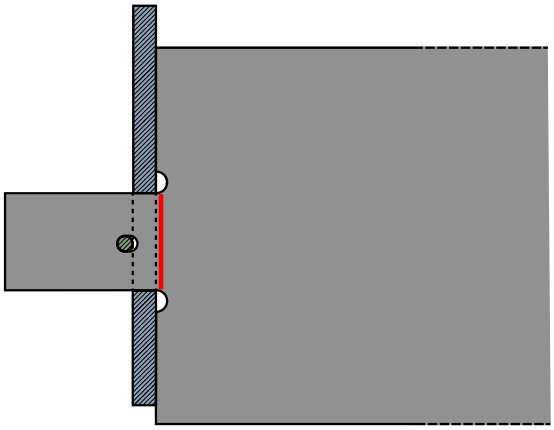


Figure 49: Yield location with hole connecting snugly

In order to generate the necessary rotational capacity, a slight chamfer will be introduced to the gap as shown in Figure 45c. Following this design alteration, yielding in tension within the beam will only occur at extremely large rotations, well beyond what can be expected in the case of simply supported beams.

In the case of bending in the weak direction of the beam, the ideal behavior would be pinned. Without yielding, for a length of 1m, the joint stiffness a_{ij} is approximately 3. However, in a dowel connection, yielding of the material around the dowel (bearing) occurs almost

immediately. In Figure 50, the moment rotation with yielding is plotted. In the linear part of the diagram, the connection with yielding is already more flexible, showing pinned behaviour ($a_{ij} < 1$) for lengths up to 2m. When the beams start yielding, softening behaviour takes place.

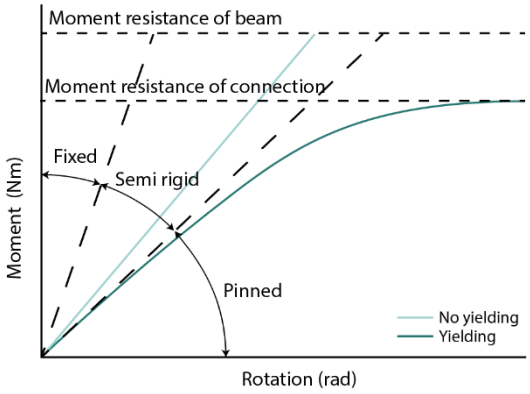


Figure 50: Moment-rotation diagram for typically sized beam-beam joint, comparing the result with and without yielding

Finally, with a perfectly circular hole, with a diameter equal to the dowel diameter, the moment rotation diagram does not show perfect linear behaviour in the early phase. The reason for this is the fact that bearing on both sides of the holes needs to take place. After one side has yielded, the rotational stiffness is decreased because in that case only one side needs further yielding for rotation.

To prevent this non-linear behaviour, a slotted hole is used. The slotted hole enables rotation capacity with bearing on only one side (see Figure 51). This creates a larger stress concentration on one side and thus faster yielding. The difference in moment-rotation behaviour is visualized in Figure 52a, where the connection with the slotted hole shows perfect linear behaviour in the initial part of the diagram. In Figure 52b, the effect of the slotted hole is shown in comparison to the circular hole. The joint stiffness exhibits a peak in the early part of the diagram, in this case resulting in non-pure pinned behaviour ($a_{ij} > 1.0$). The slotted hole slightly decreases the moment capacity of the connection, but also decreases the rotational stiffness for small bending moments.

When calculating the joint stiffness, only the first linear part of the connection is used. Therefore, the connection with the slotted hole has a much lower rotational stiffness. After full yielding, the connection behaves less stiff and ultimately has zero rotational stiffness. This, however, only occurs for large rotations

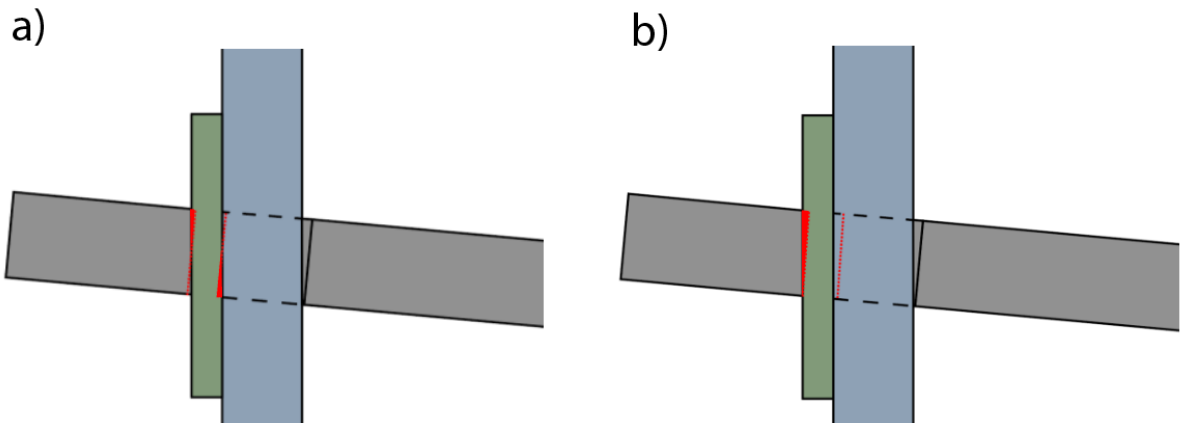


Figure 51: Bearing of dowel with a) circular hole or b) slotted hole

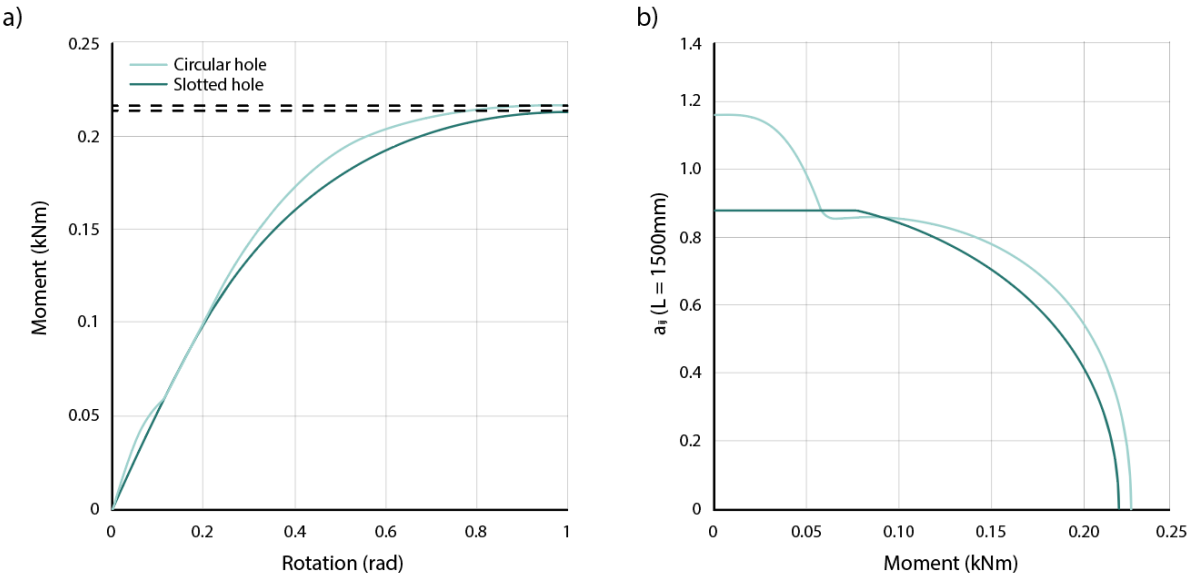


Figure 52: a) Moment-rotation diagram for the connection with a circular hole vs a slotted hole. b) a_{ij} for different moments for a circular hole vs a slotted hole

Weak direction behaviour

The joint stiffness in the weak direction of the beams are displayed for different parameters in Figure 53. In the figure, a_{ij} is shown for beams with a length of one meter.

The impact of the beam thickness on the joint stiffness is displayed in Figure 53a. A linear relationship between the upper and lower bounds is evident. For thinner elements, the joint stiffness may exceed 1. These values above 1 occur when the beam height is relatively low compared to the tenon.

The influence of dowel diameter is shown in Figure 53b. Here, a linear relationship is observed, where thicker dowels lead to higher joint stiffness. When very thick dowels are used, the joint may become excessively stiff, particularly with long beams. This behaviour is attributed to the fact that thicker dowels result in greater bearing stiffness.

The influence of the ratio of the tenon height and beam height are shown in Figure 53c. When the tenon is high with respect to the beam, the joint becomes more stiff.

The influence of eccentricity is demonstrated in Figure 53d. It appears that eccentricity does not significantly affect joint stiffness. The joint stiffness is slightly lower with larger eccentricities because for significant eccentricities, the tenon is automatically smaller compared to the beam height.

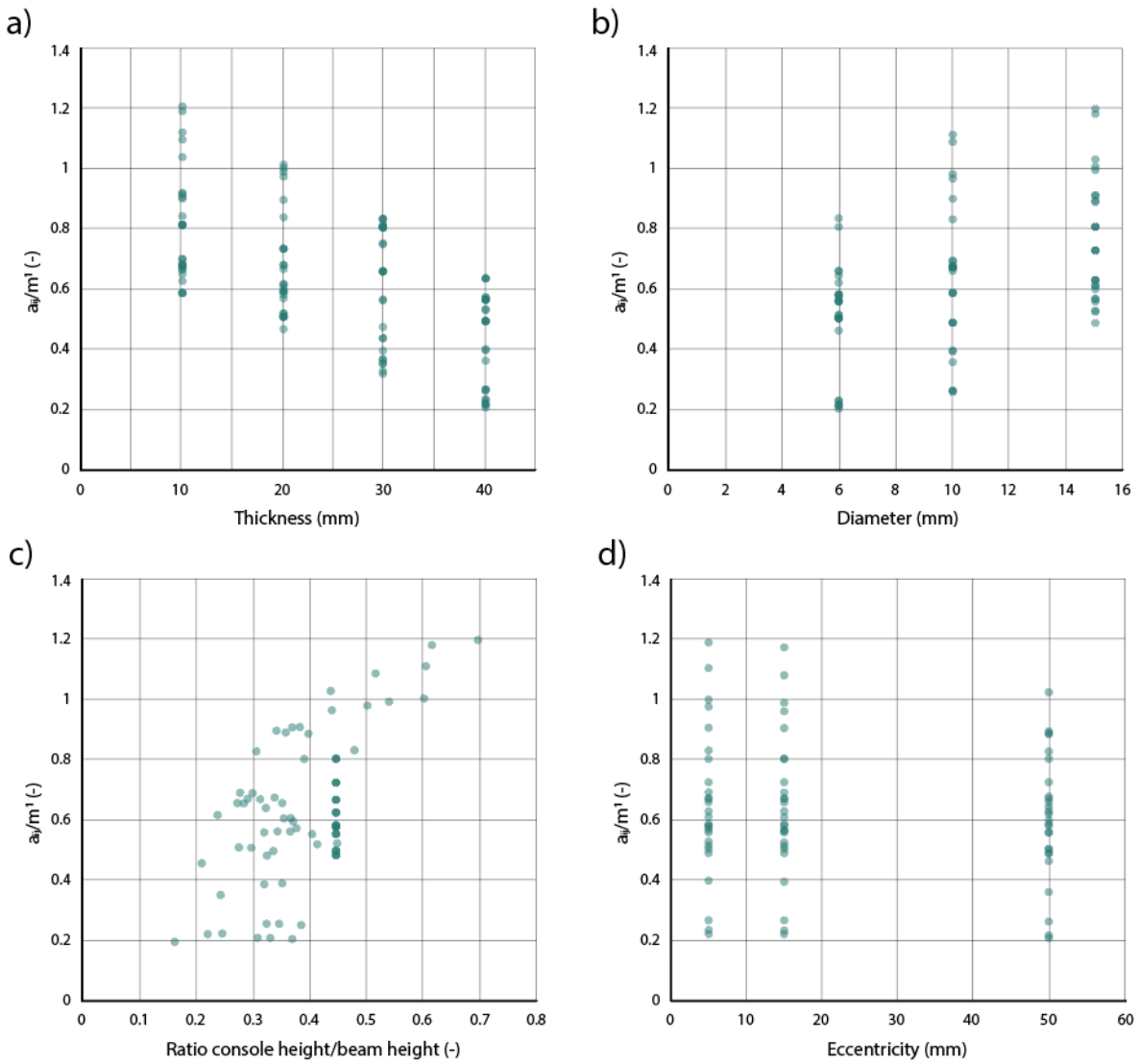


Figure 53: a_{ij}/m^1 in the weak bending direction, for a) different plate thicknesses, b) Different dowel diameters, c) ratio between the console height and beam height or d) different eccentricities. Derived from Ansys models.

Strong direction behaviour

The joint stiffness in the strong direction of the beams are displayed for different parameters in Figure 54. In the figure, a_{ij} is shown for beams with a length of one meter. In Figure 54a, the influence of the beam thickness is shown. The maximum value of the joint stiffness decreases for thicker beams.

The influence of the dowel thickness is shown in Figure 54b, where no clear relationship is visible. The bearing of the dowel is thus not the governing parameter for bending in the strong direction.

The influence of the beam height is shown in Figure 54c. The relationship between joint stiffness and beam height seems to be quadratic or linear. This can be explained by the fact that the beam height has a cubic relationship with the second moment of area of the beam, and the rotational stiffness k of the joint increases linearly for an increasing beam height.

For bending in the strong direction, the eccentricity between the beams has a large influence, as visible in Figure 54d. For a large eccentricity, the arm between the compression area and the

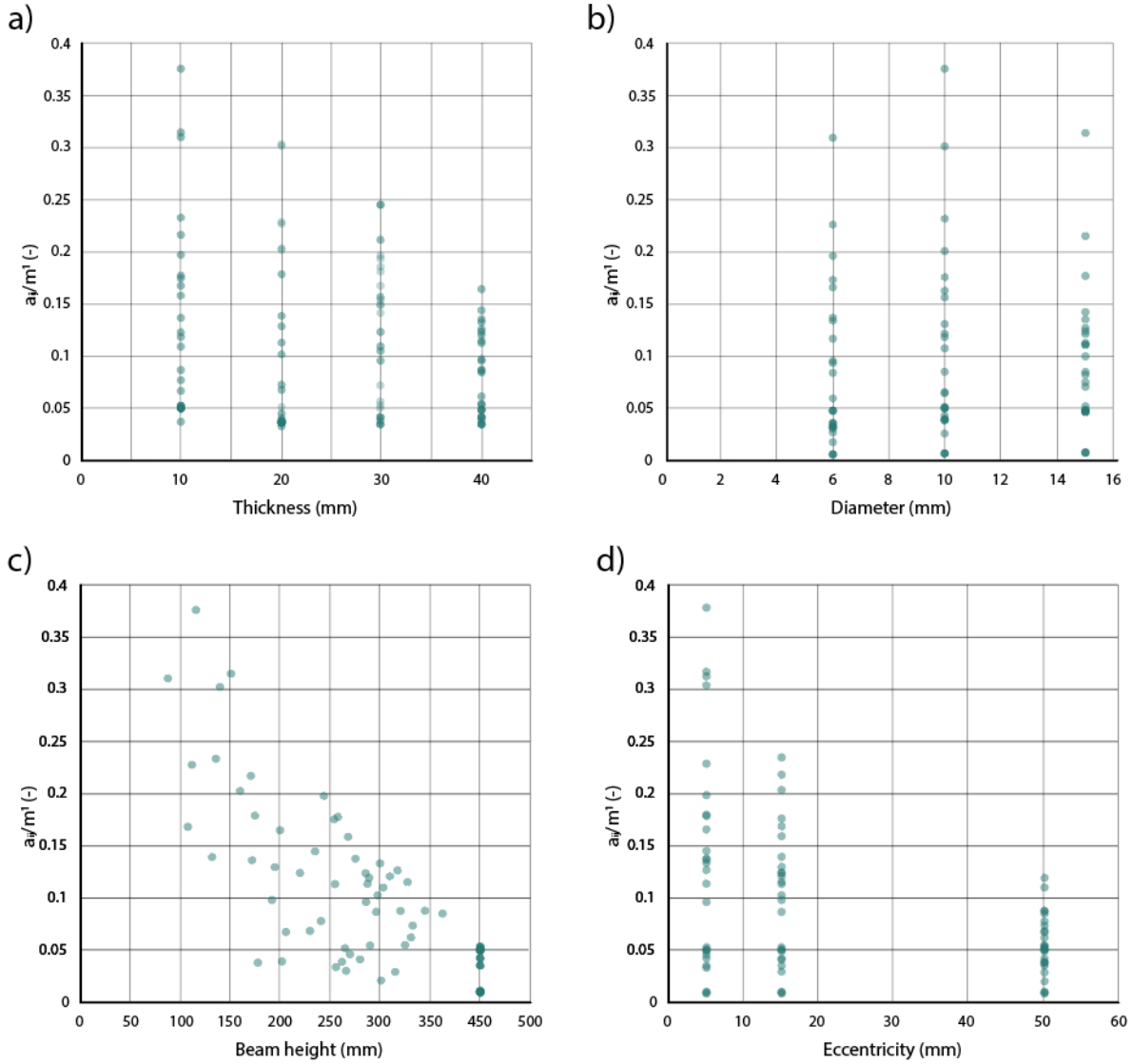


Figure 54: a_{ij}/m^1 in the strong bending direction for a) different plate thicknesses, b) different dowel diameters, c) beam height beam or d) different eccentricities. Derived from Ansys models.

dowel decreases with respect to the beam height. This results in a lower joint stiffness for large eccentricities. Note that these results are only taken for downward bending. For upward bending, an increased eccentricity is likely to result in a lower joint stiffness as well, since the upper part of the beam does not connect to the adjacent beam.

Risk analysis

In both directions, one could say it is reasonable to assume hinged behaviour between the elements. However, it might be important to check the risks of neglecting a connection stiffness.

To perform this risk analysis, the internal forces are compared for the same structure with all connections being hinged or all connections being rotationally fixed. Multiple squared-based reciprocal frames are considered, with different sizes (between 8x8m and 2x2m) and eccentricities (and thus curvature). A squared pattern layout and constant scale factor of 50% (for the center-to-center) method is used in this risk analysis.

Weak bending direction

The qualitative bending moment diagrams for bending in the weak direction (bending in the thin direction of the beam), are visualized in Figure 55. When hinged connections are assumed, there is no bending moment at the beam end ($M_{y,end}$). When the connections are fixed, there obviously are bending moments at the ends of the beam.

In the detailed design of the connection, measures have been taken to create sufficient rotation capacity. This means that even if the connection transfers a moment at the beam ends, the connection will never fail due to bending. This rotation capacity is created by bearing of the material surrounding the dowel. In the checks of the dowel the bearing width must be conservatively reduced.

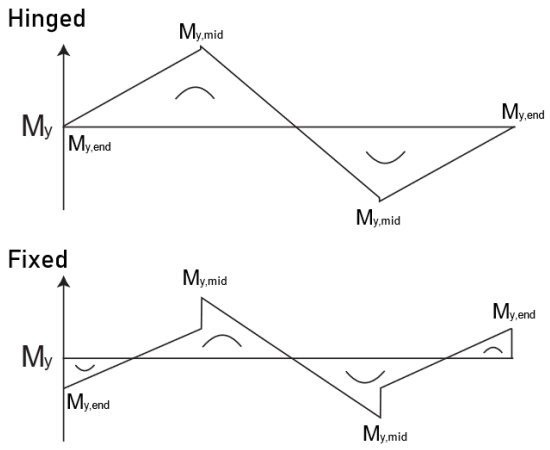


Figure 55: Moment diagrams in the weak bending direction compared for hinged or fixed end connections

The moments in the middle of the beam ($M_{y,mid}$) are also different when the end connections are moment fixed. Normally, it would be expected that the moments are lower when the ends are fixed. There however also is a jump in the bending moment caused by the moment transferred by the supported beam. This may cause $M_{y,mid}$ to be higher when the end connections are fixed.

To compare the values for $M_{y,mid}$ for different reciprocal frame sizes and eccentricities, the values are plotted in Figure 56. The hatched area is the range of the ratio between the moment when the connections are fixed or hinged. When this ratio is lower than 1.0, the value of the bending moment $M_{y,mid}$ is conservative when the connections are considered hinged. If not, $M_{y,mid}$ may be underestimated. It can thus be concluded that in some cases the bending moment is underestimated. This underestimation is however relatively small and within the limits for safe design.

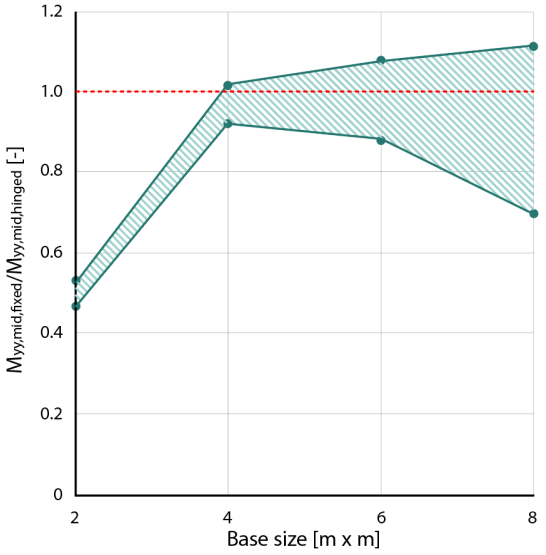


Figure 56: Ratio of bending moment in the middle of the beam in y-direction ($M_{y,mid}$) fixed/hinged.

Bending in strong direction

The joint stiffness in the strong bending direction is below 1 in most cases. However, it needs to be checked whether the structure is still safe when

the connection has some rotational stiffness in the strong direction.

The qualitative bending moment diagrams for bending in the strong direction are visualized in Figure 57. When hinged connections are assumed, the bending moment at the beam ends is underestimated. Additionally, the sign of the bending moment may be different.

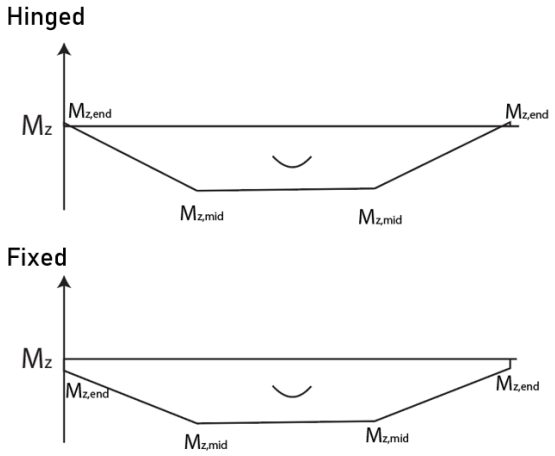


Figure 57: Moment diagrams in the strong bending direction compared for hinged or fixed end connections

The bending moments at the beam ends are quantitively compared in Figure 58 for a) small eccentricities and b) large eccentricities. In both cases, the bending moment at the beam ends are always larger when the connections are fixed. This means that the assumption of hinged connections is not always conservative.

To make a conservative assumption in the connection calculations, 5% of the bending moment in the middle of the beam ($M_{z,mid}$) is added to $M_{z,end}$. This assumption is also plotted in Figure 58. As you can see, this assumption is conservative in most cases. Only if the frames are very large with large eccentricities, the assumption may not be conservative. Those cases however do not occur in feasible reciprocal frame designs.

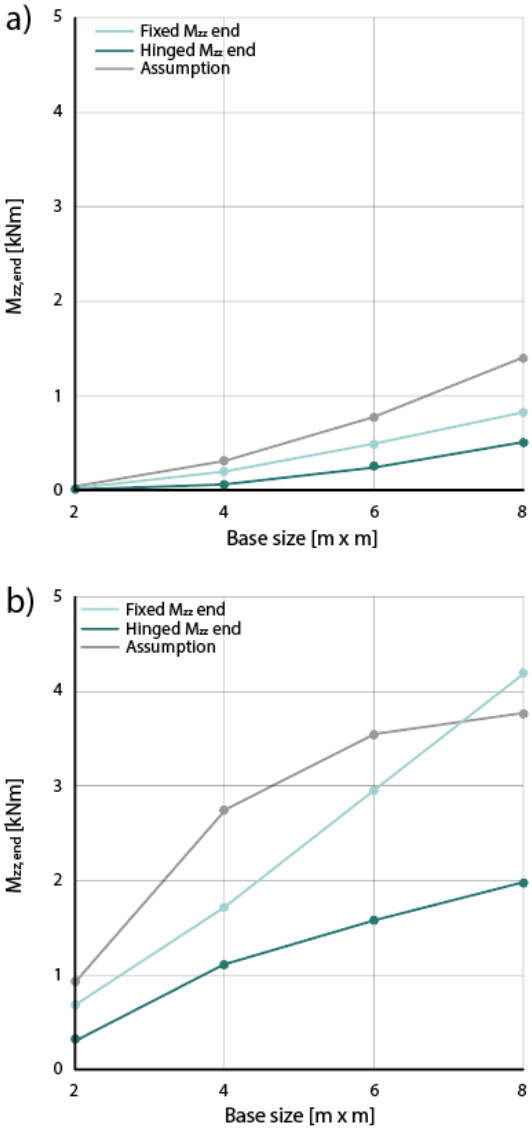


Figure 58: Bending moment at the ends of the beams with fixed connections and hinged connections. For a) 10mm b) 50mm eccentricity frames.

Similarly, the bending moments are quantitively compared at the middle of the beams in Figure 59. As visualized in the figure, the bending moments in the middle are always higher when the connections are assumed to be hinged. This means that the assumption is conservative in that case.

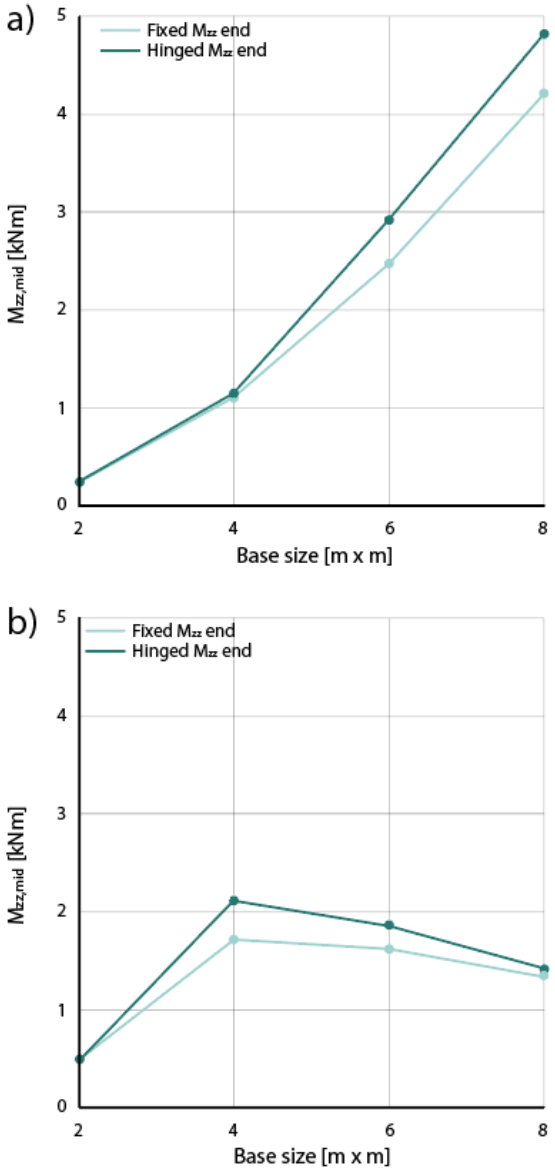


Figure 59: Bending moment at the middle of the beams with fixed connections and hinged connections. For a) 10mm b) 50mm eccentricity frames.

Conclusion

In both directions, the joint stiffness is low enough to assume pinned behaviour. For bending in the weak direction, some joint stiffness values may exceed 1. However, this is only the case for beams with small dimensions, which are not expected to have lengths exceeding 1m. Furthermore, high stiffness is observed when the dowel diameter is large, which is not typical in regular applications of reciprocal structures. For reciprocal structures with large beam elements, joint stiffness in the weak direction is a factor that may need to be considered.

In the strong direction of the beam, the joint stiffness values are lower compared to bending in the weak direction. All joint stiffness values are below 0.4, implying that beam elements with a length of 2m can also be considered hinged. Therefore, the connection can consistently be viewed as hinged.

From a risk analysis it can be concluded that assuming the connections to be pinned results in safe assumptions. However, some small precautions have to be taken in the structural calculations of the connections between the beam elements.

To ensure that the dowel has sufficient capacity after yielding in the weak direction, it is conservatively assumed that the bearing thickness is 30% of the actual thickness to disregard the yielded area. Additionally, the connection should be able to transfer 5% of the maximum bending moment in the strong direction to ensure there is sufficient capacity in the dowel.

4.3 Cladding

Once the design of the elements and the structural behaviour of the connections are known, the way the forces are placed on the structure must be established. This is significantly influenced by the cladding of the structure. Therefore, a cladding design must be determined before making the reciprocal frame designer.

As mentioned in the literary review, there are several way to weatherproof a timber reciprocal frame structure. For temporary structures, it is acceptable to apply the cladding on the interior since the deterioration of the timber is not a normative factor. However, for permanent structures, it is important that the structure is protected from the exterior. Therefore, the structure must be clad on the exterior.

Due to the nature of this research – optimization of the structure with multiple variables – it is not realistic to assume a prefabricated cladding. Therefore, a concept like the timber sheathing in the 'Frans Masereel' centre must be applied, but instead with a transparent material to allow visibility of the structure from both the interior and the exterior.

For the purpose of the research, it is imperative that the cladding does not contribute to the load bearing of the reciprocal frame. Additionally, the loads must be applied at the nodes instead of line loads along the beam. To satisfy these requirements, several cladding concepts were considered.

Concepts

Initially, an idea for applying the cladding on the exterior without applying bending moments due to eccentricity is by applying a cladding that is able to transfer compression. In that case, the structure can be connected to the foundation by simple rods that are hinged on both sides (i.e. can handle only normal forces).

Figure 60 shows the implications of using such a design. Firstly, applying a cladding that can transfer normal forces means that the cladding will transfer a significant portion of the loads, especially when the curvature of the reciprocal frame is large. Secondly, if the reciprocal frame is significantly more flexible than the cladding, the applied forces on the frame become less predictable. In extreme cases, this can even result in tension being applied on the main load bearing structure under snow loading.

This behaviour can be explained by the deformed shape. When the supporting structure is very flexible (i.e. resulting in a low spring stiffness in the diagram), the cladding will deform as visualized in grey.

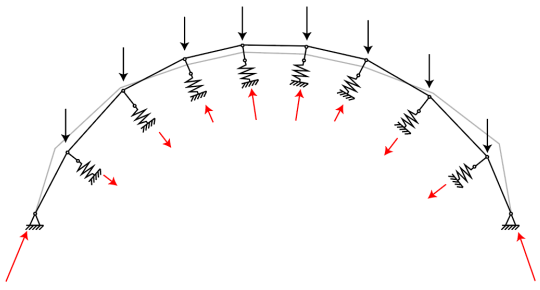


Figure 60: Diagram of the cladding a reciprocal frame that allows axial forces, supported by a flexible structure. Black: applied loads (snow), red: reaction forces.

To prevent this unpredictable behaviour, a cladding concept that does not rely on the normal force properties of the cladding must be designed. The structural behaviour in that case is visualized in Figure 61. To prevent normal forces to act in the cladding, slip must be allowed at the joints.

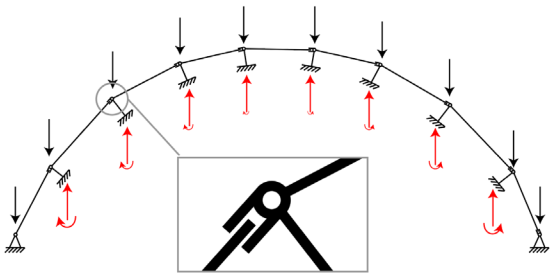


Figure 61: Diagram of the cladding a reciprocal frame with slip-joints, supported by the structure. Black: applied loads (snow), red: reaction forces.

The reaction forces of the cladding on the supporting structure in this case are much more predictable. In principle, the force acting on the cladding will be transferred through the bar to the structure. When the load is not parallel to the bar, an additional moment will be applied on the structure due to the eccentricity.

An example of a structure with a cladding that allows slip is the 'Dome of Visions' in Copenhagen, Denmark (Figure 62)(53). The dome is clad by polycarbonate sheets that are connected at several nodes by a fixed bar. In the connections between the polycarbonate sheets, small sliding is allowed. This ensures that no axial forces are generated in the cladding.



Figure 62: Cladding applied in the 'Dome of Visions' in Copenhagen, Denmark (53).

Assumed cladding design

The assumed cladding concept for the optimization in this thesis is based on the cladding that was applied in the 'Dome of Visions'. Due to fact that small sliding is allowed between the polycarbonate sheet, the structural behaviour is assumed to be like the scheme in Figure 61.

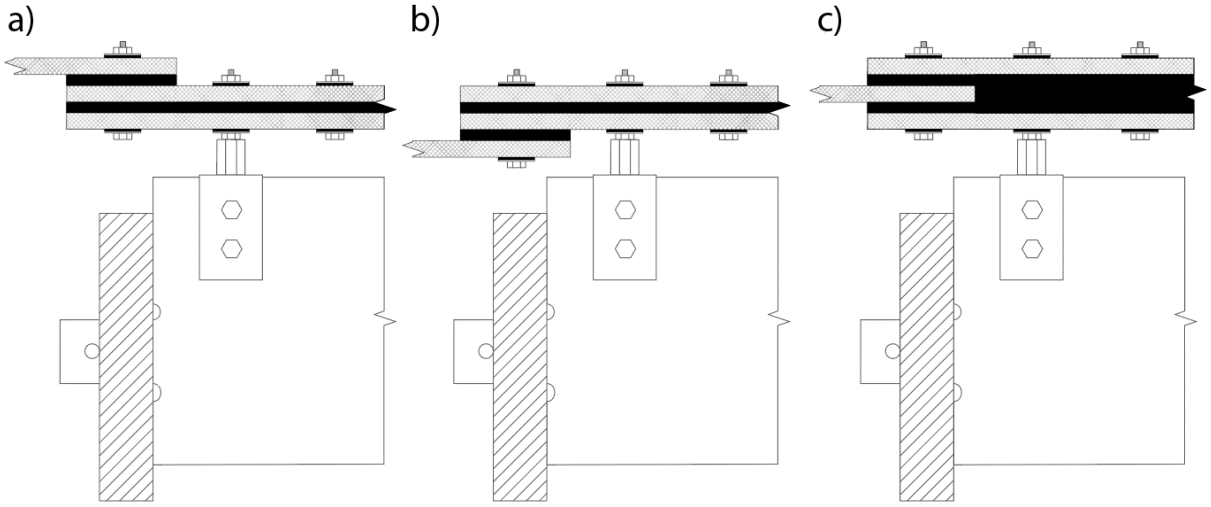


Figure 63: Cladding connection and layer detail at three different locations

Each connection between the beam elements of the reciprocal frame is also a nodal connection to the cladding. This connection is applied at the ends of the beam elements. Figure 63 shows the detail of how the cladding is connected to the beam elements as well as how the layers of polycarbonate are connected.

The cladding weatherproofed by clamping the layers of polycarbonate with a rubber-like material in between the layers. The layers overlap 50mm on all sides and the layers are clamped with rings and bolts.

Resulting from the layout of the reciprocal frame, there are three different layers of polycarbonate that connect at the nodes of the reciprocal frame. To connect the cladding at a practical location, a horizontal displacement of one bolt is applied to the connecting elements. This means that the frame is not connected where three sheets overlap (see Figure 63).

Since the bolts that connect the cladding to the structure must transfer bending moments, the bolt is strengthened by a bolt sleeve. This bolt sleeve is also used to keep the cladding at a prescribed distance from the structural elements. In this research, it is assumed that the cladding is placed at 20mm from the top side of each structural element, this allows the sheets to be slanted without touching the structural elements.

As mentioned previously, small sliding is allowed in the connections by making the holes in the polycarbonate and rubber oversized. This prevents normal forces to be transferred through the cladding.

Figure 64 shows a three-dimensional representation of the cladding. Here it is also visible that the connections to the reciprocal structure are displaced by one bolt from the locations where three sheets overlap. The connection is simply applied by lengthening the bolt and welding the bolt to a steel connector that is placed on the plywood.

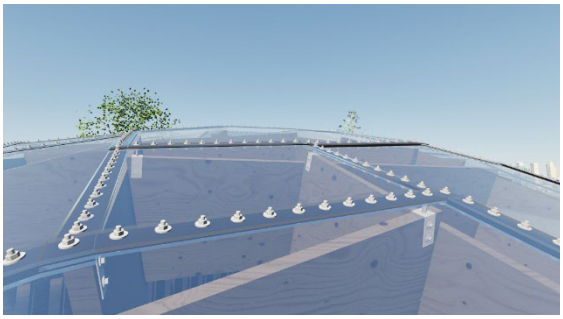


Figure 64: Closeup of connection to the reciprocal structure in context

This cladding can be applied at any reciprocal frame pattern, as long as the connections between the elements always consist of a maximum of two beams.

A full impression of the interior and exterior of a reciprocal frame with the applied cladding can be seen in Figure 65 and Figure 66.

Assumed structural behaviour

The connection to the cladding is designed in a way that the cladding does not transfer normal forces along the plane. Therefore, bending moments must be transferred through the connection.

The amount of bending moment that is transferred through the connection depends on the angle at which the force is applied. The horizontal component of

the force is used to calculate the moment that is applied at the node:

$$M_{ecc} = F_{hor} * a$$

Where the arm a is half of the beam height + 20mm that is used as a standard distance from the beams.

Additionally, the fact that the force is not applied directly on the node of the beams means that an additional shear force and a bending moment are generated in the beam. This structural behaviour is simulated by modelling the point loads at 25mm from the nodes in the FEM model.

The self-weight of the cladding is assumed to be 0.1 kN/m^2. This means that the polycarbonate sheets may be approximately 10mm thick, which is extremely conservative. The exact required polycarbonate thickness must be determined from an additional study. When the self-weight is favorable, the weight of the cladding is neglected.

For wind friction forces, the cladding is assumed to be 'rough' due to the overlapping of the polycarbonate layers and the exposed bolt ends. This means that the friction coefficient $c_{fr} = 0.02$ (54).

Other cladding designs

From an analysis in the early stages of the project, it may be concluded that applying the forces at the nodes is conservative compared to applying the forces as distributed along the beam. This means that generally other cladding designs may be applied to the structure without underestimating the forces in the structure.

Furthermore, other cladding types may add stability to the beams in the reciprocal frame, which reduces the buckling sensitivity.

Therefore, it can be concluded that the selected cladding design results in a rather conservative reciprocal frame.

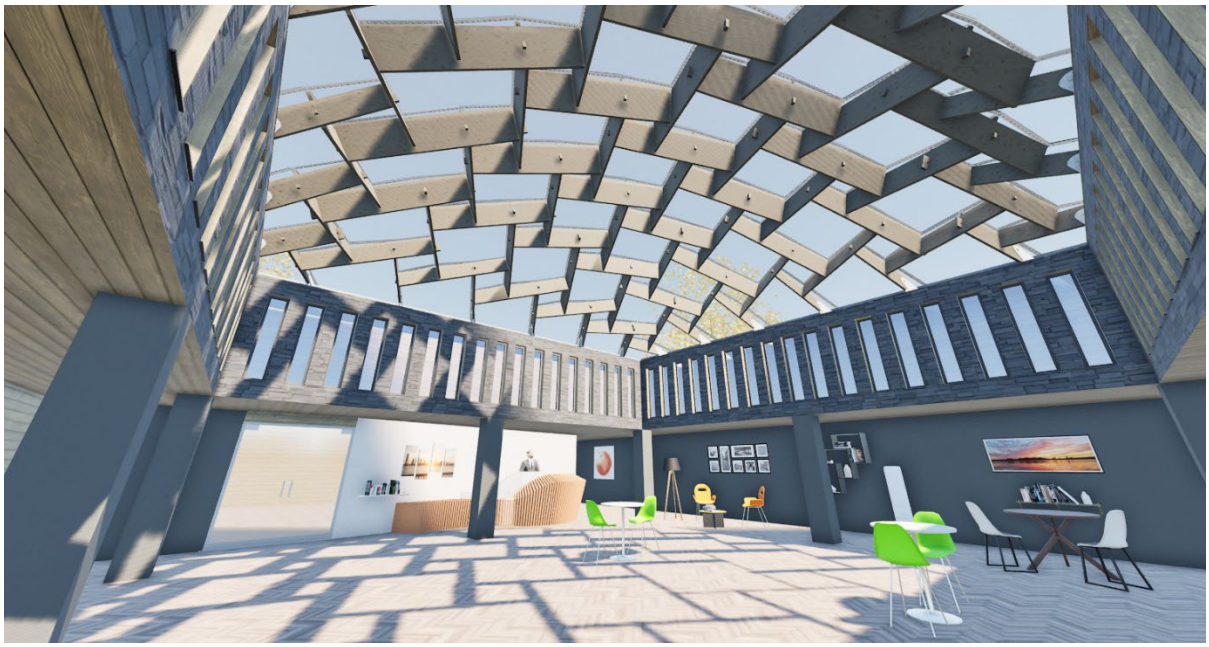


Figure 65: Impression of reciprocal roof structure with internal membrane from the building's interior

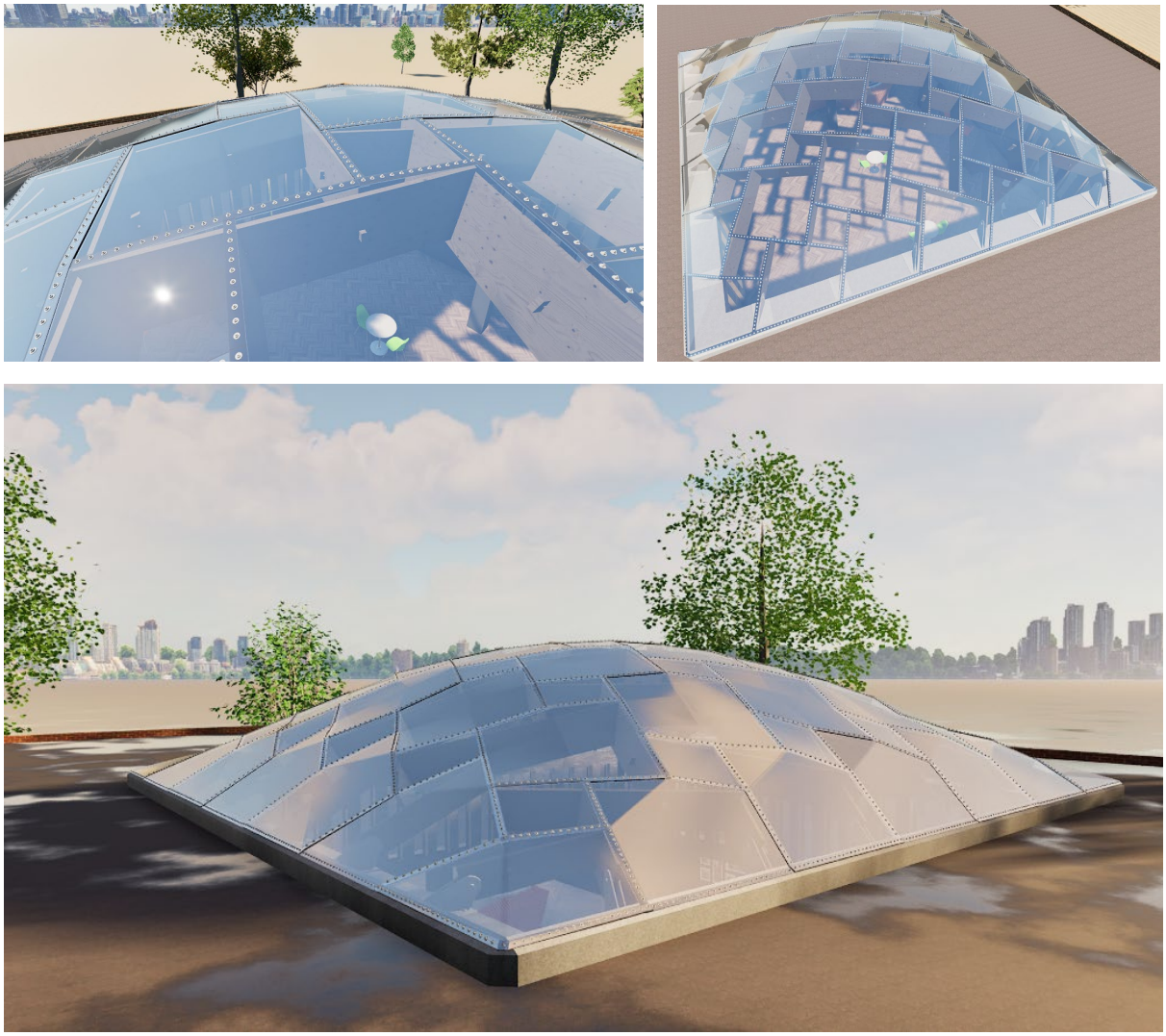


Figure 66: Impression of reciprocal roof structure with internal membrane from the building's exterior

4.4 Connection to foundation

The connection to the foundation is always assumed to be hinged for reciprocal frames. For 2d reciprocal frames, the reaction forces at the supports always act perpendicular to the surface of the frame. As the curvature (or eccentricity between the members) increases, more lateral forces are introduced.

This means that the design of the connections to the foundation is based on the curvature of the structure. To find the influence of the curvature of the reciprocal structure on the angle of the reaction force, a small parametric research has been performed.

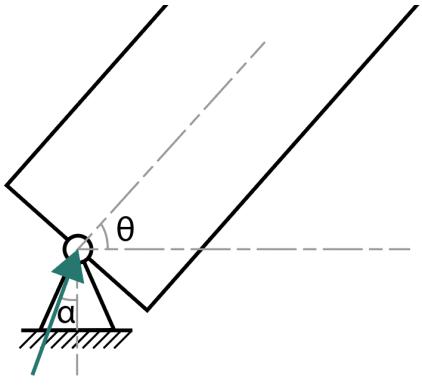


Figure 67: Angles for determination of influence reciprocal curvature on the reaction force

The angle of the beam adjacent to the support depends on the eccentricity between the members. This angle is used to compare the curvature of the reciprocal frame to the angle of the reaction force. In Figure 67, the angles that are considered are displayed.

The resulting relation between the angles – for an 8x8m, 1x1m unit reciprocal frame under uniformly distributed vertical load – is plotted in Figure 68. As expected, for a flat (2d) reciprocal frame the angle of the reaction force is 0. When there is a slight curvature, the angle of this reaction force starts increasing significantly. This increase continues upto around 15 degrees where the reaction force has an angle of 45 degrees. For larger angles, the angle of the reaction force fluctuates between 45 and 38 degrees. The exact reason for this fluctuation depends on multiple factors. Due to the complexity of reciprocal frames, this cannot exactly be quantified.

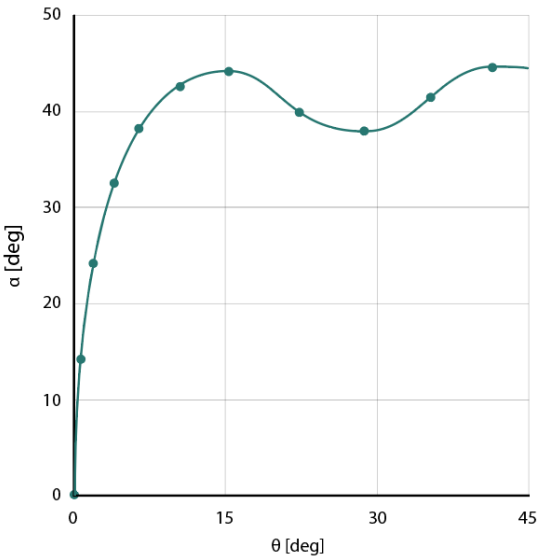


Figure 68: Angle of the reaction force α with respect to the angle of the beam θ for an 8x8m, 1x1m unit reciprocal frame loaded under an uniformly distributed vertical load

With this information, a connection to the foundation must be designed that can transfer both horizontal and vertical loads. Where the horizontal load can be equal to the vertical load. Additionally, it is important to consider the effects on the foundation of the structure. The foundation is not within the scope of this research, however one could think of solutions like a tension ring or tension cables.

An additional complexity in the connection is the fact that the beam elements are placed under three dimensional rotation (around the x, y and z axis in Figure 69).

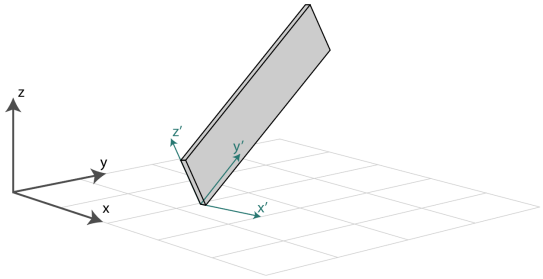


Figure 69: Beam rotation with respect to global axis

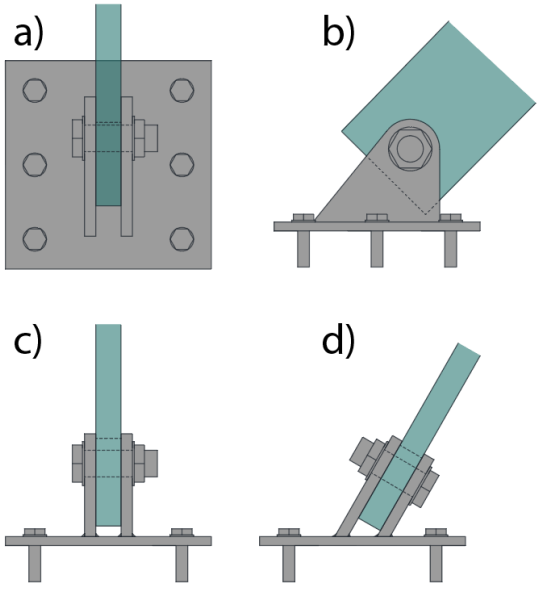


Figure 70: Principle design of connection to foundation/other structure. a) top view, b) side view, c) front view, d) front view with rotation

The resulting connection is displayed in Figure 70 where the rotation around the local x' axis is achieved by the natural hinge around the pin. The rotation around the global z axis is achieved by simply rotating the base plate on the foundation/sub structure. The only rotation that influences the connection design is the rotation with respect to the xy-plane. As visualized in Figure 70d, the rotation is achieved by welding the base plate at an angle with respect to the beam. The required rotations can be determined from the stored beam location data (see the chapter 'Reciprocal frame designer' for more details).

The sizes of the plates and bolts are determined by the forces and beam size. These connections will not be part of the optimization/calculation process.



5 Reciprocal frame designer

Knowing the prerequesites and preliminary design choices, the reciprocal frame can be designed. The reciprocal frame is generatively designed based on several design parameters (tessellation edge size, scale factor, sheet thickness, eccentricity and the tessellation gradient).

This chapter describes the workflow and methods used in the generative design of the reciprocal frames.

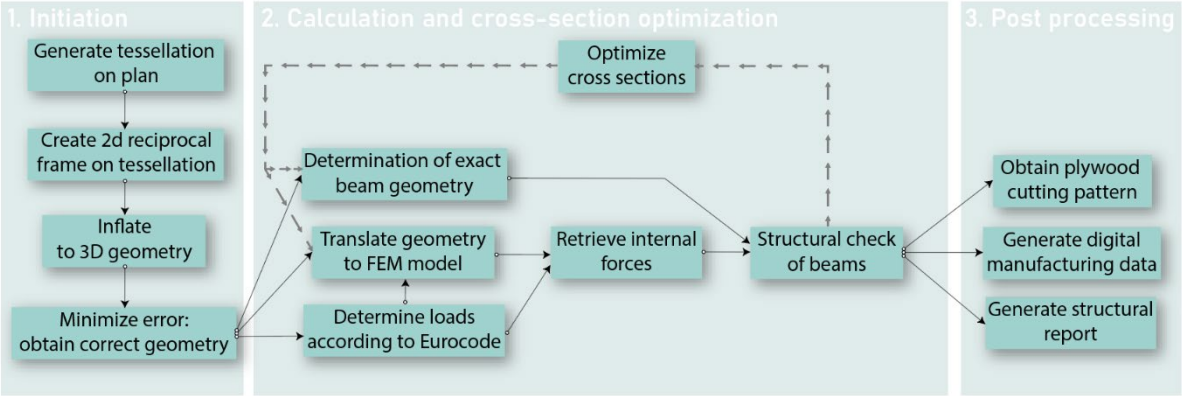


Figure 71: Flowchart for reciprocal frame designer

5.1 Workflow

The workflow for the generative reciprocal frame designer is described using the flowchart in Figure 71. The workflow consists of three main phases:

1. Initiation: creation of a reciprocal frame geometry based on several design parameters.
2. Calculation and cross-section optimization: obtaining data required for calculating unity checks of the beam elements and performing these unity checks.
3. Post processing: turning the checked and optimized reciprocal frame into usable data for digital manufacturing and a calculation report.

This process is performed based on the input plan and several design parameters that determine the morphology of the reciprocal frame.

The initiation phase is discussed in this chapter, where all steps for designing the morphology of the reciprocal frame are discussed.

The structural checks and cross-section optimization are discussed in chapter '6. Structural integrity and optimization'. In this chapter, additionally, the structural report is discussed.

Finally, the post processing for digital manufacturing is discussed in chapter '7. Digital manufacturing'

5.2 Input plan

The reciprocal frame is designed to span a user provided rectangle, defined by four corner nodes. The reciprocal frame designer designs a reciprocal frame that as closely as possible fits the input plan.

Other (non-rectangular) geometries can in theory also be used for the reciprocal frame designer. The load determination is however not automatable due to limitations in the Eurocode (e.g. wind loads can only be determined on regular shapes). Therefore, the option of generating reciprocal frames on more complicated floor plans is disabled.

5.3 Tessellation

To create a reciprocal frame geometry, firstly a 2d tessellation is 'laid over' the input plan. The applied tessellations are equilateral polygon tessellation. This type of tessellation is used because all edges in the tessellation share the same

location, there are no gaps in the tessellation and the tessellation are to a large degree uniform.

Tessellation pattern type

The tessellations that are used in the reciprocal frame designer are based on triangles, squares and hexagons. In the family of equilateral polygon tessellations, this results in the following *tessellation pattern layouts* that are considered in this research (Figure 72).

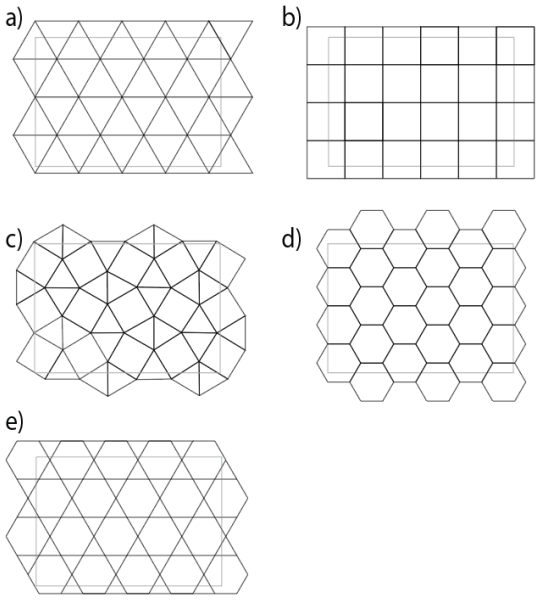


Figure 72: Tessellation pattern layouts considered in this research. a) Triangle, b) Square, c) Snub-square, d) Honeycomb, e) Trihexagon

Since the polygons are equilateral (i.e. have equal edge lengths) the whole tessellation can be scaled with a single factor*: tessellation edge size*.

In the patterns in Figure 72, the original base 'plan' is displayed underneath the tessellation. As visible in the figure, the tessellation does not always exactly match the original floor plan. To obtain the tessellation with a certain edge size that matches the base plan as closely as possible any polygons that do not have an edge in the plan are removed from the tessellation.

The tessellations is placed as such that the area that is in the resulting tessellation but not in the floor plan $(A_{tessellation} \cap A_{plan})$. This is done by manually selecting for each tessellation how it can be placed efficiently.

Tessellation density gradient

By default, the density of the tessellation is equal over the whole plane. Since the reciprocal frame is based on this tessellation, the reciprocal frame also has an uniform density. For structural optimization and/or aesthetic reasons it might however also be interesting to increase or decrease the structural density in the middle of the structure or towards the edges. Doing so might result in a reduction of (raw) material usage.

To achieve a higher density towards the center or edges of the reciprocal frame, the base 2d tessellation needs to have a variable density. The density behaviour is determined by the *gradient factor*.

To explain the theoretical background of the *gradient factor*, the tessellation and its density is flattened to a 2d problem (see Figure 73). The point density is determined using the following formula:

$$\rho_{point} = \frac{d \times n}{L}$$

Where:

- $d =$ average distance to adjacent points
- $n =$number of points
- $L =$ distance between min_x and max_x

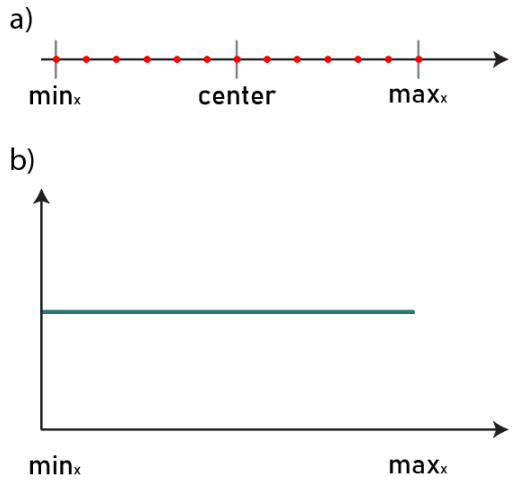


Figure 73: a) 2d representation of point density in a reciprocal frame with b) corresponding density plot

To gradually increase the density towards the center of the structure, the points are translated towards to center by a variable distance. This distance is determined by the following formula:

$$d = G_f(x) \times d_{center}$$

Where:

- $G_f(x)$ = value of the gradient function at point location x
- d_{center} = distance of point to the center

The gradient function is a parabola that is zero at min_x and max_x and has an extreme at the center (see Figure 74). The value of the extreme is the *gradient factor* G. The gradient factor determines the degree to which the gradient is increased or decreased towards the center of the reciprocal frame.

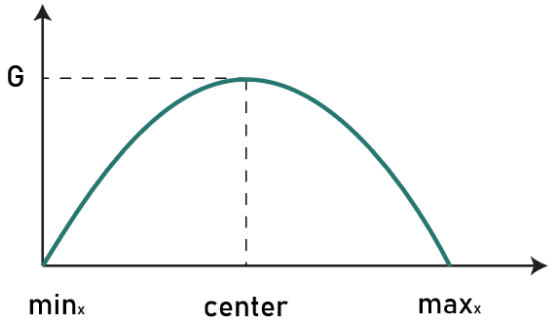


Figure 74: Function shape of the gradient function ($G_f(x)$) with extreme at center with value G

Figure 75 displays the result of applying the gradient function with *gradient factor* G = 0.5. As visible in the density plot, the point density has significantly increased towards the center of the structure whilst it has decreased towards the ends of the structure.

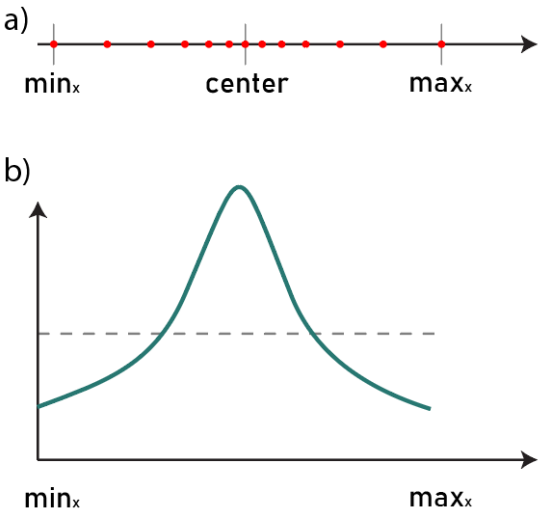


Figure 75: a) 2d representation of point density in a reciprocal frame with gradient factor G = 0.5 with b) corresponding density plot

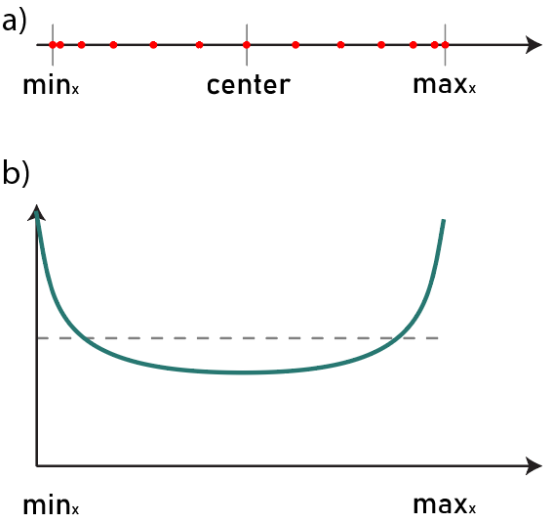


Figure 76: a) 2d representation of point density in a reciprocal frame with gradient factor G = -0.5 with b) corresponding density plot

Similarly, Figure 76 displays the result of applying the gradient function with *gradient factor* G = -0.5. Since the gradient factor is negative, the points are moved away from the center. This

results in the density plot as visualized in Figure 76b.

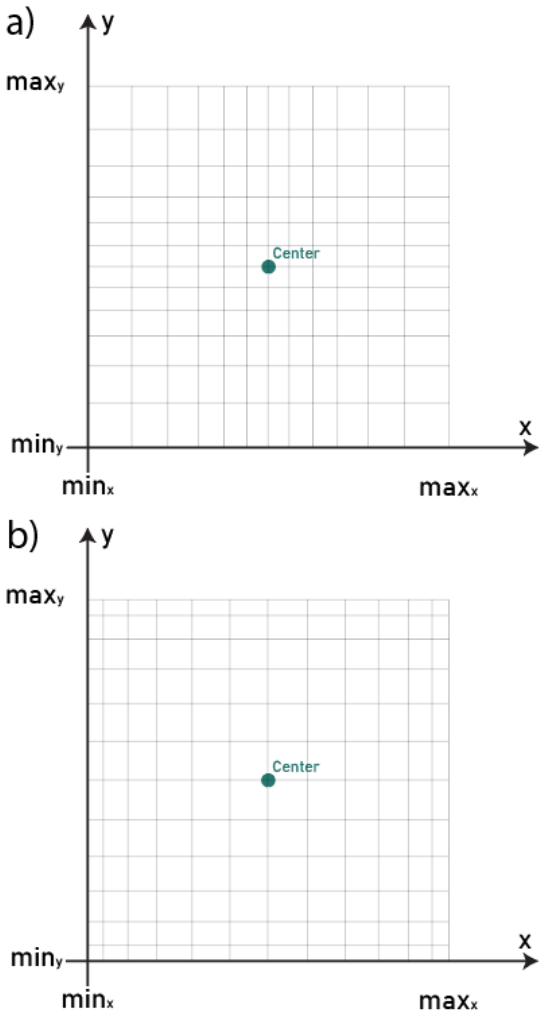


Figure 77: Gradient factor applied to a squared polygon with a) G = 0.3 and b) G = -0.3

For the 2d tessellations, these node translations are performed in x and y direction. Figure 77 shows a squared tessellation where the gradient factors have been applied.

The natural boundaries of the gradient factor are [-1, 1], where -1 means all points have moved to the edges and 1 means all points have moved to the center. To create feasible reciprocal structure, in this research, the limits of G are [-0.3, 0.3].

5.4 2d reciprocal frame

To turn the 2d tessellation into a two-dimensional reciprocal frame, the center-to-center method as described in the literary review is used.

The center-to-center method is applied by scaling each polygon in the 2d tessellation by *scale factor* S_v. A beam element is created between the center of each edge of the original polygon and the center of the right-hand edge of the scaled polygon (see Figure 78). The beams are always created with the same rotation (so connecting to the edge on the right-hand side).

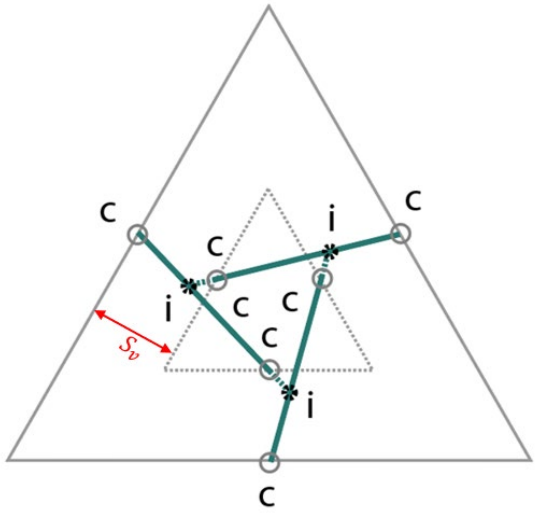


Figure 78: Center-to-center method. c = center of edge, I = intersection between beams, S_v = scale factor

Data management

The creation of the beam elements also initiates the structural element data that must be stored. To minimize computation time (which is a requirement for the iterative computations that are performed on the structure) and data storage, an indexing method for storing the data is used.

For the structure this means that there are two main 'databases'/arrays where the structural data is stored; the node data and the beam data.

In the node data the following information is stored:

- ID/index: node identifier.
- Coordinates: x, y and z positions.
- IsConstrained: Boolean to determine if point is a support and may be moved in optimization (see paragraph '5.6 Minimizing model error').
- Load data: see chapter '6. Structural integrity and optimization'.

And in the beam data the following information is stored:

- Begin node ID
- End node ID
- Begin support ID: ID of beam that supports the beam at the begin point.
- End support ID: ID of beam that supports the beam at the end point.
- Beam rotation: rotation of the beam's cross-section around the beam axis with respect to the surface plane.
- Beam dimensions: an array with all beam dimensions.
- Corresponding FEM beam ID's: see chapter '6. Structural integrity and optimization'
- Internal forces: an array with all internal forces determined from the FEM model (see chapter '6. Structural integrity and optimization')

During the initiation of the reciprocal frame, the following data would be stored for a single unit reciprocal frame (graphical representation in Figure 79):

Table 3: Node data in initiation of single unit reciprocal frame

Node ID	x	y	z	IsConstrained
1	0	1	0	True
2	0.6	0.2	0	False
3	1	1	0	True
4	0.2	0.7	0	False
5	0.5	0	0	True
6	0.7	0.8	0	False

Table 4: Beam data in initiation of single unit reciprocal frame

Beam ID	Begin node	End node	Begin support	End support
1	1	2	-1*	3
2	3	4	-1*	1
3	5	6	-1*	2

* If there is no begin support beam, the value is -1

The tables show how the indexing is used. This means that a beam is defined purely by a begin and end point, the intermediate node on the beam is not part of the beam element. For a reciprocal unit based on a polygon with n sides this means that $2n$ nodes are created and n beams.

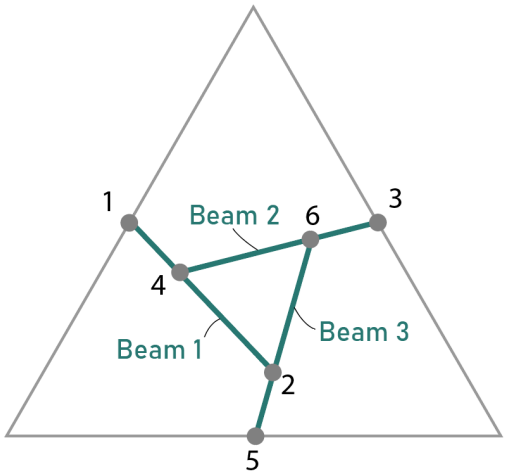


Figure 79: Graphical representation of data stored in initiation of single unit reciprocal frame

Connecting multiple single unit reciprocal frames

To create a full reciprocal frame from the multiple single unit reciprocal frames that are generated in the 2d tessellation, the single unit reciprocal frames must be connected.

Figure 80 indicates where the single unit reciprocal frames must be connected. As mentioned before, because an equilateral polygon tessellation is used, the edges always share the same center point, which makes it relatively straightforward to connect the single-unit reciprocal frames.

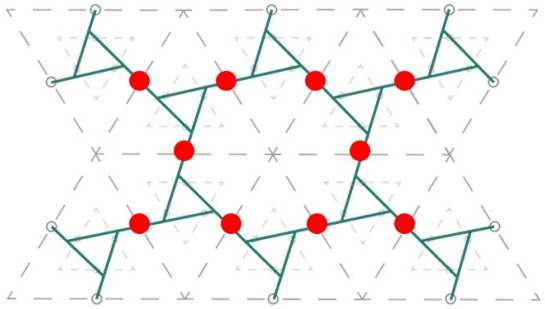


Figure 80: Location where multiple single unit reciprocal frames must be connected (red)

The connection of these separate reciprocal frames is performed in the following steps:

1. Remove duplicate nodes
2. Merging beams that share a begin/end node
3. Recalculating the position of intermediate nodes

The first step, the removal of duplicate nodes is simple; when a node shares the same x, y and z location, one of the nodes is removed. For the beam indexing this means that the removed node id must be replaced by the node if of the node that has the same location.

The second step, merging beams that share a begin/end node, is a bit more complex due to the data indexing. Figure 81 shows a graphical representation of how this is done. Firstly one of the beam elements is removed and the other beam element inherits the begin/end node ID from the removed beam. Secondly, the Begin/End support ID's are updated.

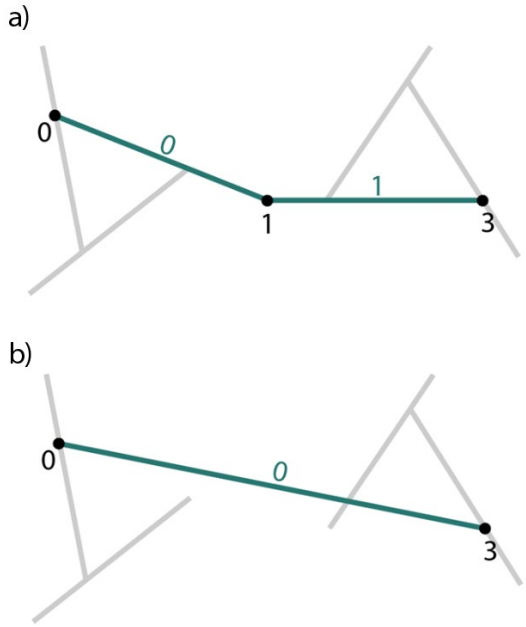


Figure 81: step 2 of connecting the single unit reciprocal frames. a) initial condition, b) situation when the beams are connected

As visible in Figure 81b, the positions of the connecting elements are not always correct after the second step. This is fixed in the third step where the intermediate nodes are moved to the locations where the beam vectors intersect.

The location of the new position is determined by calculating the vector intersection between the two beams. This is done by solving the line equation: $ax + b = cx + d$.

5.5 Inflation to 3d structure

To turn the 2d reciprocal frame into a 3d reciprocal frame structure, the 2d frame must be inflated. This inflation is achieved by creating an inter-member eccentricity. Directly determining the exact positions of each nodes for a frame with a specific eccentricity is mathematically impossible. There are however indirect solutions to solve this problem as mentioned in the literary review. In this research, a mathematical minimization is used to find the exact solution.

To aid this mathematical minimization, it is important to estimate the position of the nodes as accurately as possible. This is done by inflating the structure by moving the z-coordinates of the nodes until convergence requirements are met.

Connection beam

With the introduction of inter-member eccentricity, also so-called connection beams are introduced. This connection beam is also used to check if the convergence requirements for the inflation are met.

The connection beams are created by finding the point on the support beam that is the closest to the begin/end node of the beam.

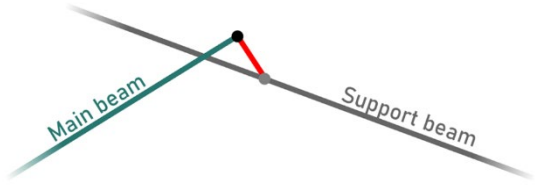


Figure 82: Creation of connection beam (red) between intermediate node on support beam (grey) and the end node of the main beam (black)

Inflation loop

When the connection beams are defined, the inflation can be performed by looping over all connection beams. The z-coordinate of the begin/end node of the main beam are increased by the required *eccentricity* for each connection beam that does not meet the initial connection beam requirements:

- $L_{connection\ beam} \geq e_{req}$
- $z_{N_{beam}} - z_{N_{connection}} \geq e_{req}$

In words: the length of the connection beam is equal to or larger than the required *eccentricity* and the z-coordinate of the beam node is *eccentricity* larger than the z-coordinate of the connection beam node.

This loop is continued until all connection beams fulfill the requirements.

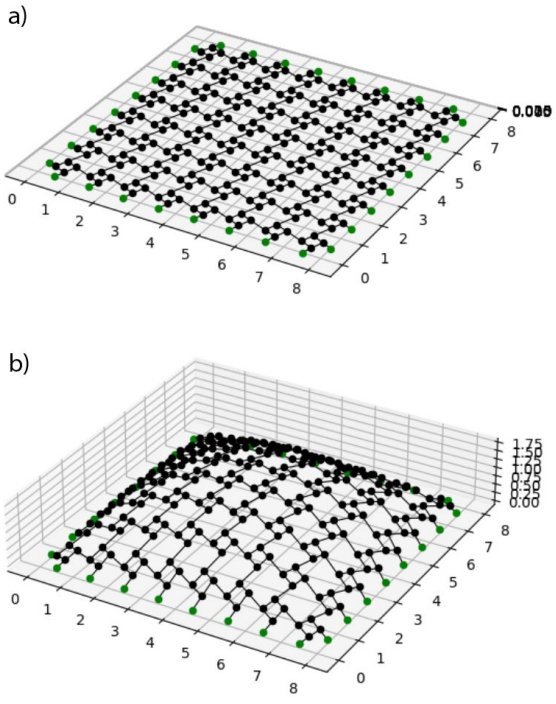


Figure 83: Reciprocal frame a) before and b) after inflation loop

Obviously, the *eccentricity* is the parameter that controls the amount of curvature there is in the reciprocal frame.

Figure 83 shows the effect of the inflation on a typical reciprocal frame structure. The resulting 3d frame gives a good estimation that can be used for the mathematical minimization.

5.6 Minimizing model error

As mentioned before, the estimated 3d reciprocal frame does not represent the actual structural behaviour of the structure. Figure 84a indicates the structural shape that may be found after inflation. When there is an eccentricity between elements, the eccentricity member should always be perpendicular to both beams (see Figure 84b).

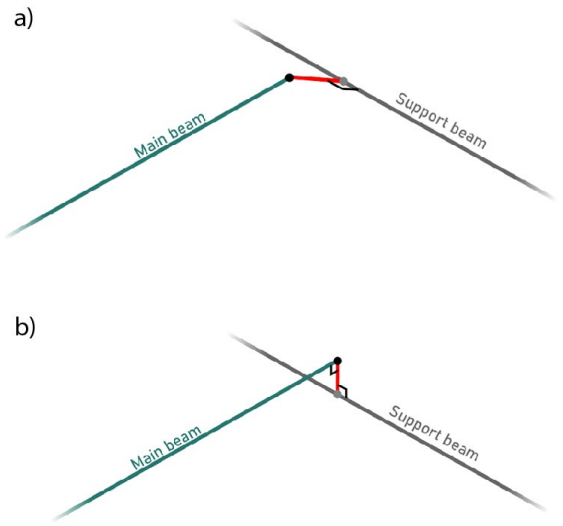


Figure 84: a) connection behaviour after inflation and b) correct connection behaviour

To make sure that both these conditions are met a mathematical minimization is applied that minimizes the model 'error'. This enables the resulting geometry to be as close as possible to the required conditions.

Connection beam error

The error of each connection beam is calculated geometrically using the following formula:

$$E_k = |sin(\theta - 90) \times L_{cb}|$$
$$+|(e - (\cos(\theta - 90) \times L_{cb}))|$$

Where:

- θ = angle between the main beam and the connection beam
- L_{cb} = length of the connection beam
- e = required eccentricity

The first part of the error function is the perpendicular condition. Since the connection beam is connected to the point on the support beam that is the closest to the end point of the main beam, the connection beam is always perpendicular to the support beam. This means that the perpendicular condition only looks at the angle between the main beam and the connection beam.

The angle between the two beams is calculated using the following formula:

$$\cos\theta = \frac{a \cdot b}{|a|\,|b|}$$

Where a and b are the direction vectors of the beams.

The second term of the error is the length condition, where it is checked whether the length of the connection beam is equal to the required eccentricity. The length condition is corrected for the perpendicular condition, which means that the error is larger when the angle is incorrect.

When both conditions are met (i.e. $\theta = 90$ and $L_{cb} = e$) the error is 0. However when one or both of the conditions are not met an error is returned (e.g. $\theta = 45$

and $L_{cb} = e$ returns $\frac{\sqrt{2}}{2}e$ for the perpendicular condition and $|e - \frac{\sqrt{2}}{2}e|$ for the length function)

Model error

The error of the full model is defined as:

$$E = \sum_{k=1}^{n} E_k^2$$

In words this is the sum of the squared value of connection beams. The error values are squared to aid convergence when minimizing the model error.

Optimization problem

To find the values for each of the coordinates that results in a model error E that is (close to) zero, a mathematical optimization must be performed. The optimization problem is described as:

Minimize $E(x_n, y_n, z_n)$

Subject to: $x_n \epsilon\, \Omega_n$
$y_n \epsilon\, \Omega_n$
$z_n \epsilon\, \Omega_n$

This means that the model error, based on the node coordinates, must be minimized. The minimization is subject to constraints of the coordinates where each of the nodes are subject to a bounding box. To make sure that the 'optimized' solution maintains the shape and uniformity of the inflated geometry, the bounding box for each node is relatively small in x and y direction: [(-2e, 2e), (-2e, 2e), (-1, 1)]. This focusses the movement of the nodes in the z-direction.

Optimization algorithm

To solve the minimization problem, the L-BFGS-B optimization is used. the L-BGFS-B is a multivariate minimization algorithm. The L-BFGS-B algorithm is used for this problem because it is efficient in memory usage which makes it efficient for high dimensional problems.

Since the problem that should be minimized is a geometrical optimization, the minimization function can be seen as continuous and differentiable. The L-BFGS-B algorithm is very suitable for such problems. Additionally, the L-BFGS-B algorithm can handle the individual bounds for each of the parameters

The L-BFGS-B algorithm finds a global minimum of the function by iteratively estimating a Hessian matrix.

For a scalar function $f(x)$ with n variables ($x_1, x_2, \dots, x_n$) the Hessian matrix H is an $n \times n$ matrix where H_{ij} is the second partial derivative with respect to x_i and x_j. This means that the Hessian matrix gives information about the curvature for all n dimensions of the problems. In other words; it tells which direction a variable should move to improve the global solution. This means that the L-BFGS-B algorithm performs directed searching to minimize the function result. This leads to relatively fast convergence for large scale problems.

Figure 85 shows the convergence diagram for a reciprocal frame with a large complexity (number of nodes > 400, which means the number of parameters is >1200). Due to the directed search algorithm, such large problem reaches convergence relatively quickly.

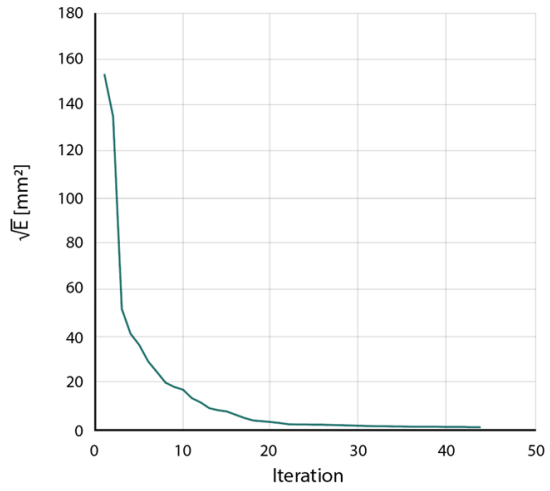


Figure 85: Typical convergence diagram for reciprocal frame with large complexity (n > 400)

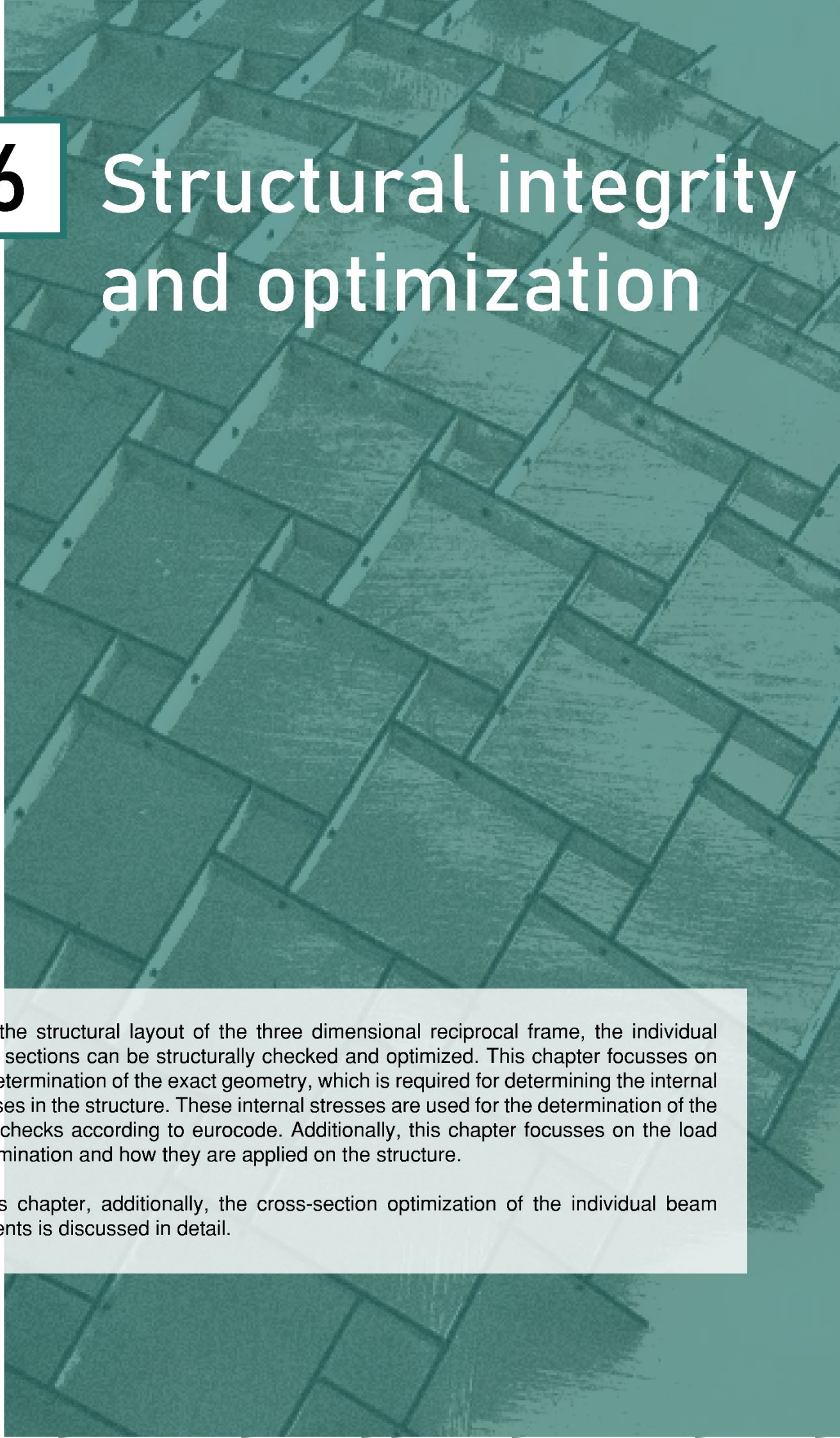
5.7 Conclusion

The structural morphology of the reciprocal frame is generated based on the following design parameters:

- Tessellation layout
- Tessellation edge size
- Tessellation gradient factor
- Scale factor
- Eccentricity

With these parameters, the reciprocal frame geometry can be controlled extensively.

In the next chapter it is explained how the exact dimensions of the beams are determined and optimized to fulfill structural requirements according to Eurocode.



6 Structural integrity and optimization

With the structural layout of the three dimensional reciprocal frame, the individual cross sections can be structurally checked and optimized. This chapter focusses on the determination of the exact geometry, which is required for determining the internal stresses in the structure. These internal stresses are used for the determination of the unity checks according to eurocode. Additionally, this chapter focusses on the load determination and how they are applied on the structure.

In this chapter, additionally, the cross-section optimization of the individual beam elements is discussed in detail.

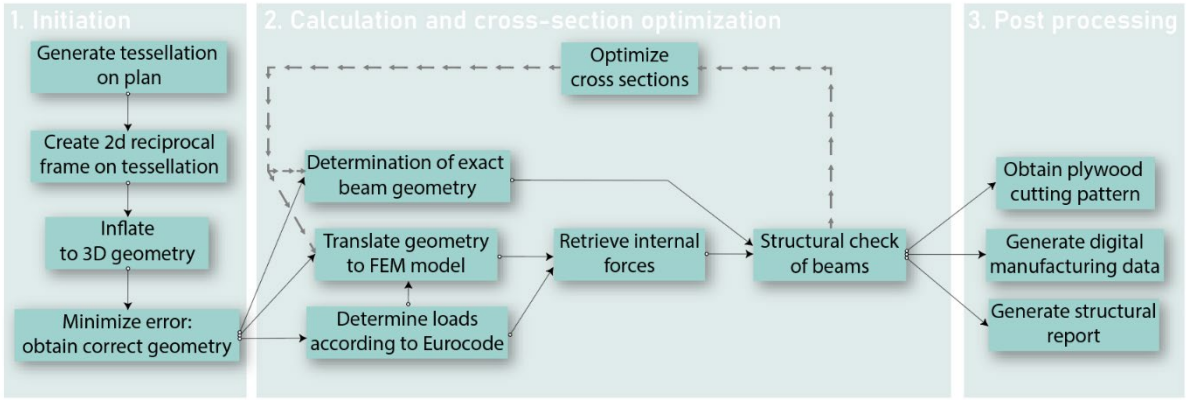


Figure 86: Flowchart for reciprocal frame designer

This chapter focusses on phase 2 of the flowchart in Figure 86, where each step is explained in detail.

6.1 Exact beam geometry

The exact beam geometry must be determined before being able to calculate the internal forces and thus the dimensioning of the structural elements. The geometry must be determined based on limited information; the begin and end node location of the structural elements and the rotation of the section around the beam axis (which is determined by the connection lines).

End and hole rotations

The rotations at the beam ends are determined by casting the beam elements as planes. The vector that is the intersection between the planes can be determined by computing the cross product of the two planes. The angle between the intersection vector and the beam vector gives the end rotation in the beam.

The planes are cast in two directions to determine the 3 dimensional end rotation, see Figure 87. In Figure 87a, the planes are cast in the local x-z planes. The intersection vector (visualized in red) is the vector parallel to the intersection line, determining rotation θ_1. In Figure 87b the planes are cast in both the local x-y plane and x-z planes. The intersection vector determines rotation θ_2.

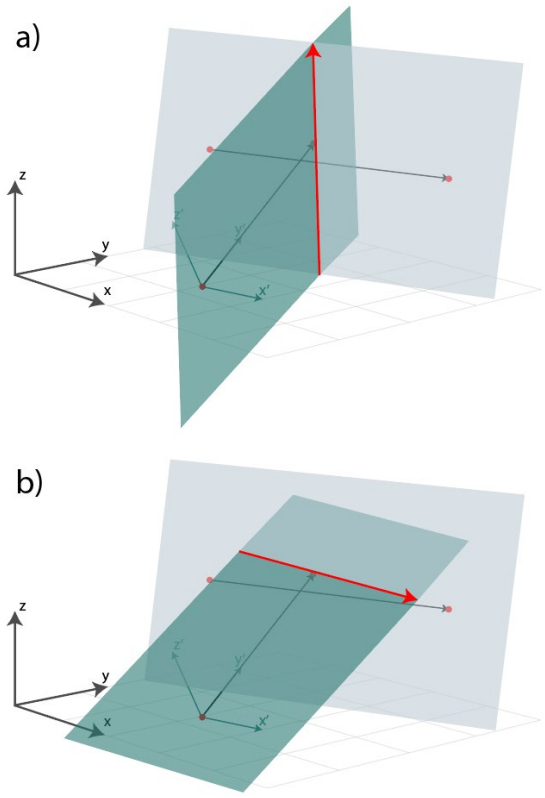


Figure 87: Beam elements cast as planes to determine end rotations

When the rotations at both the begin and the end of the beam are known, the rotations of the holes can also be determined. To fully determine the hole rotations, three angles need to be known. The first two can be determined by the end rotation of the adjacent beam$\varphi_1 = \theta_1, \varphi_2 = \theta_2$. The other rotation that must be known is the rotation around the central axis of the hole. This angle is determined by the rotation around the axis of the adjacent beam and the pitch (rotation with respect to the x-y plane) of the hole beam:

$$\varphi_3 = \theta_{ax,adj} - \theta_{pitch}$$

Initial geometry

When no minimum dimensions for the beams are specified, the minimum possible dimensions of the beams are applied (this is the starting point for the cross-section optimization process). The minimum dimensions are mostly determined by the minimum tenon size and the edge distances according to Eurocode.

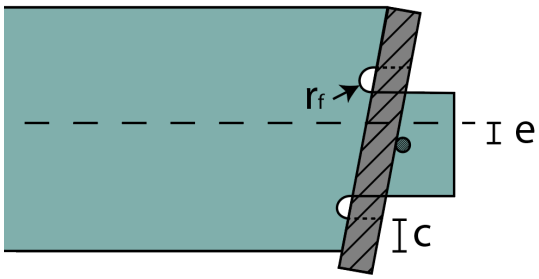


Figure 88: beam dimensions used for determining the minimum beam dimensions

According to the Eurocode, the minimum dowel (or tenon) size is 6mm (38). Additionally, the minimum edge distance is 3 times the dowel diameter. This thus means that the minimum height for the tenons is $7 \times 6mm = 42mm$.

The minimum beam height is designed as such that c (in Figure 88) is equal to the beam width. Consequently, the beam height is determined with the following formula:

$$h_{beam,min} = 42 + 4 * r_f + e + 2 * b_{beam}$$

Data storage

The beam dimensions are stored in the beam dimensions array. The geometric information that is stored in the beam element is:

- Begin/end rotation: $[\theta_{b,1}, \theta_{b,2}]$
- Hole properties: $[h, b, r_f, \varphi_{l,1}, \varphi_{l,2}, \varphi_{l,3}]$
- Tenon properties: $[h, l, d_{dow}, r_f]$

When a reciprocal element supports two elements, the properties are stored twice (for begin and end). When a reciprocal element only supports one element, the information is only stored once.

6.2 FEM modelling

To be able to calculate the internal forces in the structure, the reciprocal frame geometry must be transferred a finite element model. To be able to calculate the internal forces rather quickly, the internal forces are calculated by using a line model instead of a model with the full geometry.

In the FEM line model, the beam elements need to be split up at the location of the connection line to create an intermediate node on the beam elements. Figure 89 shows how the beam elements are split into multiple FEM beam elements. For each beam element, the corresponding FEM beam ID's are stored in the beam database.

This can later be used to determine the internal forces in the beam elements.

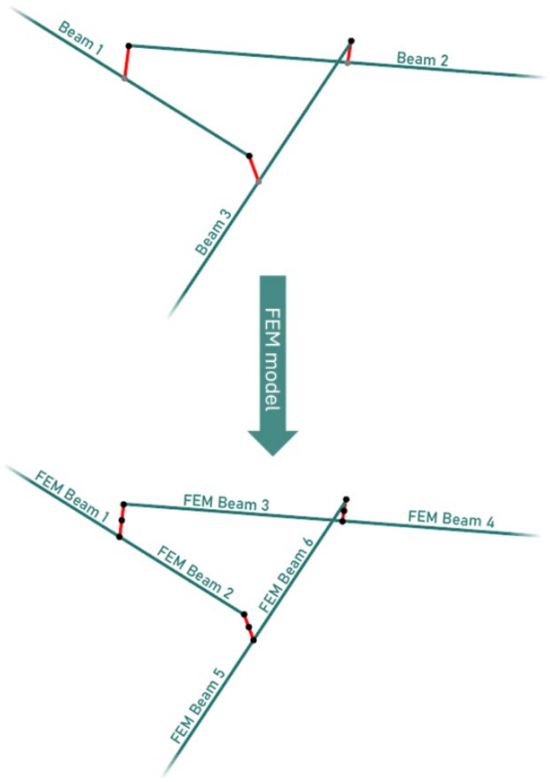


Figure 89: Reciprocal frame geometry translated to FEM model geometry

Modelling of the connection

The inter-member connection behaviour in the reciprocal frame are determined in chapter '4.2 Connection behaviour':

- Hinged in M_y and M_z
- Fixed in M_x (rotation around beam axis)

This behaviour is achieved by creating an additional intermediate node on the connection beam. The intermediate node has the behaviour listed above (see Figure 90). The connection beam elements are modelled as being infinitely stiff, this means that the connection behaviour can be seen as either fully fixed or hinged (depending on the rotation direction).

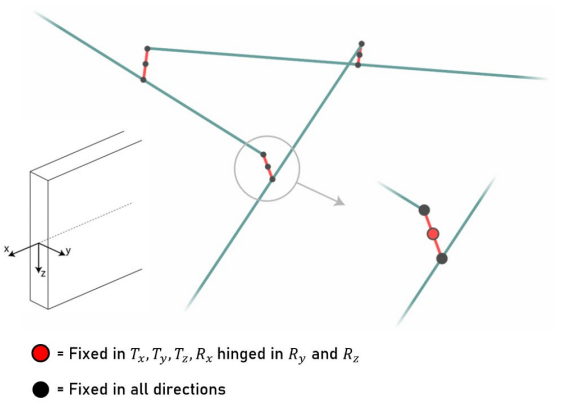


Figure 90: inter member connection detailing in the FEM model

The supports of the reciprocal frame are simply modelled as hinges at the end of the beam. Any moment caused by the eccentricity to the connection to the foundation is not expected to influence the flow of forces due to the large stiffness in the connection.

FEM model properties

The FEM calculations are performed in the open-source FEM modelling software 'NextFEM' (55). The FEM model performs a three dimensional linear static structural analysis. The model includes shear deformations, which is important due to the rather low shear modulus of plywood.

In the FEM model, the plywood is assumed to behave linear-elastic orthotropic. As mentioned previously, assuming linear-elastic behavior is safe when the stresses are expected to be rather low.

The FEM model material properties depend on the quality of plywood that is used. When no specific stiffness properties are provided, the following material properties are assumed (see Table 5). These properties are expected to resemble plywood behaviour for various standard thicknesses. When the

exact stiffness properties for a certain type of plywood sheet are known, they can manually be entered.

Table 5: Material properties plywood in the FEM model. Derived from(36).

Density	ρ	460	kg/m^3
Young's modulus	E_1	6682	MPa
	E_2	5318	MPa
	E_3	5318	MPa
Shear modulus	G_{12}	350	MPa
	G_{13}	52	MPa
	G_{23}	38	MPa
Poisson ratio	v_{12}	0.04	
	v_{13}	0.191	
	v_{23}	0.248	

The FEM model automatically splits the FEM beam elements into multiple parts to be able to accurately calculate the internal forces in the beam elements.

6.3 Load determination

For the load determination, it is assumed that the building is situated in the Netherlands. This means that all load determinations are based on the Dutch national annex of the Eurocode.

The load cases that are considered for the reciprocal frame to act as a roof structure are: permanent loads, wind loads, imposed loads, snow loads and temperature loads.

Permanent load

The permanent load on the structure is determined by the weight of the structural elements and the weight of the cladding material. The weight of the cladding is assumed as $0.2\ kN/m^2$. This value can be altered by the designer if necessary. In practice, the distance between the structural elements might alter the density of the cladding material. In this research, that effect is ignored.

Imposed loads

The roof is of category H which means that an imposed load of $1{,}0\ kN/m^2$ is applied (or $4 - 0{,}2\alpha\ kN/m^2$ when the roof slope is $15° \leq \alpha \leq 20°$). This load specification acts on a designated area measuring $10\ m^2$, as stipulated by the Eurocode (56). This area should be acting on the most impactful location on the structure. Since the loads are automatically calculated, the loads are assumed to be distributed across a square around the central point of the structure. When testing on several reciprocal structures this load locations seemed to be most influential. When the optimized structure is going to be applied in real life, it is advised to apply the imposed loads on other areas.

In instances where the structural area is less than $10\ m^2$, the aforementioned imposed load is uniformly applied over the entire area. When the length or width of the area is smaller than $\sqrt{10}$, the force is not acting over the square but over a rectangle where the width is equal to the width of the structure.

Wind load

The determination of the wind loads on the structure is based on the schematization presented in Figure 91, which is provided in the Eurocode NEN-EN 1991-1-4 (57).

It is important to note that the geometrical configuration of the structure may deviate from the circular base as provided in the figure, as the base of the structures are square or rectangular. However, the presence of double curvature within the dome aligns

most closely with this theoretical representation of wind loads.

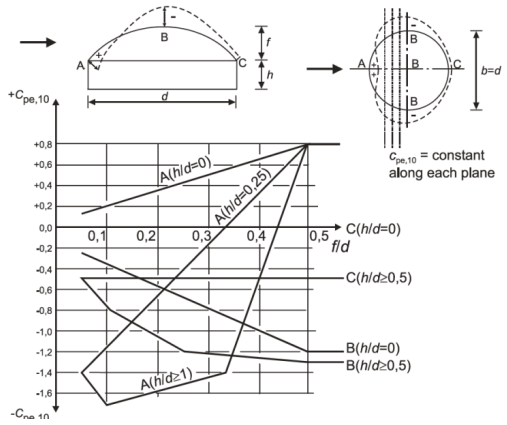


Figure 91: Recommended values of external pressure coefficients for domes acc. Eurocode NEN-EN1991-1-4 (57)

The extreme wind pressure $q_p(z)$ is determined by the highest point in the structure. This value is multiplied with $C_{pe,10}$ as derived from Figure 91.

For the wind loads, the location of the structure influences the load determination. Therefore, the designer must determine the wind area, surrounding environment (built/unbuilt) and the height of the base of the reciprocal frame.

When the reciprocal frame has a low curvature, the wind loads on the roof are considered to be acting on a flat roof acc. NEN-EN1991-1-4 7.3.2. The constraint is a maximum slope of $-5° \leq \alpha \leq 5°$. This translates into $\frac{f}{d} = 0.5$ in Figure 91.

Snow load

The determination of the snow loads on the structure is based on the schematization provided in the Eurocode NEN-EN 1991-1-3 (58) (Figure 92). The code prescribes two distinct cases.

For case (i), a uniformly distributed load is imposed over the full area of the structure, excluding parts where the structure has a slope larger than 60 degrees. This method is rather straightforward, assuming a blanket distribution of snow load across the structure.

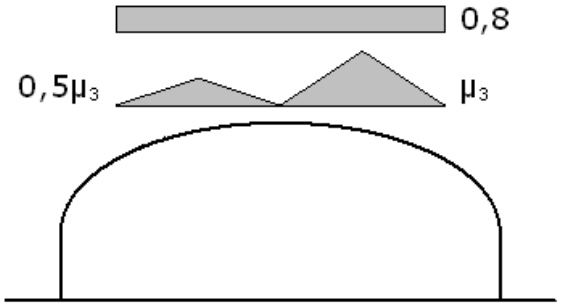


Figure 92: Snow load shape coefficients for cylindrical roof

In the second case (ii), the snow load is considered to be accumulated at the sides of the dome. For dome-like structures, this load condition might be normative over the equally distributed load.

The snow load coefficient in this case is determined geometrically. This is done by first determining the center point, or line, of the reciprocal structure. This center point/line is the location where the distance to each of the edges of the base polygon is equal.

Using the central axis as a reference, the cumulative snow load coefficient is derived. This involves computing the distances from each point to both the edge of the base polygon and the central point/line. The snow load coefficient is determined by the following expressions:

If $d_{mid} > L_{tot}/2$:

$$\mu = \mu_3 * 2 * \left(1 - \frac{d_{mid}}{L_{tot}}\right)$$

If $d_{mid} \leq L_{tot}/2$:

$$\mu = \mu_3 * \frac{2d_{mid}}{L_{tot}}$$

Where:

- $\mu_3 = 0.2 + 10\frac{h}{b}$ (acc. Eurocode NEN-EN-1991-1-3 clause 5.3.5) (58)
- L_{tot} = Distance to edge + distance to center line
- d_{mid} = Distance to the center line/point
- μ = Snow load coefficient

Note that in principle, the reduction on the left hand side in Figure 92 ($0.5\mu_3$) is neglected, and the full load is used on both sides. This is done to reduce the number of load combinations.

Temperature loads

The thermal actions on the structure are determined according to the Eurocode NEN-EN 1991-1-5 (59). According to Table 5.2, the maximum outside temperature is $T_{max} + T_{1,2,3}$ where $T_{max} = 30°C$ and $T_{1,2,3} = 10/20\,°C$ depending on color of the structural elements. The minimum temperature is $T_{min} = -25\,°C$. This results in a maximum temperature difference of $65 - 75\,℃$. However, the installation temperature is always between 0 and 30 ℃. Resulting in a maximum temperature difference of 40 to 50 ℃ expansion and -55 ℃ shrinkage. In cases where the structure is entirely enclosed within a controlled internal environment, the thermal loads are less extreme.

6.4 Load combinations

Similarly to the determination of the loads, the load combinations are determined according to the Dutch national annex of the Eurocode. Resulting in the load combinations for ULS as summarized in Table 6, and SLS as summarized in Table 7.

The consequence class is a user input in the reciprocal frame designer. The consequence class determines the factor K_{FI} (CC1: 0.9, CC2: 1.0, CC3: 1.1). Since the reciprocal structure is a roof structure, the ψ factor for the imposed loads in the ULS is 0. Other ψ factors for wind snow and temperature are 0 according to the Dutch national annex of the Eurocode. Therefore, all ψ factors are 0 for ULS.

	Permanent	Imposed	Wind	Snow	Temperature
LC1 (ULS)	$\kappa_{FI} * 1.35$	0	0	0	0
LC2 (ULS)	$\kappa_{FI} * (1.35 * 0.89)$	$\kappa_{FI} * 1.5$	0	0	0
LC3 (ULS)	$\kappa_{FI} * (1.35 * 0.89)$	0	$\kappa_{FI} * 1.5$	0	0
LC4 (ULS)	0.9	0	$\kappa_{FI} * 1.5$	0	0
LC5 (ULS)	$\kappa_{FI} * (1.35 * 0.89)$	0	0	$\kappa_{FI} * 1.5$	0
LC6 (ULS)	$\kappa_{FI} * (1.35 * 0.89)$	0	0	0	$\kappa_{FI} * 1.5$

Table 6: ULS load combinations used to find the maximum forces in the structure

	Permanent	Imposed	Wind	Snow	Temperature
LC7 (SLS)	1	0	0	0	0
LC8 (SLS)	1	0	1	0	0
LC9 (SLS)	1	0	1	0	0
LC10 (SLS)	1	0	0	1	0
LC11 (SLS)	1	0	0	0	1

Table 7: SLS load combinations used to find the deformations of the structure

The structure is checked for four wind directions; in both positive and negative x- and y-direction. The structure will also be checked for two types of snow loads, evenly distributed snow and accumulated snow. This results in a total of 13 load combinations for the ultimate limit state.

For timber design, the strength of the material that is used in the calculations depends on the load duration. This is done by introducing the modification factor (k_{mod}) that ranges from 0.6 (permanent action) to 1.1 (instantaneous action). The application of the k_{mod} factor will be considered in the structural calculations.

In the SLS load combinations, the imposed load is not considered. The reason for this is the fact that the imposed load only acts on the structure in the case of maintenance of the roof. All other factors are equal to 1.

6.5 Determining point loads

When the load distribution is known, the loads can be applied to the structure in the FEM model. As mentioned in the preliminary design, the point loads are assumed to act on the beam nodes. To obtain the load value and direction for each node, additional computation needs to take place.

To obtain the area of forces that acts on each node, a Voronoi diagram containing each of the points is made. A Voronoi diagram is a tessellation pattern in which the plane is subdivided in cells enclosing the portions of the plane that are closest to the points, see Figure 93 for an example Voronoi diagram.

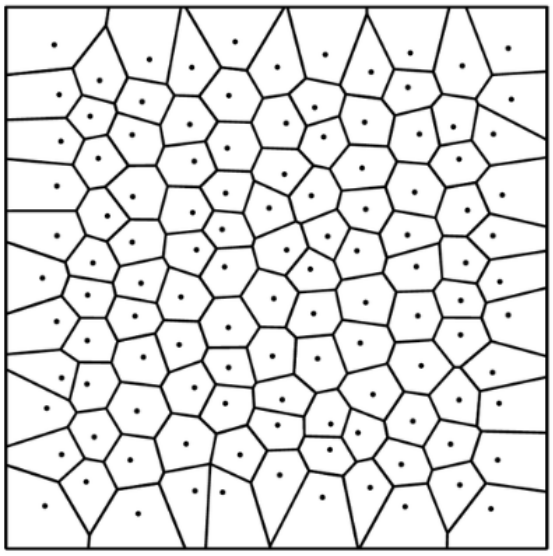


Figure 93: Example Voronoi diagram used to obtain the area per node (60)

Using the area and location of the node, the exact point load can be determined for each of the nodes. For all load cases except wind loads, the forces act downwards (in the -z direction).

For wind loads, the forces act normal to the surface of the curvature of the surface. To obtain the vectors normal to the surface at each node, the cross-product method is used. To compute the normal, the covariance matrix of the neighbouring vectors is calculated. After that, the eigenvector corresponding to the smallest eigenvalue is searched, resulting in the normal direction.

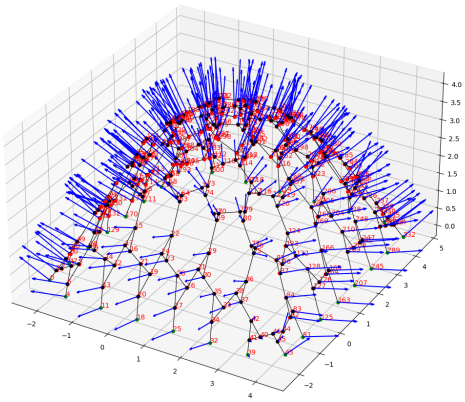


Figure 94: Example of normal vectors at each node for a reciprocal frame

Figure 94 shows this method being applied to a curved reciprocal frame. As visible in the figure, the normal vectors can quite accurately be determined using the method described above.

Due to limitations in the FEM software, the wind node forces are split into a separate force in the x-,y- and z-direction. This results in the loading as visualized in Figure 95.

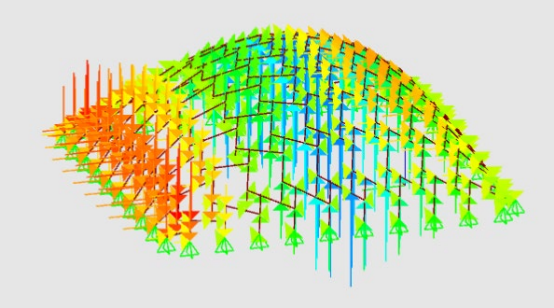


Figure 95: Example wind loading in NextFEM

Local moment caused by cladding eccentricity

As mentioned in chapter '4.3 Cladding', local bending moments are created at the places where the cladding is connected to the structure due to the fact that the cladding is placed on the exterior.

Wind loads are acting normal to the plane of the reciprocal frame, therefore no additional bending moments are generated in those cases. However, snow loads do not perpendicular to the reciprocal frame. In those cases, the additional local bending moment must be calculated.

The bending moment is calculated by calculating the angle between the force and the normal vector at the node.

$$\cos\theta = \frac{a \cdot b}{|a||b|}$$

Using the angle, the load vector can be decomposed into a component acting parallel to the normal vector $v_{\parallel}$ and a component acting perpendicular to the normal vector $v_{\perp}$. The latter can be split into a x-and y-component ($v_{\perp,x}$ and $v_{\perp,y}$) to be able to calculate the bending moment in the two main directions:

$$M_x = |v_{\perp,x}| \cdot a$$

$$M_y = |v_{\perp,y}| \cdot a$$

Where:

- a = arm of the cladding to the neutral axis of the beam ($= \frac{h_{beam}}{2} + 20mm$)
- $|v_{\perp,x}|$ = length of the x-component of the perpendicular component of the force vector
- $|v_{\perp,y}|$ = length of the y-component of the perpendicular component of the force vector.

Data storage

The load data is stored in the node database, where the load and moment value for each load case is stored, as well as the normal vector.

6.6 Obtaining FEM forces

With all the information provided above, NextFEM can compute the internal forces in each of the members. This data is retrieved from NextFEM and stored in the beam data using the FEM beam ID's stored in the beam data.

Due to the loads only being applied at the nodes, the extremes are always found at the begin, end or intermediate nodes. This means that for each of the force components (N, V_x, V_y, M_y, M_z and T) only the value at each of the nodes must be stored. For the bending moments,

the bending moment can be different at the left hand or right hand side of a node (due to the eccentricity). In those cases the most extreme value is stored.

6.7 Flow of forces

Before being able to start optimizing the reciprocal structure, it is important to understand how the forces flow through the structure. The curvature of the structure has a large influence on the flow of forces. Therefore two reciprocal frames are discussed and compared; one with a small (near-zero) eccentricity, and one with a large eccentricity (0.1 and 60mm respectively.

The flow of forces is also dependent on the load case, the load cases with an interesting flow of forces are also discussed in more detail.

For this comparison an 8x8m reciprocal frame with an edge size of 1m are compared. The loads on the structure are determined with the following parameters:

- Consequence class: CC2
- Wind area: II
- Unbuilt
- Rough surface

Normal forces

The normal forces in a reciprocal frame with very little curvature, exposed to snow loads, are visualized in Figure 96. The normal forces in this structure are relatively small. A fan-like pattern can be observed in the normal force diagram. This means that the normal force is not equal in all of the elements, despite the uniformly distributed load.

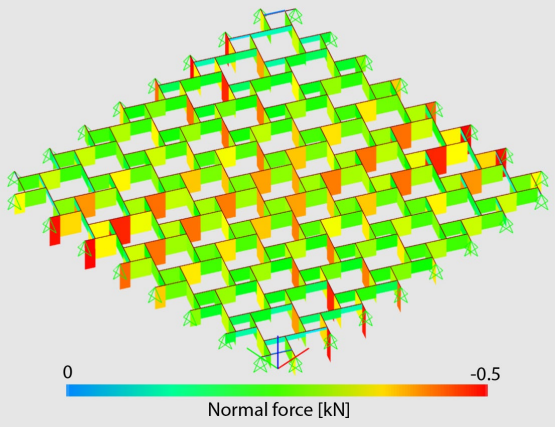


Figure 96: Normal forces in an 8x8m square reciprocal frame, edge size = 1m, e = 0.1mm, load = snow load

In Figure 97 the normal force diagram for the same structure with a larger eccentricity is visualized. The same fan-like behaviour can be observed. This means there is a stiffer load path along these fan-lines. Additionally, the normal forces are significantly higher when the reciprocal frame is more curved.

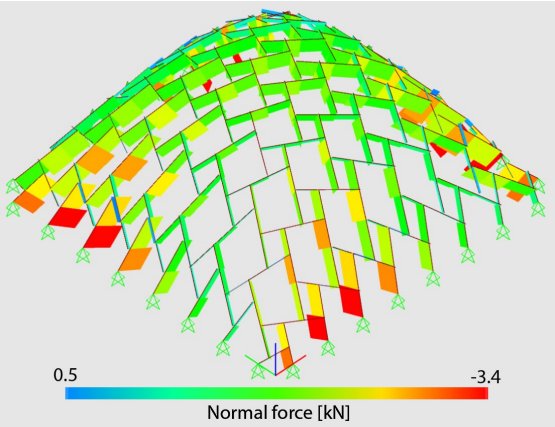


Figure 97: Normal forces in an 8x8m square reciprocal frame, edge size = 1m, e = 60mm, load = snow load

The normal force behaviour as observed can be explained by looking at the deformation under loading (Figure 98). The structure seems to rotate in the xy plane (as visualized with the arrow) due to the snow loading. The reason for this rotation is the fact that the elements are relatively flexible in the weak axis. This rotating deformation causes the fan-like normal force behaviour.

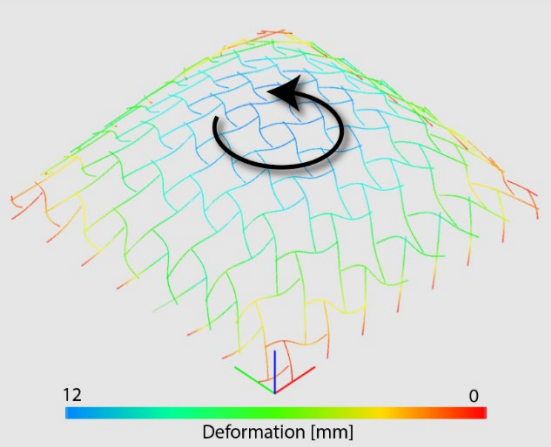


Figure 98: Deformation of an 8x8m square reciprocal frame, edge size = 1m, e = 60mm, load = snow load

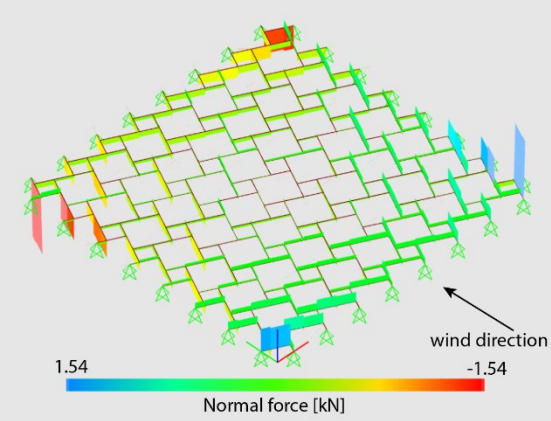


Figure 99: Normal forces in an 8x8m square reciprocal frame, edge size = 1m, e = 0.1mm, load = wind load (flat roof)

In the case of wind loads, a similar kind of pattern is observable for both the low and high eccentricity reciprocal frame (see Figure 99 and Figure 100). In that case however, the normal forces are opposing each other. Resulting in compression on the one side and tension on the other. This is likely caused by wind friction since that is the only horizontal component in case of a flat roof. The wind friction also causes local bending moments due to the cladding eccentricity. This generates the most extreme normal forces at the corners of the frame. Note: the wind force for the flat roof is significantly different than the wind load on the dome. The comparison is made to qualitatively compare the internal forces.

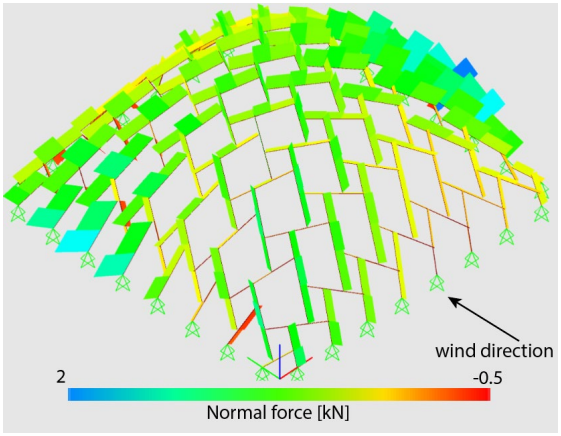


Figure 100: Normal forces in an 8x8m square reciprocal frame, edge size = 1m, e = 60mm, load = wind load (dome)

Moments

For a reciprocal frame with a low eccentricity, the bending moments in the strong beam axis (M_{zz}) behave as expected; the more towards the center, the higher the bending moments (see Figure 101). Due to the hinged inter-member behaviour (and the almost zero eccentricity), there are no moments at the beam ends.

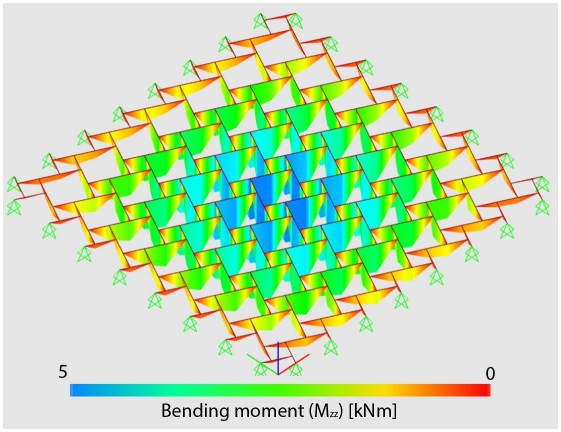


Figure 101: Bending moment (M_{zz}) in an 8x8m square reciprocal frame, edge size = 1m, e = 0.1mm, load = snow load

When the eccentricity between the members is increased, and there thus is a large curvature in the reciprocal

frame, the normal force distribution changes significantly. Firstly, the maximum bending moment is decreased significantly (see Figure 102). Additionally, a negative bending moment is created. This is caused by the fact that the load is not uniformly distributed over the whole area (snow loads may be neglected when the surface angle is larger than 60 degrees).

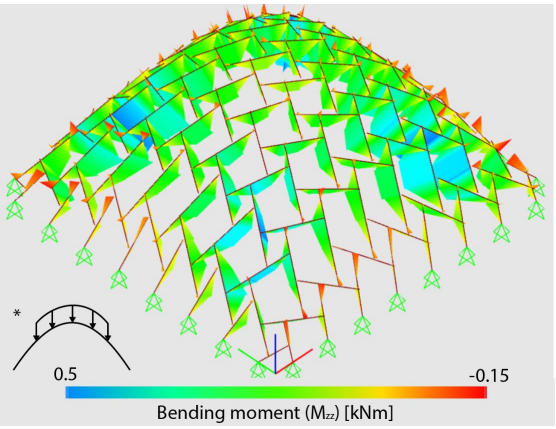


Figure 102: Bending moment (M_{zz}) in an 8x8m square reciprocal frame, edge size = 1m, e = 60mm, load = snow load * = load diagram

Additionally, it can be observed that the bending moment at the ends of the beams are not necessarily zero. This is caused by the combination of eccentricity and normal force that acts on these locations.

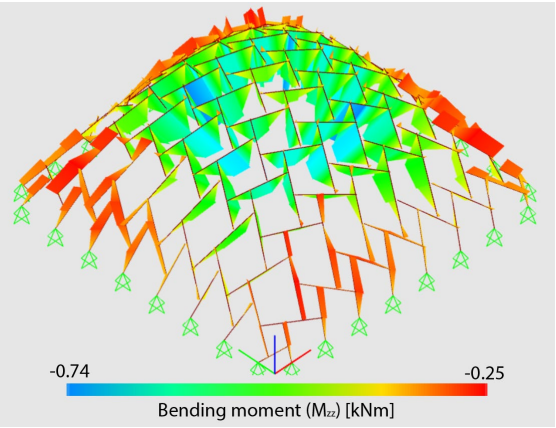


Figure 103: Bending moment (M_{zz}) in an 8x8m square reciprocal frame, edge size = 1m, e = 60mm, load = accumulated snow load

The effect of negative bending moment is increased when the accumulated snow load is considered (see Figure 103). The reason for this is the fact that this type of loading creates bending out of the plane of the 'dome'. So even though the total force on the structure is lower, the extreme bending moments are higher.

When looking at wind loads, the behaviour of the bending moments depend on the type of wind loading that is considered. For low eccentricity reciprocal frame, the wind loading considered is a combination of wind suction and compression as on a flat roof. This results in the moment distribution as visualized in Figure 104.

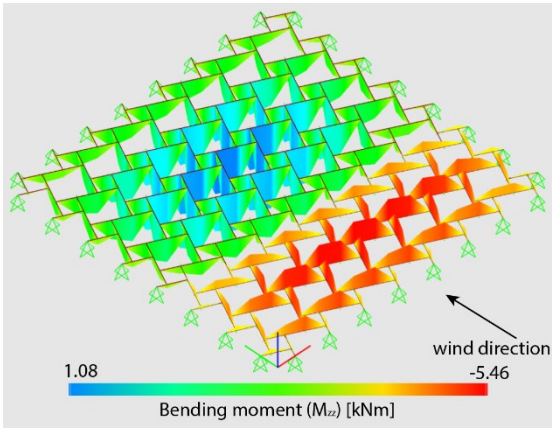


Figure 104: Bending moment (M_{zz}) in an 8x8m square reciprocal frame, edge size = 1m, e = 0.1mm, load = wind load

When the reciprocal frame has more curvature, the bending moment due to wind loads changes significantly. The wind loading changes to wind loads associated with a dome. The resulting bending moment behaviour (see Figure 105) is caused by the same rotation effect as when looking at the normal forces. Due to wind suction, this rotation is reversed, resulting in the pattern being opposing the pattern when considering snow loads.

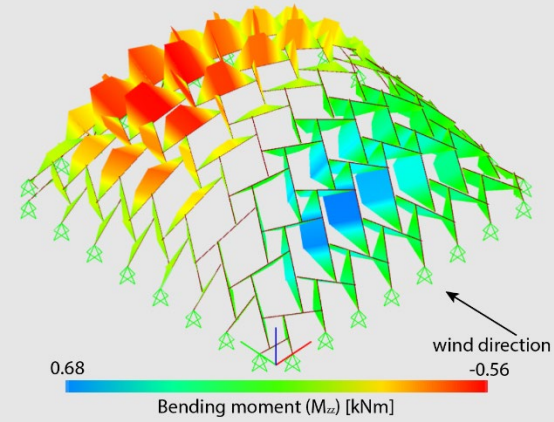


Figure 105: Bending moment (M_{zz}) in an 8x8m square reciprocal frame, edge size = 1m, e = 60mm, load = wind load

When looking at the bending in the weak axis (M_{yy}), the behaviour between a low and high eccentricity reciprocal frame is the most significant. When the eccentricity is 0.1mm, the bending in the weak axis is negligible. However, for reciprocal frames with a larger eccentricity, bending in the weak axis becomes more significant (Figure 106).

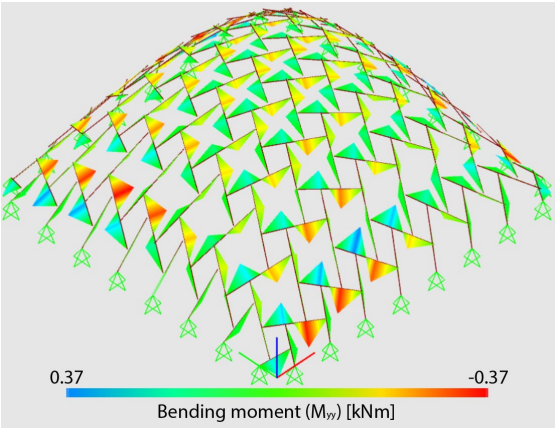


Figure 106: Bending moment (M_{yy}) in an 8x8m square reciprocal frame, edge size = 1m, e = 60mm, load = snow load

This out of plane bending is caused by the normal forces in the adjacent beams. Since the beams connect at intermediate points on the beam, this normal force must be transferred by bending. For planar elements, this bending may be rather unfavorable.

Deformations

As visible in Figure 98, the deformation of the reciprocal frames is mostly caused by rotation when the eccentricity is large. The deformation in z-direction when the structure is exposed to snow load is only 12mm ($< \frac{span}{500}$). This means that the deformations are not extremely large.

When the eccentricity in the reciprocal frame is small, this rotating behaviour is completely gone. The deformation in that case is only caused by bending of the elements (see Figure 107). In result, the displacement in z-direction is significantly larger (170mm ($> \frac{span}{500}$)). Therefore, curving the reciprocal frame results in significantly smaller deformations.

Additionally, the deformation behaviour for a low-eccentricity reciprocal frame, may result in water accumulation.

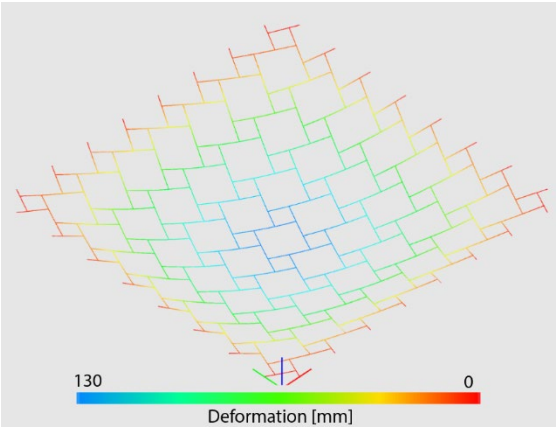


Figure 107: Deformation of an 8x8m square reciprocal frame, edge size = 1m, e = 0.1mm, load = snow load

Reaction forces

For a flat reciprocal frame, the reaction forces are almost purely in z-direction, except when for instance wind friction acts on the surface. Figure 108 shows the reaction forces in z-direction for a low eccentricity reciprocal frame loaded

by snow. The reaction force is not equal in every support. The more to the center of an edge, the higher the reaction force.

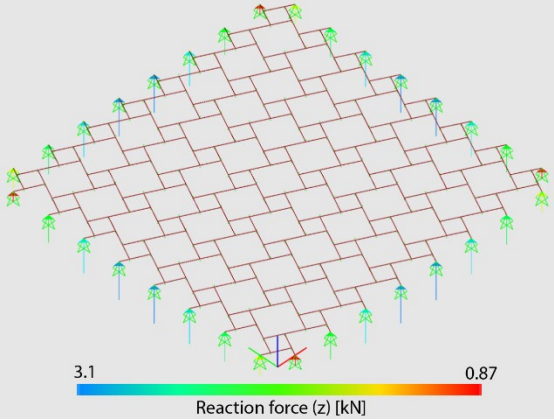


Figure 108: Reactions in z-direction for an 8x8m square reciprocal frame, edge size = 1m, e = 0.1mm, load = snow load

In the reactions of a reciprocal frame with a large eccentricity (Figure 109), the rotation behaviour can again be observed. The horizontal forces are counteracting the rotation that takes place.

Additionally, the reactions in z-direction are not larger in the center of the edges, but more towards one side.

Tessellation pattern

The tessellation pattern does not influence the structural behaviour for a non-curved reciprocal frame. The bending moment behaviour remains the same.

For curved reciprocal frames, the internal forces change when the pattern changes. When looking at the triangular reciprocal frame pattern, the rotating deformation is not there because the internal rotations are counteracting each other (see Figure 110). This means that triangular reciprocal frame elements add stability against rotation, resulting in a more uniform loading. The relation between bending in the strong- and weak beam axes remains.

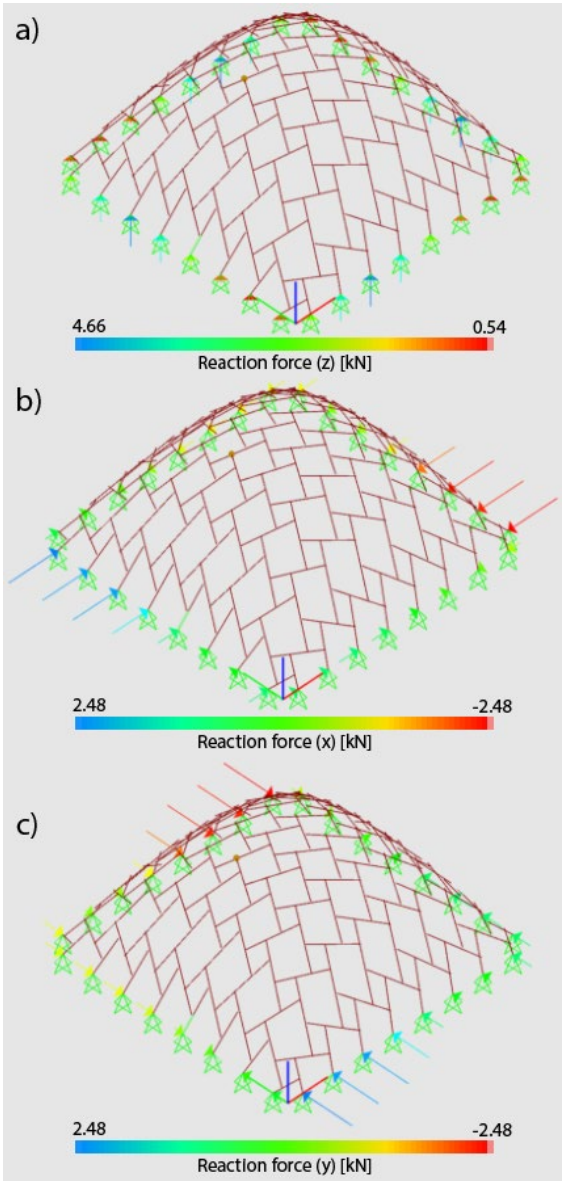


Figure 109: Reactions for an 8x8m square reciprocal frame, edge size = 1m, e = 60mm, load = snow load. a) = reaction in z-direction, b) = reaction in x-direction, c) = reaction in y-direction

Similarly, for patterns containing hexagons, more stability is generated in the frame. this results in a uniform flow of forces (see Figure 111). Therefore, it can be concluded that the square pattern reciprocal frame produces the least stability resulting in less uniform loading.

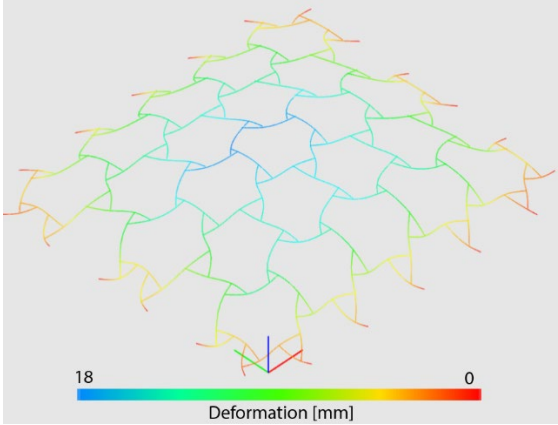


Figure 110: Deformation of an 8x8m triangle reciprocal frame, edge size = 1m, e = 25mm, load = snow load

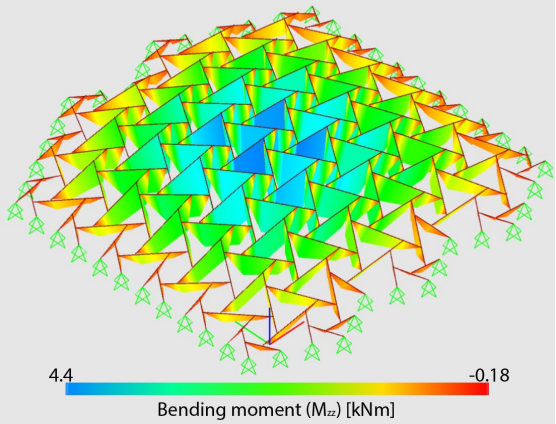


Figure 111: Bending moment (M_{zz}) in an 8x8m hexagonal reciprocal frame, edge size = 1m, e = 25mm, load = snow load

6.8 Structural checks

During the determination of the dimensions of all beam elements Eurocode unity checks are performed to ensure the integrity of the beam elements under the loading conditions. Since all elements are made from timber (plywood), Eurocode 5 is used to ensure compliance with the prescribed requirements (38). Eurocode 5 provides a set of guidelines and specifications for the design and construction of timber elements, including beams. The unity checks defined in Eurocode 5 are used to verify that the beam's strength and serviceability limits are not exceeded.

The first set of unity checks that are performed on each beam are the checks on the global cross section. For these checks, the holes in the beam are neglected.

Global section checks

Due to the nature of reciprocal structures, pure compression and/or tension never exists in the structure. Therefore, the beams are checked for a combination of bending and compression and or tension, according to NEN-EN 1995-1-1 6.2.3 and 6.2.4. As mentioned previously, the complete cross-section without the holes is considered.

Additionally, the section without holes is checked on shear in both directions according to NEN-EN 1995-1-1 6.1.4 and on torsion according to NEN-EN 1995-1-1 6.1.8.

Stability checks

The structural elements must also be checked on stability to prevent (local) buckling of the structure. Firstly, stability with biaxial bending is considered (acc. NEN-EN 1995-1-1 6.3.2). In principle, the buckling length of each of the beams is taken as the system length ($L_{eff} = L$). However, there are some load conditions where other buckling lengths apply.

In Figure 112, the typical normal force distributions are visualized. In each of these cases, another buckling length is considered (since not every part is loaded in compression).

In case a) the buckling length is equal to the system length, where the applied

force in the calculations is the largest normal force in the beam.

In case b), only the begin and end part are loaded in compression. Therefore, only buckling in these parts is considered. With one end connected to the rest of the beam, this connection can be considered fixed. This results in $L_{eff} = L_{part} * 0.7$.

In case c), 2 adjacent parts are loaded in compression. The end that is connected to the part of the beam loaded in tension can be considered fixed. This thus results in $L_{eff} = (L_{part1} + L_{part2}) * 0.7$.

Finally, there are also cases where the beam is loaded in pure tension (case d)). In those cases, buckling may be ignored.

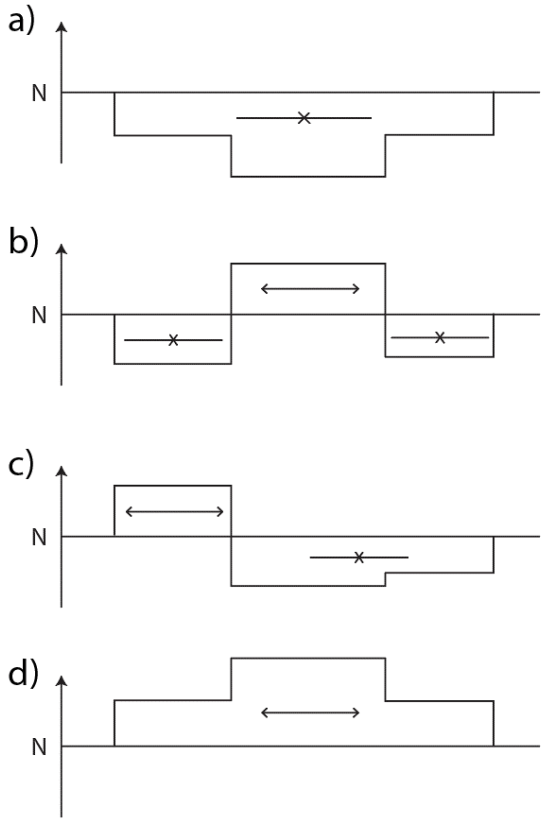


Figure 112: Typical normal force distributions in reciprocal beam elements

The holes in the beam may also result in a reduced buckling resistance. This reduction is also considered in the computation of the buckling resistance in cases a and b. To determine the reduced buckling resistance FEM calculations must be performed.

To reduce the computation time for the unity checks, these FEM calculations have been performed in advanced for the whole design range of the holes. To calculate the reduced buckling resistance caused by the holes in the beam, a multi- and cross polynomial regression on the FEM data has been performed. The model predicts the buckling load of the element and compares it to the same element without holes.

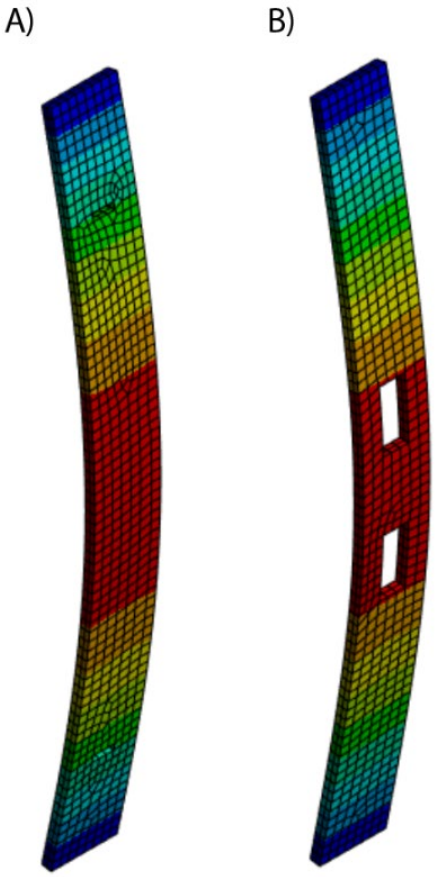


Figure 113: Buckling deformation according to Ansys model where the buckling reduction is a) 0.97, b) 0.79

To train the model, a parametric Ansys model has been set up to generate a dataset containing over 1000 samples. These samples encompass diverse combinations of the specified parameters, effectively capturing the interaction among parameters. Figure 115 shows a schematization of the FEM calculations that have been performed.

The analysis takes into account the ratio of the hole width to beam width λ_{width}, the ratio of the hole height to column height λ_{height} and the ratio of the distance to the edge of the beam to the column height λ_{dist} . A parameter sensitivity analysis has been conducted, revealing that the eccentricity of the hole has no significant influence on the result of the buckling load. Additionally, column dimension have no influence since the gap dimension are taken as ratios instead of dimensions.

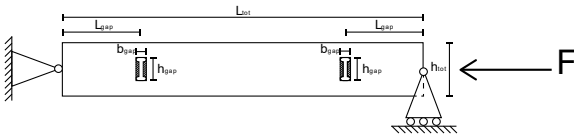


Figure 115: Schematization of Ansys model with $\lambda_{width} = L_{tot}/b_{gap}$, $\lambda_{height} = h_{tot}/h_{gap}$ and $\lambda_{dist} = L_{gap}/L_{tot}$

A multi-and cross polynomial regression has been performed to account for nonlinearity and interactions among parameters. The model establishes relationships that enable the estimation of the reduced moment of inertia with a high degree of accuracy. The result of the model is described in the following equation:

$$\alpha = 1.114 - 0.297 * \lambda_{width}^2 + 13.34 * \lambda_{height}^2 - 0.29 * {\lambda_{dist}}^2 - 4.753 * \lambda_{width} * \lambda_{height} - 0.496 * \lambda_{width} * \lambda_{dist} - 4.682 * \lambda_{height} * \lambda_{dist}$$

The coefficient of determination (R^2) is 0.97, which is close to 1 meaning that there is a strong correlation between predicted and observed data. Additionally, a low standard deviation of 0.05 underscores the model's precision in approximating the actual outcomes

Since the buckling resistance is linearly dependent on the second moment of area of a column (I), the reduced buckling resistance is simulated by reducing the moment of inertia with the predicted value α: $I_{red} = I * \alpha$.

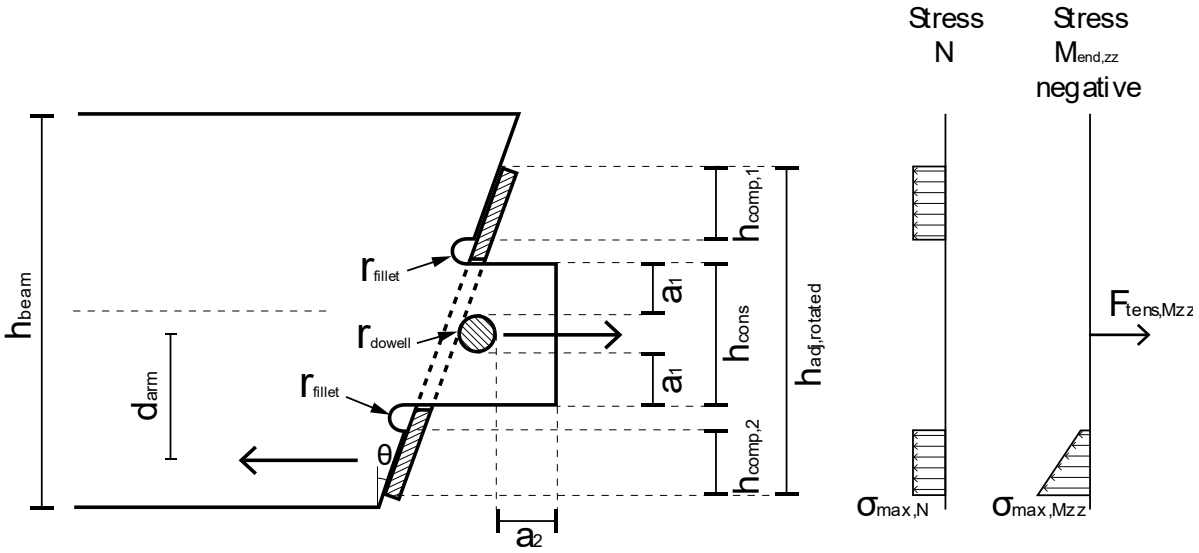


Figure 114: Dimensions and internal forces of tenon, schematized

Tenon checks

The beams are supported at the ends with a part that is lower than the main section. To make sure that tension can flow through the beam, the beam is fastened with a dowel through the tenon. The internal forces in this tenon cannot directly be calculated from the FEM model, due to the way the connection at the end of the beam is designed.

As mentioned in the preliminary design, the connections are considered to be hinged. However, still some moment is transferred through the tenons due to the inter member eccentricity. Additionally, to be conservative, 5% of the bending in the middle of the beam is applied at the ends.

These tenons are considered to be connection checks, meaning that the partial factor for these checks is $\gamma_M = 1.3$.

Determining tension force in the tenon

Figure 114 shows a schematization of the end connection of the beam. The connection can transfer bending moment in the strong direction by creating an arm between the dowel and the compressive area.

To compute the tensile force within the connection due to bending in the strong direction, it is assumed that the dowel is the sole component responsible for transferring tension, acting at a single point. This assumption leads to a linear stress distribution either in the upper or lower compression region (denoted as $h_{comp,1}$ or $h_{comp,2}$), depending on the direction of the bending moment. To calculate $F_{tens,Mzz}$ and the maximum compression stress $\sigma_{max,Mzz}$,the neutral axis for bending around the tension point and the compression area needs to be determined.

To obtain the normal force and stresses due to bending moment, additional computation are required. In principle, the forces in the tenon will be limited to pure tension and shear.

Figure 116 depicts two scenarios for calculating the forces at the beam end. The neutral axis can in principle be calculated using $y_{cg} = \frac{2}{5}d$. However, this

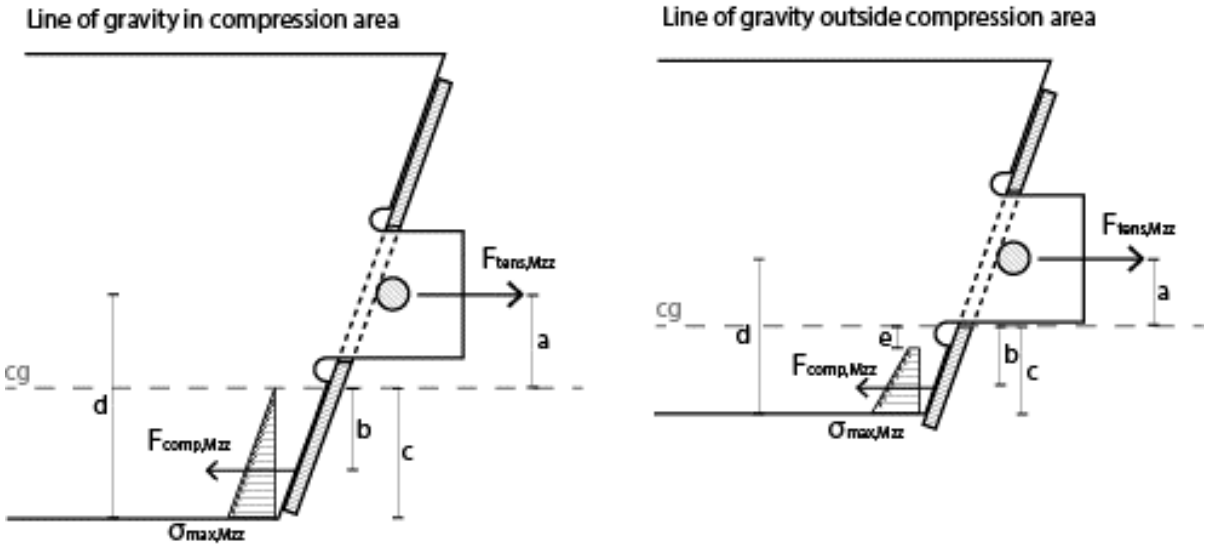


Figure 116: cases for line of gravity at the inter-member connections where line of gravity is in compression are (left) or outside the compression area (right)

formula may not apply when the neutral axis falls outside the compressive area, as the compressive stress distribution is not purely triangular in that case.

In cases where the line of gravity does not lie within the compressive area, it is impossible to directly ascertain its position using a formula. In such instances, we must make an assumption and verify whether a = b. In this project, this determination is made through an iterative process involving various assumed positions for the neutral axis. When the distance to the tensile force equals the distance to the compressive force, the assumed neutral axis is considered to be correct. When the position of the neutral axis is known, the forces $F_{tens,Mzz}$ and $F_{comp,Mzz}$ can be computed by dividing the moment over the length of the arm between the forces. Using $F_{comp,Mzz}$, in turn, the compressive stress can be calculated using the stress profile.

Tension checks

With the force $F_{tens,Mzz}$ known, the tension in the tenon can be checked. At the place of the dowel, the cross section is weakened. This area is used to determine the tensile stress: $\sigma_{t,Ed} = F_{t,Ed}/A_{net}$. According to Eurocode 5, there is no requirement to consider stress concentrations in these types of connection checks.

The tension forces in the tenon also cause stress concentrations at the locations indicated with σ_{peak} in Figure 117. This stress concentration is not part of standard Eurocode procedure, and will therefore be checked.

Since the checks on all elements need to be able to be performed rather quickly (to speed up the iterative processes), the stress concentrations are predicted using a predictive model. This predictive model is trained using over 1000 Ansys simulations. It considers the following parameters/ratios:

- h/H = ratio tenon height/beam height
- b/H = ratio beam width/beam height
- r/h = ratio corner radii/tenon height
- θ_1 = in-plane rotation of beam end
- θ_2 = out-of-plane rotation of beam end

From an Ansys parameter sensitivity analysis, it is found that all variables mentioned above have a large significance on the resulting peak stress. The methodology of creating this predictive model is discussed in more detail in chapter '6.9 Stress concentration prediction'.

The predictive model calculates a stress concentration value k_t so that: $\sigma_{peak} = k_t \sigma_{nom}$. The predicted peak stress is in turn checked. This stress may not exceed the yield tensile stress of the material.

Tenon shear

One of the most important features of the tenon is the ability to transfer shear forces. This way the vertical forces on the beam can be transferred to the supports or supporting beams. The shear capacity of the tenon is checked according to Eurocode 5.

According to Eurocode 5; *for beams with rectangular cross-sections and where grain runs essentially parallel to the length of the member, the shear stresses at the notched support should be calculated using the effective (reduced) depth* h_{ef} (38). Additionally, a reduction factor k_v

needs to be calculated to reduce the shear capacity of the material. Eurocode does not explicitly explain why this reduction needs to be used, but it is likely to do with shear stress concentrations. The reduction factor k_v is calculated using NEN-EN 1995-1-1 formula 6.62, and should never by higher than 1.

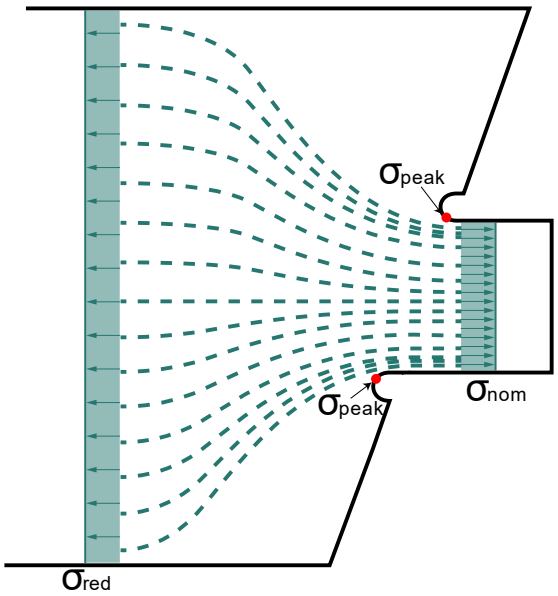


Figure 117: stress concentration in tenon due to tension

Support stresses

To be able to transfer shear forces through the tenons, the forces are transferred between the member with compression on a rather small areas (see Figure 118).

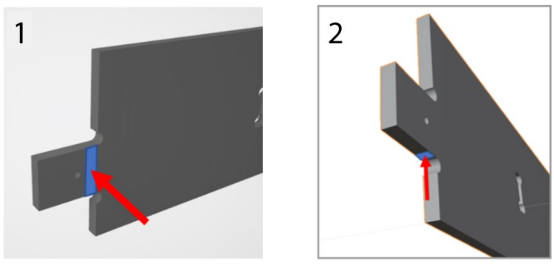


Figure 118: Support stresses at tenons

For the first case, the stresses act perpendicular to the grain, therefore in these cases the normal stress may not exceed the compressive yield stress perpendicular to the grain ($f_{c,0,d}$).

In the second case, the stresses act parallel to the grain, which means that the stresses may not exceed the compressive yield stress parallel to the grain ($f_{c,90,d}$).

Dowel checks

With F_{tens} known, the dowels used to transfer the tension force can also be checked. These dowels operate by transferring the tension forces across two shear planes.

To ensure the adequacy of the connection's design, Eurocode 5 offers several checks. Initially, specific boundary conditions, known as edge distances, are introduced. According to NEN-EN-1995-1-1, table 8.5 (38), the distance from the unloaded edge to the dowel should be a minimum of three times the dowel diameter.

The dowel itself undergoes two critical checks: one for shear in the two shear planes and another for yielding under lateral loads.

Compression at beam ends

As indicated in Figure 114, at the end of the beam, there are compressive forces caused by compression in the beam and bi-axial bending at the beam end. The compressive stress due to normal force is calculated using:

$$\sigma_N = N_{beam}/((h_{comp,1} + h_{comp,2}) * b)$$

The stresses caused by bending in the strong axis, caused by M_z are calculated by calculating the second moment of area of the compressive side of the

beam $I_{z,end}$. The maximum stress is found using the following formula:

$$\sigma_{Mz} = \frac{M_{z,end}}{2*I_{z,end}} * c$$

The maximum total bending stress is found by superposition. This stress should be lower than the resistance perpendicular to the grain $f_{c,90,d}$. This is perpendicular to the grain because this stress acts perpendicular to the grain on the adjacent beam. Resulting in the following unity check:

$$\sigma_{comp,Ed} = \sigma_N + \sigma_{Mz} \leq f_{c,90,d}$$

Stress concentration around holes

The holes in the beams, which are utilized to support other beams, introduce stress concentrations around the holes. There are two distinct types of stress concentrations, each occurring at a different location around the gap:

1. **Normal stress concentration:** This type of stress concentration arises due to the presence of the hole and its impact on the distribution of normal and bending stresses within the beam.
2. **Shear stress concentration:** The shear stress concentration is another consequence of the holes and is associated with the distribution of shear stresses due to bi-axial shear and torsion. Additionally, the local shear caused by the point load of the supported beam, only acts on the material below the gap, on two shear planes.

Normal stress concentrations

According to Eurocode 5, Linear elasticity may be assumed, this allows superposition of stress concentrations. To determine the normal stress concentrations, the stress concentration caused by normal force and bi-axial bending are thus combined.

From a predictive model, trained by 1.124 Ansys simulations, the stress concentration values are determined. The predictive model requires several variables as input (visualized in Figure 119):

- h/H: height ratio (height h is taken as height after rotation)
- r/h: radius ratio (with respect to rotated height)
- b/h: width ratio, where width is the total width of the gap
- d/H: d = beam thickness
- θ_1, θ_2, θ_3: hole rotations

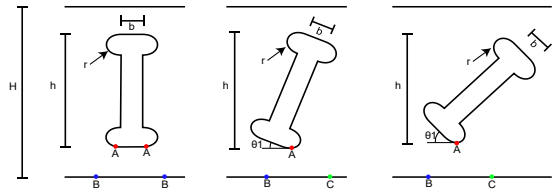


Figure 119: Variables used to determine stress concentrations around the hole

For the hole rotations, it is important to note that they are chained Euler rotations, meaning that one rotation will influence the other. The rotations are performed in the order: rotation around x-axis, rotation around z-axis and rotation around y-axis. The rotations are based on the local coordinate system of the beam.

When the stress concentrations are calculated, the peak stress can be calculated by multiplying concentration value K_t with the applied stress, contrary to the more conventional method of multiplying with the nominal stress. The reason for this is the fact

that it is difficult to manually determine the nominal stress when the hole is rotated. This results in the following set of normal peak stresses:

- $\sigma_{peak,N} = k_{t,N} * \sigma_{applied,N}$
- $\sigma_{peak,My} = k_{t,My} * \sigma_{applied,My}$
- $\sigma_{peak,Mz} = k_{t,Mz} * \sigma_{applied,Mz}$

Resulting in the following peak stress, and unity check:

$$\sigma_{peak,\sigma} = \sigma_{peak,N} + \sigma_{peak,My} + \sigma_{peak,Mz} \leq f_{t,0,d}$$

Shear stress concentrations

For the shear stress concentrations, the same variables are used to predict the stress concentration values. This results in the following set of equations:

- $\sigma_{peak,T} = k_{t,T} * \sigma_{applied,T}$
- $\sigma_{peak,Vy} = k_{t,Vy} * \sigma_{applied,Vy}$
- $\sigma_{peak,Vz} = k_{t,Vz} * \sigma_{applied,Vz}$

Resulting in the following peak stress, and unity check:

$$\sigma_{peak,\tau} = \sigma_{peak,T} + \sigma_{peak,Vy} + \sigma_{peak,Vz} \leq f_{v,d}$$

These peak stresses do not occur at the same locations as the normal stress concentrations occur, as visualized in Figure 120.

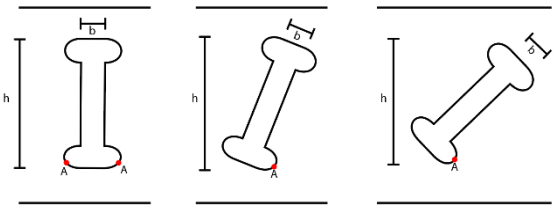


Figure 120: Locations for shear stress concentration

Additionally, shear stresses caused by the local point load occur in the two shear planes situated below the hole (see Figure 121). These shear stresses are calculated separately from the stress concentration, because these will not take place in the same place. The shear stress unity check in this point will be calculated using the methodology similar to the tenons. This means that reduction factor k_v is also calculated for this location.

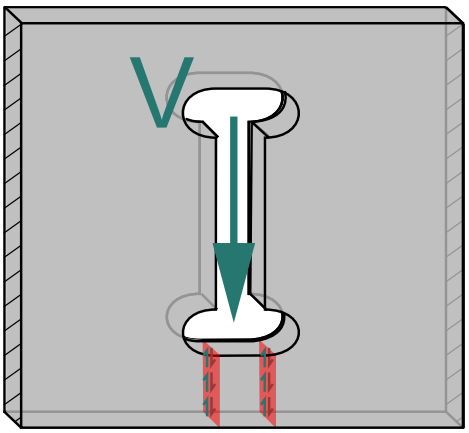


Figure 121: shear stresses due to local force

6.9 Stress concentration prediction

The stress concentrations mentioned in previous paragraphs can be determined using FEM calculations. However, the beam calculations are part of an iterative process, for instance for the cross section optimization. Therefore, FEM calculations for each separate element would require too much computation time. Too speed up the process of determining the stress concentration, a predictive model is made using 1.124 pre-calculated Ansys FEM calculations per load case.

The pre-calculated Ansys FEM calculations aim to discover the full design range of the holes in the beams (variable, range):

- Ratio h/H : [0.1,0.9]
- Ratio r/H : [0.05,0.3]
- Ratio h/b : [0.1,0.5]
- $\theta_1, \theta_2, \theta_3$: [0°, 45°]

Using the multiple pre-calculated Ansys simulations, a predictive model can be trained that predicts the stress concentration value K_t based on the known data. To make sure the predictive model is accurate, the model is trained with 80% of the data and tested with 20% of the remaining data.

As mentioned previously, in the design with timber (or plywood), linear elasticity of the material may be assumed according to the Eurocode. Therefore, the stress concentration factors for each of internal force components may be calculated separately.

FEM model properties

The parametric FEM model calculates the stress concentration using a static structural solver. The material properties of the test material are summarized in Table 8.

Table 8: Material properties plywood in the FEM model. Derived from (36)

Density	ρ	460	kg/m^3
Young's modulus	E_1	6682	MPa
	E_2	5318	MPa
	E_3	5318	MPa
Shear modulus	G_{12}	350	MPa
	G_{13}	52	MPa
	G_{23}	38	MPa
Poisson ratio	v_{12}	0.04	
	v_{13}	0.191	
	v_{23}	0.248	

The FEM model setup is different for obtaining the K_t for the normal force stress concentration or the shear force stress concentration. The mesh size is set at 10mm for all elements. However, to prevent underestimation of the peak stresses, the mesh is refined at the locations where peak stresses occur. For this refinement a simple mesh sensitivity analysis is performed. The refinement is described as number of elements on each of the line segment. A qualitative graph of the sensitivity analysis performed for several layouts is displayed in Figure 122.

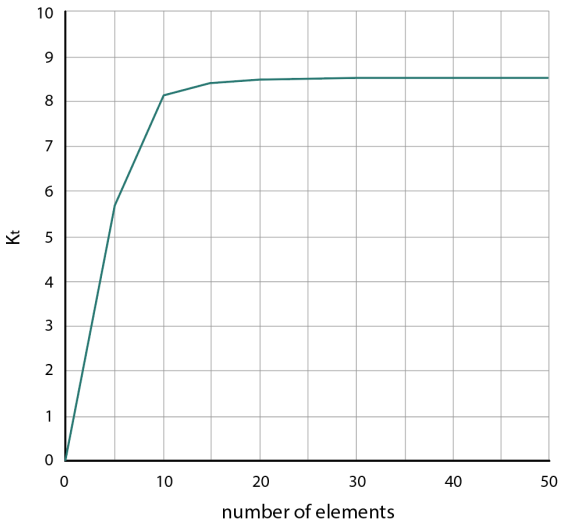


Figure 122: Quantitative graph for mesh size sensitivity analysis

Overall, this means that for 20 elements per line segment at the stress concentration, the resulting stress concentration may be assumed as accurate. This results in the meshing as visualized in Figure 123

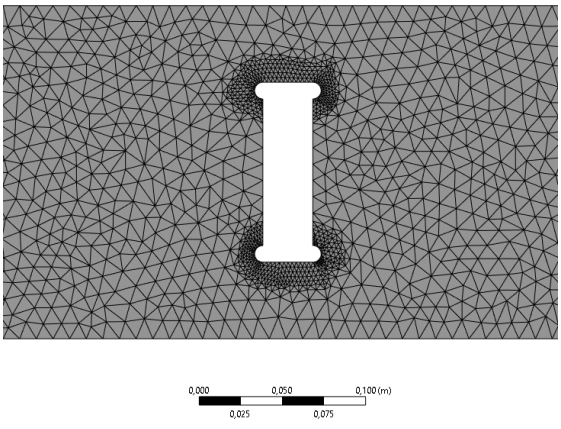


Figure 123: Mesh used for FEM calculations of Kt prediction, from Ansys

Normal force stress concentration

The normal force stress concentration consists of three components. A graphical representation of the 3d FEM

model to obtain the K_t values is schematized in Figure 124. The model has three load cases; normal force, bending in-plane and bending out-of-plane. The distance to the hole from the edges of the beam (L_{gap}) is at least equal to the beam height to make sure the stresses can be distributed well. The total beam length (L_{tot}) is minimally $2 \times h_{beam}$ but is selected to be at least 1m.

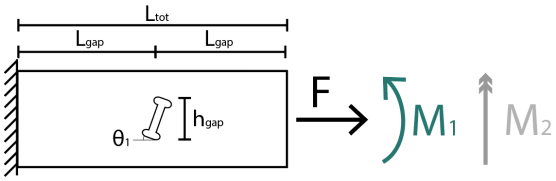


Figure 124: Ansys FEM mode setup for normal stress concentrations with three load cases. Black = Normal force, Green = Bending in-plane, Grey = Bending out-of-plane.

Stress concentration due to tension

In the case of pure tension the applied tension stress is simply calculated by $\sigma_{applied} = F/A$. The stress concentration value is calculated as $K_t = \sigma_{applied}/\sigma_{peak}$ where σ_{peak} is found by the FEM model.

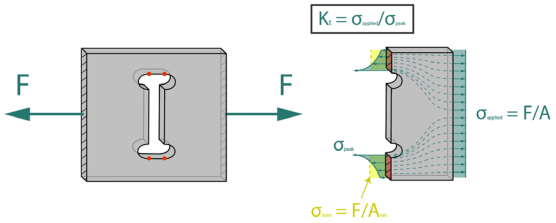


Figure 125: Graphical representation of stress concentrations due to tension

The resulting stress concentrations for h/b = 0.1 and θ = [0,0,0] are plotted in Figure 126. As visible in the figure, increasing the hole height significantly increases the stress concentration around the hole. Additionally, the influence of the fillet radius can be seen from the plot. Increasing the fillet radius can quite significantly decrease the K_t value, especially when the h/H ratio is relatively low.

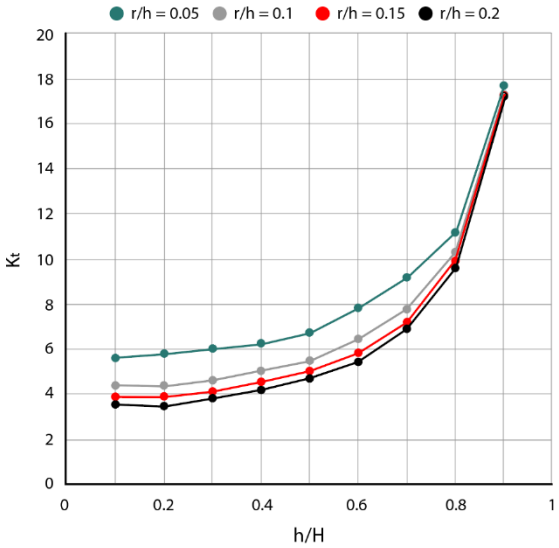


Figure 126: Stress concentration K_t around hole in pure tension, with h/b = 0.1 and θ = [0,0,0] for different values of r/h

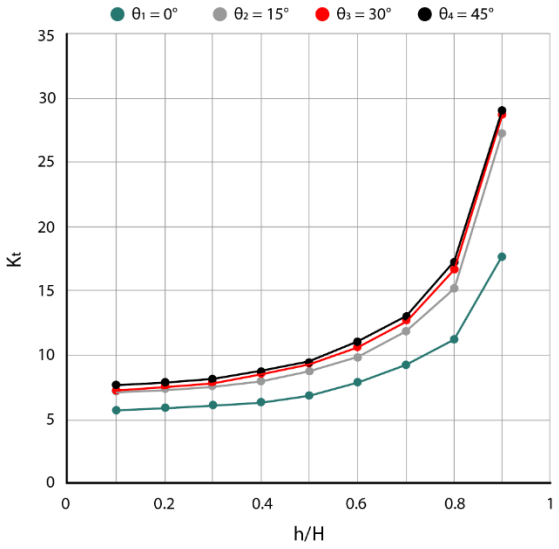


Figure 127: Stress concentration K_t around hole in pure tension, with h/b = 0.1, r/h = 0.1 and θ = [θ_1,0,0] for different values of θ_1

Figure 127 shows the same plot but now shows the results for different rotations around the main hole axis (with h/b = 0.1, r/h = 0.1 and θ = [θ_1,0,0]). Here it can be seen that rotating the hole also has a significant influence on the stress concentration, as more rotation results in higher stress concentrations. For the

other two rotations, the effects are similar, but less extreme.

Finally, the influence of ratio h/b is plotted in Figure 128 where the narrower the hole, the less significant the stress concentration.

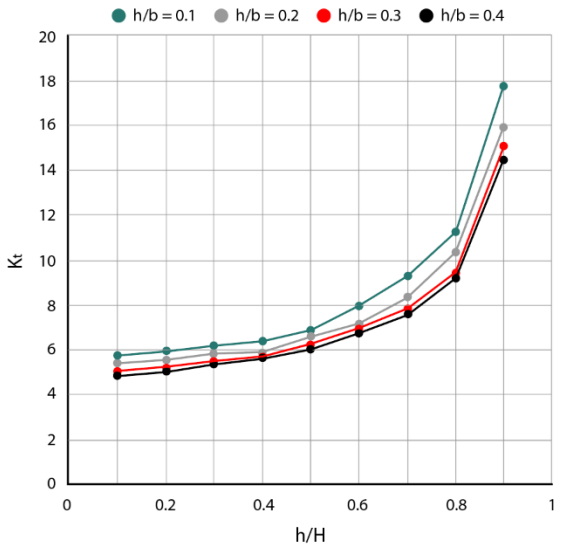


Figure 128: Stress concentration K_t around hole in pure tension, with r/h = 0.1 and θ = [0,0,0] for different values of h/b

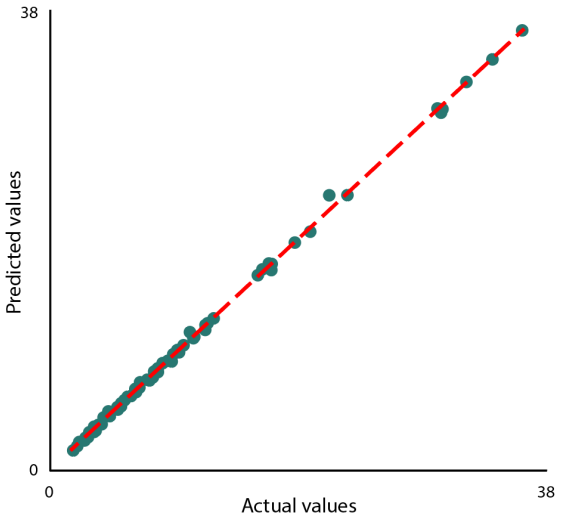


Figure 129: Predicted vs. actual K_t values for stress concentration due to pure tension, with ideal line (red)

As visible, all of the parameters influence the final value for the K_t. To overcome this complexity, a 6th order linear model is used to predict the value of K_t.

Figure 129 shows the accuracy of the predictive model, as the predicted values are almost equal to the actual (training) data. The red line indicates where the points should be for perfect predictions. This means that the predictive model can quite accurately predict the K_t values. The accuracy of the fit can also be expressed by the R^2 value: $R^2 = 0.98$.

Stress concentration due to bending in-plane

Similar to pure tension, bending in-plane also causes a stress concentration around the hole. The applied bending stress is simply computed using the Euler-Bernoulli beam theory. The stress concentration factor is then calculated by: as $K_t = \sigma_{applied}/\sigma_{peak}$

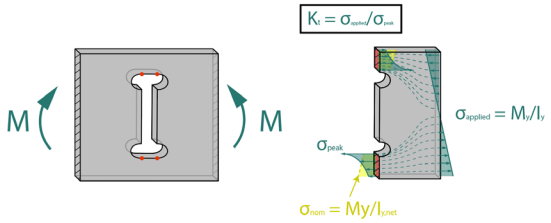


Figure 130: Graphical representation of stress concentrations due to bending in-plane

Similar influences for the parameters as for pure tension are found. The only difference here is that the stress peak can occur at the edge of the plate when the hole height is relatively small. Figure 131 shows this behaviour for a specific set of parameters. As visible in the figure, the stress concentration around the hole is below one for h/H < 0.32. this is caused by the fact that the stress concentration is based on the applied stress instead of the nominal stress.

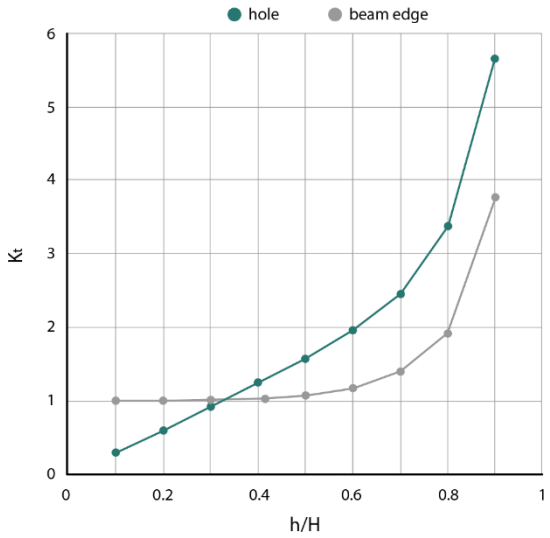


Figure 131: Stress concentration due to bending out-of-plane for h/b = 0.1, r/h = 0.1 and θ = [0,0,0] at beam edge and hole

For low h/H values, the stress concentration at the beam edge can be slightly above one, in those cases these values of K_t are applied in the calculations.

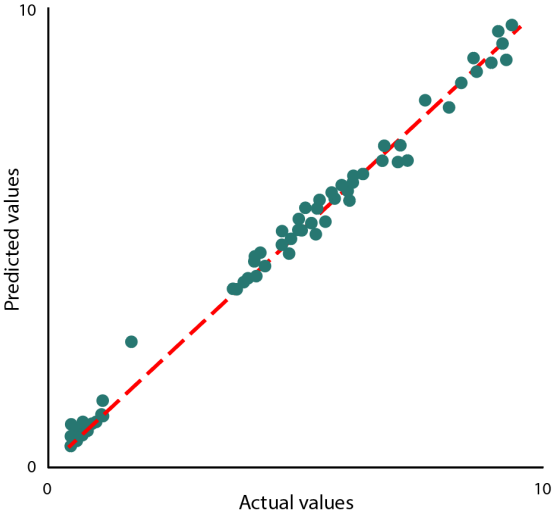


Figure 132: Predicted vs. actual K_t values for stress concentration due to bending in-plane, with ideal line (red)

Figure 132 shows the accuracy of the 6th-order linear predictive model for bending in plane. Similar to the predictive model for pure tension, the 6th order linear model can predict the K_t values quite accurately. The R^2 in this case is 0.95.

Stress concentration due to bending out-of-plane

Stress concentrations can also be caused by bending out of the beam plane. This behaviour is visualized in Figure 133.

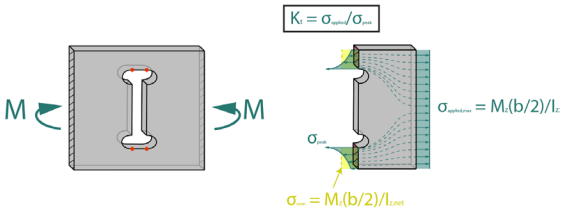


Figure 133: Graphical representation of stress concentrations due to bending out-of-plane

The influences of the parameters are different to those of bending in plane and pure tension force. The main differences are displayed in Figure 134. Firstly, a lower h/H might result in a higher stress concentration. Secondly, the influence of the width of the hole is much less significant. The influence of the rotations is similar to that of the other two types of stress concentrations.

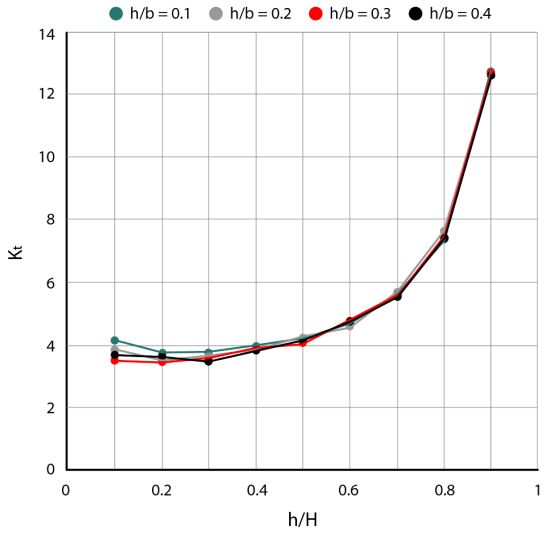


Figure 134: Stress concentration K_t around hole in bending out-of-plane, with r/h = 0.1 and θ = [0,0,0] for different values of h/b

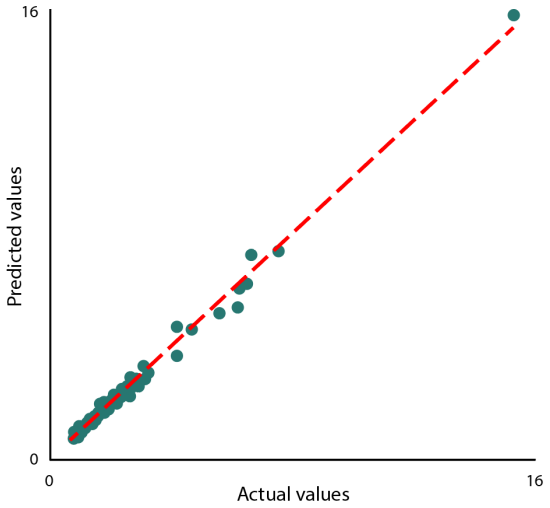


Figure 135: Predicted vs. actual K_t values for stress concentration due to bending out-of-plane, with ideal line (red)

Figure 135 shows the accuracy of the 6th-order linear predictive model for bending out-of-plane. The 6th order linear model can predict the K_t values quite accurately. The R^2 in this case is 0.94.

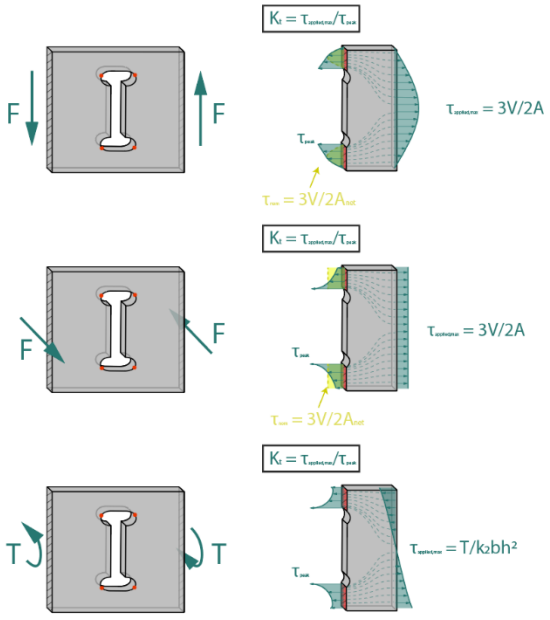


Figure 136: Graphical representation of stress concentrations due to shear in both directions and torsion

Shear force stress concentrations

Similar to the normal force concentration, predictive models are trained for predicting the shear stress concentrations. The influence of the parameters are similar to those of the normal force stress concentrations.

The shear force concentrations that are considered are displayed in Figure 136. These are also superimposed to find the true stress peak. A graphical representation of the 3d FEM model to obtain the K_t values is schematized in Figure 137. The model has three load cases; normal force, bending in-plane and bending out-of-plane. The edge distances are the same as those for the normal force stress concentrations.

Respectively, the trained models have the following R^2 values:

- Shear in-plane: $R^2 = 0.89$
- Shear out-of-plane: $R^2 = 0.95$
- Torsion: $R^2 = 0.90$

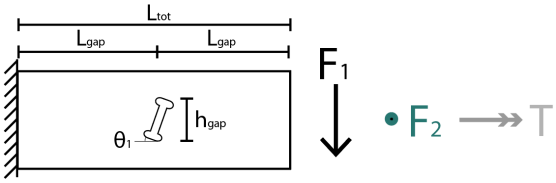


Figure 137: Ansys FEM mode setup for normal stress concentrations with three load cases. Black = Shear in-plane, Green = shear out-of-plane, Grey = torsion

Additionally, there are no large outliers that would result in unsafe design. This means that the resulting K_t values can thus be used rather safely for predicting the stress concentrations.

The stress concentration values for the shear are not as large as the K_t values for the normal stress concentrations. This means that the stress concentration caused by shear is not expected to be governing.

The location of the stress concentrations are not the same as the normal stress concentrations, therefore

these stress concentrations do not have to be combined in a structural check.

6.10 Section optimization

With all the unity check calculations in place, the cross sections can be optimized by finding the smallest possible beam dimensions that result in fulfilling all the unity checks. This optimization is performed by looping over the second phase of the reciprocal frame designer (Figure 86).

Optimization parameters

For the optimization of the beam dimensions, the following parameters can be optimized (see Figure 138):

- Beam height: h_{beam}
- Tenon heights: $h_{cons,l}$ and $h_{cons,r}$
- Dowel radii: $r_{dowel,l}$ and $r_{dowel,r}$
- Fillet radius: r_{fillet}

In practice, the fillet radius does not influence the stress concentrations very significantly (because the ratio h/H is often quite low). Therefore, the fillet radius is not included in the optimization process. This results in a total of 5 parameters to be optimized for each beam element.

Interdependencies

Optimizing each of the parameters using a mathematical minimization solver is not possible because the parameters of one beam influence the behaviour of adjacent beams. Mathematical minimization solvers can generate combinations of parameters that are not feasible.

The interdependencies of the parameters are summarized in Figure 139. As visible in the figure, the main

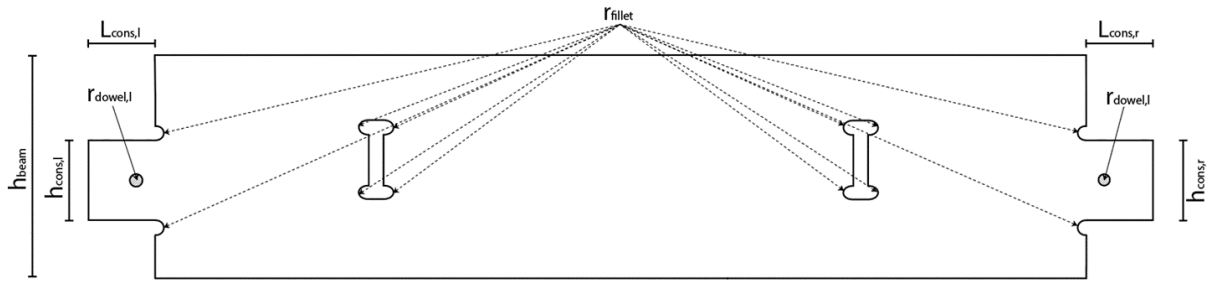
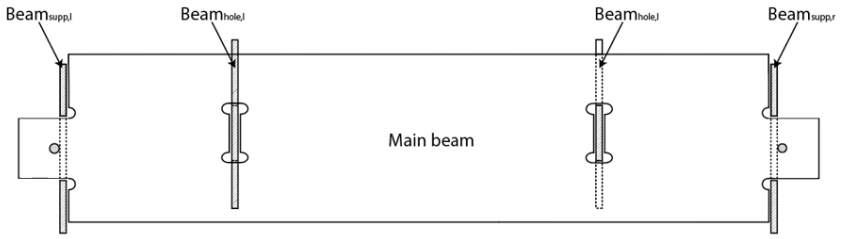


Figure 138: Beam with parameters that can be optimized in cross-section optimization



	Main beam			beam$_{supp,l}$		beam$_{supp,r}$		beam$_{hole,l}$		beam$_{hole,r}$	
	height	console,l	console,r	height	console	height	console	height	console	height	console
Main section checks	x							x	x	x	x
Dowel checks L	x	x		x							
Dowel checks R	x		x			x					
Console checks L	x	x		x							
Console checks R	x		x			x					
Connection check L	x	x		x							
Connection check R	x		x			x					
Stress concentration hole L	x								x		
Stress concentration hole R	x										x

Figure 139: Overview of beam element in the context of adjacent beams, including a table with interdependencies, visualizing for the beam checks which parameters influence the beam checks

section checks are not only influenced by the main beam properties, but also the height and tenon size of the beams at the hole($Beam_{hole}$). Additionally, the stress concentrations around the holes are influenced by the dowel heights of the hole beams.

Additionally, the dowel and tenon checks of the main beam are influenced by the height of the support beams ($Beam_{supp}$).

Step-by-step optimization

To overcome the problems with interdependencies in the cross-section optimization, a custom part-by-part optimization technique is developed. The flowchart of this optimization technique is shown in Figure 140 (on page 98).

The optimization technique consist of three main phases and an initiation phase.

Inititation

Since reciprocal frames are statically indeterminate, the internal forces are influenced by the cross sections of the structural elements. Initially, some geometry is required to calculate the internal forces in the structure. In the cross section optimization process, the minimum possible beam heights are used to calculate the internal forces.

Using these internal forces, the unity checks of all structural elements are calculated. When all unity checks are satisfied, the minimum beam height is accepted as optimal solution. If this is not the case, the three phase optimization process is initiated.

Phase 1: tenon optimization

In phase 1, the minimum required heights for the tenons are calculated. These minimum tenon heights are based on the support stresses in the tenons and the shear in the tenons.

As visible in the flowchart, for both tenons in each beam, the unity checks are performed. When the unity checks are not satisfied, the tenon height is incremented with increment factor a (1mm). Additionally, the beam height is incremented accordingly to make sure the tenon is not larger than the beam height. When the unity checks are satisfied, the tenon height is accepted as minimum tenon height.

Phase 2: dowel optimization

The tension force in the tenon/dowel is dependent on the height of the beam since the beam height influences the arm between the dowel and the compression area. This means that in principle for all dowel sizes the unity checks can be satisfied.

To tackle this problem, in phase 2, the dowel dimension is sought which results in the lowest possible beam height. This is done by iterating over the possible dowel dimensions and storing their required beam height in a list.

As visible in the flowchart, for each beam, for both tenons, the list of dowels is iterated. The tenon height is the maximum height of either the tenon height found in phase 1, or the tenon height based on the edge distance requirements. For this combination of tenon and dowel, the beam height is computed so that the dowel unity checks are satisfied.

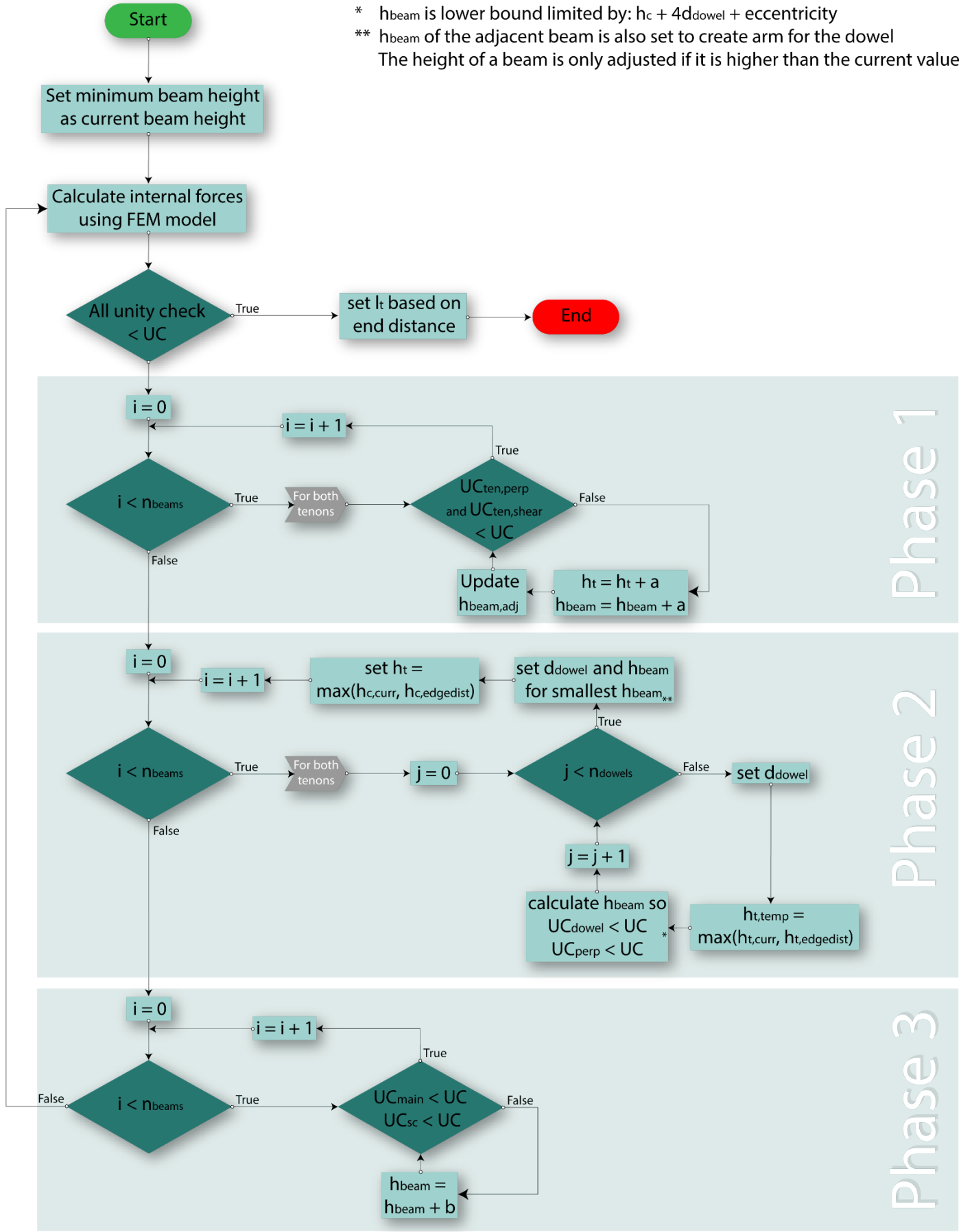


Figure 140: Flowchart of step-by-step optimization process, used to find the optimal cross-section dimension for each beam

Additionally, the compression checks at the beam ends must be satisfied.

When this is done for all of the possible tenon dimensions, the dowel dimensions resulting in the lowest beam height are accepted as optimal solution. When h_{beam} is smaller than the current h_{beam} , the value for h_{beam} is not updated. Additionally, the beam height of the adjacent beam is incremented (if necessary) so the arm can be generated (if the adjacent beam is too low, the full compression area might not be usable resulting in a smaller arm).

Phase 3: main section optimization

When both the dowel and tenon dimensions are known, the unity checks of the main section and stress concentrations can be performed. To satisfy these unity checks, only the beam heights can be increased.

The flowchart for this phase is thus relatively straightforward. For all beams the unity checks for the main section and the stress concentration are performed. When the unity checks are not satisfied, the cross section height is increased with increment factor b. This process is looped until the unity checks are satisfied.

Convergence

The three main steps are looped until the unity checks just before phase 1 are satisfied. In that case, the cross sections satisfy the unity checks with the actual internal forces corresponding to the structure with the same cross sections.

Mathematically, the convergence criterion can be described with the following formula:

$$\forall_i \, UC_i - UC_{max} \leq 0$$

This means that for all beams i, the unity check minus the maximum allowed unity check value should be smaller than or equal to zero.

This cross-section optimization method can be seen as a *monotonic sizing optimization*. The optimization process is monotonic because the cross-section values can only be increased. This leads to fast convergence, but the found solution may not be the global minimum.

An additional constraint for the cross section optimization, besides element unity checks, is the global unity check of the maximum serviceability deformation. When the deformation is too large, all cross section heights are increased until the deformation requirements are satisfied. The deformation in practice was never found to be normative.

Solution

The cross section data and corresponding internal forces that is found in the optimization problem is stored in the beam information. All additional convergence data is not stored.

Governing unity checks

After optimization, each beam has a unity check close to the allowed maximum unity check. What unity check is governing depends on the location in the structure.

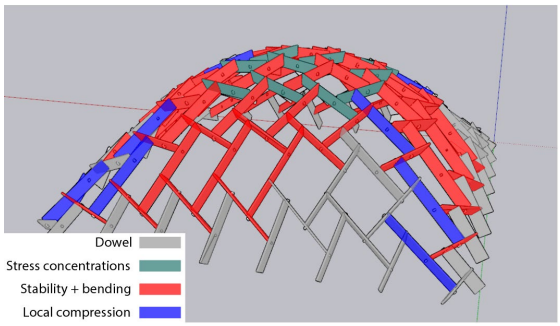


Figure 141: Governing unity check type in an 8x8m reciprocal frame structure

Figure 141 displays the governing unity check in a typical reciprocal frame structure. The governing unity check depends on the loading of each element and the optimization method. When the dowel or local compression are governing, the beam height did not have to be incremented for bending, stress concentrations or stability. This occurs most around the edges of the reciprocal frame.

Figure 142 shows more details on the load cases, where the aspect that has the largest impact on the unity check is displayed. As visible, on the top of the structure, bending in the strong axis is most significant.

Elements that are placed more horizontally, are governed by bending in the weak beam axis. And elements that are placed vertically are governed by stability.

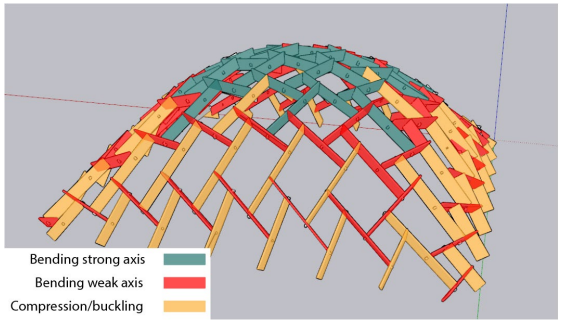


Figure 142: Governing load case, most important factor in check

6.11 Structural report

As a structural engineer, it is important to be able to show the calculations that are performed on the structure, to be able to convince other people that the structure is structurally sound.

The reciprocal frame designer automatically generates a structural calculations report using the cross section data and internal force data as described in the previous paragraph.

The user/designer has a few options as to what should be in the structural report. Firstly, a full report can be generated where all the steps of the calculations are performed for all unity checks (see Annex 1.2). This may result in very extensive calculation reports of a few thousand pages. To reduce the size of the full report, the user may choose to remove the internal force diagrams from the structural report.

Secondly, a report containing the unity check summary for each beam element can be generated (see Annex 1.1). Due to the large amount of unity checks that are performed, this may still result in a rather large calculation report. The report is however a lot more insightful.

7 Digital manufacturing

In the previous chapters, all data is gathered to be able to create an optimized reciprocal frame from plywood sheets. The next step in the process is to be able to transform that data into information that is comprehensive for digital manufacturing and (manual) assembly.

In this chapter, the process of translating all structural data into digital manufacturing data. Firstly, .stl files (containing 3d geometric information) are generated for each of the beam elements. Secondly, cutting patterns are generated so the digital manufacturing tools can effectively obtain the 3d elements from the sheets.

Finally, it will be explained how the structure can be assembled on-site. To explain and test this process, a few scale models have been made. These test models are also displayed in this chapter.

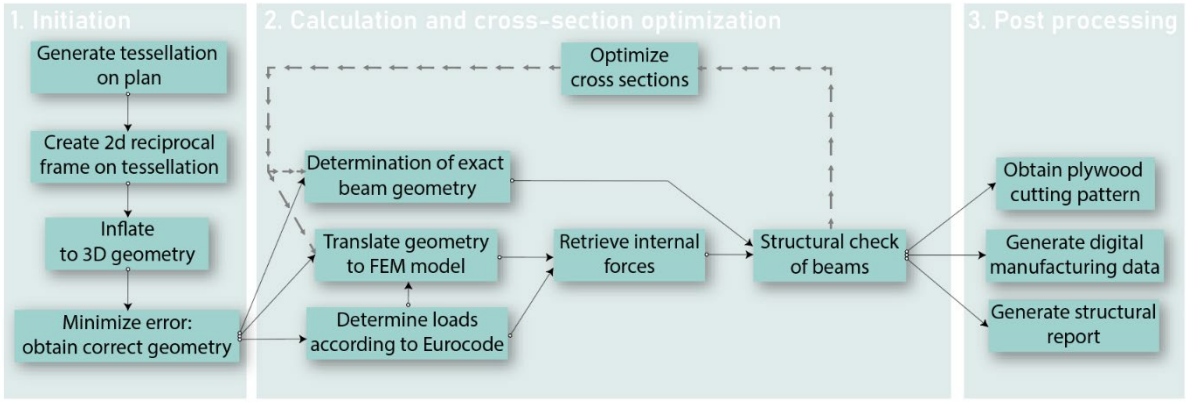


Figure 143: Flowchart for reciprocal frame designer

This chapter focusses on phase 3 of the flowchart in Figure 143, where each step is explained in detail.

7.1 Digital manufacturing data

To be able to automatically produce the structural elements from plywood sheets, the exact three-dimensional geometry of the beams must be known.

There are several methods to store this three-dimensional geometry. The reciprocal frame designer translates the geometry into .STL files. STL-files are a 3D file format where the model is composed of a triangular surface mesh. This means that the model is split into hundreds of small triangles. STL files are commonly used for 3d printing purposes, but they can also be used for (3D) CNC machining.



Figure 144: Example STL file of beam element

A downside of the STL file format is the fact that circular shapes are split into many straight edges. Advanced CNC software can handle these circularities, but the software and machine must be configured to obtain the correct resulting shapes.

Figure 144 shows an STL file that is automatically generated by the reciprocal frame designer. As visible in the figure, the ends and holes are rotated in such a way that three-dimensional manufacturing is required.

Besides using the STL files for production, they can also be used to visualize the full structure. This does not only allow the designer to check the structure, but also allows communication with contractors or other design disciplines. Figure 145 shows the combined STL model, where it can be seen that the end and hole rotations are obtained correctly.

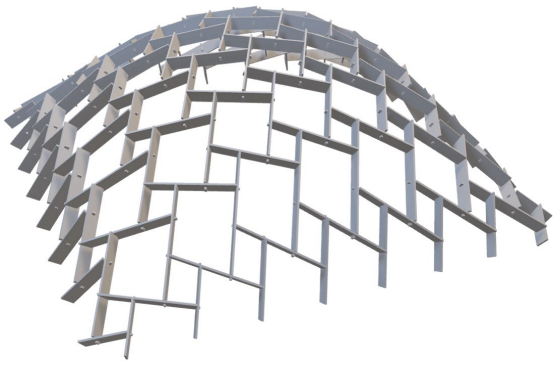


Figure 145: Full reciprocal frame structure STL

Geometry determination

The three dimensional geometry is obtained purely using geometric relationships between the structural elements, as explained in chapter '6. Structural integrity and optimization'.

Additionally to the end rotation, the exact position of the beam elements must be defined as a coordinate and rotation system. This enables the combination of multiple STL files.

To do so, the aircraft principles for rotations are used: yaw, pitch roll. This means that an aircraft rotation can be obtained with three rotations around its principal axes, but the rotations must be performed in the proper order. The yaw gives the bearing, the pitch will give the elevation and the roll gives the banking angle.

The yaw can be obtained by the differences in the x and y coordinates of the begin and end point: $yaw = \tan^{-1}\left(\frac{\Delta y}{\Delta x}\right)$. The pitch then is found by the relation between the relation between the difference in z coordinate and the length on the horizontal plane between the begin and end point: $pitch = \tan^{-1}\left(\frac{\Delta z}{\sqrt{\Delta x^2+\Delta y^2}}\right)$. Finally, the roll is a predefined value that is obtained in the initial phase of the reciprocal frame designer.

Combining these three angles and performing the Euler rotations in the specified order will result in the exact location of the beam element.

Fillet radius

As mentioned before, the fillet radius was omitted from the structural optimization. The fillet radius is instead selected from the minimum allowed fillet radius for CNC milling. These minimum values are summarized in Table 1 in chapter '3. Literary review'.

7.2 Cutting pattern

For (raw) material efficiency it is important to obtain the beam elements from as few plywood sheets as possible. To do so, bin packing algorithms as described in chapter '3. Literary review' are used. These algorithms try to find the most optimal way to place the elements in a 'box'.

Bin packing algorithms are so called NP-hard algorithms, which means there is no known algorithm that can solve all instances of the problem. In the case of packing the beam elements in the plywood sheets, it means that there is not one algorithm that will give the most optimal result (global minimum).

To tackle the NP-hardness, multiple bin packing algorithms are ran for each instance of the reciprocal frame; the shelf algorithm, guillotine algorithm, maximal rectangle algorithm and skyline algorithm. Since the bin packing problems is an offline bin packing problem (all geometry is known before performing the algorithm), the beams can be sorted – based on height or length) before bin packing. This will typically aid the bin packing algorithm and thus result in fewer sheets required.

An example bin packing solution is shown in 'Annex 2.1: Plywood cutting pattern of a non-optimized RF'. Where the most optimal bin packing solution is visualized for an 8x8m reciprocal frame

that is not optimized for plywood sheet reduction. As visible in the cutting pattern, the plywood sheets are not fully used resulting in a lot of waste material. This stipulates the importance of optimizing for raw material instead of e.g. total beam volumes.

Digital manufacturing

For digital manufacturing, the cutting pattern simply means that each beam element gets a sheet number and a (x,y) location from where to start cutting the STL beam. This data can directly be obtained from the bin packing algorithms, and is stored in the beam elements.

The bin packing includes a margin between the elements for the CNC router to be able to pass as well as some margin on the edges. These margins are applied by simply enlarging the elements geometry by $2d$ in both x and y direction and then displacing the coordinate by d in both x and y direction.

Scale model manufacturing

For this research, scale model elements can only be created by laser-cutting 2d beam elements. This means that all 3d beam information is 'lost'. Additionally, the margin between elements is not required due to the near-zero laser thickness.

To be able to automatically create a laser cutting pattern, the 2d element geometry needs to be exported to a 2d line based file format. In the case of the reciprocal frame designer, this is the DXF file format. For each beam element a DXF is created and then combined on a sheet to enable automatic laser cutting. Figure 146 shows an automatically generated laser cutting pattern for a scale model, where the DXF files for all beams are combined into a single cutting pattern sheet.

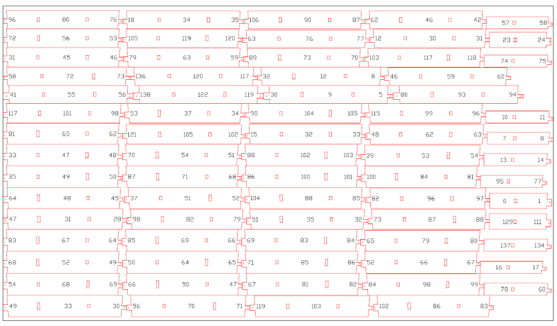


Figure 146: Laser cutting pattern for scale model using combined DXF files. Red is for cutting and black for engraving

7.3 Construction method

Reciprocal frames can be difficult to construct due to their large complexity. Therefore, numbering is applied to the beam elements to clarify construction (see Figure 147). The number in the middle of the beam is the beam ID, and the number on the ends of the beam are the ID's of the beams that they should connect to.



Figure 147: Numbering on a beam element

The reciprocal frame can be constructed in the order of the beam ID's, starting at ID 0. The constructors can be aided by an additional overview drawing including beam ID's.

Structural safety during construction

During construction of the reciprocal frame, the structural integrity of the structure should be maintained. To do so, each free end should be supported during construction. Do to the curvature

in the reciprocal frame, the support should be both horizontal and vertical.

These supports can be created by using building props (Dutch: Stempels) underneath the free ends. The horizontal support can be generated by placing the building prop at a slight angle, aligned with the beam direction.

Alternatively, no horizontal supports may be used. This would require the inter-member connections to act moment fixed. Due to the low connection stiffness this may result in slight sagging of the structure. This is acceptable if the structure is raised at the end by moving the end points inwards.

The exact behaviour of the structure in the second case is not tested and/or calculated. Additional research and engineering is required to ensure safety.

7.4 Physical test models

To test whether the digitally designed structures can also be constructed in reality, a few scale models have been constructed. The scale models are also used to check whether the digitally determined geometry (end rotations etc.) are correct.

Hand sawn model

Firstly, a simple hand sawn test model has been generated in the early stage of the reciprocal frame designer development. This model was predominantly used to test if the computer-calculated end rotations and hole locations were correct. Additionally, this model was used to test if the indexing method as displayed in Figure 147 is working.

The hand sawn model is a simple 12 element reciprocal frame. The frame is based on a squared tessellation.

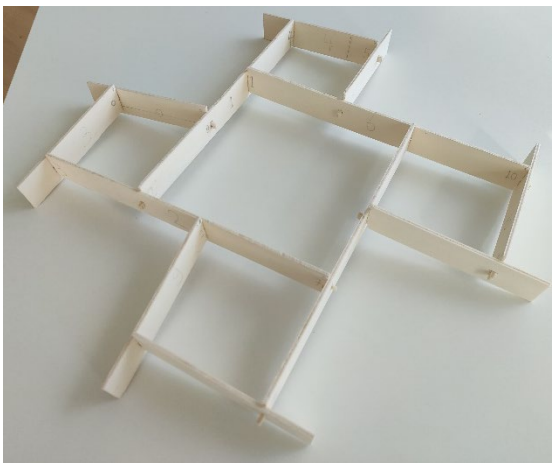


Figure 148: Hand sawn test model, scale 1:5

Laser cut model

After the hand sawn model gave confirmation of the geometry and the construction method, it was time to test the same on a more complex reciprocal frame. Additionally, the automatically generated cutting patterns and DXF files were tested with this model.

The following parameters for the reciprocal frame designer were used in for the scale model:

- Sheet thickness: 30mm
- Base polygon: 8x8m
- Tessellation pattern: squared
- Pattern gradient: 0.1
- Edge size: 1m
- Eccentricity: 0.4m
- Scale factor: 0.4

Resulting in reciprocal frame with 144 beam elements, where the beam elements have a maximum length of 1.71m.

The scale model is shown in Figure 149, the scale model manufacturing method

as described earlier has been performed to generate the test model.

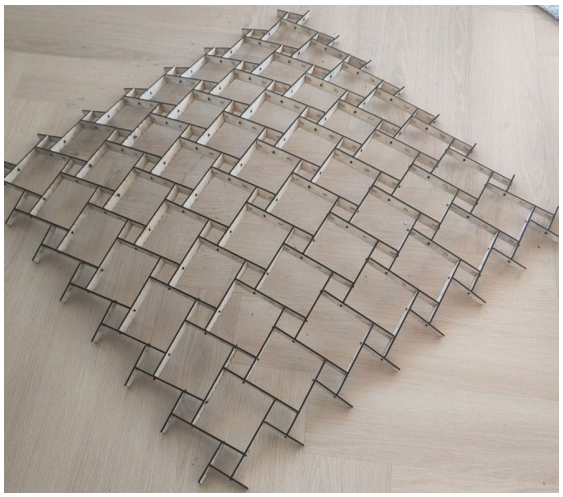


Figure 149: Laser cut scale model for an 8x8m, squared tessellation reciprocal frame, scale 1:10

The test model was obtained from two 3x400x700mm plywood sheets using an automatically generated laser cutting pattern (Figure 150).

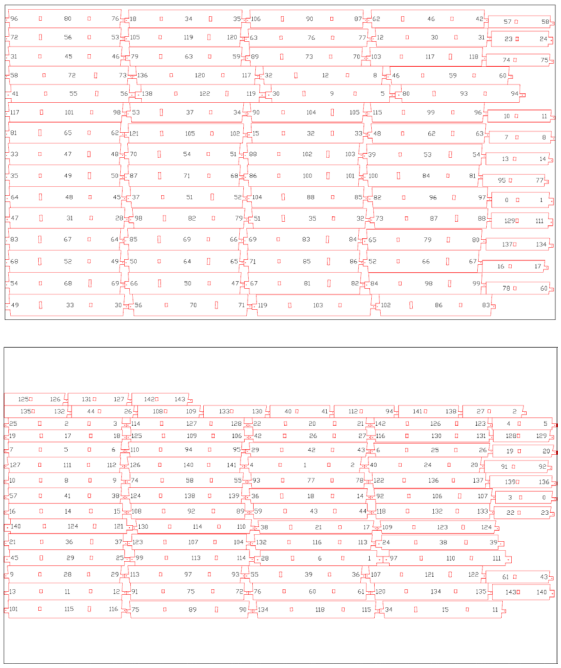


Figure 150: 3x400x700mm cutting patterns used for the laser cut scale model



8 Parametric optimization

To be able to automatically optimize the parameters that are used in the reciprocal frame, an algorithm can be used to reduce the manual user input. The goal of the parametric optimization, is to reduce the number of plywood sheets that are used for obtaining the beam elements

This chapter discusses what optimization algorithm is used and how the algorithm can be tweaked to perform optimally. The results of this optimization are discussed in the second half of the next chapter.

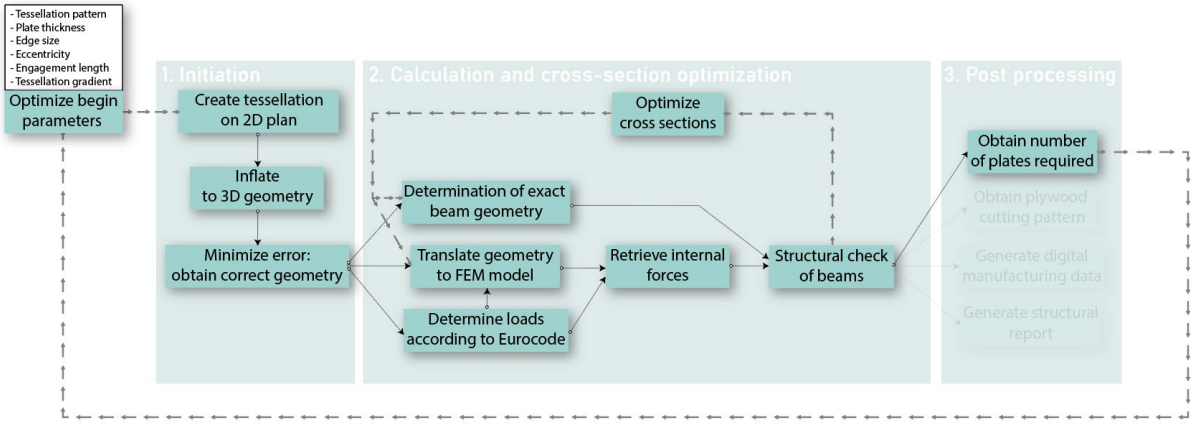


Figure 151: flowchart of reciprocal frame designer with parametric optimization loop

To truly optimize a reciprocal frame structure, the combination of parameters that used for designing the reciprocal frame resulting in the least amount of material required to create the reciprocal frame must be found. The flowchart in Figure 151 shows the process of this optimization. The whole reciprocal frame design tool is looped with different begin parameters. The post processing part is dropped for the parameter optimization.

8.1 Optimization goal

The optimization of structures is often based on minimizing the volume of the structural elements. A factor that is often forgot in this optimization goal is the amount of material that is required to produce said structural elements.

For structural materials like steel or concrete, the volume of the elements is almost equal to the volume of material required to create such element. For timber, and especially plywood, these volumes may lie further apart.

A structure with optimized cross sections and a layout that results in the lowest beam volume may result in large amounts of waste material when the elements are obtained from the plywood sheets. For this reason, the optimization target for this parametric optimization is minimizing the amount of plywood sheets that are required to produce the beam elements.

8.2 Optimization problem

The geometry of the reciprocal fame is based on a set of design parameters:

- Base rectangle dimensions
- Tessellation pattern
- Tessellation edge size
- Tessellation density gradient
- Scale factor
- Eccentricity

The sizes of the beam elements are in turn based on the load conditions, sheet thickness and maximum allowed value for the unity check.

For the optimization, the target is to find the combination of design parameters resulting in the most material-efficient reciprocal frame for certain span dimensions, when exposed to the user entered load conditions. The optimization problem can thus be expressed as:

Minimize $V_{sheets} = f(\mathrm{TP}, \mathrm{ES}, \mathrm{E}, \mathrm{SF}, \mathrm{DG}, \mathrm{T})$

Subject to:

- Plywood sheet size
- Maximum unity check
- Load conditions

This means the minimization goal is stated as the volume of the sheets that are required to create the beam elements. This volume is a function of the previously mentioned design parameters. This optimization is subject to the design parameters mentioned in the expression of the optimization problem.

This minimization can then be performed for different base rectangle dimensions.

8.3 Optimization algorithm

The reciprocal frame designer is used to obtain the total volume of plywood sheets that is required for a certain combination of parameters. This can be seen as a black-box function; this means that the only thing known about the function is the value that comes out. For optimization algorithms this means that no additional information can be obtained from the function (e.g. the derivative function).

A second important consideration is the fact that evaluations are very 'expensive' (i.e. time consuming). For large problems, the reciprocal frame designer may need several minutes to compute an optimized structure.

Parameter space

Besides the tessellation pattern and the plywood sheet thickness, all parameters are so called 'continuous-variables', which means they can have any real number value. The plywood sheet thickness is constrained to the typically produced plywood sheet thicknesses, meaning this is a so-called 'discrete parameter'.

The tessellation pattern parameter is constrained to five possible tessellation pattern designs. A downside of the tessellation pattern is that the set of optimal free design parameters may be different for each pattern. This will confuse any optimization algorithm and must therefore be removed from the optimization process. To incorporate this parameter in the optimization, the optimization should be performed for each pattern.

The resulting design space is thus a five dimensional design space with (parameter, type):

- Edge size continuous
- Eccentricity continuous
- Scale factor continuous
- Density gradient continuous
- Sheet thickness discrete

All the parameters additionally should be constrained to remain in a feasible design region.

Bayesian optimization algorithm

The Bayesian optimization algorithm suits the design space and problem best because the algorithm can make most out of limited evaluations.

The algorithm is most optimal for optimization over continuous design spaces with less than 20 dimensions. Additionally, the algorithm tolerates stochastic noise in function evaluations (61). This means that the algorithm allows a non-smooth function, which is

expected for the reciprocal frame results (a slight change in a parameter may result in more plywood sheets to be used and thus a jump in raw material volume).

The Bayesian optimization algorithm is very efficient for expensive black-box functions because it selects the sample location efficiently. The algorithm creates a surrogate function for the objective and determines the uncertainty in the representative function using machine learning (with the Gaussian process regression). It uses an acquisition function determined based on the representative function to determine where to sample.

Integer encoding

The Bayesian optimization algorithm is not able to handle discrete parameters directly. Therefore, the plywood sheet thickness parameter should be encoded to be an integer value when performing the data acquisition.

Integer encoding means that a continuous encoding is used in the optimization process. This integer encoding then is rounded to the nearest plywood sheet thickness.

Bounds

The Bayesian optimization algorithm uses bounds for each of the parameters. These bounds are defined by the maximum and minimum value each of the parameters can possibly have.

Gaussian process regression

GP regression is a Bayesian statistical approach for modeling functions. Since the objective function (the function that describes the behaviour of each parameter) is unknown, the optimization algorithm treats it as a random function and places a prior over it.

The prior function captures the assumptions about the function's behaviour. The prior function is updated after obtaining more evaluations of the functions. This prior is then used to form the posterior distribution. Finally, the posterior distribution is used to create the acquisition function that in place is used to determine where to sample the function next.

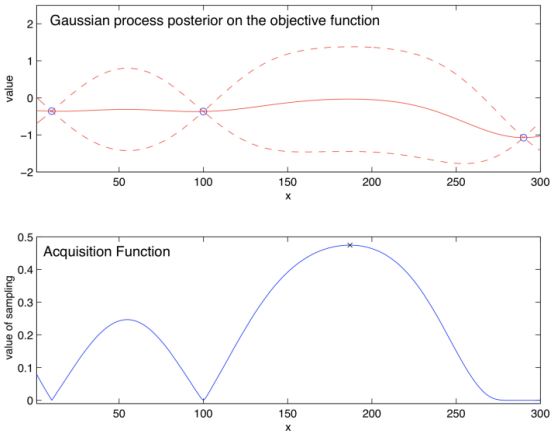


Figure 152: Gaussian process and acquisition visualized (61)

This process is illustrated in Figure 152. The (unknown) objective function is drawn in red. The prior is illustrated in the red dotted lines. In this case the upper and lower confidence bounds are used. The acquisition function shows the locations at which the confidence bounds are highest, meaning there is the most uncertainty.

Exploration vs. exploitation

The Bayesian optimization algorithm can be used to both explore and exploit the objective function. Exploration means that the algorithm is used to

'explain' the objective function without looking for an optimal value.

Exploitation means that the Bayesian optimization algorithm is used to search for the optimal value. When the Bayesian optimization algorithm focusses too much on exploitation, a global minimum value may be missed.

The balance between exploration and exploitation depends on the acquisition function that is used for the Bayesian optimization. There are three main acquisition functions that can be used in Bayesian optimization:

- Upper confidence bound
- Expected improvement
- Probability of improvement

Upper confidence bound

The UCB function balances exploration and exploitation by selecting points where the UCB is maximized. The upper confidence bound is calculated as the mean plus a multiple of the standard deviation of the predictive distribution of the objective function

This is a tunable parameter that controls the trade-off between exploration and exploitation. This tunable parameter is kappa (κ) which is between 0.1 (focus on exploitation) and 10 (focus on exploration).

The difference between the behaviour is visualized in Figure 153 and Figure 154. When $\kappa = 0.1$, the focus is on exploitation. This can be seen by the fact that the points are focused around the peak. Note that the maximum peak of the (unknown) objective function is missed in this case.

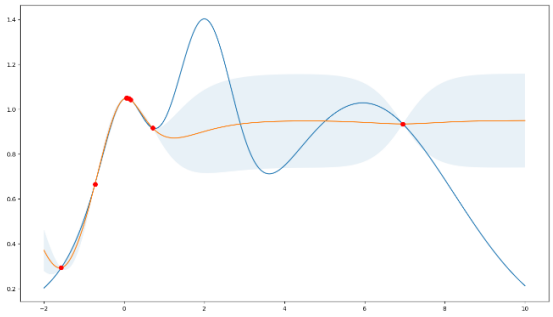


Figure 153: Example of acquisition function 'upper confidence bound' with $\kappa = 0.1$

When $\kappa = 10$, the focus is on exploration, which can be seen by the fact that the points are spread evenly in the design space. In this case, the peak is found, but more acquisitions are required to find this value

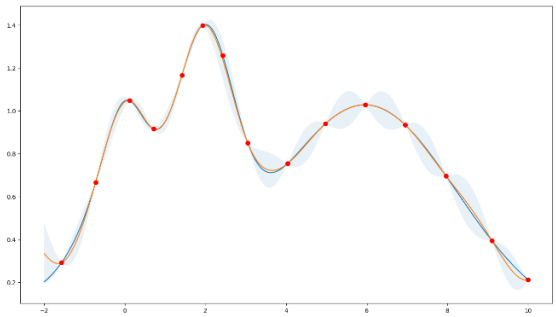


Figure 154: Example of acquisition function 'upper confidence bound' with $\kappa = 10$

Expected improvement

The expected improvement acquisition function selects the points where the expected improvement over the current best observation is maximized. It thus quantifies how much improvement is expected by evaluation the objective function at a given point compared to the current best observation.

The expected improvement acquisition function is useful when the objective function is noisy.

The amount of exploration/exploitation when using expected improvement can be tuned with the parameter x_i which is

between 0.0 (prefer exploitation) and 0.1 (prefer exploration).

The difference between the behaviour for the different x_i values is visualized in Figure 155 and Figure 156. When $x_i = 0.0$ the focus is on exploitation, which can be seen by the fact that there are more points around the peaks. When $x_i = 0.1$ the focus is on exploration, which can be seen by the wide spread between the points.

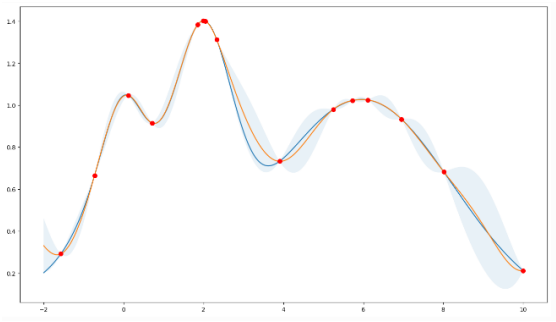


Figure 155: Example of acquisition function 'expected improvement' with $x_i = 0.0$

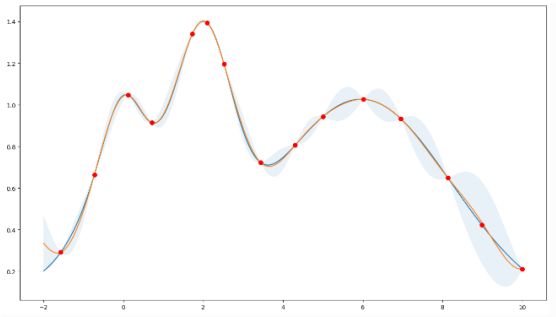


Figure 156: Example of acquisition function 'expected improvement' with $x_i = 0.1$

Probability of improvement

The probability of improvement acquisition function selects the points where the probability of improvement over the current best observation exceeds a threshold. Probability of improvement is used when the objective function is uncertain and when it is desirable to balance exploration and exploitation.

The amount of exploration/exploitation when using probability of improvement can be tuned with the parameter x_i which is between 0.0 (prefer exploitation) and 0.1 (prefer exploration).

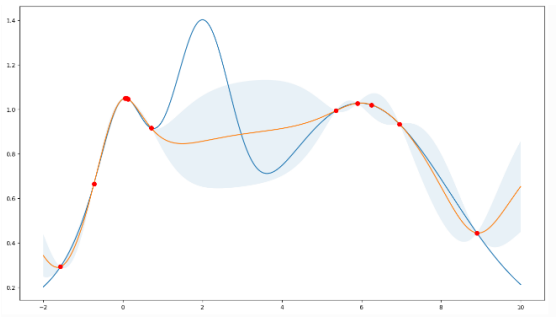


Figure 157: Example of acquisition function 'probability of improvement' with $x_i = 0.0$

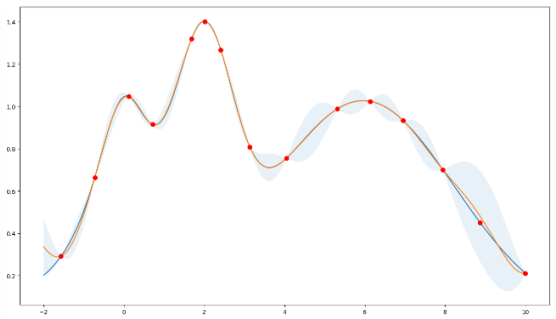


Figure 158:Example of acquisition function 'probability of improvement' with $x_i = 0.1$

The difference between the behaviour for the different x_i values is visualized in Figure 157 and Figure 158. When $x_i = 0.0$ the focus is on exploitation, this can be seen by the fact that most points are located around the peaks. However, the global maximum is not observed in this case. When $x_i = 0.1$, the points are evenly spread. In this case the focus is on exploitation.

Applied acquisition function

For the design space of optimizing the reciprocal frame dimensions, the most effective acquisition function is the expected improvement function. The reason for this is that it is focused on finding a global minimum. Additionally, the expected improvement function has

the quality of handling a noisy objective function.

Noise handling

Another tuning parameter in the Bayesian optimization is the alpha value that influences the gaussian process.

For instance when dealing with discrete parameters, it is useful to increase the alpha parameter. Increasing the alpha parameter makes the gaussian process more flexible.

8.4 Optimization approach

There are multiple methods to optimize the design parameters to find the optimal structure in terms of raw material. Initially, one could consider applying the Bayesian algorithm to all parameters:

- Edge size
- Eccentricity
- Scale factor
- Density gradient
- Sheet thickness

However, the Bayesian optimization algorithm might create infeasible combinations. Additionally, it might take the algorithm a while to learn the influences of the parameters because the algorithms have a strong interaction (e.g. when the edge size is small, the eccentricity has a larger influence).

Initial exploration

To reduce the number of combinations and infeasible results, an initial exploration is used. This exploration is made by exploring the design region in terms of edge size and eccentricity since these parameters are expected to have the largest influence on the end result.

In this research, the number of structural elements has been limited to approximately 500 due to computation time. Therefore, the design region for the edge size is between an edge size that generates approximately 500 beam elements and the edge size resulting in beams that are longer than the plate dimensions.

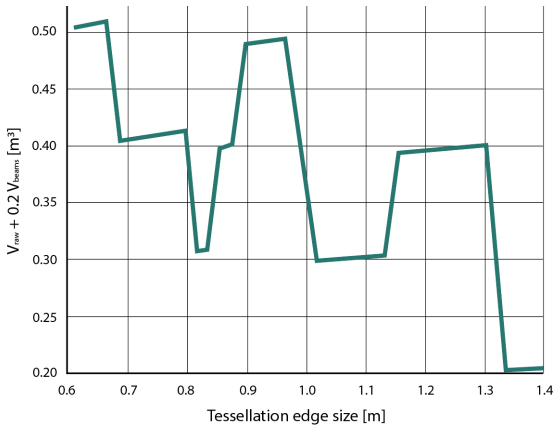


Figure 159: Initial exploration analysis for a 4x4m squared reciprocal frame

From an initial exploration analysis for a 4x4m span, local minima were found when the edge size creates a tessellation that matches the base plan as closely as possible (Figure 159). For a square tessellation this means that the plan dimension should be devisable by the edge size. This generates a structure with no unnecessarily large span.

The span with a certain edge size that is closest to the required span can be calculated using a ceiling function: $L_{add} = \lceil x/L_{plan} \rceil * x$. The graph for a 4x4m squared reciprocal frame is plotted in Figure 160. The local minima in the initial exploration analysis match closely with the lowest spans in the ceiling function. Therefore, it can be concluded that it is appropriate to only calculate the structure at divisions of the

span sizes since the minima are always found at those locations.

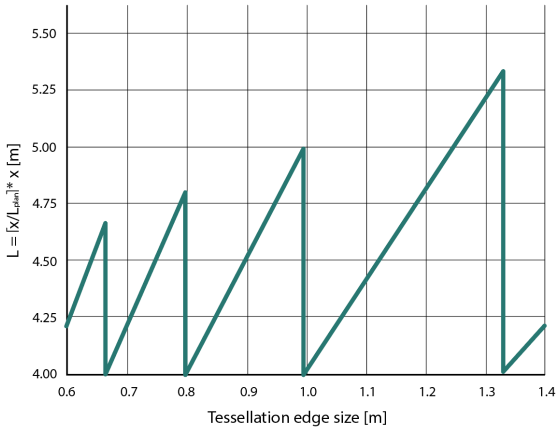


Figure 160: Ceiling function to require span with a certain edge size in a squared tessellation for a 4x4m reciprocal structure

For the other patterns it is more difficult to find the edge sizes for which the grids match the base plan as close as possible since the tessellations do not have the same width as height. In this research, the edge sizes for which the grids match the base plan as closely as possible are manually calculated.

With the edge sizes within the design region and as divisions of the plan dimensions, the number of sheets required per layout can be calculated. From these calculations a minimum (or a few minima can be found). These minima are the locations on which further analysis should be performed to find the true minimum.

Optimizing to minimum

The remaining reciprocal frame parameters that result in the minimum required sheets is calculated using the Bayesian optimization. In principle, the fitness function can be defined as the volume of the sheets that are required. To further guide the optimization, the a fraction of the volume of the beam elements is added to the fitness function. This results in the following (updated) minimization function:

Minimize $V_{sheets} + 0.2V_{beams}$

$$= f(\sout{\text{TP}}, \text{ES}, \text{E}, \text{SF}, \text{DG}, \text{T})$$

Subject to:

- Plywood sheet size
- Maximum unity check
- Load conditions

As mentioned before, the acquisition function for the Bayesian optimization is the 'expected improvement' function. The tuning parameters are focused on exploitation $(x_i = 0.001)$ and allow significant noise: $\alpha = 0.2$.

The results and process of the parametric optimization is discussed using an example case (with assumed boundary conditions) in 9.2 Parametric optimization results.

9 Results

The results of the recirpocal frame designer as well as the parametric optimization are discussed in this chapter. The reciprocal frame designer has a graphical user interface to make the software usable for someone with limited knowledge on sofware engineering. The range of options and their accompanying results are discussed in the first part of this chapter.

In the second part of the chapter, the parametric optimization is discussed. The influences of each of the parameters are discussed based on an 8x8m design plan. The optimization is performed for 2440x1220mm plywood sheets.

9.1 Reciprocal frame designer

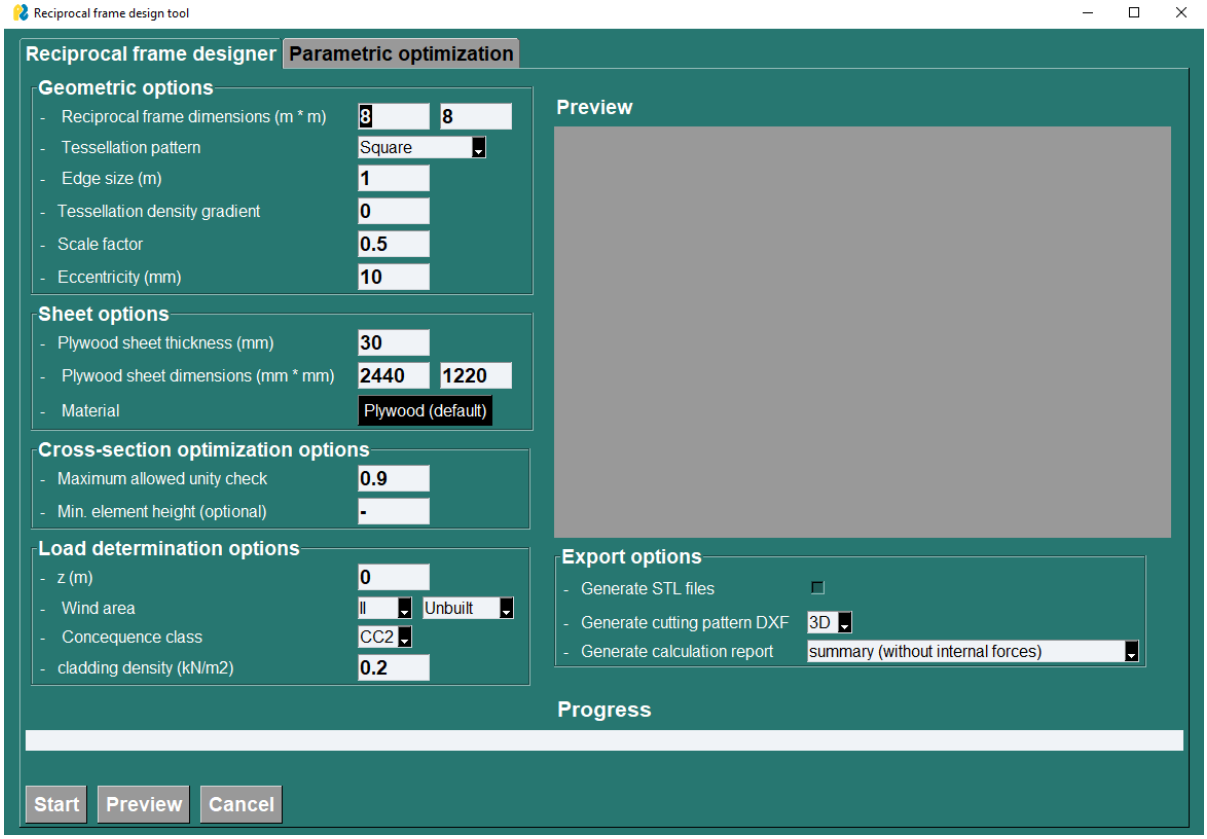


Figure 161: Graphical user interface of the reciprocal frame designer

To make designing reciprocal frames with the parameters mentioned in chapter '5. Reciprocal frame designer' easy for people with limited programming knowledge, a reciprocal frame design tool has been developed. The graphical user interface (GUI) of the reciprocal frame design tool is visualized in Figure 161. Besides controlling the reciprocal frame geometry, loading and export settings can be controlled in the GUI. A manual for using the reciprocal frame design tool can be found in Appendix 1: User manual.

Geometric options

The geometric options control the geometry of the reciprocal frame. The reciprocal frame geometry that results from the combination of geometric options can be previewed by clicking preview in the bottom of the GUI. The influence of the different parameters and their resulting geometries will be discussed in the following paragraphs.

Note: Under each of the figures, the geometric parameters that are used for the visualization are represented as an array: [tessellation pattern, edge size, tessellation density gradient, scale factor, eccentricity]. All other relevant parameters are explicitly mentioned.

In each figure showing the structure as a line geometry, green represents a support node, black a normal node and red an intermediate node.

<u>Reciprocal frame dimensions</u>

The first parameters that are used for determining the reciprocal frame

dimensions are the dimensions of the base of the reciprocal frame. This determines the base tessellation that is used for determining the reciprocal frame geometry, and thus also the resulting reciprocal frame.

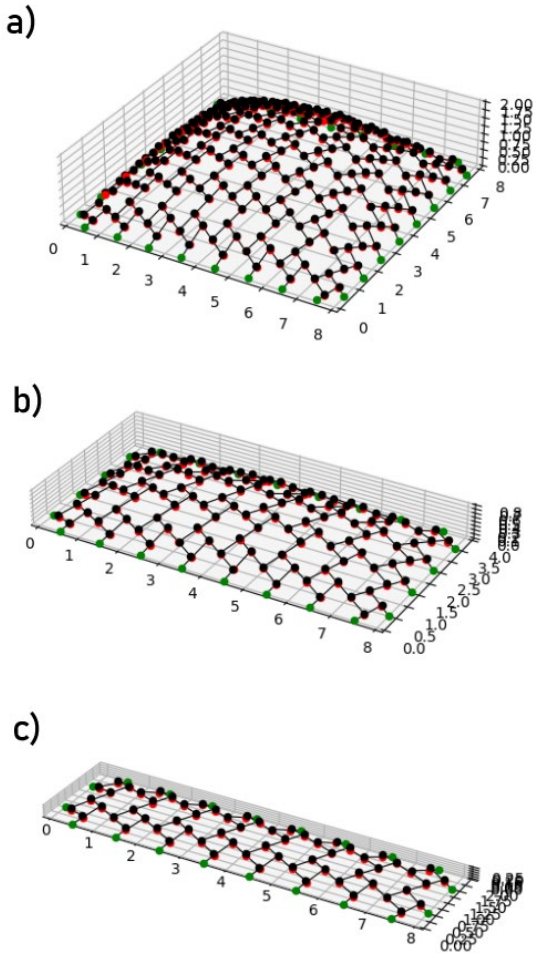


Figure 163: Reciprocal frame geometry for different b x h ratios for the reciprocal frame dimensions [Square, 1, 0, 0.5, 40] a) 8x8m, b) 4x8m and c) 2x8m

The resulting reciprocal frames for different ratios of reciprocal frame dimensions are visualized for different reciprocal frame dimensions in Figure 163.

Tessellation patterns

The tessellation pattern that is applied directly determines the pattern of the beam elements. In this research, 5 different tessellation patterns are applied: Square, Triangle, Snub-Square, Honeycomb and Trihexagon. The resulting reciprocal frame geometry based these tessellation patterns are visualized in Figure 162.

A different set of parameters is required to create the same fineness of structure, or the same curvature for each of the patterns. To get a clear graphic representation of the effect of the tessellation pattern, the geometric parameters are chosen as such that the resulting geometry generally has the same shape.

Edge size

The edge size determines the mesh-size of the tessellation and thus the fineness of the resulting reciprocal frame. A reciprocal frame with the same dimensions and geometric parameters

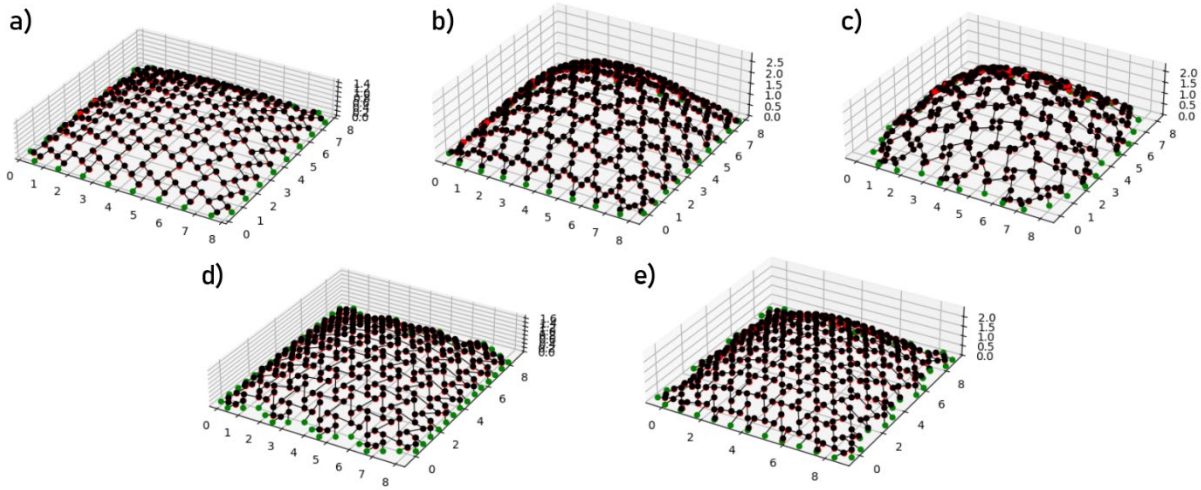


Figure 162: Reciprocal frame geometry for different patterns: a) [square, 1, 0, 0.5, 20], b) [triangle, 1, 0, 0.5 15], c) [snub-square, 1, 0, 0.5, 15], d) [honeycomb, 0.7, 0, 0.5, 25], e) [trihexagon, 0.83, 0, 0.5, 25]

(except for the edge size) are visualized in Figure 164. This also shows how the parameters influence each other, as for a lower edge size there is more curvature with the same eccentricity.

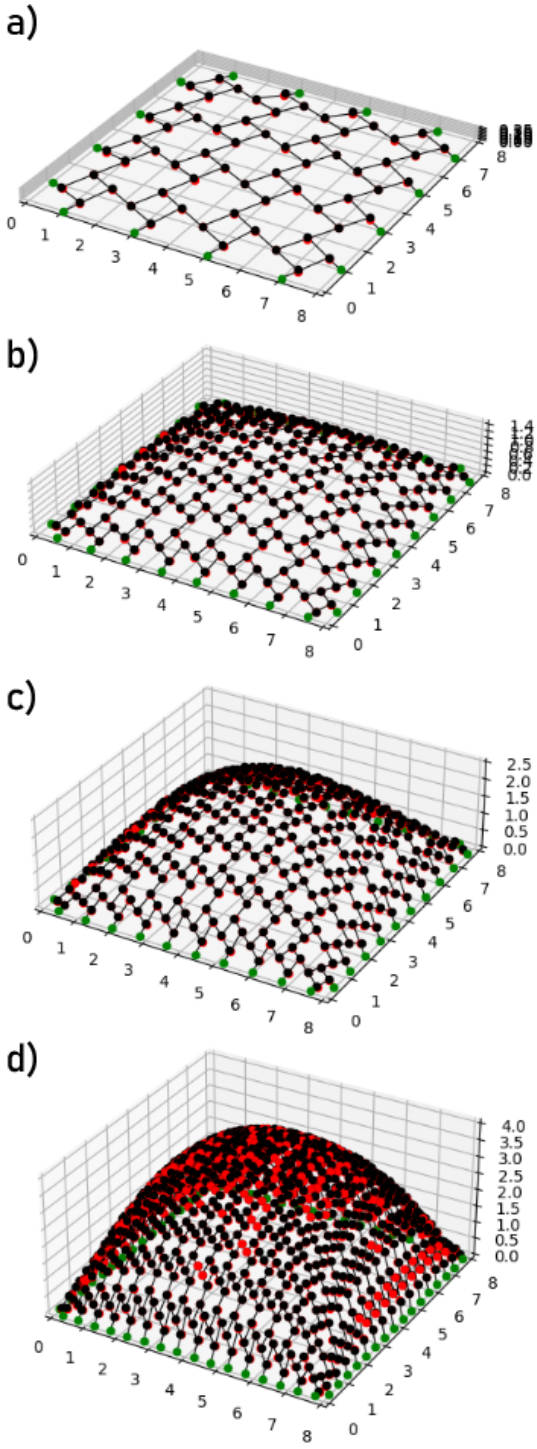


Figure 164: Reciprocal frame geometry for 8x8m reciprocal frame with different edge sizes [square, x, 0, 0.5, 30] a) x = 2m, b) x = 1m, c) x = 0.8m and d) x = 0.5m

Tessellation density gradient

The tessellation density gradient can be used to influence the density of the tessellation at the center of the structure compared to the density on the edges of the structure. The influence of the density gradient on the resulting reciprocal frame structure is visualized in Figure 165.

In the figure it can be seen that the tessellation density gradient also changes the (amount of) curvature in the structure. The two structures below have the same geometric parameters except for the density gradient.

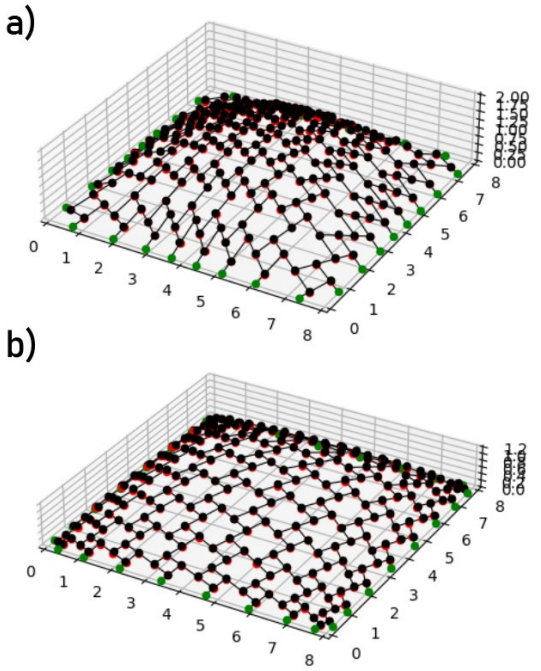


Figure 165: Geometry for an 8x8m reciprocal frame [square, 1, x, 0.5, 30] with tessellation gradient: a) x = 0.3, b) x = -0.3

Scale factor

The scale factor determines the amount of scaling that takes place in the center-to-center method. As a result, it determines the locations where the beams are supported along the adjacent beam. For a scale factor of 0.5, the beams seem to connect at the most

neutral locations (at ¼ and ¾ of the beam). A low scale factor results in the connections being closer to the middle of the adjacent beams, and a high scale factor results in the connections being closer to the ends of the adjacent beams. The influence of the scale factor can be seen in Figure 166.

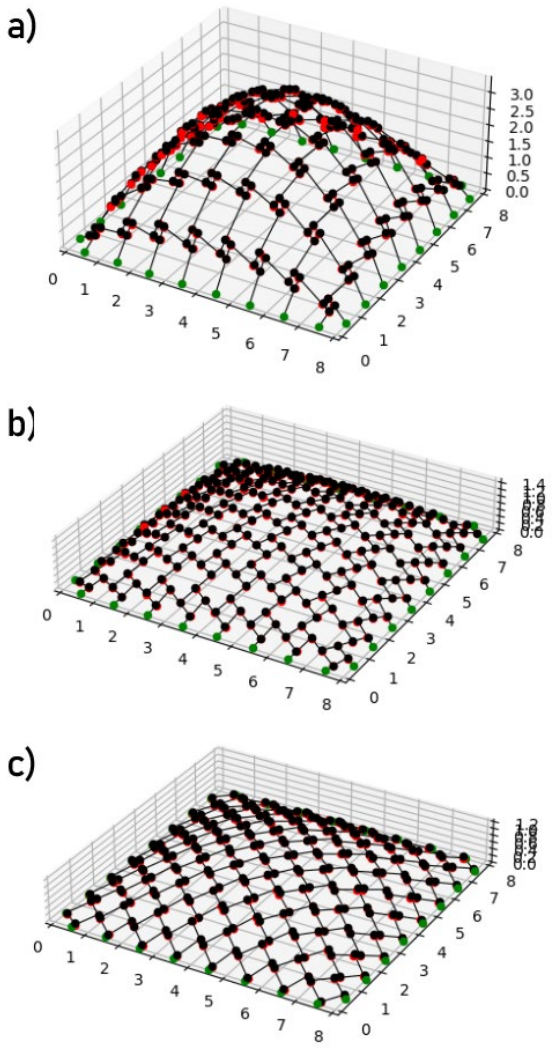


Figure 166: Geometry for an 8x8m reciprocal frame [square, 1, 0, x, 30] with scale factor: a) x = 0.2, b) x = 0.5 and c) x = 0.8

As a result of the locations of the connections, the scale factor also determines the amount of rotation the beam elements have with respect to the base tessellation. A low scale factor results in a large rotation with respect to the base square (near 45°) and a high scale factor results in a small rotation.

Again, this parameter also influences the amount of curvature in the reciprocal frame. Since the connections are closer to each other for small scale factors, the eccentricity has a larger effect (as can be seen in Figure 166a. The opposite is also true, when the connections are far away from each other, the eccentricity has a smaller effect (as can be seen in Figure 166c).

Eccentricity

The final parameter that determines the reciprocal frame geometry is the eccentricity. This parameter determines how much eccentricity there is between all elements (in all connections). As a result, the curvature of the reciprocal frame can be controlled using this parameter.

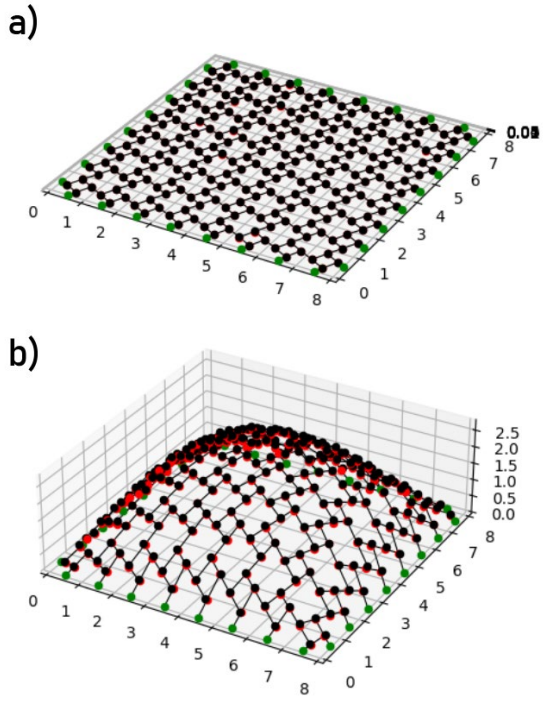


Figure 167: Geometry for an 8x8m reciprocal frame [square, 1, 0, 0.5, x] with eccentricity: a) x = 1mm and b) x = 50mm

The influence of the eccentricity on the resulting reciprocal frame can be seen in Figure 167. A small eccentricity results in an (almost) flat reciprocal frame and a large eccentricity results in a large curvature. As seen earlier however, the eccentricity is not the only parameter that influences the curvature. Therefore, one should be careful with assuming a curvature based on a certain scale factor.

Sheet options

The sheet options in the GUI correspond to the material and dimension of the plywood sheets from which the reciprocal frame should be made. The plywood sheet dimensions determine the maximum dimensions of the beam elements. This means that the boundary conditions of feasible reciprocal frames depend on the sheet size.

The thickness of the sheets influences the stresses in the beam and thus the optimal sizes of the beam elements. Figure 168 shows the same reciprocal structure with different sheet (or element) thicknesses. The resulting optimized section heights differ significantly between the sheet thicknesses.

As a result, much more (2.4x1.2m) sheets are required when using thinner plywood sheets. However, when we compare the volume of the sheets that are required, it does not mean that the solution with the fewest sheets results in the model with the leas timber volume required. The respective volumes for 15mm, 21mm, 30mm and 40mm are: $4.02m^3, 2.13m^3, 1.87m^3$ and $2.50m^3$. In this case, using 30mm sheets would thus be the most efficient. The reason for this is the fact that with 30mm sheets, the beams have approximately the same height as for 40mm with less thickness.

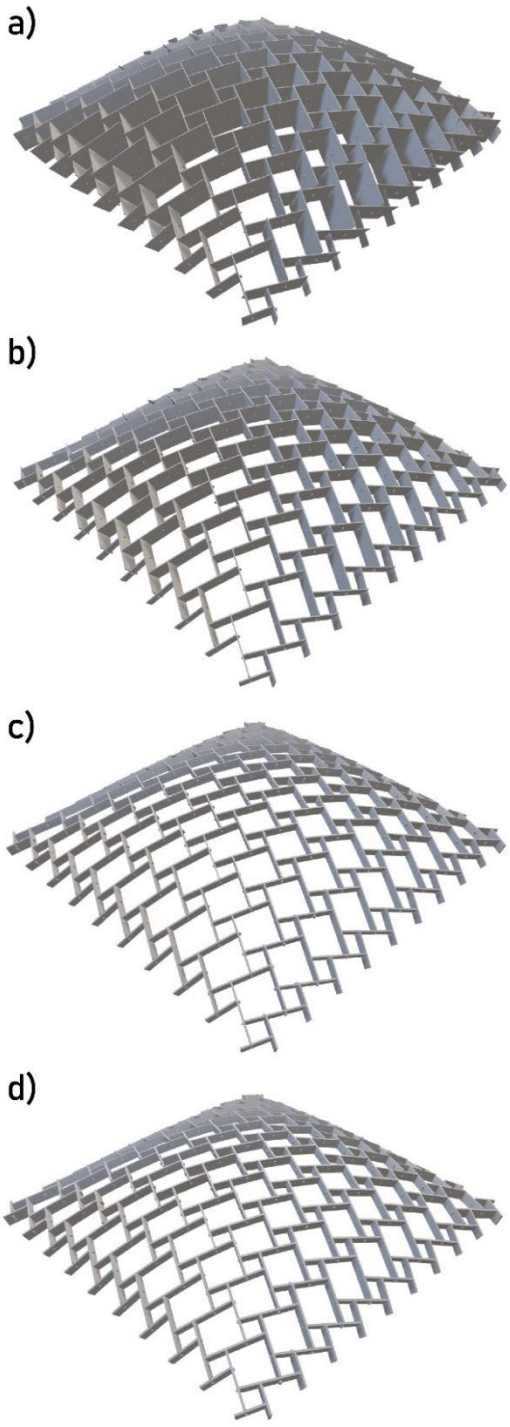


Figure 168: Cross-section optimized beam geometry for an 8x8m reciprocal frame [square, 0.8, 0, 0.5, 20] with sheet thickness a) 15mm, b) 25mm, c) 30mm and d) 40 mm

The material is also of large influence of the optimization. In this research, all structures have been calculated using 'standard' plywood design strengths and stiffnesses (acc Wieringa et al. (51)). Using other material properties may result in significantly different results.

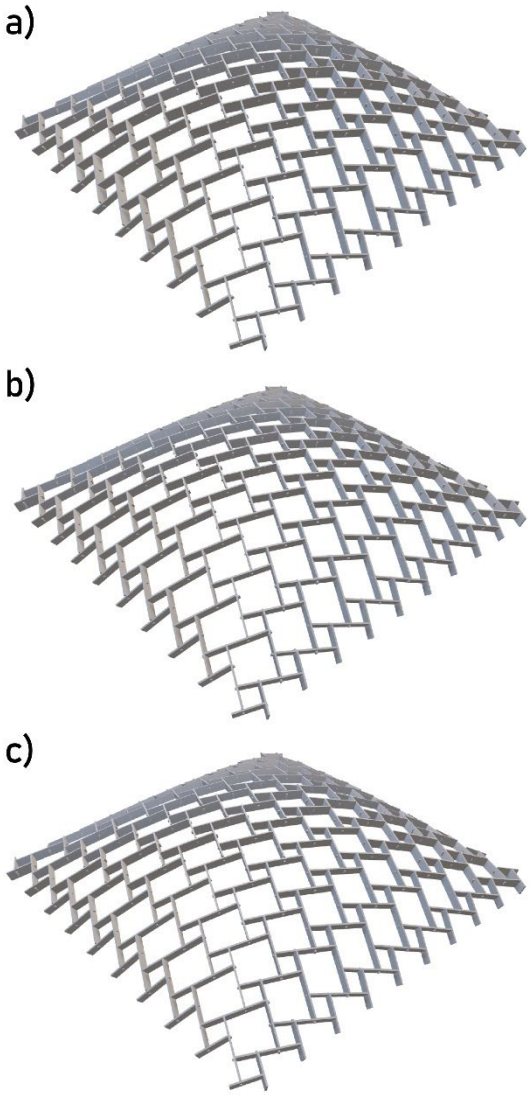


Figure 169: Cross-section optimized beam geometry for an 8x8m reciprocal frame [square, 0.8, 0, 0.5, 20] with 30mm sheets for with a maximum unity check of: a) 0.6, b) 0.8 and c) 1.0

Cross-section optimization options

The cross-section optimization options in the GUI correspond to the parameters that are used during the cross-section optimization. The minimum beam height can be entered when the user wants to have certain minimum beam dimensions for aesthetical reasons.

The maximum unity check can be used by designers to determine the amount of margin in the unity checks. It is not advisable to design with a maximum unity check of 1.0 since small differences in loading or self-weight might result in unity check values above 1.0

The influence of the maximum unity check is visualized in Figure 169, where the same structure has been optimized for a maximum unity check of respectively 0.6, 0.8 and 1.0. The resulting beam heights do not seem to differ significantly, however when looking especially in the center of the structure, the beam heights are lower when a unity check of 1.0 is allowed. This can also be seen when looking at the amount of 2.4x1.2m sheets required; respectively 27, 21 and 18.

Load determination options

The load determination options influence the Eurocode loads that are placed on the structure. The 'z' parameter influences the base height of the structure. This influences the wind pressure and thus the wind load. Additionally, the wind area also influences the wind pressure.

The consequence class influences the load combination factor K_{FI} that is used in the determination of the load combinations. This means that the resulting structure also changes based on the consequence class. These differences are visualized in Figure 170.

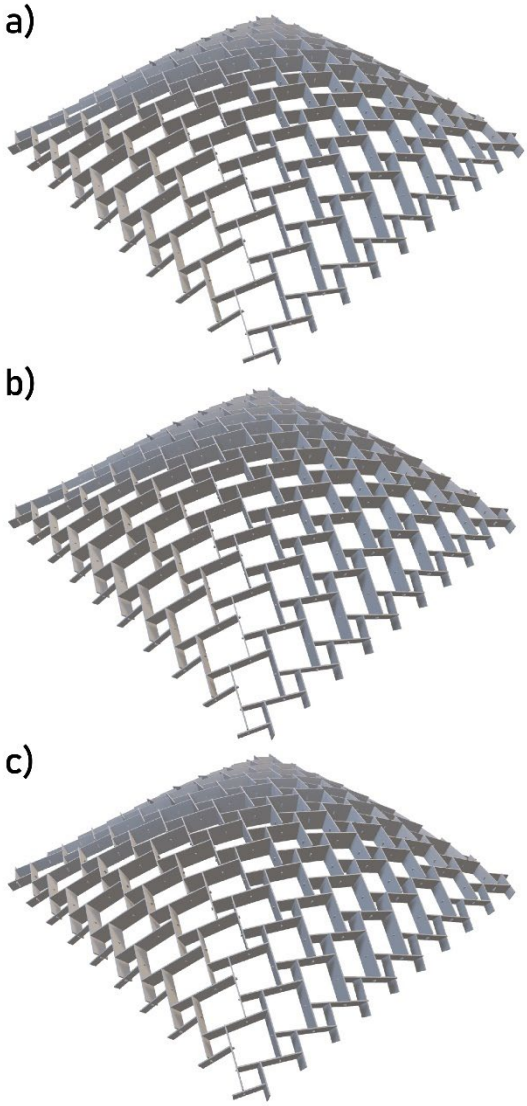


Figure 170: Cross-section optimized beam geometry for an 8x8m reciprocal frame [square, 0.8, 0, 0.5, 20] with 30mm sheets for consequence class a) CC1, b) CC2 and c) CC3

The differences in the cross-sections do not seem to be very large. However, when we look at the number of 2.4x1.2m plywood sheets required to make this structure, there are quite some differences. Respectively, the number of sheets required are: 32, 34 and 38.

Note: the consequence class only influences the load combination factor, other requirements for specific consequence classes (e.g. secondary load paths) are not considered in this comparison and research.

Export options

The export options can be used to control what should be exported from the reciprocal frame designer. The STL files can be used for the CNC production of the elements. Figure 171 shows an example STL file of one beam element. The element data is fully three-dimensional, which means that no additional information is required to create such beam element.

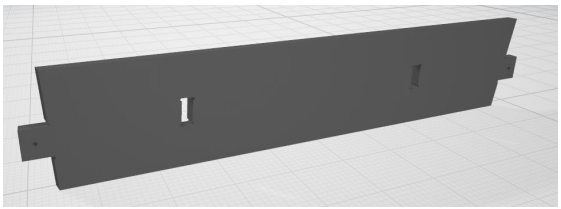


Figure 171: Example of an STL file that can be used for 3d CNC production

Additionally, full STL models are created which can be used to visualize the structure within its architectural context.

The exported cutting pattern is discussed in chapter '7.2 Cutting pattern'. The cutting pattern can be used to determine the location on the sheet from which the beam should be obtained. This location is determined by the aforementioned bin-packing algorithm(s). Annex 2: Plywood cutting pattern shows examples of the cutting patterns both before and after the parametric optimization.

Finally, a calculation report is automatically generated by the reciprocal frame design tool. The user can control whether to generate a full report (with intermediate steps) or a report with only the unity checks

(optionally with or without the internal force diagrams in the beam elements).

'Annex 1: Calculation reports' shows example calculation reports that have automatically been generated for a typical reciprocal frame structure.

9.2 Parametric optimization results

Conditions for the optimization

For a clear comparison of all factors in the parametric optimization, example structural conditions are assumed. This way, the results are consistent and comparative.

For the parametric optimization, the following parameters are assumed:

- Reciprocal frame dimensions: 8x8m
- Plywood sheet dimensions: 2440x1220mm
- Maximum allowed unity check: 0.8
- Base height z: 3m
- Wind area II, Unbuilt
- Consequence class: CC2
- Cladding density: 0.2 kN/m^2

The reciprocal frame dimensions are selected as such that the number of elements are not excessive, keeping the computation times per iteration below an hour. The plywood sheet dimensions are selected to suit the industry standard dimensions. The other parameters are selected to give a typical/average result.

Initial exploration

As mentioned in chapter '8. Parametric optimization', the parametric optimization is performed in two steps. Firstly, the areas of interest are searched using the initial exploration. The goal of the initial exploration is focused on limiting the search area of the edge size. This drastically improves the Bayesian optimization process as less iterations are required because 'bad' parts of the optimization are quickly eliminated

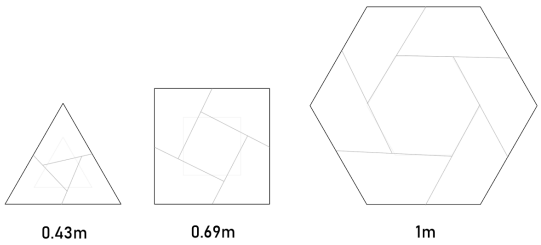


Figure 172: Equilateral polygons that are used in the tessellation (to scale, with the same edge size) and their resulting reciprocal frame geometry with $S_f = 0.5$ (corresponding beam length indicated below the figure)

The initial exploration is performed for all different tessellation patterns, as the pattern is a large influence on what tessellation edge sizes are promising. A large part of this influence can be derived by looking at the shapes that make up the tessellation. As can be seen in Figure 172, a hexagon with the same edge size is significantly larger than a triangle or square with the same edge size. The resulting reciprocal beam geometry is thus also larger for hexagons. Therefore, the optimal edge sizes are expected to be smaller for

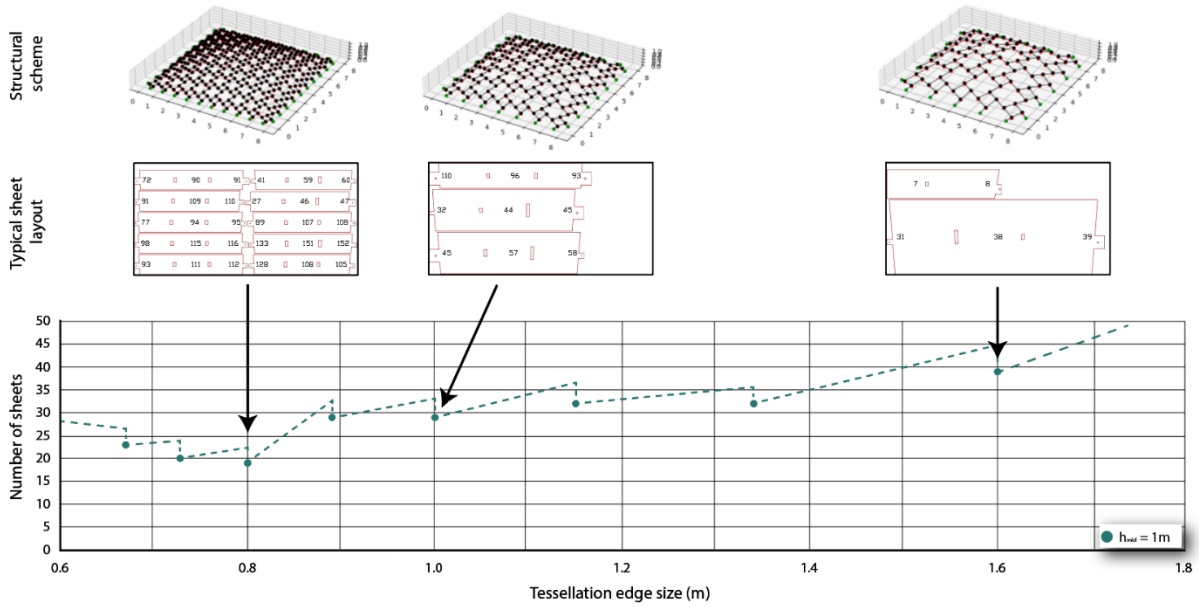


Figure 173: Initial exploration for Square tessellation pattern with center height h_{mid} = 1m

patterns containing hexagons than for patterns that consists of purely triangles or squares.

Square tessellation pattern

The results of the initial exploration for the square polygon tessellation is visualized in Figure 173, where the number of sheets required to make the reciprocal frame is plotted against the tessellation edge size. The corresponding typical cutting pattern for each sheet and the corresponding structural geometry is visualized for some interesting locations. The dots indicate the locations at which the results are obtained, and the dotted lines is the expected trend based on previous results.

As can be seen in Figure 173, there is a significant 'dip' in the number of sheets required when the edge size is 0.8. This dip can be explained by the fact that 2 elements fit on one row in the sheet instead of one.

On the left side of the graph, there is an upward trend which means that the larger the edge size the more sheets there are required to make the structure. This upward trend is less steep when you would compare it to the total volume of the beams. The reason for this is the fact that for larger edge sizes, a larger part of the sheet can be used resulting in less cutting loss.

When the same tessellation is compared for a different center height, $h_{mid} = 2m$, the dip seems to shift a bit towards the smaller edge sizes (see Figure 174). The reason for this is the fact that the beam elements are more stretched to create the desired shape.

Another observation that can be seen in the figure is the fact that increasing the center height to 2m, in this case, does not result in solutions with fewer sheets required. This means that the optimal solution is not always the most curved solution.

Unlike the other tessellation patterns, which will be discussed later, the square tessellation pattern seems to be very efficient when it is flat. This behaviour can be seen in Figure 175, where the

results are visualized for a center height of 0m.

The same dip in the graph is found when the edge size is 0.8. However, the most apparent part of the graph is the fact that there are very few sheets required when the edge size is 1.6. With this edge size, beam elements exactly fit on the sheet in the width.

Structurally, this pattern is more efficient when flat compared to the other tessellations for a few reasons. Firstly, the stress concentrations are lower when the holes in the beam are not rotated (so when the beams are perpendicular). Secondly, the square pattern is efficient when flat because the elements are loaded purely in torsion due to the fact the beam are perpendicular. This means that there is little normal force in the structure, meaning that no buckling behaviour prevents the elements to be long.

As a result of this initial exploration, the area of interest for finding the structure

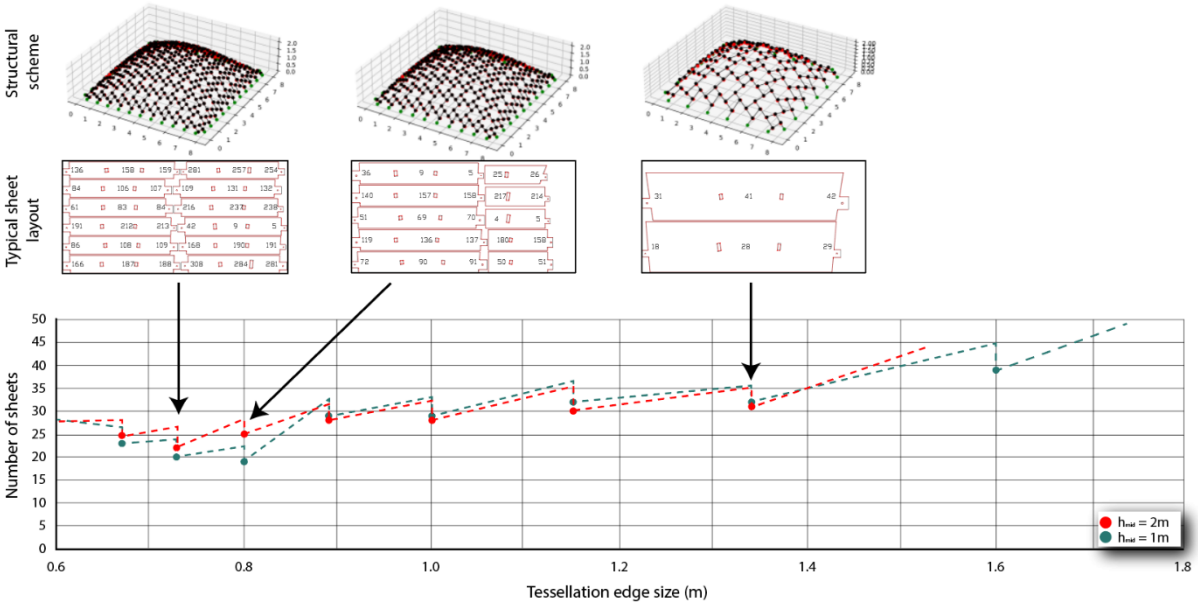


Figure 175: Initial exploration for Square tessellation pattern with center height $h_{mid} = 2m$

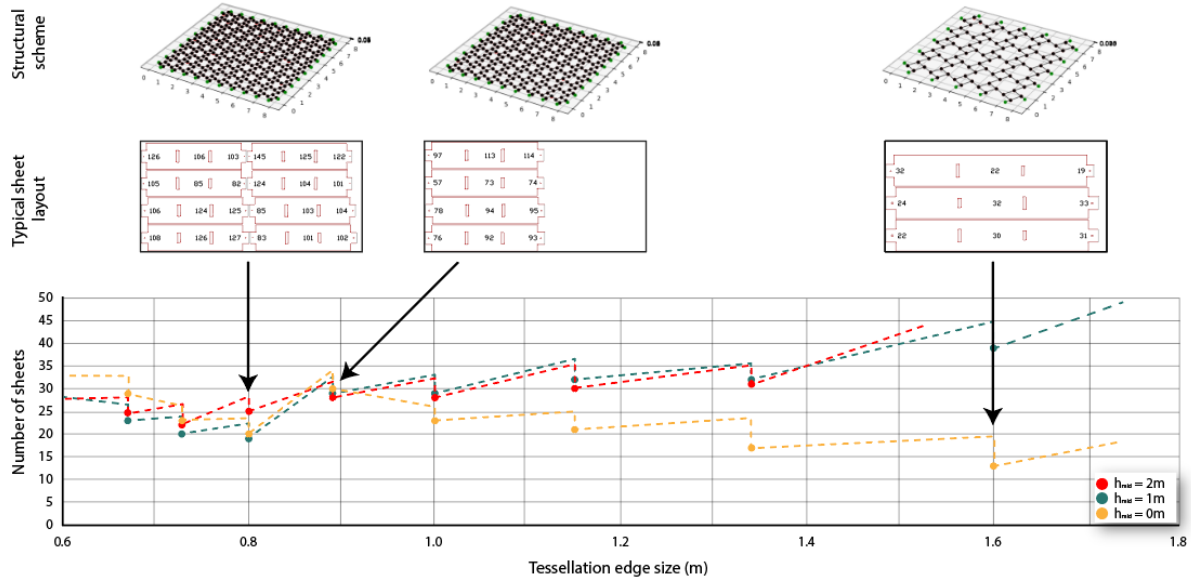


Figure 174: Initial exploration for Square tessellation pattern with center height h_{mid} = 0m

that uses the least amount of plywood sheets, is for tessellation edge sizes between 0.73m and 0.8m.

In this chapter, only the most important findings of the initial exploration are elaborated. The full internal exploration graphs for the square tessellation can be found in Appendix 3.1, figure 1-4.

Triangle tessellation pattern

The results of the initial exploration of the triangle tessellation pattern with a center height of 1m is visualized in Figure 176. The behaviour of the edge size with respect to the number of sheets required is similar to that of the square tessellation pattern.

The region after the dip however is more stretched. The reason for this is the fact that the beam heights still drastically decrease by decreasing the edge size. This means that there is more cutting loss, but also much less volume required for the beam elements.

Another striking difference between the triangular tessellation and the square tessellation pattern is the area before the 'dip' in the graph. For the triangular tessellation pattern, this part of the graph is much steeper. This is caused by the fact that the triangular pattern is much less structurally efficient when there are large spans. This can be seen by the required beam height when the edge size is 1.7, where beam height is almost equal to the sheet height.

When the center height increases, the dip in the graph does not move in this case (see Appendix 3.2, figure 2). The reason for this is the fact that the increased structural efficiency weighs up to the increased cutting loss caused by the fact that some elements are too large to fit two elements on the sheet. This highlights the fact that the optimization of the reciprocal frames with respect to raw material is a balancing act between structural efficiency and cutting efficiency.

Contrary to the square tessellation, the triangular tessellation pattern is not as efficient when flat (i.e. $h_{mid} = 0$). This is caused by the fact that the beams are not connected perpendicularly. This

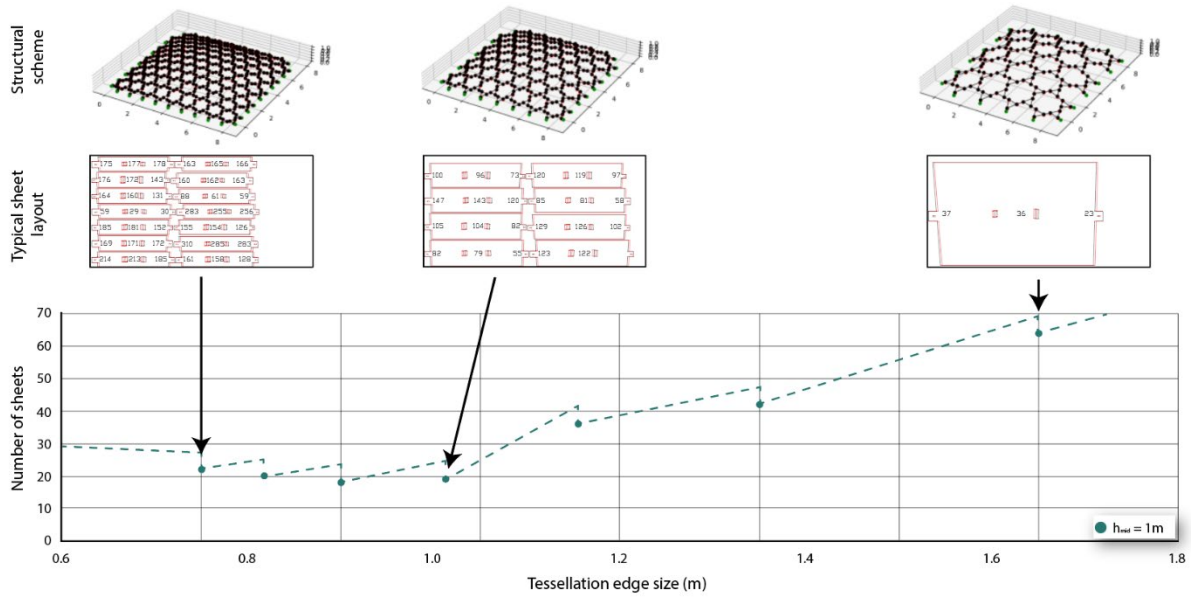


Figure 176: Initial exploration for Triangle tessellation pattern with center height h_{mid} = 1m

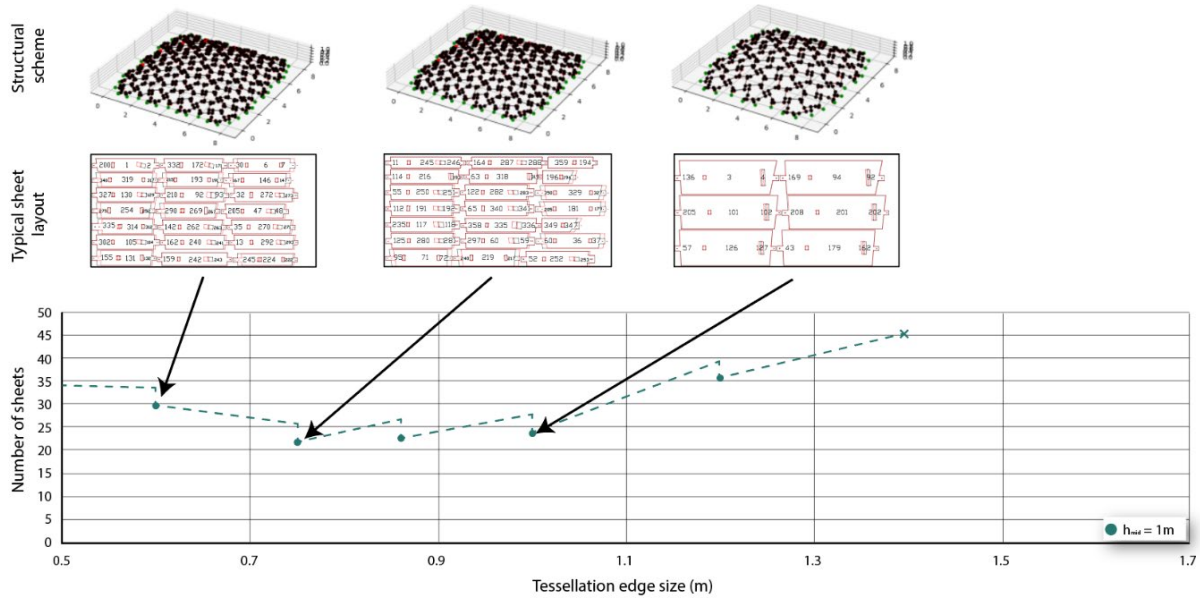


Figure 177: Initial exploration for Snub-Square tessellation pattern with center height $h_{mid} = 1m$

causes an increase in stress concentrations due to the additional rotations of the holes. These results are visualized in Appendix 3.2, figure 3.

The area of interest for the triangular tessellation is between 0.83 and 1.03m.

Snub-Square tessellation pattern

The results of the initial exploration of the triangle tessellation pattern, with a center height of 1m, is visualized in Figure 177. The behaviour of the snub-square tessellation pattern is similar to those of the triangular and square tessellation patterns. For the Snub-Square tessellation, not all elements have the same length due to the combination of triangles and squares in the tessellation. As a result, there is still a dip when the edge size is 1.0 but the dip is more outstretched, where another minimum is found when the edge size is 0.73.

The range of the possible design region for the snub-square tessellation is much smaller compared to the previously mentioned tessellation patterns, as for an edge size of around 1.4m, the structure cannot be created from 1.2x2.4m plywood sheets. This is caused by the fact that the beams required for that layout are higher than the smallest sheet dimension.

When the center height of the reciprocal frame is increased to 2m, the design region becomes larger (see Appendix 3.3, figure 2). This means that for large edge sizes, this makes the structure more efficient. Also for the smaller edge sizes, the reciprocal frame becomes more efficient when the center height is increased.

The behaviour when the center height is 0m is similar to that of the triangular tessellation pattern, which means that the structure is less efficient when flat.

As a result of the initial exploration of the snub-square tessellation pattern, the search region for the edge size is between 0.74m and 1.0m.

Honeycomb tessellation pattern

Figure 178 shows the results of the initial exploration of the honeycomb tessellation pattern. As expected, the

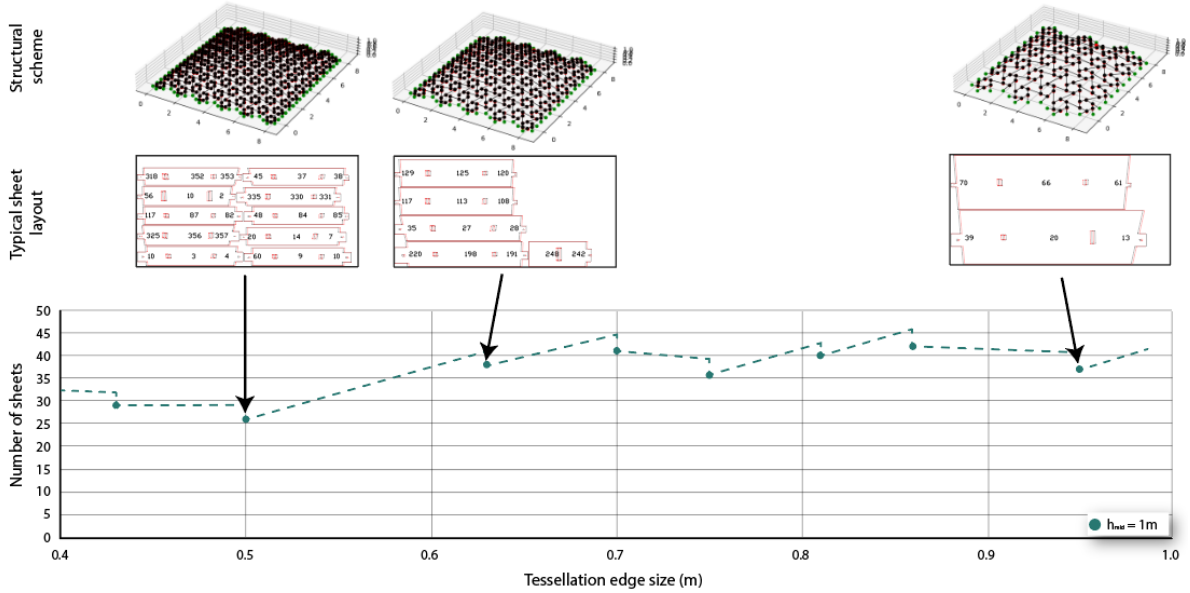


Figure 178: Initial exploration for Honeycomb tessellation pattern with center height h_{mid} = 1m

area of interest regarding the tessellation edge size for the honeycomb pattern is much smaller (caused by the size difference for an equilateral hexagon).

As a result, the 'dip' in the graph of the number of sheets required is found at 0.5m edge size. Similarly to the other patterns, this dip is found when two elements fit in a row on the sheet.

The behaviour before the dip seems to be more constant compared to the other tessellations. This is likely caused by the fact that the number of elements increases more rapidly compared to the other tessellations. For each element, the length of the tenons is added to the total element, meaning that the material usage automatically increases when there are more elements. As a result, the increase of beam height is counteracted by less additional loss.

When the center height is increased to 2m ($h_{mid} = 2m$), the differences in the number of sheets required is less significant than for the other patterns (see Appendix 3.4, figure 2).

For this tessellation, even the results when $h_{mid} = 0m$ follows the same results. The only difference is the fact that the dip is not very apparent anymore. This means that when you would apply the honeycomb pattern for a 2d structure, the cutting efficiency is not a large influence in the resulting amount of sheets required.

As a result of the initial exploration for the honeycomb tessellation pattern, the search region for the tessellation edge size is between 0.43 and 0.5m.

Trihexagon tessellation pattern

The final tessellation pattern that is considered in this research is the trihexagon tessellation pattern, which consists of a combination of hexagons and triangles. The results of the initial exploration is visualized in Figure 179. In this case, the dip in the graph is found at a an edge size between the honeycomb and the triangle pattern. This makes sense as the element is also between the lengths that are created with these tessellation patterns.

The 'dip' in the graph occurs at an edge size of 0.74m. After the dip, the results

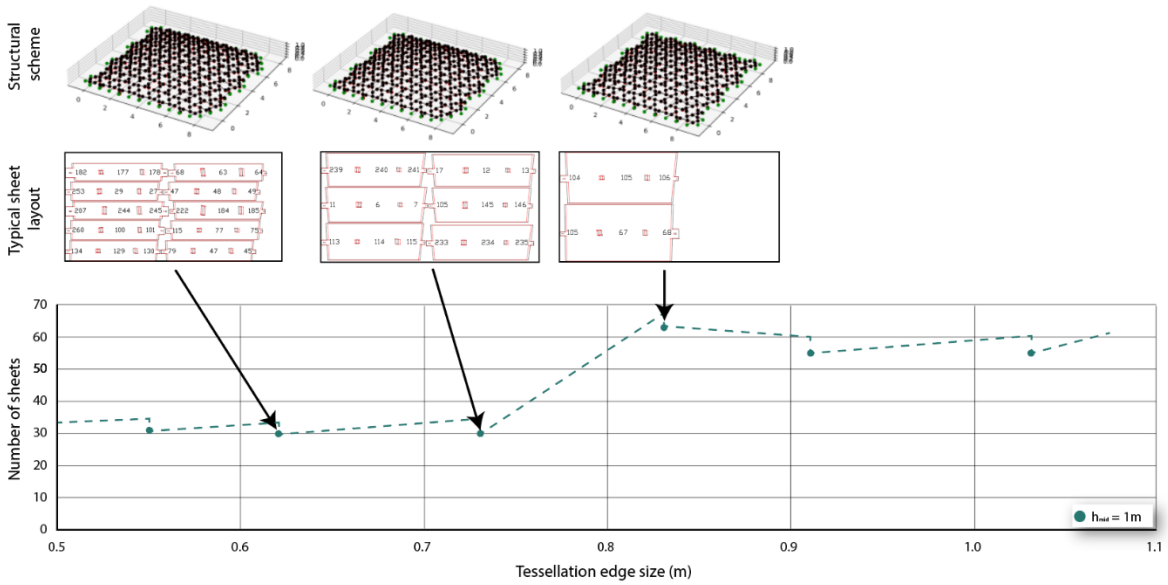


Figure 179:Initial exploration for Trihexagon tessellation pattern with center height h_{mid} = 1m

remain relatively constant. This is caused by the fact that when the beam lengths are approximately half the beam size, the sections are still relatively high. This means that decreasing the edge size will result in smaller sections (but more cutting loss).

The results of the trihexagon are relatively similar independent of the center height of the reciprocal structure (see Appendix 3.5, figure 2-4). This means that the dip in the graph does not really move, and that the value at the dip is almost equal. The only observed difference is found when the center height is 0m. When the edge size is relatively large, a smaller amount of sheets is used. This is caused by the fact that there is no compression (and thus buckling) when there is no curvature.

As a result of this initial exploration, the search area of the tessellation edge size is between 0.55 and 0.74m.

Bayesian optimization

After the area of interest is found, the Bayesian optimization is applied to find a complete optimum. As mentioned in chapter '8. Parametric optimization', the optimization goal of the Bayesian optimization is:

Minimize $V_{sheets} + 0.2V_{beams}$

This means that the most optimal result is found when the number of sheets is the lowest, and the accompanying beam volume is the lowest.

Sheet thickness

To be able to see the direct influence of the sheet thickness on the amount of material that is used, the Bayesian optimization algorithm is applied for an edge size of: 15mm, 21mm, 30mm and 40mm.

The results of these optimizations can be found in Appendix 3, where the amount of sheets and the volume of sheets for each sheet thickness are summarized for each tessellation pattern.

When observing the results for - for example - the square tessellation pattern in Figure 180, it is noticeable that the volume of the sheets required to make the structure is largely dependent on the sheet thickness.

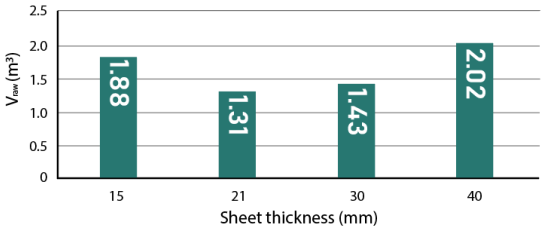


Figure 180: The volume of sheets (V_{raw}) required to make a square tessellation pattern, 8x8m, reciprocal frame

When a beam is loaded in pure uniaxial bending – and influences like lateral torsional buckling are neglected – the beam gets more efficient when the height becomes larger with respect to the width. This is not the case for reciprocal frames because the bending is biaxial. Therefore, it can be seen that when the beam thickness is too small, the volume of sheets requires increases significantly. Additionally, when the elements are larger, it becomes increasingly more difficult to efficiently pack the beam elements into the bins (read: sheets).

Figure 181 shows the optimal structural shapes for each of the sheet thicknesses. *Note: there are multiple structural shapes that can be made from the same number of sheets*. Interestingly, the thinner the sheets, the more curvature there is in the most optimal structure. This means that the out-of-plane bending is not necessarily governing.

This means that bending in the middle of the structure is a governing factor. The larger the curvature, the smaller the bending moment in the middle of the section. This limits the beam height in the middle of the reciprocal frame.

The out-of-plane bending is likely to have a smaller influence as the bending stiffness out of plane becomes extremely low. This means that less forces are transferred using the bending out-of-plane path. Instead, the flow of forces is more shear-focused.

For increasing beam thicknesses it becomes less important to reduce the moment in the middle of the reciprocal frame, and the bending out-of-plane becomes more significant. Therefore, in those cases, the amount of curvature is significantly lower.

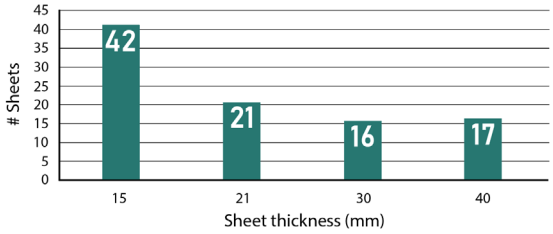


Figure 182: Number of sheets (V_{raw}) required to make a square tessellation pattern, 8x8m, reciprocal frame

When expressing the result of the 4 Bayesian optimizations in terms of amount of sheets required (see Figure 182), it is noticeable the effect of the lower sections that can result from the

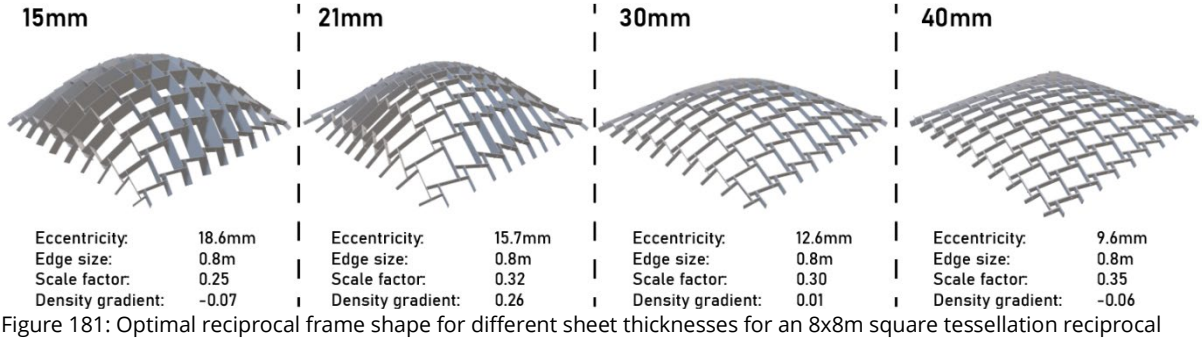


Figure 181: Optimal reciprocal frame shape for different sheet thicknesses for an 8x8m square tessellation reciprocal frame

section optimization with 30mm thick elements, is not significant enough to result in a lower sheet volume compared to the result for 21mm thick elements.

These results are relatively similar for each tessellation pattern, where 21mm is the most efficient sheet thickness. The only outlier that is found is the trihexagon tessellation pattern. In that case, 30mm thick sheets are the most efficient (see Figure 183).

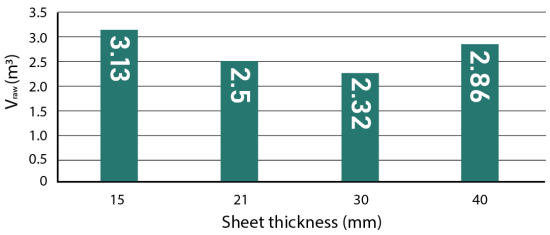


Figure 183: The volume of sheets (V_{raw}) required to make a trihexagon tessellation pattern, 8x8m, reciprocal frame

For the tessellation patterns with a relatively narrow search region in terms of edge size (square and triangle), the resulting optimal shape has the same edge size. For the other patterns, for a low sheet thickness, the optimal edge size is smaller compared to the optimal edge size for thicker patterns.

The full results can be found in Appendix 3, where figures 5 and 6 and the accompanying pictures below show the results of the optimization for each sheet thickness.

Scale factor

One of the factors that is included in the Bayesian optimization is the scale factor. The scale factor controls the location of the connections along the beam. A high scale factor will move the connections towards the middle of the beams whilst a low scale factor will move the connections towards the ends of the beam.

Generally, the behaviour as depicted in Figure 185 is observed for each tessellation pattern. This means that when the scale factor is lower, generally, the structure becomes more efficient. In a 3d reciprocal frame, this can be explained by the fact that the smaller the scale factor gets, the more the structure behaves like a normal space frame. This means that the normal forces have to transfer a shorter path towards adjacent nodes, resulting in less out-of-plane bending.

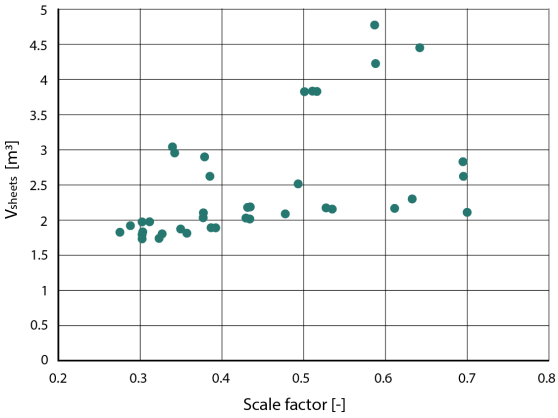


Figure 184: Scale factor plotted against the volumes of sheets obtained from the Bayesian optimization of an 8x8m square tessellation reciprocal frame

The scale factor is lower-bound limited by the distance to the end of the beam. The distance must at least be equal to the beam height in order to make sure the forces can flow around the hole as expected. For the upper bound, the scale factor is limited by the fact that the holes cannot touch each other (after rotation). The distance between the holes must at least be equal to the beam height as well to make sure the area can transfer reaction forces adequately.

Tessellation density gradient

The tessellation density gradient parameter is suggested in this research as it can enable a more efficient reciprocal frame by creating more density. Generally, this behaviour can be confirmed by the data that was obtained during the parametric optimization. As visualized in Figure 185, when the tessellation density gradient is positive, the amount of sheets is reduced.

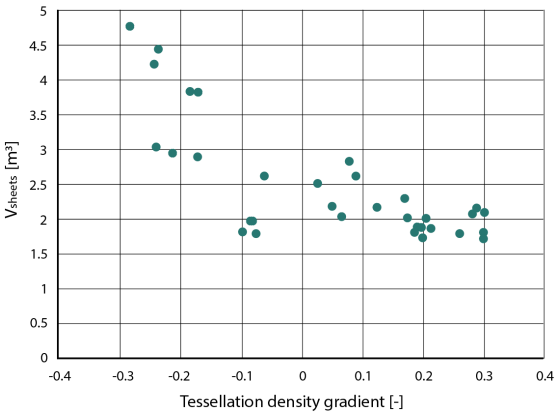


Figure 185: Tessellation density gradient plotted against the volumes of sheets obtained from the Bayesian optimization of an 8x8m square tessellation reciprocal frame

In the results however, another phenomenon is observed. When the tessellation density gradient is slightly negative, minima are also found.

When the reciprocal frame is translated from 2d to 3d, the beam elements are stressed as the nodes are moved in z-direction, but not in the x- or y-direction. A slightly negative tessellation density gradient counteracts this behaviour, and enables the beam elements to be more similar in length. This makes packing the elements in the available sheet size a lot more efficient.

In Figure 189 the optimal shape after optimization for each of the tessellation patterns is visualized. As can be seen in the figure, a high tessellation density gradient seems to be the most efficient for the square tessellation pattern, where the density is significantly higher in the center of the structure. However, there are multiple solutions for the same tessellation pattern that uses the same amount of sheets. Therefore, the square tessellation pattern can also be efficient with a slight negative tessellation density gradient.

For the other tessellations the most optimal geometry has a slightly negative density gradient (between -0.05 and -0.1). This means that the optimization in that case was production focused instead of structurally focused.

Comparing tessellation patterns

After optimizing all parameters for each tessellation pattern, a fair comparison between the material efficiency of each pattern can be made.

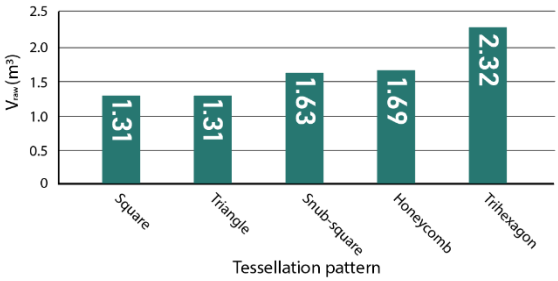


Figure 186: Comparison of sheet volume required to make an 8x8m reciprocal frame for each tessellation pattern

Figure 186 shows a direct comparison between the tessellation patterns. The square and triangle tessellation patterns seem to be equally efficient after optimization, as the same amount of sheets are required to make those reciprocal frames.

The snub-square tessellation pattern. Is slightly less efficient. There are multiple reasons to be found for the reduced efficiency. Firstly, it is impossible to fit the tessellation exactly to the 8x8m plan. This means that an additional, unnecessary, part is added to the span of the structure.

Another reason for the reduced efficiency is the fact that the beam elements do not have an equal length due to the combination of triangles and squares in the pattern.

Finally, the snub-square pattern is also less efficient structurally. As can be seen in Figure 189, several load-paths are formed, where the height of the elements is significantly larger than the surrounding elements. This means that a small part of the structure needs to carry a significant part of the loads on the structure.

The honeycomb structure is also less efficient compared to the triangle and square pattern. The reason for this cannot necessarily be found in the structural behaviour. The difference in this case is found by looking at the number of beams required to make the tessellation (see Figure 187).

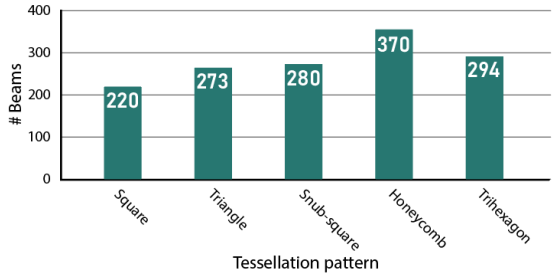


Figure 187: Comparison of number of beams required to make an 8x8m reciprocal frame for each tessellation pattern

The honeycomb pattern uses much more elements compared to the other patterns. The reason for this can be found by the fact that a small edge size must be used to create elements that are short enough to be packed efficiently on the sheets. As mentioned before, each element creates an automatic additional loss of material caused by the tenons on the ends of the beams.

Additionally, similar to the snub-square pattern. It is impossible to exactly fit the polygon tessellation on the 8x8m plan. This means that some additional span is created when applying this pattern.

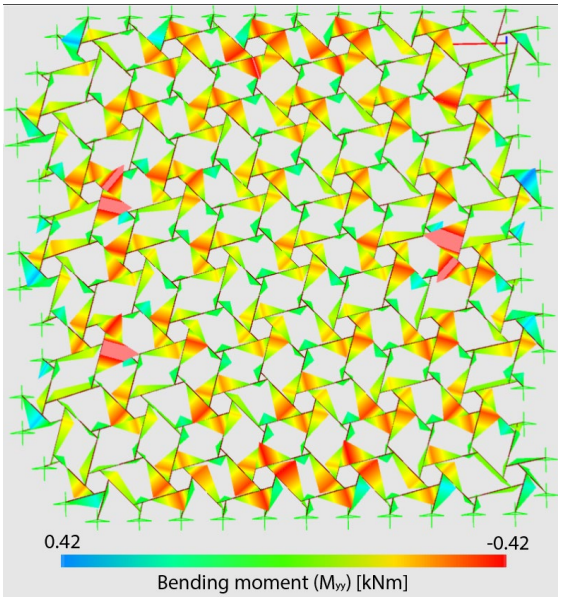


Figure 188: Out of plane bending moment in 8x8 trihexagon reciprocal frame (top view)

Finally, the trihexagon pattern seems to be significantly less efficient compared to the other tessellation patterns. Besides the reasons posed for the other tessellation patterns, this tessellation pattern also seems to be structurally less efficient. A similar amount of sheets is used for the pattern when compared to the snub-square and honeycomb pattern. However, in the case of the

trihexagon pattern, the sheets have a thickness of 30mm instead of 21mm.

The reason for this structural inefficiency can be found by looking at the out-of-plane bending moments, see Figure 188. The hexagonal shapes seem to have a higher stiffness compared to the triangular shapes. Because of this, the hexagons must transfer most out of plane bending forces. This means that all elements must have larger section sizes because all elements are connected to the hexagon on at least one side.

Scale models

To be able to compare the resulting structures physically and aesthetically, structural scales models (1:20) have been made for each of the tessellation patterns. The base plate of the models are open which allows people to look at the model from the bottom, simulating the look from the interior of a building.

The scale models are automatically used to test/showcase the reciprocal frame designer output. Pictures of the resulting scale models are attached to this thesis in Annex 3.

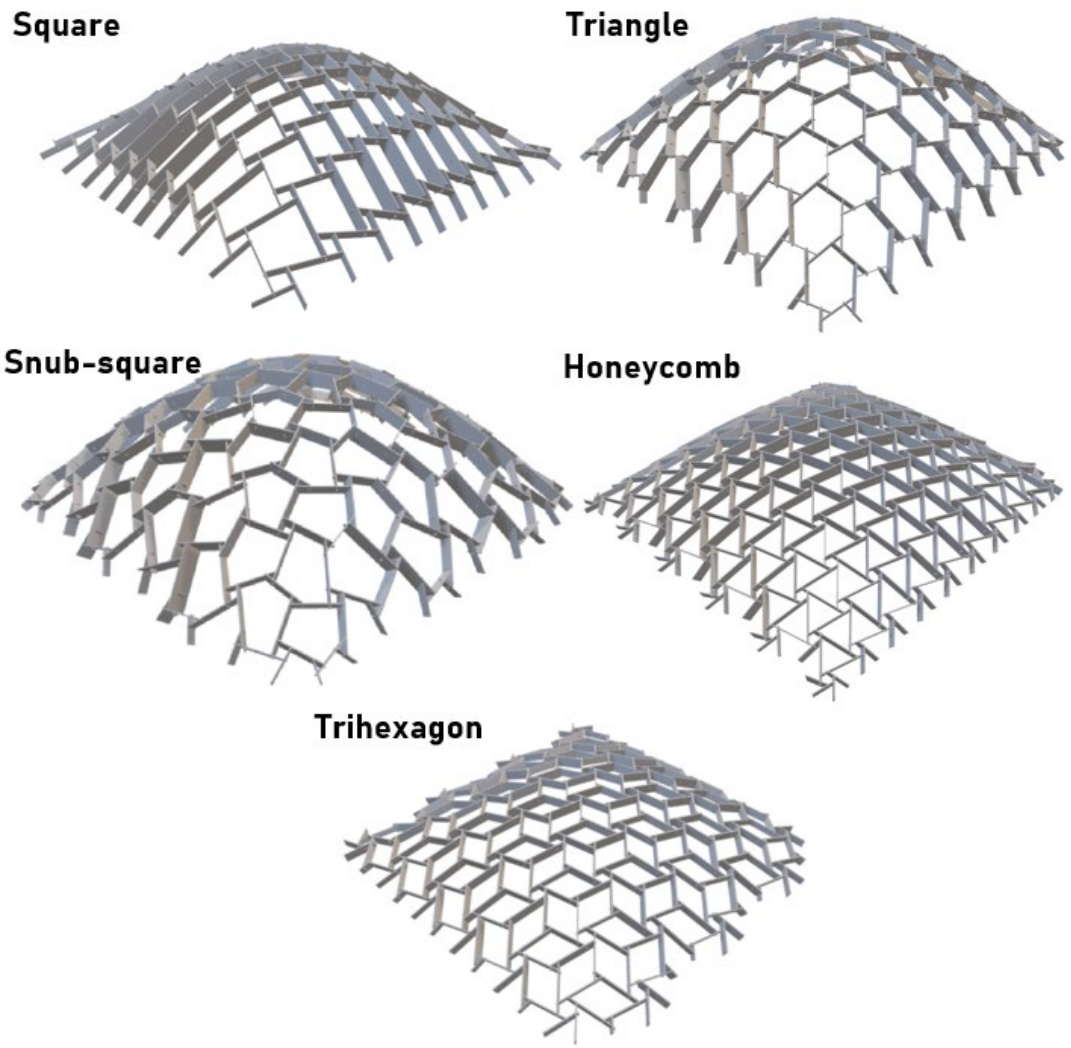


Figure 189: Most efficient reciprocal frame geometry for each tessellation pattern found by applying the Bayesian optimization algorithm

10. Conclusions

To answer the research question, a reciprocal frame designer tool has been developed that generatively designs a plywood reciprocal frame and optimizes the cross sections of the individual cross sections in the structure. As an output, digital manufacturing data is generated that can be used to automatically fabricate the components that make up the reciprocal frame.

The generative design is performed by applying the center-to-center method on a two-dimensional equilateral polygon tessellation. The geometry is then inflated to a three-dimensional reciprocal frame by moving the z-coordinates of the nodes until a set of boundary conditions is met. Finally, the exact structural shape is found by mathematically minimizing the model error by applying the L-BFGS-B algorithm.

The cross-section optimization is performed by applying a custom step-by-step optimization method. This method is a monotonic sizing optimization, meaning that the opima can only be found by increasing the cross-sectional heights. As a result, the solution converges fast. However, the found structural sections may not be a global minimum.

From the parametric optimization results, it can be concluded that the structure does not necessarily have to be optimal if only the individual cross-sections are optimized. There is a large potential for optimization by optimizing or tweaking the parameters that make up the generative design.

In the approach proposed in this thesis, a reciprocal frame structure can be designed by the following set of parameters:

- Tessellation pattern
- Tessellation edge size
- Scale factor
- Eccentricity
- Tessellation density gradient
- Sheet thickness

Each of these parameters have a significant influence on the resulting amount of material (plywood sheets) required. The following conclusions can be drawn from the parametric optimization.

(1) The tessellation pattern is of significant influence on the resulting amount of material required when designing a reciprocal frame out of plywood. In the example case that was used for the parametric optimization, the triangular and square tessellation are the most efficient patterns. The other patterns are less efficient due to a number of causes:

- **How well the tessellation fits on the initial rectangular floorplan.** The square and rectangular tessellation result in less unnecessary span when compared to the other patterns
- **The structural efficiency of the resulting geometry.** The reciprocal frames where different polygons are applied in the tessellation seem to be less efficient. This is likely caused by a

difference in stiffness over parts of a structure.

- **The amount of elements required to obtain certain beam lengths**. Patterns that include hexagons have relatively long elements compared to the other tessellations. This means that the optimum uses significantly more beam elements whilst the elements have the same length. This is unfavorable for, for instance, buckling. Therefore, the resulting optimum structures have less curvature.
- **The equality of the resulting beam lengths**. Some polygon tessellations automatically result in different beam lengths due to the combination of different polygons in the tessellation (e.g. the snub-square tessellation). This makes is more difficult to efficiently pack the beam elements on the plywood sheets.

The trihexagon polygon tessellation is significantly less efficient than the other tessellation patterns due to a combination of the aforementioned factors.

(2) The edge size is another significant parameter when optimizing a reciprocal frame structure. When optimizing this parameter in the initial exploration, it was observed that this parameter clearly shows the difference in optimizing for structural volume or raw material. Since the focus in this research is on optimizing for raw material, it can be seen that there is a large drop in amount of sheets required when the edge size is as such that two rows of beam elements can be fitted on a plywood sheet. The resulting optimum however does not represent the optimum when designing for the volume of the structural elements.

(3) Local minima in raw material usage when the edge sizes are as such that it enables the polygon tessellation to fit the rectangular plan as closely as possible. This is the case because if the tessellation does not fit the plan closely, an additional, unnecessary, span has to be covered.

(4) The scale factor that is used in the center-to-center method also influences the resulting amount of plywood sheets that are required. For the example case, it was found that decreasing the scale factor to the lower bound generally gives more optimal solutions. The influence of this parameter is less significant than the edge size or tessellation pattern, but can be used to tweak the structure to become more optimal.

(5) The influence of the eccentricity parameter is impossible to define, as the resulting curvature of the reciprocal frame is not only a function of the eccentricity, but also the density gradient, scale factor and edge size.

(6) The influence of the curvature, however, can be found especially in the initial exploration. The center height in the structure rather significantly influences the resulting number of plywood sheets. The sweet spot of the curvature is dependent on the tessellation pattern (as well as the other variables). The sweet spot is found by

balancing between the reduction of the moment in the center of the frame and the out-of-plane bending moment and normal force in the elements.

(7) The tessellation density gradient can be used to optimize the reciprocal frames in two ways. One focusses on optimizing the structural behaviour, whilst the other focusses on optimizing for the cutting loss. When the tessellation density gradient is positive (i.e. the density is higher in the middle of the structure), there are more beam elements where the moments are higher, resulting in a more efficient structure. When the tessellation density gradient is slightly negative, the lengths of the beam elements become more equal. This makes retrieving the elements from the plywood sheets more efficient, resulting in fewer sheets required to make the structure.

(8) Finally, the sheet thickness significantly influence the volume of the plywood sheets that are required, as well as the most optimal reciprocal frame geometry. When the sheet thickness becomes too large, elements have the minimum beam height making the structure less efficient. And when the sheet thickness becomes too low, elements become too high making it less efficient to retrieve them from the plywood sheets. For the example reciprocal frame dimensions, 21mm is the most efficient plywood sheet thickness.

To conclude, the reciprocal frame design tool can effectively be used in combination with the Bayesian optimization algorithm to find the optimal reciprocal frame for a certain rectangular floor plan under a set of boundary (load) conditions. The results of the parametric optimization are only obtained for a specific design case. From these results, scale models have been made to test the digital manufacturing data.

This research proposes an approach for designing and optimizing reciprocal frames in which multiple assumptions were made. These assumptions were made to find the structure with the lowest material required, however it cannot be guaranteed that these assumptions led to the most optimal end result.

11. Recommendations

The proposed approach for optimally designing reciprocal from plywood structures is not guaranteed to be the most efficient method. Therefore, in future research it might be useful to propose other design methods or tweak the method proposed in this research with different initial design parameters/choices. For instance the element shape was determined by comparing four proposed beam designs. There might however be other designs that proof to be more efficient. Further research on the optimal beam morphology could result in even more efficient plywood reciprocal frames.

The approach of finding the reciprocal frame geometry is based on multiple assumptions. Firstly, in this research the method of transforming the tessellation to a reciprocal frame is the center-to-center method. This method was applied because it enables a quick and straightforward determination of reciprocal frame geometry. However, it might structurally not be the most efficient design approach. Also, it results in different geometries when applying other design methods. These other geometries might be structurally more efficient, or be more aesthetically pleasing.

This research is limited to squared plans simply caused by the limitations of (wind) load determination in the Eurocode. When a computationally quick method for determining the wind loads on more organic shapes is implemented, this constraint could be released from this research. This would enable designers to optimize plywood reciprocal frames for more organic, non-rectangular plans.

The results of the parametric optimization in this research are limited to one example case of an 8x8m reciprocal frame with a specific set location parameters and for 2.4x1.2m sheets. The effect and influence of the design parameters is not expected to behave significantly different when applied to other dimensions or locations. However, for the quality of the results, it is advised to apply the parametric optimization to multiple designs to check the consistency of the influence of the parameters and the results.

The calculation of the stress concentrations by a pre-trained parametric model has been effective to keep the structural optimization rather quick. However, before applying the resulting geometry in a real-life scenario, the full model should be FEM tested to see the influences of local stress concentrations.

Finally, no true-scale tests have been performed on the resulting structure. This means that the assumed structural behaviour cannot be confirmed by true scale laboratory testing. The structural behaviour as found in the FEM models should be tested to confirm the models. Additionally, all practical tests that have been performed were performed on scale models. This means that it should still be tested whether the structures can also constructed in true scale.

12. Literature

1. Dutch Green Building Council. Whole life carbon: position paper [Internet]. Den Haag; 2021 Sep [cited 2022 Nov 3]. Available from: https://www.dgbc.nl/publicaties/position-paper-whole-life-carbon-44
2. Dutch Green Building Council. Leidende principes - DGBC Roadmap Whole life Carbon.
3. LETI. LETI Embodied Carbon Primer [Internet]. London; 2020 Jan. Available from: www.LETI.london
4. PE LCA study of US sawn hardwood [Internet]. 2012 [cited 2024 Jan 22]. Available from: https://www.americanhardwood.org/fileadmin/docs/
5. Nguyen Q. How Sustainable Is Plywood? Here Are the Facts [Internet]. 2012 [cited 2023 Apr 22]. Available from: https://impactful.ninja/how-sustainable-is-plywood/
6. AWS. Architectural Woodwork Standards [Internet]. 2009. Available from: www.awmac.com,
7. Kellert SR, Heerwagen J, Mador M. Biophilic Design: The Theory, Science and Practice of Bringing Buildings to Life. John Wiley & Sons; 2008.
8. Godthelp T, Jorissen A, Habraken APHW, Godthelp TS, Jorissen AJM, Habraken APHW, et al. The Timber Reciprocal Frame Designer: Free Form Design to Production Design to Production of Reciprocal Frame Structures [Internet]. 2019. Available from: https://www.researchgate.net/publication/336642227
9. Su Y, Ohsaki M, Wu Y, Zhang J. A numerical method for form finding and shape optimization of reciprocal structures. Eng Struct. 2019 Nov 1;198.
10. Chilton JC. Building with Air View project PhD research View project [Internet]. 1992. Available from: https://www.researchgate.net/publication/299629210
11. Shah S. DEPLOYABLE RECIPROCAL FRAME STRUCTURES: DEPLOYABLE MODULE Deployable Module. 2021.
12. Gelez S, Saby V. Nexorades, facing an emergency situation. International Journal of Space Structures. 2011;26(4):359–62.
13. Popovic Larsen O. RECIPROCAL FRAME ARCHITECTURE [Internet]. 2008 [cited 2023 May 11]. Available from: https://casaeco.files.wordpress.com/2012/03/reciprocal-frame-architecture.pdf
14. Nagy M, Csóka L, Katona V. The role of symmetry in reciprocal frame structures. Symmetry: Culture and Science. 2019;30(1):15–24.
15. Pugnale A, Sassone M. Structural Reciprocity: Critical Overview and Promising Research/Design Issues. Nexus Netw J. 2014;16(1):9–35.

16. Petrović M, Ilić I, Mijatović S, Šekularac N. The Geometry of Timber Lamella Vaults: Prototype Analysis. Buildings. 2022 Oct 1;12(10).

17. Li CQ. Designing KREOD. [cited 2023 May 11]; Available from: https://evolute.at/download/130129_designing_KREOD_web.pdf

18. Bergis L, De Rycke K. FRANS MASEREEL CENTRUM [Internet]. 2017 [cited 2023 May 11]. Available from: https://daf9627eib4jq.cloudfront.net/app/uploads/2019/02/LIST_FMC_annex_structure.pdf

19. Anastas Y, Rhode-Barbarigos L, Adriaenssens S. Design-to-construction workflow for cell-based pattern reciprocal free-form structures. Journal of the International Association for Shell and Spatial Structures. 2016 Jun 1;57(2):159–76.

20. Habraken A, Godthelp SIDstudio bv T. Digital path towards Timber Reciprocal Frame Structures. Vol. 66. 2021.

21. Rizzuto J, Saïdani M, Chilton JC. Polyhedric space structures using reciprocally supported elements of various cross-sections. Journal of the International Association for Shell and Spatial Structures. 2001;42:149–59.

22. Baverel OLS. NEXORADES: A FAMILY OF INTERWOVEN SPACE STRUCTURES 1411. 2000.

23. Anastas Y, Rhode-Barbarigos L, Adriaenssens S. Design-to-construction workflow for cell-based pattern reciprocal free-form structures. Journal of the International Association for Shell and Spatial Structures. 2016 Jun 1;57(2):159–76.

24. Godthelp T, Jorissen A, Habraken APHW, Godthelp TS, Jorissen AJM, Habraken APHW, et al. The Timber Reciprocal Frame Designer: Free Form Design to Production [Internet]. 2019. Available from: https://www.researchgate.net/publication/336642227

25. Mellado N, Song P, Yan X, Fu CW, Mitra NJ. Computational Design and Construction of Notch-Free Reciprocal Frame Structures. 2014;181–97. Available from: http://geometry.cs.ucl.ac.uk/projects/2014/rf-aag

26. Song P, Fu CW, Goswami P, Zheng J. Reciprocal Frame Structures Made Easy.

27. Pugnale A, Parigi D, Kirkegaard PH, Sassone M. The Principle of Structural Reciprocity. IABSE-IASS Symposium 2011 [Internet]. 2011 [cited 2023 Dec 18]; Available from: https://vbn.aau.dk/en/publications/the-principle-of-structural-reciprocity-history-properties-and-de-2

28. Asefi M, Bahremandi-Tolou M. Design challenges of reciprocal frame structures in architecture. Journal of Building Engineering. 2019 Nov 1;26.

29. Brocato M. Reciprocal frames: Kinematical determinacy and limit analysis. International Journal of Space Structures. 2011 Dec 1;26(4):343–58.

30. Tunç E. Shaping a timber reciprocal frame structure. 2015.

31. Melenbrink N, Pedersen S, Raman S. RECIPROCAL FRAME BY NATHAN MELENBRINK, SAMO PEDERSEN AND SHIBU RAMAN [Internet]. 2014 [cited 2024 Jan 25]. Available from: https://frameweb.com/article/reciprocal-frame-by-nathan-melenbrink-samo-pedersen-and-shibu-raman

32. Corio E. An innovative sail-shaped shelter for the Ancient Ships Archaeological site of Pisa Conception and parametric design. 2016 [cited 2024 Jan 26]; Available from: https://etd.adm.unipi.it/theses/available/etd-11212016-151530/unrestricted/tesi.pdf

33. Bollinger+Grohmann. Frans Masereel Centrum. Kasterlee; 2019.

34. Tosic Z, Krasic S, Stojic D. Constructive system of reciprocal frames in terms of contemporary architecture. Facta universitatis - series: Architecture and Civil Engineering. 2018;16(3):415–23.

35. United States Environmental Protection Agency. AP-42, CH 10.5: Plywood Manufacturing. [cited 2024 Jan 29]; Available from: https://www3.epa.gov/ttnchie1/ap42/ch10/final/c10s05.pdf

36. Habraken IAPHW, Rozemeijer IGJ. Finite Element Analysis of Interlocking Timber Connections in Plywood Diaphragm Floors: Optimizing Form for Strength. 2023.

37. Dinwoodie JM. Timber—a review of the structure-mechanical property relationship. J Microsc. 1975 May 2;104(1):3–32.

38. European Committee for Standardisation. Eurocode 5: Timber structures, Part 1-1: General rules and rules for buildings [Internet]. 2022 [cited 2022 Nov 1]. Available from: https://www.briswarenhuis.nl

39. Schlick J. Is Water Jet Cutting Wood Possible? [Internet]. 2022 [cited 2023 Jun 4]. Available from: https://www.techniwaterjet.com/can-waterjet-cut-wood/

40. Hazir E, Koc KH. Optimization of wood machining parameters in CNC routers: Taguchi orthogonal array based simulated angling algorithm. Maderas: Ciencia y Tecnologia. 2019;21(4).

41. CNC-Cut-to-Size-Guidelines [Internet]. Darra; 2020 [cited 2023 Jun 4]. Available from: https://www.plywoodandpanel.com.au/wp-content/uploads/2020/03/CNC-Cut-to-Size-Guidelines.pdf

42. Hubs. Reducing CNC Machining Costs: Design Tips [Internet]. [cited 2023 Jun 4]. Available from: https://wiki.imal.org/howto/good-cnc-design-practice

43. Zehmakan AN. Bin Packing Problem: A Linear Constant-Space 3/2-Approximation Algorithm [Internet]. [cited 2023 Jun 11]. Available from: https://arxiv.org/ftp/arxiv/papers/1610/1610.08820.pdf

44. Paul E. Black. NP-hard, in Dictionary of Algorithms and Data Structures [Internet]. National Institute of Standards and Technology (NIST); 2021 [cited 2023 Jun 11]. Available from: https://xlinux.nist.gov/dads/HTML/nphard.html

45. Jylänki J. A Thousand Ways to Pack the Bin-A Practical Approach to Two-Dimensional Rectangle Bin Packing [Internet]. 2010 [cited 2023 Jun 11]. Available from: http://pds25.egloos.com/pds/201504/21/98/RectangleBinPack.pdf

46. Paul E. Black. Big-O notation, in Dictionary of Algorithms and Data Structures [Internet]. National Institute of Standards and Technology (NIST); 2019 [cited 2023 Jun 11]. Available from: https://xlinux.nist.gov/dads/HTML/bigOnotation.html

47. Albers S. Bin packing 1. Problem definition and general observations [Internet]. 2008 [cited 2023 Jun 11]. Available from: https://ac.informatik.uni-freiburg.de/lak_teaching/ws07_08/algotheo/Slides/13_bin_packing.pdf

48. Pilkey WD, Pilkey DF, Bi Z. Peterson's Stress Concentration Factors [Internet]. 4th ed. Hoboken: John Wiley & Sons; 2020. Available from: https://onlinelibrary.wiley.com/doi/book/10.1002/9781119532552

49. Dr. John McGuire. Notes on Semi-Rigid Connections [Internet]. 1995 Jul [cited 2023 Nov 3]. Available from: https://femci.gsfc.nasa.gov/semirigid/

50. Leichti RJ, Hyde RA, French ML, Camillos SG. The Continuum of Connection Rigidity in Timber Structures. Wood and Fiber science [Internet]. 1999 [cited 2023 Nov 3];32(1). Available from: https://core.ac.uk/download/pdf/236633215.pdf

51. Wieringa E, Suiker ASJ, Habraken APHW, Rozemeijer GJ. Finite Element Analysis of Interlocking Timber Connections in Plywood Diaphragm Floors: Optimizing Form for Strength [Internet]. 2023 [cited 2023 Nov 3]. Available from: https://pure.tue.nl/ws/portalfiles/portal/306714154/Wielinga_1017980_ABP_Suiker_MSc_thesis.pdf

52. Wang T, Wang Y, Crocetti R, Wålinder M. In-plane mechanical properties of birch plywood. Constr Build Mater [Internet]. 2022 Jul 18 [cited 2023 Nov 3];340. Available from: https://www.sciencedirect.com/science/article/pii/S0950061822015252

53. Tejlgaard K, Jepsen B. Behance. 2013 [cited 2024 Mar 28]. Dome of Visions. Available from: https://www.behance.net/gallery/8369477/Dome-of-Visions

54. European Committee for Standardisation. Eurocode 1: Actions on structures, Part 1-4: Wind loads [Internet]. European Committee for Standardisation; 2022 [cited 2022 Nov 1]. Available from: https://www.briswarenhuis.nl

55. NextFEM [Internet]. NextFEM SRLS ; 2018 [cited 2024 Feb 26]. Available from: https://www.nextfem.it/it/home/

56. European Committee for Standardisation. Eurocode 1: Actions on structures. Part 1-1: Denisties, self-weight, imposed loads for buildings [Internet]. BRISwarenhuis; 2022 [cited 2022 Oct 31]. Available from: https://www.briswarenhuis.nl/

57. European Committee for Standardisation. Eurocode 1: Actions on structures, Part 1-4: Wind loads [Internet]. European Committee for Standardisation; 2022 [cited 2022 Nov 1]. Available from: https://www.briswarenhuis.nl

58. European Committee for Standardisation. Eurocode 1: Actions on structures, Part 1-3: Snow loads [Internet]. European Committee for Standardisation; 2022 [cited 2022 Nov 1]. Available from: https://www.briswarenhuis.nl/

59. European Committee for Standardisation. Eurocode 1: Actions on structures, Part 1-5: General actions - Thermal actions [Internet]. 2022 [cited 2023 Aug 15]. Available from: www.briswarenhuis.nl

60. Wolfram S. A New Kind of Science. Wolfram Media; 2002.

61. Frazier PI. A Tutorial on Bayesian Optimization. 2018 Jul 8; Available from: http://arxiv.org/abs/1807.02811

62. Mellado N, Song P, Yan X, Fu CW, Mitra NJ. Computational Design and Construction of Notch-Free Reciprocal Frame Structures. 2014;181–97. Available from: http://geometry.cs.ucl.ac.uk/projects/2014/rf-aag

12.1 Figures

Figure 1: Log peeling to create plywood sheets

Retreived from AWS. Architectural Woodwork Standards [Internet]. 2009. Available from: www.awmac.com

Figure 4: Rf units and resulting tessellations and 3d approximations, derived from Mellado et al.

Mellado N, Song P, Yan X, Fu CW, Mitra NJ. Computational Design and Construction of Notch-Free Reciprocal Frame Structures. 2014;181–97. Available from: http://geometry.cs.ucl.ac.uk/projects/2014/rf-aag

Figure 5: Simple reciprocal structure

Shah S. DEPLOYABLE RECIPROCAL FRAME STRUCTURES: DEPLOYABLE MODULE Deployable Module. 2021. Available from: https://papers.cumincad.org/data/works/att/caadria2021_107.pdf

Figure 6: Typical medieval floor grillage configuration and Figure 7: Da Vinci's sketches in the Codex Atlantico, resketched by A. E. Piroozfar

Popovic Larsen O. RECIPROCAL FRAME ARCHITECTURE [Internet]. 2008 [cited 2023 May 11]. Available from: https://casaeco.files.wordpress.com/2012/03/reciprocal-frame-architecture.pdf

Figure 8: Casa Negre roof, designed by Josep Maria Jujol, Photo: Jaime Segura.

Pugnale A, Sassone M. Structural Reciprocity: Critical Overview and Promising Research/Design Issues. Nexus Netw J. 2014;16(1):9–35.

Figure 9: Section and detail of Zollinger lamella roof design.

Petrović M, Ilić I, Mijatović S, Šekularac N. The Geometry of Timber Lamella Vaults: Prototype Analysis. Buildings. 2022 Oct 1;12(10).

Figure 10: KREOD pavilion in London, designed by Chun Qing Li

Li CQ. Designing KREOD. [cited 2023 May 11]; Available from: https://evolute.at/download/130129_designing_KREOD_web.pdf

Figure 11: Frans Masereel Centrum roof structure

Retreived from: Bergis L, De Rycke K. FRANS MASEREEL CENTRUM [Internet]. 2017 [cited 2023 May 11]. Available from: https://daf9627eib4jq.cloudfront.net/app/uploads/2019/02/LIST_FMC_annex_structure.pdf

Figure 20: Generating a 3d reciprocal frame by mapping a 2d tessellation onto a 3d surface [edited]

Retreived from: Godthelp T, Jorissen A, Habraken APHW, Godthelp TS, Jorissen AJM, Habraken APHW, et al. The Timber Reciprocal Frame Designer: Free Form Design to Production Design to Production of Reciprocal Frame Structures [Internet]. 2019. Available from: https://www.researchgate.net/publication/336642227

Figure 23: Example of a dome-like reciprocal frame

Retreived from: Godthelp T, Jorissen A, Habraken APHW, Godthelp TS, Jorissen AJM, Habraken APHW, et al. The Timber Reciprocal Frame Designer: Free Form Design to Production Design to Production of Reciprocal Frame Structures [Internet]. 2019. Available from: https://www.researchgate.net/publication/336642227

Figure 24: Example sketch of a notching joint between two beams, used in a reciprocal frame designed by N. Melenbrink et al..

Retreived from: Melenbrink N, Pedersen S, Raman S. RECIPROCAL FRAME BY NATHAN MELENBRINK, SAMO PEDERSEN AND SHIBU RAMAN [Internet]. 2014 [cited 2024 Jan 25]. Available from: https://frameweb.com/article/reciprocal-frame-by-nathan-melenbrink-samo-pedersen-and-shibu-raman

Figure 25: example of a beam cut to allow for a friction joint

Retreived from: Popovic Larsen O. RECIPROCAL FRAME ARCHITECTURE [Internet]. 2008 [cited 2023 May 11]. Available from: https://casaeco.files.wordpress.com/2012/03/reciprocal-frame-architecture.pdf

Figure 26: reciprocal beams connected with metal pins

Retreived from: Tunç E. Shaping a timber reciprocal frame structure. 2015. Available at: https://papers.cumincad.org/cgi-bin/works/paper/caadria2021_107

Figure 27: Mortise and tenon joint, as used in 'Reciprocal-Framed Grid Shell'

Corio E. An innovative sail-shaped shelter for the Ancient Ships Archaeological site of Pisa Conception and parametric design. 2016 [cited 2024 Jan 26]; Available from: https://etd.adm.unipi.it/theses/available/etd-11212016-151530/unrestricted/tesi.pdf

Figure 28: Sheeting applied to reciprocal structure in Frans Masereel centrum in Belgium

Bollinger+Grohmann. Frans Masereel Centrum. Kasterlee; 2019. Available from: https://b-b.be/nl/portfolio/frans-masereel-centrum

Figure 29: KREOD pavilion in London, designed by Chun Qing Li

Li CQ. Designing KREOD. [cited 2023 May 11]; Available from: https://evolute.at/download/130129_designing_KREOD_web.pdf

Figure 30: Aluminium panel cladding as used in the work by Z. Tošić et al.

Tosic Z, Krasic S, Stojic D. Constructive system of reciprocal frames in terms of contemporary architecture. Facta universitatis - series: Architecture and Civil Engineering. 2018;16(3):415–23.

Figure 31: Log peeling to create plywood sheets

AWS. Architectural Woodwork Standards [Internet]. 2009. Available from: www.awmac.com

Figure 32: Undercut in corners to be able to fit a rectangular element

Hubs. Reducing CNC Machining Costs: Design Tips [Internet]. [cited 2023 Jun 4]. Available from: https://wiki.imal.org/howto/good-cnc-design-practice

Figure 43: Diagrams of beams having pinned, semi-rigid, and rigid end fixity: (A) loading, (B) qualitative bending shape

Leichti RJ, Hyde RA, French ML, Camillos SG. The Continuum of Connection Rigidity in Timber Structures. Wood and Fiber science [Internet]. 1999 [cited 2023 Nov 3];32(1). Available from: https://core.ac.uk/download/pdf/236633215.pdf

Figure 44: The continuum of joint stiffness versus normalized minimum natural frequency

Leichti RJ, Hyde RA, French ML, Camillos SG. The Continuum of Connection Rigidity in Timber Structures. Wood and Fiber science [Internet]. 1999 [cited 2023 Nov 3];32(1). Available from: https://core.ac.uk/download/pdf/236633215.pdf

Figure 46: Schematization of stress strain behaviour used in the FEM model (green) and the stress strain behaviour from tests (black)

Wang T, Wang Y, Crocetti R, Wålinder M. In-plane mechanical properties of birch plywood. Constr Build Mater [Internet]. 2022 Jul 18 [cited 2023 Nov 3];340. Available from: https://www.sciencedirect.com/science/article/pii/S0950061822015252

Figure 62: Cladding applied in the 'Dome of Visions' in Copenhagen, Denmark

Tejlgaard K, Jepsen B. Behance. 2013 [cited 2024 Mar 28]. Dome of Visions. Available from: https://www.behance.net/gallery/8369477/Dome-of-Visions

Figure 91: Recommended values of external pressure coefficients for domes acc. Eurocode NEN-EN1991-1-4

European Committee for Standardisation. Eurocode 1: Actions on structures, Part 1-4: Wind loads [Internet]. European Committee for Standardisation; 2022 [cited 2022 Nov 1]. Available from: https://www.briswarenhuis.nl

Figure 93: Example Voronoi diagram used to obtain the area per node

Wolfram S. A New Kind of Science. Wolfram Media; 2002. Available from: https://mathworld.wolfram.com/VoronoiDiagram.html

Appendix 1: User manual

The reciprocal frame designer/optimizer tool consists of two main parts. Firstly, reciprocal frame can be generated (with optimized cross sections) for a set of design parameters as described in the 'reciprocal frame designer' chapter. Secondly, the design set of parameters can be optimized to minimize the raw material (plywood sheets) required to fabricate the structure. These two functions are split into two tabs in the graphical user interface (= GUI). This manual explains how the software can be used, detailed information about the internal processes in the tool is provided in the report and/or other appendices.

Reciprocal frame designer

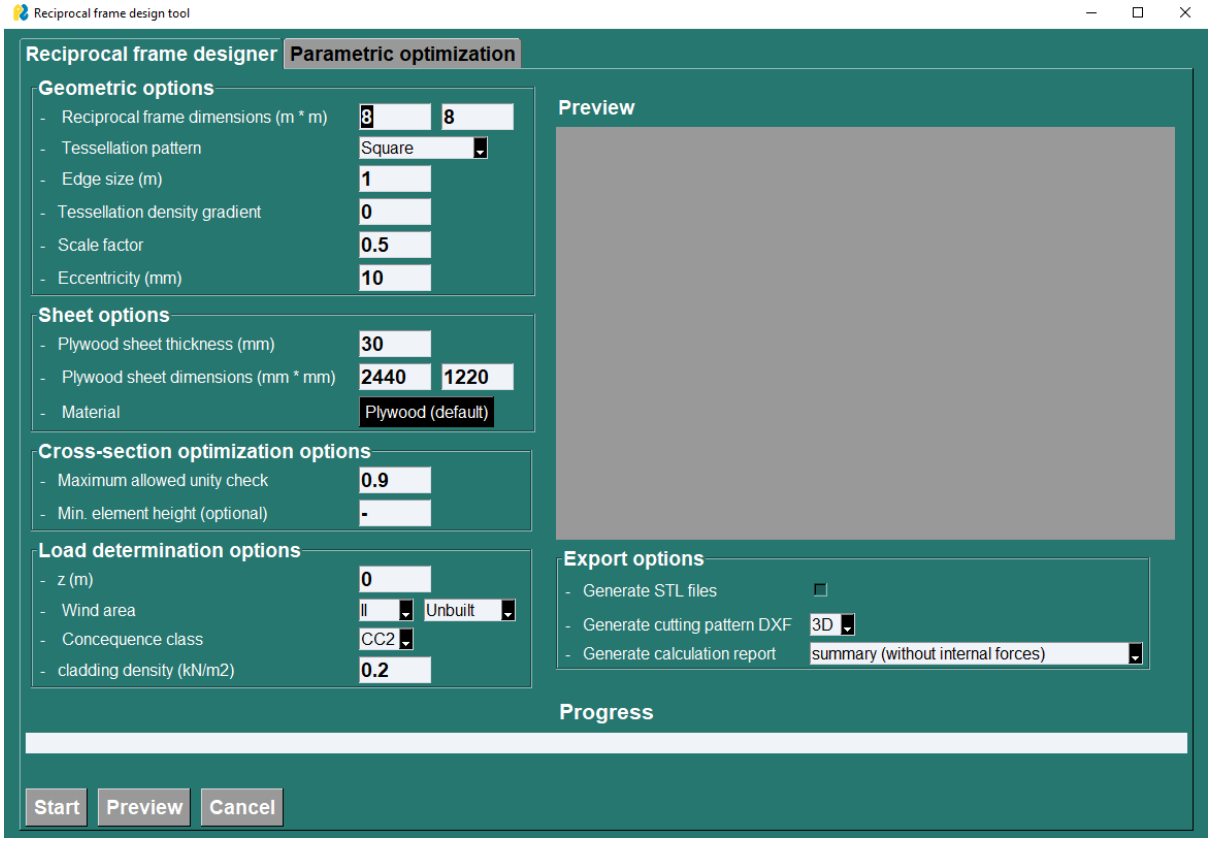


Figure 1: GUI of reciprocal frame designer

Figure 1 shows the graphical user interface of the first part of the reciprocal frame designer tool. On this tab, a reciprocal frame can be generated based on certain design parameters (under the header 'Geometric options'). The cross sections of the generated reciprocal frame are generated with the provided optimization and load options. Finally, digital manufacturing data (i.e. STL files, cutting patterns and a calculation report) are generated. The cutting pattern is based on the sheet options as provided under the header 'Sheet options'.

Getting started

The best method to work with the reciprocal frame designer is to work from top to bottom, as described below.

Geometric options

To get started, firstly the dimensions of the base of the reciprocal frame must be entered. This base is used as a minimum span in x- and y direction. The generated reciprocal frame may end up larger than these dimensions; when the dimensions are not devisable by the edge size of the tessellation pattern. Additionally, some patterns may not generate a perfectly rectangular reciprocal frame due to the nature of the pattern. E.g. an equilateral triangle tessellation can never be rectangular.

The second option to select is the tessellation pattern, this influences the layout of the structural elements. The layout of the structural elements is determined by applying the center-to-center method to the tessellation.

The edge size of the tessellation is the next parameter. This parameter determines the density of the tessellation. As mentioned before, be careful in selecting a correct edge size, as some edge sizes may result in a structure larger than the base polygon. Additionally, care should be taken that the edge size is not too small as this may result in long computation time.

The next parameter that can be selected is the tessellation density gradient. This is a value between -1 and 1, where -1 means the density is increased towards the edges (and as a result decreased towards the center of the polygon). And 1 means the density is decreased towards the edges and increased towards the center. The density gradient does not add or remove beam elements, it only affects the placement of the beams. It is advised to keep these values between -0.5 and 0.5 as more extreme values may result in non-feasible reciprocal frames.

The scale factor is a factor that is used in the center-to-center method in determining the position of the intermediate supports on the beams. This value should be between 0.1 and 0.9. Check the generated structure to make sure that the intermediate supports are not too close to the beam ends, as the structural calculations may not be valid in those cases.

Finally, the eccentricity is another parameter that can be entered. The eccentricity determines the amount of curvature that is present in the reciprocal frame. For a 2d reciprocal frame, the eccentricity should be 0.

Sheet options

Under the sheet options, the dimensions of the sheet that is used to create the reciprocal frame can be entered. The sheet thickness influences the sizes of the cross sections, as the thinner the sheet, the thinner the beams and thus the more structural height is required. The sheet dimensions are used to determine the cutting pattern. If only one of the structural elements is too large to fit on the sheet, the design tool will generate an error. The remaining data will still be generated.



When the button 'material' is clicked, a popup will appear where different values for the orthotropic elasticity and yield stresses can be entered. The standard material is picked from literature sources

Cross-section optimization options

Under the cross-section optimization options, the engineer can enter what unity check is allowed for each of the cross sections. The unity checks are determined according to Eurocode 5 with the Dutch national annex. In early design, engineers may want to reduce the unity check for extra margins.

Additionally, the minimum height of the beam elements may be entered. If for instance from an aesthetical point of view, the designer wants to have beams with a certain minimum height, the value can be entered here. If no value is entered, the minimum beam height is determined according to Eurocode checks.

Load determination options

Under the load determination options, all values that are used in the Eurocode to determine the loads can be entered. Some additional design variables (e.g. surface roughness) cannot be entered here, if that is the case, the reciprocal frame designer always calculates the structure based on the most conservative value.

For the value z(m), the height of the base of the reciprocal frame can be entered. If the frame is placed on the floor, this value may be entered as 0. If the structure is placed on for instance a roof, the z value can be adjusted here.

For the cladding density, the load of the cladding material must be entered. It can be difficult to estimate the density since the inter-member spans are not known on beforehand. Therefore, this value may be adjusted or taken conservatively during design.

Export options

In the right bottom of the GUI, the export options can be entered. The first option is to generate STL files. If the box is checked, the STL files of the individual members as well as a combined model are generated. This process may take a while, therefore this box must only be checked if the user is completely certain of a design.

The second option is to generate a DXF file for the cutting pattern. There are three options: 3D, 2D and no. When 3d is entered, a cutting pattern 3d projection is generated. This can be used to combine the STL data and determine the location on the sheet where the element should be cut from. When 3d is entered, a 2d cutting pattern is generated. This can be used when the structure should be made using a 2d cutting technique. This means that the structural calculations may not be accurate, therefore this option must only be used for creating scale models to be cut using for instance laser cutting.

Note: if a scale model is made, it is advised to adjust the sheet size accordingly. For instance when the scale model must be made from a 600x800mm sheet and the scale of the model is 1:10, the sheet that should be entered here is 6000x8000mm.

Finally, the settings of a calculation report can be entered. When no is selected, no calculation report is generated. When full is selected, all unity checks on the beams with intermediate calculations will be generated. This will result in an extensive calculation report (approximately 8 pages per element; for an 8x8m reciprocal frame with edge size = 1m, this generates a report of approximately 1000 pages). When summary (without internal forces) is selected, for each element a table will be generated where each unity check is summarized. When summary (with internal forces) is selected, the same table will be generated, but additionally the internal force diagrams for each load case are generated.

Examples of the structural report can be found in annex 1 of this report.

Preview

Before starting the calculation process, a preview can be generated by clicking the 'preview' button in the bottom of the GUI. A preview will be generated in a few seconds (depending on the complexity of the frame) in the preview window (see figure 2). Using this preview, the designer can decide if the combination of parameters is satisfactory.

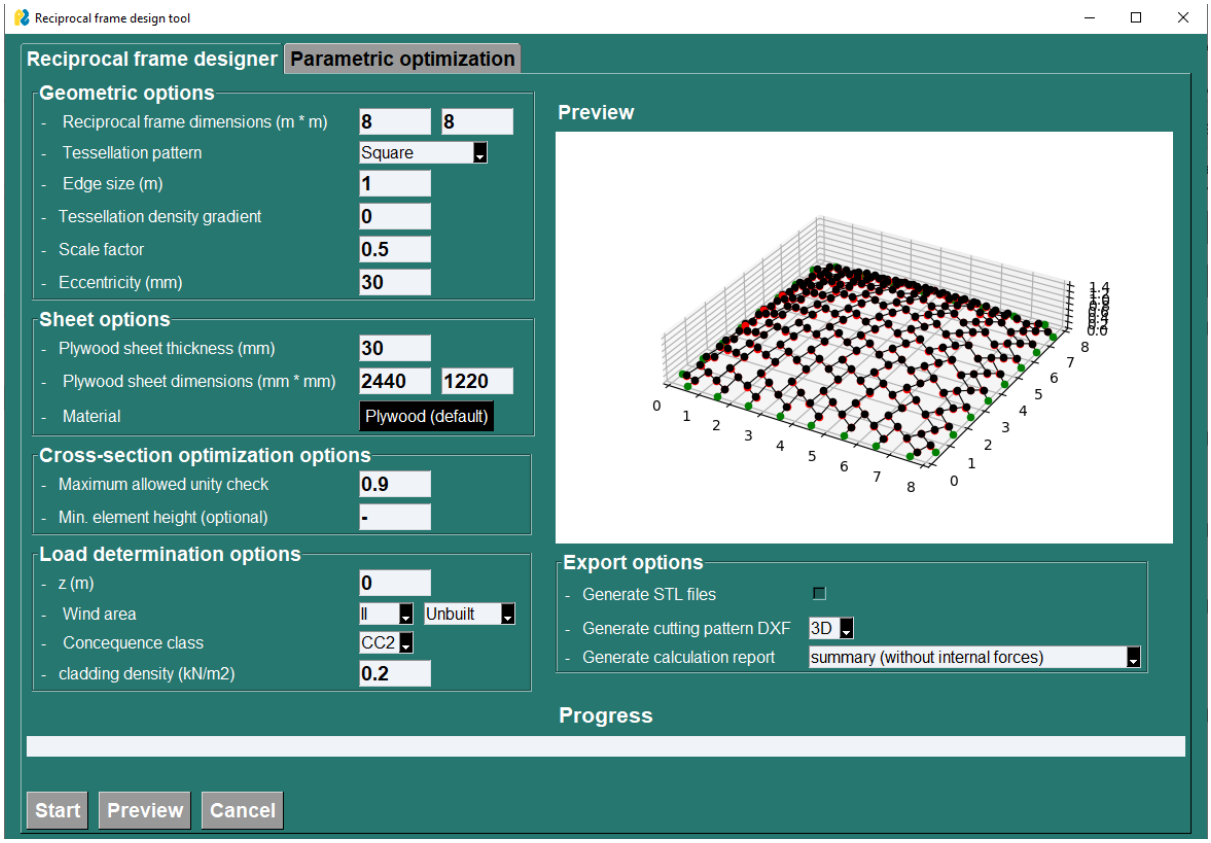


Figure 2: GUI of reciprocal frame designer with preview

Starting the calculation

When the start button is clicked, the full calculation process is started. The process of the calculations can be seen in the bar at the bottom, as well as what part of the calculation is performed.

Firstly a preview is also generated when start is clicked. Then, when the resulting shape is calculated, the final morphology is displayed in the window.

The cancel button can be clicked at any time, exiting all calculation and progress.

Output folder

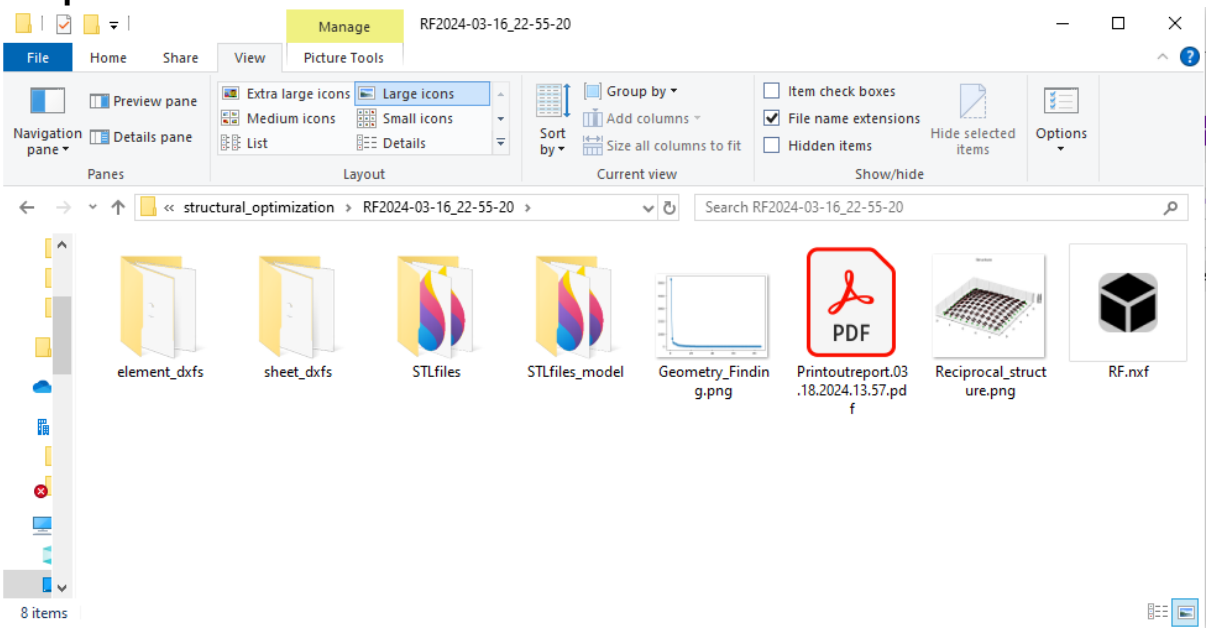


Figure 3: output folder of reciprocal frame designer

The resulting output files are outputted in a folder RF[date] which is located in the program files. In the folder 'element_dxfs', the 2d shape of each element is generated. In the folder 'sheet_dxfs', the cutting patterns for each of the sheets is generated.

The STL files are generated in the folder STL files of the individual elements, where the 0-point of the elements is on the same location as of the cutting pattern. Therefore, these files can be used to cut from the sheets. In the folder 'STLfiles_model', the beam elements are generated on their 'real' positions, as well as a combined model with all of the elements combined.

Additionally, the printout report (calculation report), image of the structure, the FEM model file (Next-FEM file) and the optimization convergence plot are outputted in the folder.

Parametric optimization

The second option is to optimize the geometric properties for the set of boundary conditions. This optimization can be performed under the tab 'parametric optimization' (see figure 4). In principle, the optimizer will run the previous tab with different sets of parameters until the combination resulting in the least sheets required is found.

The layout of the left side of the GUI is similar to that of the 'reciprocal frame designer' tab. The difference here is that a range can be entered. Additionally, each variable can be locked, meaning that that variable will not be part of the optimization.

The reciprocal frame dimensions and tessellation pattern are always locked because these cannot be part of the optimization. The other variables can in principle bee 'free'. In that case, the most optimal value of the parameter is sought in the entered range. The automatically generated ranges are empirical suggestions. The ranges can however be widened or narrowed if this is deemed necessary.

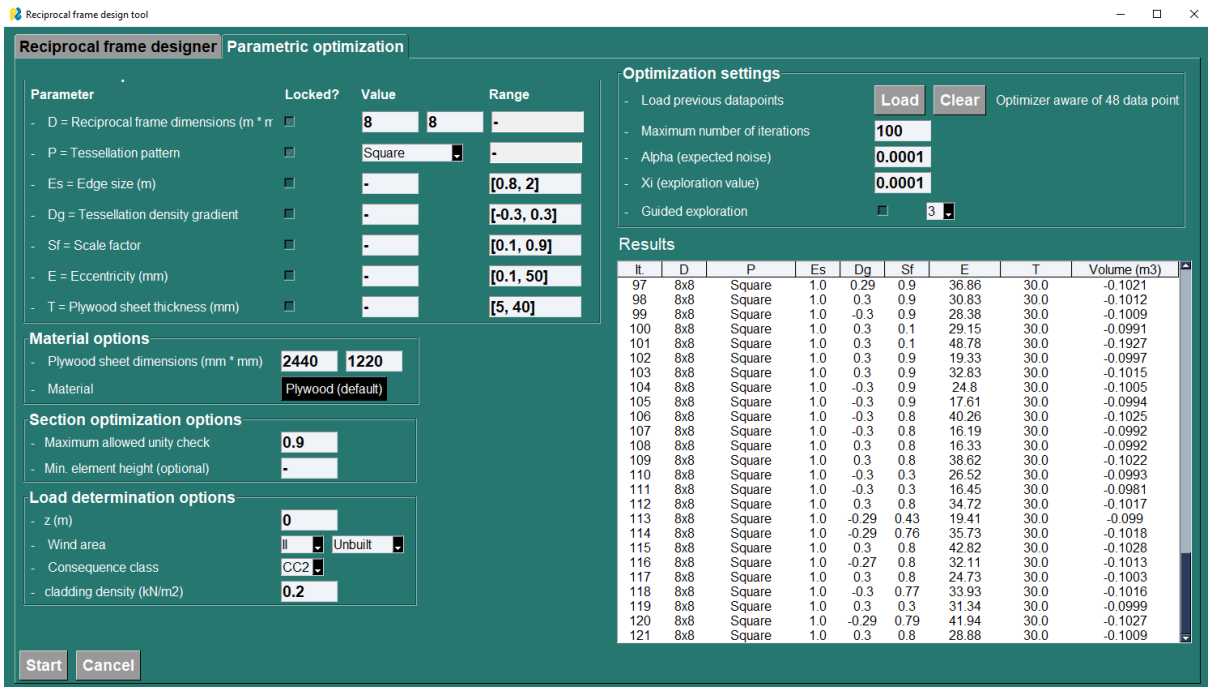


Figure 4: GUI of reciprocal frame designer parametric optimization tab

The material options, section optimization options and load determination options are similar to that of the reciprocal frame designer tab.

Optimization settings

An important part of this tab are the optimization settings. These settings will be used to steer the Bayesian optimization algorithm. The first option is to load previous datapoints. When load is clicked, a message will be displayed with how many datapoints are found.

It is important to check whether the previous datapoints connect well to the boundary conditions that are generated now; the dimensions, load conditions and sheet dimensions must be the same, otherwise the algorithm will get confused and the results may be sub-optimal.

If the previous datapoints do not connect to the optimization that must be performed now, the previous datapoints must be cleared. This can be done by clicking the 'clear' button. In that case, the previous datapoints are neglected. Note: this process is irreversible, previously generated data cannot be retrieved.

The next setting is the maximum number of iterations, this number is used to stop the optimization process after a certain number of iterations. Note; this excludes the imported datapoints. If 48 datapoints are loaded, and the maximum number of iterations is 148, the optimizer will stop only after 148 iterations (or 100 'new' iterations).

The next settings are the noise and exploitation values. The working of these variables is explained in the report under 'parametric optimization'. Basically, the lower the value of alpha, the least noise is tolerated in the optimization process.

Additionally, the kappa value is used to determine the amount of exploitation or exploration that must take place. When this value is (close to) 0, the algorithm will focus on exploitation (e.g. finding the minimum value). When the value is 0.1, the algorithm will focus on 'explaining' the whole design space.

Additionally, the exploration may be guided by 'probing' datapoints at spread out locations. This can be done by clicking the box. The value that is selected is used to determine how many values are used for each range. So if the range is [0, 1] and the value is 4 this means that the variable is probed with 0, $\frac{1}{3}$, $\frac{2}{3}$, 1.

The guided exploration can be used if the designer does not have an idea where the possible best solution can be found. This way, the algorithm gets spread out information and can optimize at the most promising areas.

Result

The results of each step are displayed in the table where the volume indicates the amount of material required for that combination. The algorithm will always converge at the 'best' combination, which means that the parameters at the bottom of the table will generate the most efficient design.

When the export data is required for the most optimal design, the parameters must be entered in the 'reciprocal frame designer' tab.

Appendix 2: Detailed structural calculations

On each of the structural elements, the following unity checks are performed for the main cross section:

1. Tension parallel to the grain (NEN-EN 1995-1-1, 6.1.2)
2. Compression parallel to the grain (NEN-EN 1995-1-1, 6.1.4)
3. Shear (NEN-EN 1995-1-1, 6.1.7)
4. Torsion (NEN-EN 1995-1-1, 6.1.8)
5. Combined biaxial bending and tension (NEN-EN 1995-1-1, 6.2.3)
6. Combined biaxial bending and compression (NEN-EN 1995-1-1, 6.2.4)
7. Compression or combined compression and bending (NEN-EN 1995-1-1, 6.3.2)
8. Bending or combined bending and compression (LTB) (NEN-EN 1995-1-1, 6.3.3)

Additionally, the following checks are performed for the dowels:

9. Dowel embedment (NEN-EN 1995-1-1, 8.2.2 g+h)
10. Dowel yielding (NEN-EN 1995-1-1 8.2.2 j+k)
11. Dowel shear failure

Besides, the tenons are checked with the following checks:

12. Compression parallel to the grain (NEN-EN 1995-1-1, 6.1.4)
13. Compression perpendicular to the grain (NEN-EN 1995-1-1, 6.1.5)
14. Tension in the net-section
15. Stress concentration due to tension
16. Tenon shear (including stress concentration (NEN-EN 1995-1-1, 6.5.2)

The beam ends are checked with the following check:

17. Compression perpendicular to the grain (NEN-EN 1995-1-1, 6.1.5)

Finally, the following checks are performed to check stress concentrations at the holes:

18. Normal stress concentration
19. Shear stress concentration
20. Shear on reduced section

The details about these checks will be discussed in the following paragraphs.

1. Tension parallel to the grain

For tension parallel to the grain, the following expression must be satisfied (acc. NEN-EN 1995-1-1, 6.1.2):

$$\sigma_{t,0,d} \leq f_{t,0,d}$$

This means the unity check can be described as:

$$\frac{\sigma_{t,0,d}}{f_{t,0,d}} \leq UC_{max}$$

Where:

- $\sigma_{t,0,d}$ = design tensile stress along the grain: $\sigma_{t,0,d} = \frac{N_{Ed}}{A}$
- N_{Ed} = Maximum normal force (maximum tensile force along the beam)
- $f_{t,0,d}$ = $\frac{f_{t,0,k}}{\gamma_m} * k_{mod}$
- $f_{t,0,k}$ = characteristic tensile strength par. to the grain (material property)
- γ_m = partial factor for material properties (1.2 for plywood)
- k_{mod} = Modification factor for duration of load and moisture content
- UC_{max} = Maximum allowed unity check

The k_{mod} factor depends on the load case for the forces:

- Permanent: $k_{mod} = 0.6$
- Imposed loads: $k_{mod} = 0.8$
- Wind loads: $k_{mod} = 1.1$
- Snow loads (even): $k_{mod} = 0.8$
- Snow load (accumulated): $k_{mod} = 0.9$
- Thermal forces: $k_{mod} = 0.8$

These k_{mod} and γ_m factors apply to all unity checks, except when mentioned explicitly that the factors deviate.

2. Compression parallel to the grain

The unity check for compression parallel to the grain is described as: (acc. NEN-EN 1995-1-1, 6.1.4)

$$\frac{\sigma_{c,0,d}}{f_{c,0,d}} \leq UC_{max}$$

Where:

- $\sigma_{c,0,d}$ = design tensile stress along the grain: $\sigma_{c,0,d} = \frac{N_{Ed}}{A}$
- N_{Ed} = Minimum normal force (maximum compression force in the beam)
- $f_{c,0,d}$ = $\frac{f_{c,0,k}}{\gamma_m} * k_{mod}$
- $f_{c,0,k}$ = char. compression strength par.to the grain (material property)

3. Shear

The unity check for shear is described as (NEN-EN 1995-1-1, 6.1.7):

$$\frac{\tau_d}{f_{v,d}} \leq UC_{max}$$

Where:

- τ_d = design shear stress: $\tau_d = \frac{3V_{Ed}}{2A}$
- V_{Ed} = maximum absolute shear force
- $f_{v,d}$ = $\frac{f_{v,k}}{\gamma_m} * k_{mod}$
- $f_{v,k}$ = characteristic shear strength (material property)

4. Torsion

The unity check for torsion is described as (NEN-EN 1995-1-1, 6.1.8):

$$\frac{\tau_{tor,d}}{k_{shape} f_{v,k}} \leq UC_{max}$$

Where:

- $\tau_{tor,d}$ = design torsion stress: $\frac{3T_{Ed}}{8bh^2}\left[1 + 0{,}6095\frac{h}{b} + 0{,}8865\left(\frac{h}{b}\right)^2 - 1{,}8023\left(\frac{h}{b}\right)^3 + 0{,}91\left(\frac{h}{b}\right)^4\right]$
- T_{Ed} = maximum design torsional moment
- $f_{v,k}$ = characteristic shear strength
- k_{shape} = reduction factor for shape: $\min\left(1 + 0{,}15\frac{h}{b}; 2{,}0\right)$

5. Combined biaxial bending and tension

The following unity checks have to be satisfied for combined bending and tension, as described in NEN-EN 1995-1-1, 6.2.3:

$$\frac{\sigma_{t,0,d}}{f_{t,0,d}} + \frac{\sigma_{m,y,d}}{f_{m,y,d}} + k_m \frac{\sigma_{m,z,d}}{f_{m,z,d}} \leq UC_{max}$$

$$\frac{\sigma_{t,0,d}}{f_{t,0,d}} + k_m \frac{\sigma_{m,y,d}}{f_{m,y,d}} + \frac{\sigma_{m,z,d}}{f_{m,z,d}} \leq UC_{max}$$

Where:

- $\sigma_{t,0,d}$ = design tension stress: $\frac{N_{Ed}}{A}$
- $\sigma_{m,y,d}$ = design bending stress in y-direction: $\frac{M_{y,Ed}}{W_y}$
- $\sigma_{m,z,d}$ = design bending stress in z-direction: $\frac{M_{z,Ed}}{W_z}$
- W_y, W_z = section moduli in resp. y- and z-direction
- $f_{t,0,d}$ = $\frac{f_{t,0,k}}{\gamma_m} * k_{mod}$
- $f_{t,0,k}$ = characteristic tensile strength par. to the grain (material property)
- $f_{m,d}$ = $\frac{f_{m,k}}{\gamma_m} * k_{mod} * k_h$
- $f_{m,k}$ = characteristic bending strength (material property)
- k_h = size factor modification factor
- k_m = re-distribution factor (acc. 6.1.6 (2), $k_m = 0{,}7$)

To make sure the check is satisfied for all locations in the section, the check is performed at the three beam parts. The typical force distributions are visualized in Figure 1-3. The check is performed at all parts loaded in tension with the respective maximum (absolute) moments.

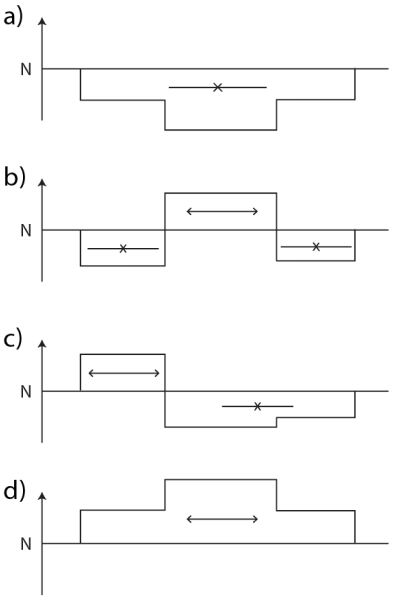


Figure 1: Possible normal force distribution in reciprocal beam element

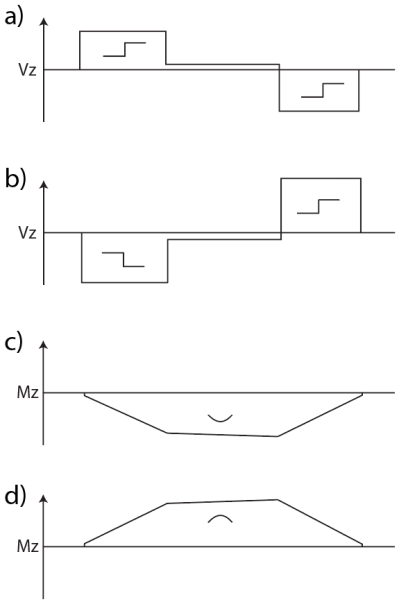


Figure 2: Possible shear and bending distribution in z-direction

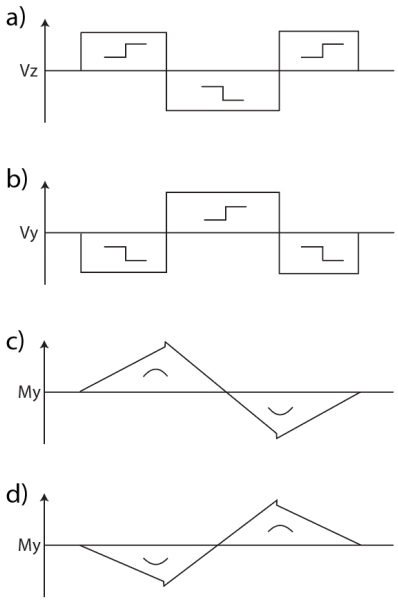


Figure 3: Possible shear and bending distribution in y-direction

6. Combined biaxial bending and compression

The following unity checks have to be satisfied for combined bending and compression, as described in NEN-EN 1995-1-1, 6.2.3:

$$\left(\frac{\sigma_{c,0,d}}{f_{c,0,d}}\right)^2 + \frac{\sigma_{m,y,d}}{f_{m,y,d}} + k_m \frac{\sigma_{m,z,d}}{f_{m,z,d}} \leq UC_{max}$$

$$\left(\frac{\sigma_{c,0,d}}{f_{c,0,d}}\right)^2 + k_m \frac{\sigma_{m,y,d}}{f_{m,y,d}} + \frac{\sigma_{m,z,d}}{f_{m,z,d}} \leq UC_{max}$$

Where:

- $\sigma_{c,0,d}$ = design compression stress: $\frac{N_{Ed}}{A}$
- $\sigma_{m,y,d}$ = design bending stress in y-direction: $\frac{M_{y,Ed}}{W_y}$
- $\sigma_{m,z,d}$ = design bending stress in z-direction: $\frac{M_{z,Ed}}{W_z}$
- W_y, W_z = section moduli in resp. y- and z-direction
- $f_{c,0,d}$ = $\frac{f_{c,0,k}}{\gamma_m} * k_{mod}$
- $f_{c,0,k}$ = char. compressive strength par. to the grain (material property)
- $f_{m,d}$ = $\frac{f_{m,k}}{\gamma_m} * k_{mod} * k_h$
- $f_{m,k}$ = characteristic bending strength (material property)
- k_h = size factor modification factor
- k_m = re-distribution factor (acc. 6.1.6 (2), $k_m = 0{,}7$)

The design normal force and bending moments are selected similarly as for the combined biaxial bending and tension check. That means that each beam part that is loaded in compression is checked with the respective maximum (absolute) bending moments in both y- and z-direction.

7. Compression or combined compression and bending (stability)

The following unity checks should be satisfy for combined compression and bending when checking for stability (NEN-EN 1995-1-1 6.3.2):

$$\frac{\sigma_{c,0,d}}{k_{c,y} f_{c,0,d}} + \frac{\sigma_{m,y,d}}{f_{m,y,d}} + k_m \frac{\sigma_{m,z,d}}{f_{m,z,d}} \leq UC_{max}$$

$$\frac{\sigma_{c,0,d}}{k_{c,z} f_{c,0,d}} + k_m \frac{\sigma_{m,y,d}}{f_{m,y,d}} + \frac{\sigma_{m,z,d}}{f_{m,z,d}} \leq UC_{max}$$

The only addition compared to the previous check is the addition of the stress increase factor due to deflection ($k_{c,y}$ and $k_{c,z}$):

- $k_{c,y}$ = $\frac{1}{k_y + \sqrt{k_y^2 - \lambda_{rel,y}^2}}$
- $k_{c,z}$ = $\frac{1}{k_z + \sqrt{k_z^2 - \lambda_{rel,z}^2}}$
- k_y = $0{,}5\left(1 + \beta_c\left(\lambda_{rel,y} - 0{,}3\right) + \lambda_{rel,y}^2\right)$
- k_z = $0{,}5\left(1 + \beta_c\left(\lambda_{rel,z} - 0{,}3\right) + \lambda_{rel,z}^2\right)$
- β_c = factor for element straightness (= 0,1 for plywood (6.29))
- $\lambda_{rel,y}$ = $\frac{\lambda_y}{\pi}\sqrt{\frac{f_{c,0,k}}{E_{0,05}}}$
- $\lambda_{rel,z}$ = $\frac{\lambda_z}{\pi}\sqrt{\frac{f_{c,0,k}}{E_{0,05}}}$
- $E_{0,05}$ = fifth percentile value of the modulus of elasticity par. to the grain
- λ_y = slenderness ratio y-direction = $\frac{L_{eff}}{\frac{I_{y,red}}{A}}$
- λ_z = slenderness ratio z-direction = $\frac{L_{eff}}{\frac{I_z}{A}}$
- $I_{y,red}$ = reduced second moment of area due to holes in the section (see 'Stability Checks')

The effective length L_{eff} is determined based on what parts of the element are loaded in compression. As visible in Figure 1, there are cases where the full beam element is loaded in compression. In that case, $L_{eff} = L$ (system length). There are also cases where only one part of the beam is loaded in compression (for instance c) inverted), in that case $L_{eff} = 0.7L_{comp}$, where L_{comp} is the length of the part loaded in compression. One side of the beam can be considered 'fixed' since the beam section is continuous on one side. When only the middle part is loaded in compression (inverted b)), $L_{eff} = 0.5L_{comp}$ because both sides are 'fixed'. When two parts are loaded in compression (for instance c)), $L_{eff} = 0.7L_{comp}$. The second moment of area is always reduced, even if there is only compression in part of the beam.

8. Bending or combined bending and compression (LTB)

The lateral torsional stability is verified with the following unity check (acc. NEN-EN 1995-1-1 6.3.3.):

$$\left(\frac{\sigma_{m,d}}{k_{crit} f_{m,d}}\right)^2 + \frac{\sigma_{c,0,d}}{k_{c,z} f_{c,0,d}} \leq UC_{max}$$

Where:

- $\sigma_{m,d}$ = design bending stress: $\frac{M_z}{W_z}$
- $f_{m,d}$ = $\frac{f_{m,k}}{\gamma_m} * k_{mod} * k_h$
- $f_{m,k}$ = characteristic bending strength (material property)
- $\sigma_{c,0,d}$ = design compression stress: $\frac{N_{Ed}}{A}$
- $f_{c,0,d}$ = $\frac{f_{c,0,k}}{\gamma_m} * k_{mod}$
- $f_{c,0,k}$ = char. compressive strength par. to the grain (material property)
- $k_{c,z}$ = reduction value, see 7
- k_{crit} = reduction value for critical bending stress
- = $\begin{cases} 1 & for\ \lambda_{rel,m} \leq 0{,}75 \\ 1{,}56 - 0{,}75\lambda_{relm} & for\ 0{,}75 < \lambda_{rel,m} \leq 1{,}4 \\ \frac{1}{\lambda_{rel,m}^2} & for\ 1{,}4 < \lambda_{rel,m} \end{cases}$
- $\lambda_{rel,m}$ = $\sqrt{\frac{f_{m,k}}{\sigma_{m,crit}}}$
- $\sigma_{m,cirt}$ = $\frac{\pi\sqrt{E_{0,05} I_Z G_{0,05} I_{tor}}}{l_{ef} W_y}$
- $E_{0,05}$ = fifth percentile value of modulus of elasticity parallel to grain
- $G_{0,05}$ = fifth percentile value of shear modulus parallel to grain
- I_z = second moment of area about the weak axis z
- I_{tor} = torsional moment o inertia
- l_{ef} = effective length of the beam (= conservatively 1,0L)

This check is also performed at all locations where there is bending or bending and compression. The effective length is always equal to the system length. The check with the maximum compression stress is only performed at the part that is loaded with that stress.

9. Dowel embedment

Additionally, the embedment failure of the dowel is checked using the following formula:

$$F_{v,Rk,emb} = f_{h,i,k} * t * d \leq F_{Ed}$$

Or

$$\frac{F_{Ed}}{F_{v,Rk,emb}} \leq UC_{max}$$

Where:

- F_{Ed} = Design tensile force in the dowel
- t = plywood sheet thickness
- d = dowel diameter
- $f_{h,i,k}$ = characteristic embedment strength of plywood
  = $0{,}082 * (1 - 0{,}01 * d) * \rho$
- ρ = plywood density

10. Dowell yielding

The yield check is performed using an Eurocode formula where the characteristic load-carrying capacity per shear plane is calculated using (with $\beta = 1$ and neglecting the axial withdrawal capacity):

$$F_{v,Rk,yd} = 1.15\sqrt{2M_{y,Rk}f_{h,1,k}d}$$

Resulting in the following unity check:

$$\frac{F_{Ed}}{F_{v,Rk,yd}} \leq UC_{max}$$

With:

- $M_{y,Rk} = 0.3 * f_{t,k} * d^{2.6}$ characteristic fastener yield moment
- $f_{h,i,k} = 0.082 * (1 - 0.1 * d) * \rho$ characteristic embedment strength

11. Dowel shear failure

The unity check for shear is described as (NEN-EN 1995-1-1, 6.1.7):

$$\frac{\tau_d}{f_{v,d}} \leq UC_{max}$$

This check is also performed for the dowel, where $f_{v,d}$ is the design shear strength for the dowel material.

12. Compression parallel to the grain (tenon)

The compression parallel to the grain in the tenon acts on the area as indicated in Figure 4(2). The check of this compression is performed as follows:

$$\frac{\sigma_{c,0,d}}{f_{c,0,d}} \leq UC_{max}$$

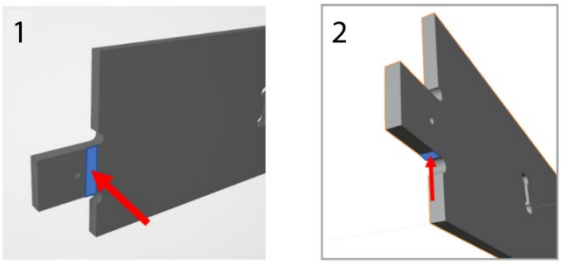


Figure 4: compression stresses in the tenons

Where:

- $\sigma_{c,0,d}$ = design tensile stress along the grain: $\sigma_{c,0,d} = \frac{V_{Ed}}{A}$
- V_{Ed} = Maximum shear force normal to the compression plane
- $f_{c,0,d}$ = $\frac{f_{c,0,k}}{\gamma_m} * k_{mod}$
- $f_{c,0,k}$ = char. compression strength par.to the grain (material property)

13. Compression perpendicular to the grain (tenon)

The compression perpendicular to the grain in the tenon acts on the area indicated in Figure 4(1). The check for this compression is performed as follows:

$$\frac{\sigma_{c,90,d}}{f_{c,90,d}} \leq UC_{max}$$

Where:

- $\sigma_{c,90,d}$ = design tensile stress perpendicular to the grain: $\sigma_{c,90,d} = \frac{V_{Ed}}{A}$
- V_{Ed} = Maximum shear force normal to the compression plane
- $f_{c,90,d}$ = $\frac{f_{c,90,k}}{\gamma_m} * k_{mod}$
- $f_{c,90,k}$ = char. compression strength perp. to the grain (material property)

14. Tension in the net-section

The tension from the dowel flows through the tenon. According to the Eurocode, the net-section should also be checked. This check is performed using the following formula:

$$\frac{\sigma_{t,0,d,net}}{f_{t,0,d}} \leq UC_{max}$$

Where:

- $\sigma_{t,0,d,net}$= design tensile stress along the grain in net area: $\sigma_{t,0,d} = \frac{F_t}{A_{net}}$
- F_t = tension force in the dowel
- $f_{t,0,d}$ = $\frac{f_{t,0,k}}{\gamma_m} * k_{mod}$
- $f_{t,0,k}$ = characteristic tensile strength par. to the grain (material property)

15. Stress concentration due to tension

Between the tenon and the main section, the tension forces flow around the corners. This leads to a stress concentration that must be checked:

$$\frac{\sigma_{t,0,d,conc}}{f_{t,0,k}} \leq UC_{max}$$

Where:

- $\sigma_{t,0,d,net}$= concentrated tensile stress along the grain: $\sigma_{t,0,d} = \frac{F_t}{A} * k_t$
- F_t = tension force in the dowel
- $f_{t,0,k}$ = characteristic tensile strength par. to the grain (material property)

16. Tenon shear

The tenons support the beam by shear. This shear must be checked with a reduction due to shear stress concentration. This stress concentration is specified in the Eurocode, resulting in the following unity check:

$$\tau_{d,z} = \frac{1.5V_{Ed}}{bh_{ef}} \leq k_v f_{v,d}$$

$$\tau_{d,y} = \frac{1.5V_{Ed}}{bh_{ef}} \leq f_{v,d}$$

Or:

$$\frac{\tau_{d,z}}{k_v f_{v,d}} + \frac{\tau_{d,y}}{f_{v,d}} \leq UC_{max}$$

Where:

- V_{Ed} = design shear stress in the tenon
- b = plywood sheet thickness
- h_{ef} = effective height of the tenon

k_v is a value that takes account for the shear stress concentration:

$$k_v = \frac{k_n\left(1 + \frac{1{,}1i^{1.5}}{\sqrt{h}}\right)}{\sqrt{h}\left(\sqrt{\alpha(1-\alpha)} + 0{,}8\frac{x}{h}\sqrt{\frac{1}{\alpha} - \alpha^2}\right)}$$

Where:

- i = notch inclination = 0 in this project
- h = beam depth (mm)
- x = distance from line of action of the support reaction to the corner of the notch (mm)
- α = $\frac{h_{ef}}{h}$
- k_n = 5 for plywood

17. Compression perpendicular to the grain

Due to bending at the beam end, compression is created to create an arm with the tension in the dowel. This compression is parallel to the grain for the beam considered, but acts perpendicular to the grain on the adjacent beam. Therefore, the unity check is as follows:

$$\frac{\sigma_{c,90,d}}{f_{c,90,d}} \leq UC_{max}$$

The determination of the maximum normal stress depends on the location of the line of gravity of the couple between the compression area and the tenon. When the line of gravity is in the compression area:

$$\sigma_{max,M_{zz}} = \frac{M_{zz}}{I} * b$$

Where:

- b = distance to cg, indicated in Figure 5
- I = second moment of area of the compressive area with respect to cg
  = $\frac{1}{12} * w * c^3$
- w = beam width
- c = height of compression area

If the line of gravity is outside the compression area, the determination of I changes:

- I = $\frac{1}{12} * w * c^3 + w * (\frac{c}{2})^2$

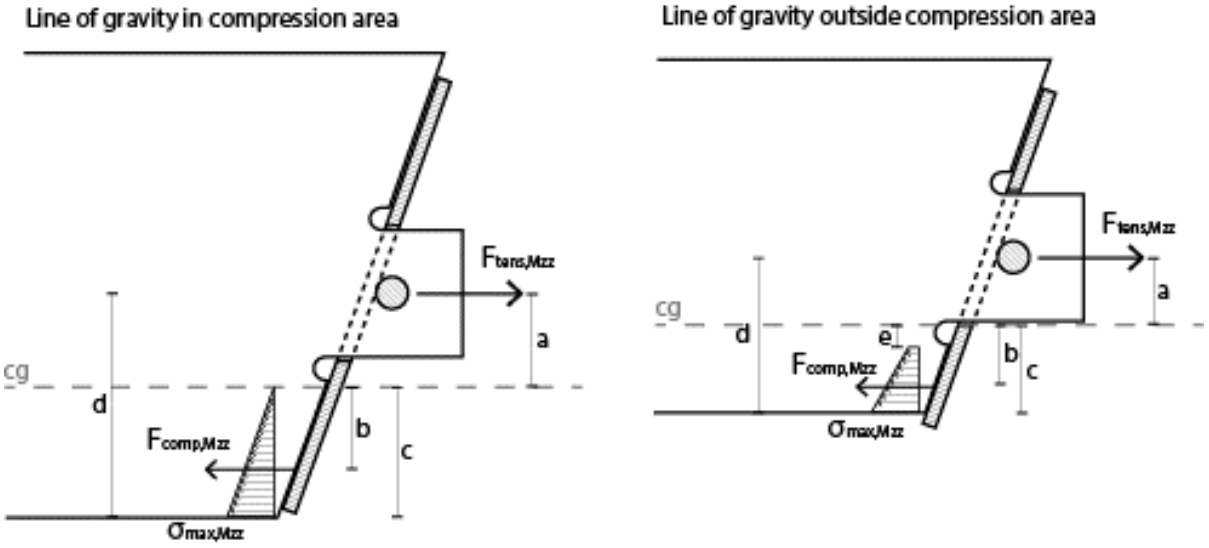


Figure 5: determination of maximum normal stress

18. Normal stress concentration

The stress concentrations around the holes are checked using the following unity checks:

$$\frac{\sigma_{t,0,conc}}{f_{t,0,d}} \leq UC_{max}$$

Where:

- $\sigma_{t,0,conc}$ = design normal stress concentration
  = $\sigma_N * k_{t,N} + \sigma_{M_y} * k_{t,M_y} + \sigma_{M_z} * k_{t,M_z}$
- $k_{t,N}, k_{t,M_y}, k_{t,M_z}$ = stress concentration factors determined using predictive model
- $\sigma_N, \sigma_{M_y}, \sigma_{M_z}$ = normal stresses without hole

19. Shear stress concentration

Similarly the stress concentrations around the holes are checked for shear (on another location):

$$\frac{\tau_{d,conc}}{f_{v,d}} \leq UC_{max}$$

Where:

- $\tau_{d,conc}$ = design shear stress concentration
  = $\sigma_{V_y} * k_{t,V_y} + \sigma_{V_z} * k_{t,V_z} + \sigma_T * k_{t,T}$
- $k_{t,V_y}, k_{t,V_z}, k_{t,T}$ = stress concentration factors determined using predictive Model
- $\sigma_{V_y}, \sigma_{V_z}, \sigma_T$ = shear stresses without hole

20. Shear on the reduced cross-section

Finally, the shear on the area below the hole must be checked (see Figure 6). The unity check for this stress is as follows:

$$\frac{\tau_{d,red}}{f_{v,d}} \leq UC_{max}$$

Where:

- $\tau_{d,red}$ = design shear stress below hole: $\tau_d = \frac{3V_{Ed,z}}{4A_{red}}$
- $V_{Ed,z}$ = Shear force at the hole in the z-direction
- A_{red} = reduced shear area: $b * h_{red}$
- $f_{v,d}$ = $\frac{f_{v,k}}{\gamma_m} * k_{mod}$
- $f_{v,k}$ = characteristic shear strength (material property)

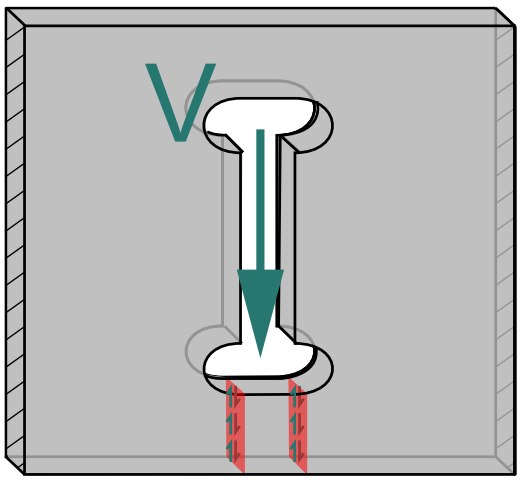


Figure 6: shear planes for reduced cross-section unity check

Appendix 3: Parametric optimization overviews

The following pages show an overview of the parametric optimization process for each of the tessellation patterns:

- Appendix 3.1: Square pattern
- Appendix 3.2: Triangle pattern
- Appendix 3.3: Snub-Square pattern
- Appendix 3.4: Honeycomb pattern
- Appendix 3.5: Hex-Tri pattern

On each of the pages, firstly the initial exploration focused on the edge size (in combination with curvature) is shown. Where in each of the four tables (Table 1 – 4), there is a focus on the resulting structure and edge sizes for different middle heights of the structure.

When the initial exploration is completed, the focus is shifted to the parametric optimization where there is a focus on the sheet thickness. Tables 5 and 6 respectively show the volume of raw material required per sheet thickness and the number of sheets per sheet thickness (after parametric optimization). Finally, the structural shapes and accompanying parameters are summarized on the bottom of the page.

Appendix 3.1: Square tessellation – parametric optimization

Edge size & curvature

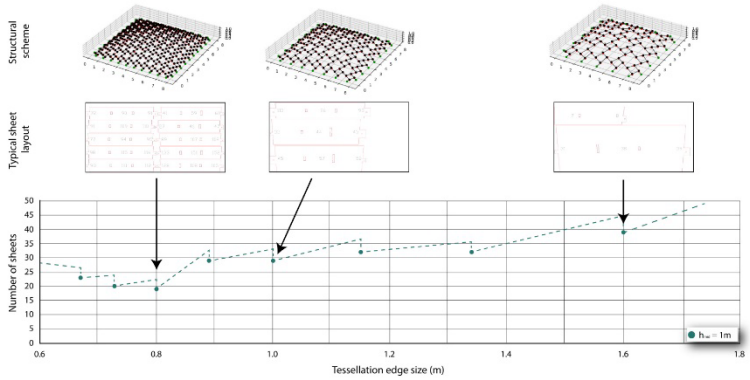


Figure 1: Influence of tessellation edge size on number of sheets required (with scheme and sheet layout for h_{mid} = 1m)

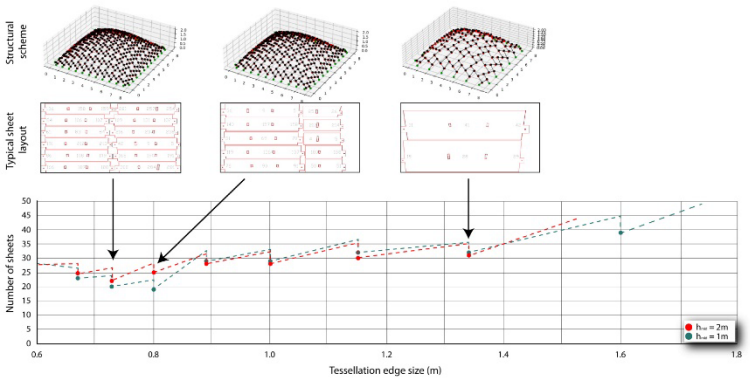


Figure 2: Influence of tessellation edge size on number of sheets required (with scheme and sheet layout for h_{mid} = 2m)

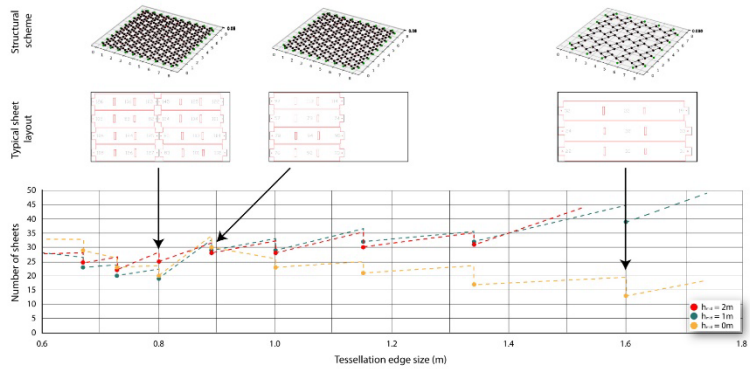


Figure 3: Influence of tessellation edge size on number of sheets required (with scheme and sheet layout for h_{mid} = 0m)

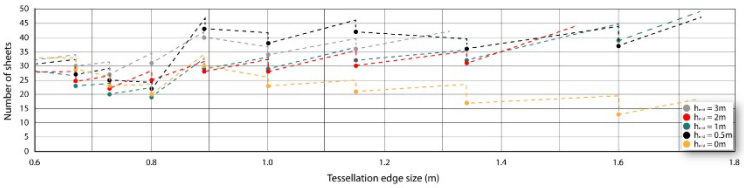


Figure 4: Influence of tessellation edge size on number of sheets required (combined)

Sheet thickness

Table 5: Raw material required to create reciprocal frame for different sheet thicknesses

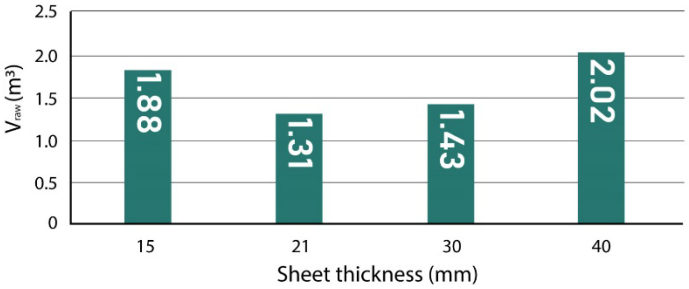
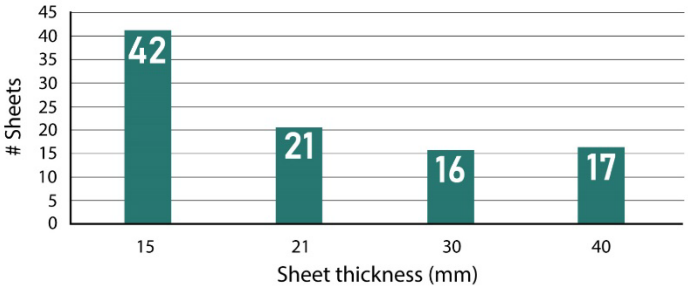
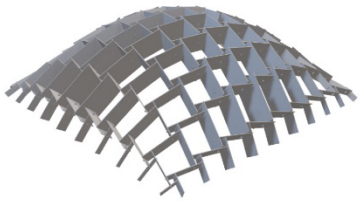


Table 6: Number of sheets required to create reciprocal frame for different sheet thicknesses



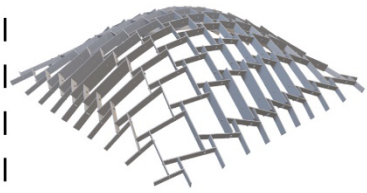
Most optimal reciprocal frame shape for sheet thicknesses (note: there may be multiple layouts with the same amount of sheets)

15mm



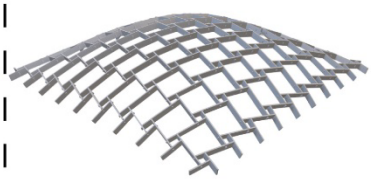
Eccentricity:	18.6mm
Edge size:	0.8m
Scale factor:	0.25
Density gradient:	-0.07

21mm



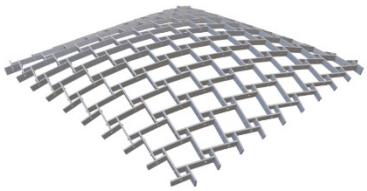
Eccentricity:	15.7mm
Edge size:	0.8m
Scale factor:	0.32
Density gradient:	0.26

30mm



Eccentricity:	12.6mm
Edge size:	0.8m
Scale factor:	0.30
Density gradient:	0.01

40mm



Eccentricity:	9.6mm
Edge size:	0.8m
Scale factor:	0.35
Density gradient:	-0.06

Appendix 3.2: Triangle tessellation – parametric optimization

Edge size & curvature

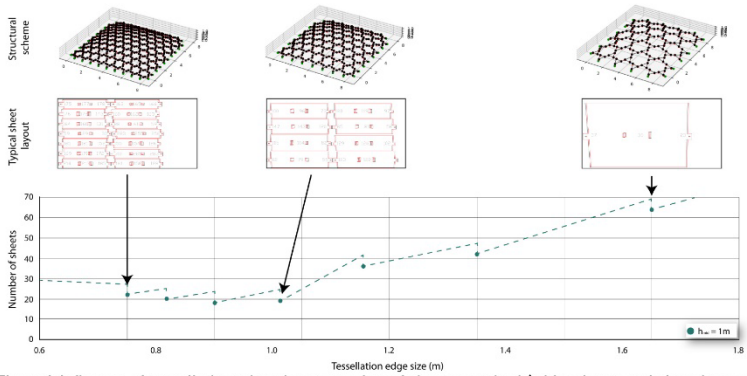


Figure 1: Influence of tessellation edge size on number of sheets required (with scheme and sheet layout for h_{mid} = 1m)

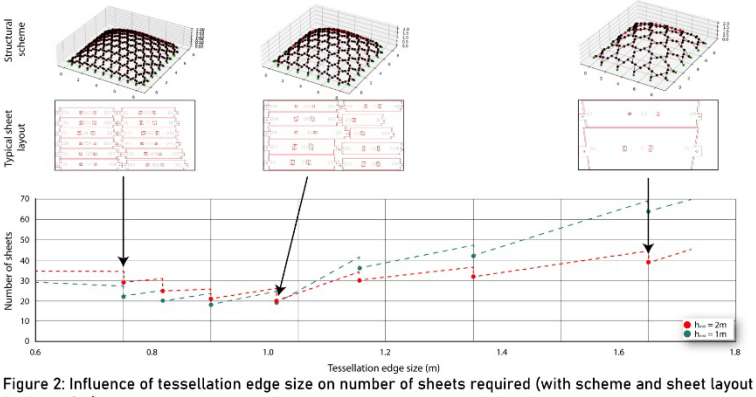


Figure 2: Influence of tessellation edge size on number of sheets required (with scheme and sheet layout for h_{mid} = 2m)

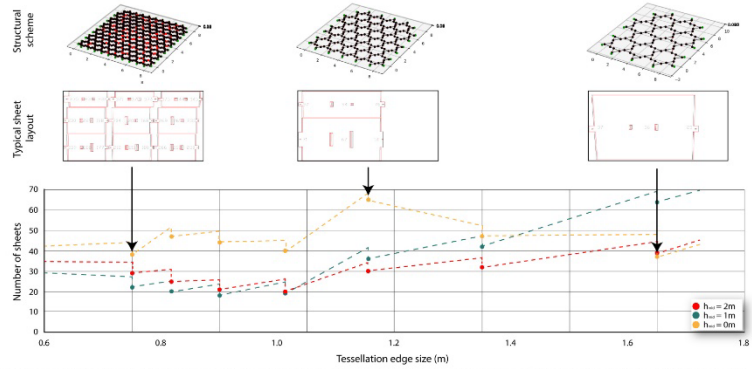


Figure 3: Influence of tessellation edge size on number of sheets required (with scheme and sheet layout for h_{mid} = 0m)

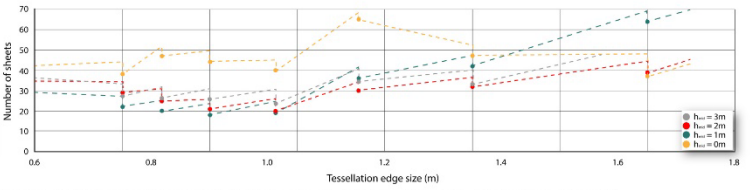


Figure 4: Influence of tessellation edge size on number of sheets required (combined)

Sheet thickness

Table 5: Raw material required to create reciprocal frame for different sheet thicknesses

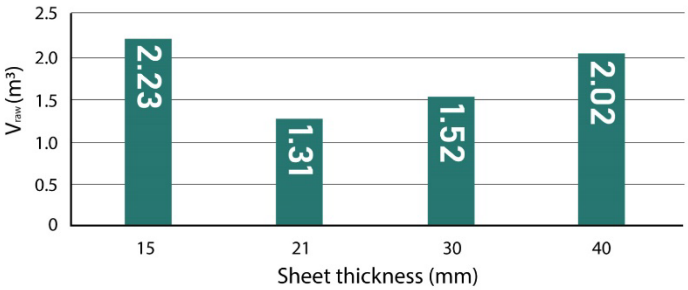
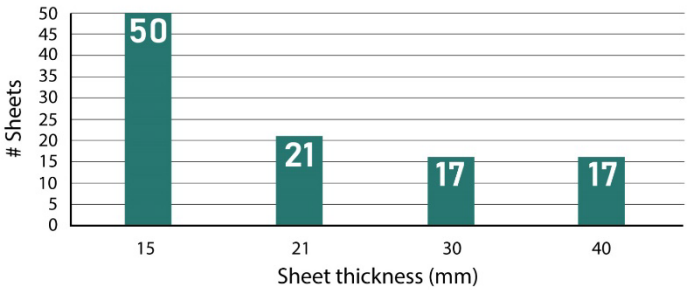
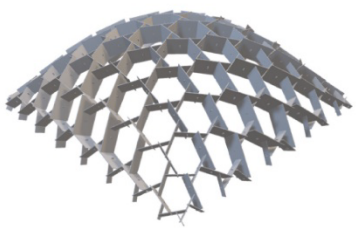


Table 6: Number of sheets required to create reciprocal frame for different sheet thicknesses



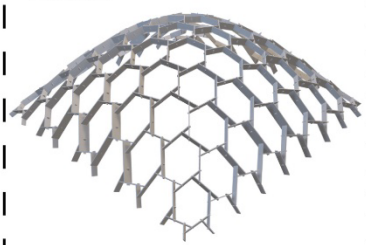
Most optimal reciprocal frame shape for sheet thicknesses (note: there may be multiple layouts with the same amount of sheets)

15mm



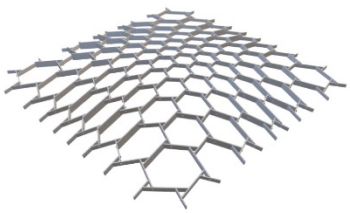
Eccentricity:	22.4mm
Edge size:	1.0m
Scale factor:	0.50
Density gradient:	-0.16

21mm



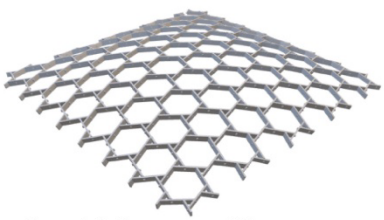
Eccentricity:	15.9mm
Edge size:	1.0m
Scale factor:	0.28
Density gradient:	-0.08

30mm



Eccentricity:	3.2mm
Edge size:	1.0m
Scale factor:	0.25
Density gradient:	0.3

40mm



Eccentricity:	5.9mm
Edge size:	0.8m
Scale factor:	0.39
Density gradient:	-0.06

Appendix 3.3: Snub-Square tessellation – parametric optimization

Edge size & curvature

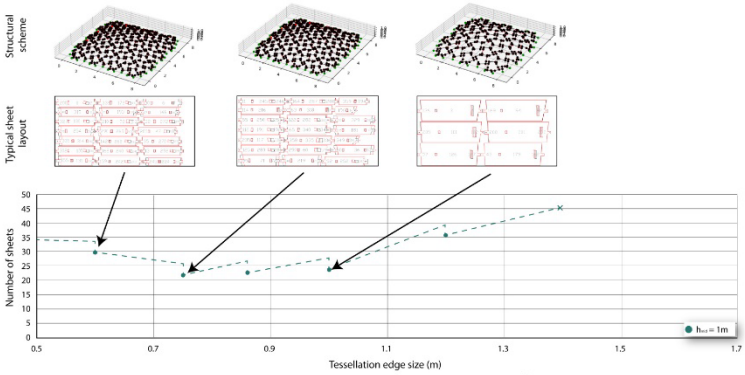


Figure 1: Influence of tessellation edge size on number of sheets required (with scheme and sheet layout for h_{mid} = 1m)

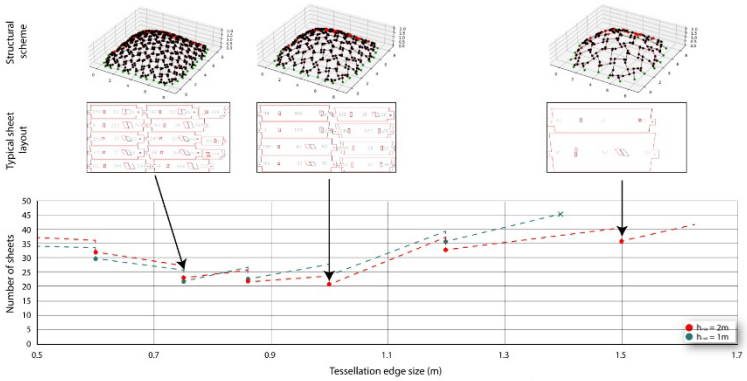


Figure 2: Influence of tessellation edge size on number of sheets required (with scheme and sheet layout for h_{mid} = 2m)

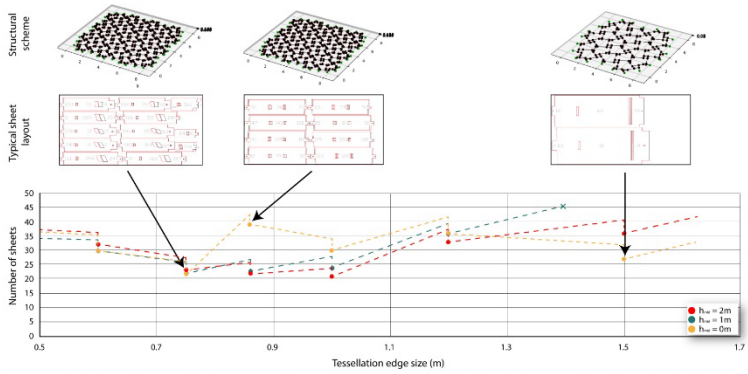


Figure 3: Influence of tessellation edge size on number of sheets required (with scheme and sheet layout for h_{mid} = 0m)

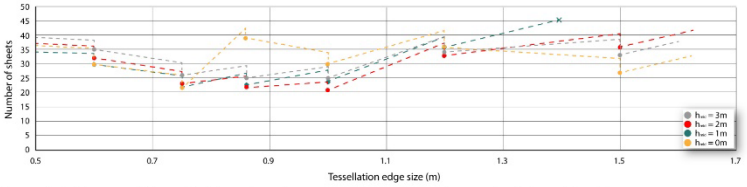


Figure 4: Influence of tessellation edge size on number of sheets required (combined)

Sheet thickness

Table 5: Raw material required to create reciprocal frame for different sheet thicknesses

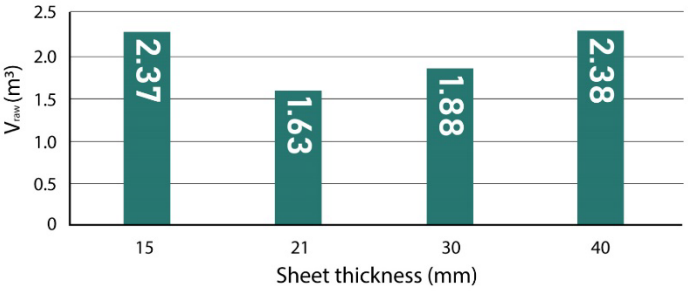
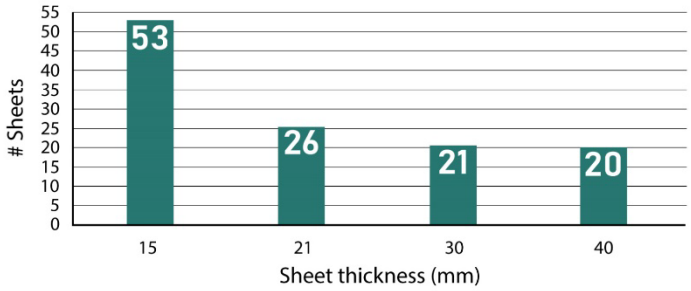
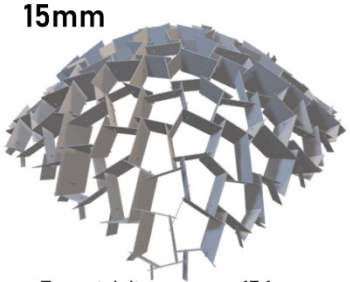


Table 6: Number of sheets required to create reciprocal frame for different sheet thicknesses



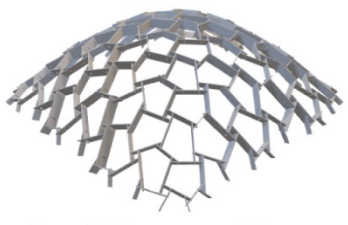
Most optimal reciprocal frame shape for sheet thicknesses (note: there may be multiple layouts with the same amount of sheets)

15mm



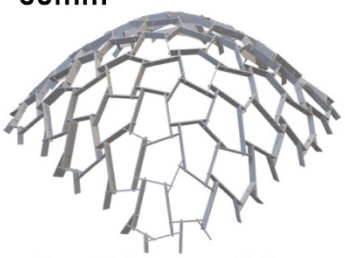
Eccentricity:	17.1mm
Edge size:	0.86m
Scale factor:	0.31
Density gradient:	-0.08

21mm



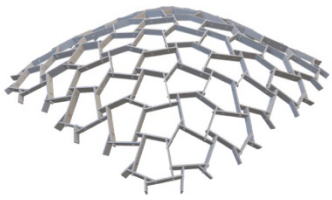
Eccentricity:	14.5mm
Edge size:	0.86m
Scale factor:	0.31
Density gradient:	-0.08

30mm



Eccentricity:	18.6mm
Edge size:	1.0m
Scale factor:	0.31
Density gradient:	-0.08

40mm



Eccentricity:	11.9mm
Edge size:	1.0m
Scale factor:	0.35
Density gradient:	-0.06

Appendix 3.4: Honeycomb tessellation – parametric optimization

Edge size & curvature

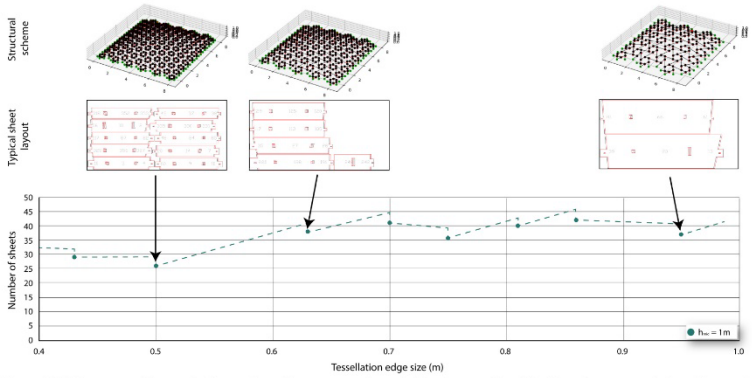


Figure 1: Influence of tessellation edge size on number of sheets required (with scheme and sheet layout for h_{mid} = 1m)

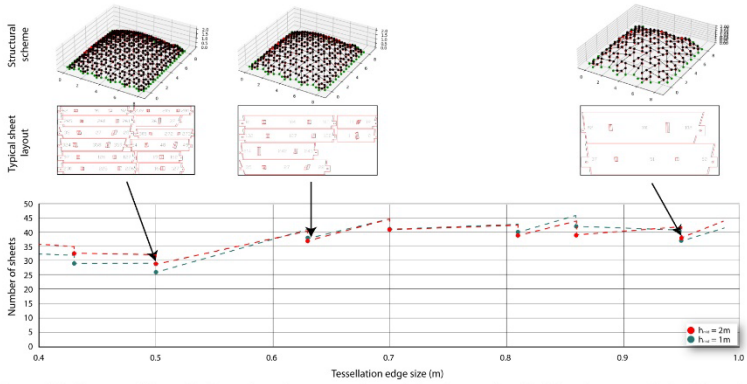


Figure 2: Influence of tessellation edge size on number of sheets required (with scheme and sheet layout for h_{mid} = 2m)

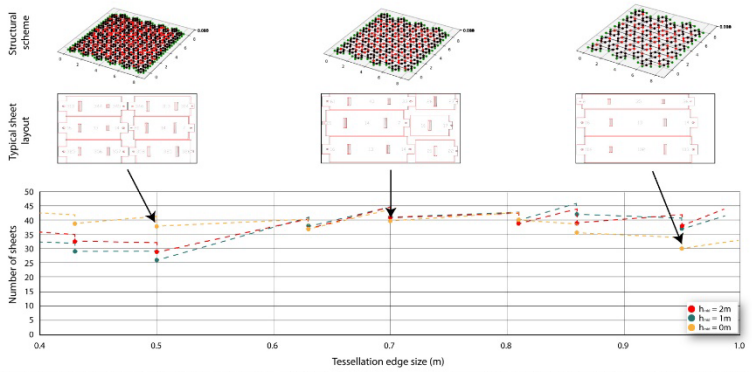


Figure 3: Influence of tessellation edge size on number of sheets required (with scheme and sheet layout for h_{mid} = 0m)

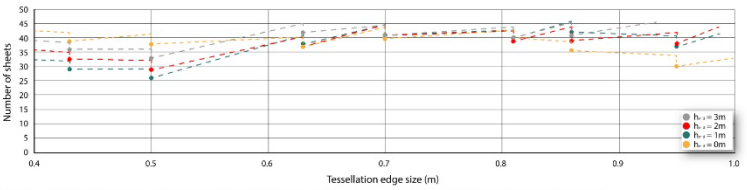


Figure 4: Influence of tessellation edge size on number of sheets required (combined)

Sheet thickness

Table 5: Raw material required to create reciprocal frame for different sheet thicknesses

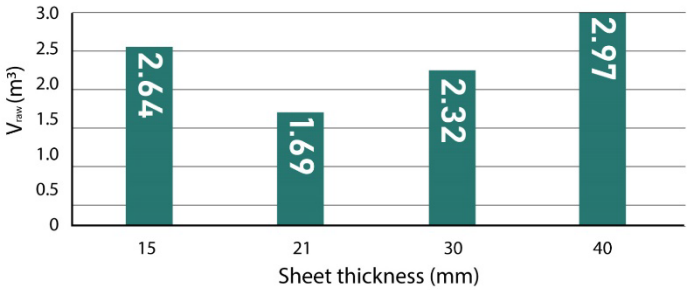
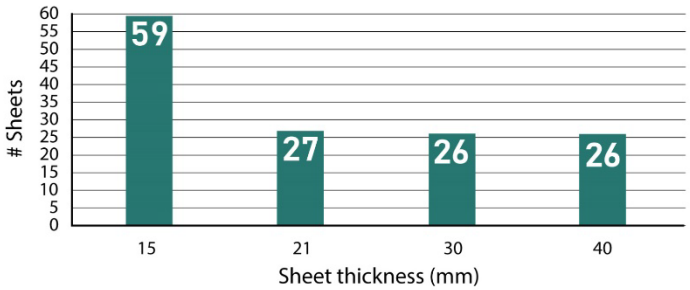
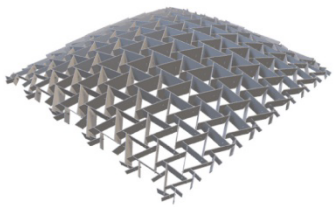


Table 6: Number of sheets required to create reciprocal frame for different sheet thicknesses



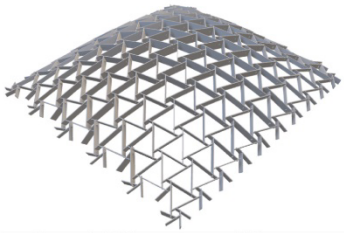
Most optimal reciprocal frame shape for sheet thicknesses (note: there may be multiple layouts with the same amount of sheets)

15mm



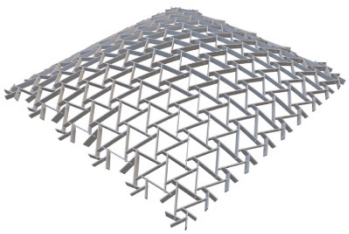
Eccentricity:	9.2mm
Edge size:	0.5m
Scale factor:	0.41
Density gradient:	-0.14

21mm



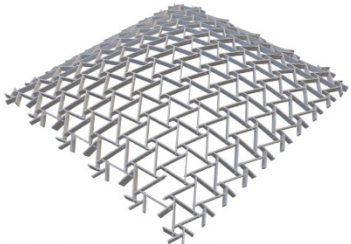
Eccentricity:	9.6mm
Edge size:	0.5m
Scale factor:	0.30
Density gradient:	-0.07

30mm



Eccentricity:	9.2mm
Edge size:	0.5m
Scale factor:	0.38
Density gradient:	-0.06

40mm



Eccentricity:	8.1mm
Edge size:	0.5m
Scale factor:	0.35
Density gradient:	-0.06

Appendix 3.5: Hex-Tri tessellation - parametric optimization

Edge size & curvature

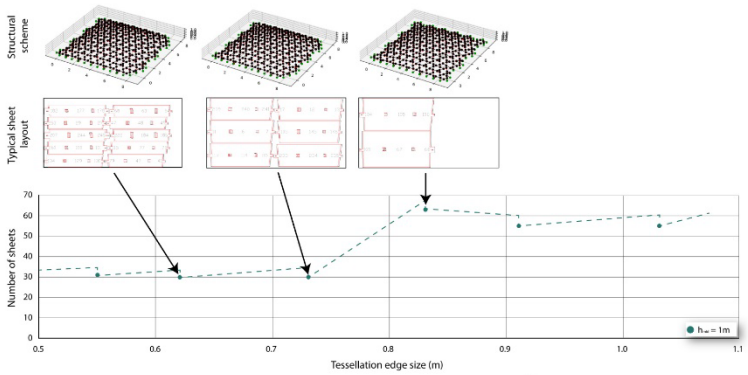


Figure 1: Influence of tessellation edge size on number of sheets required (with scheme and sheet layout for h_{mid} = 1m)

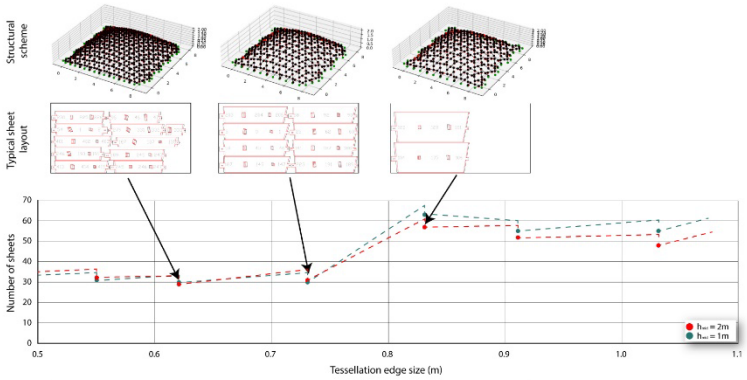


Figure 2: Influence of tessellation edge size on number of sheets required (with scheme and sheet layout for h_{mid} = 2m)

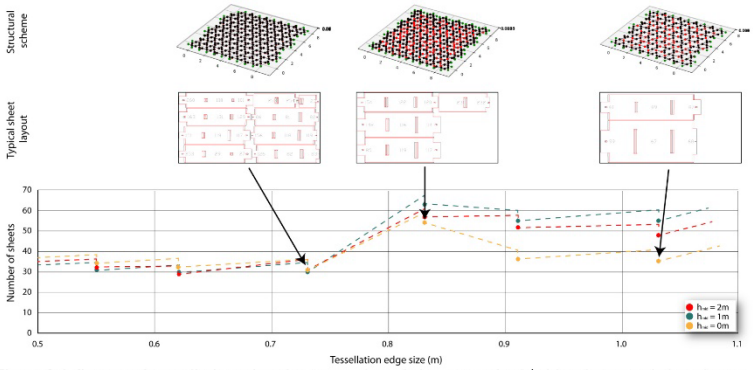


Figure 3: Influence of tessellation edge size on number of sheets required (with scheme and sheet layout for h_{mid} = 0m)

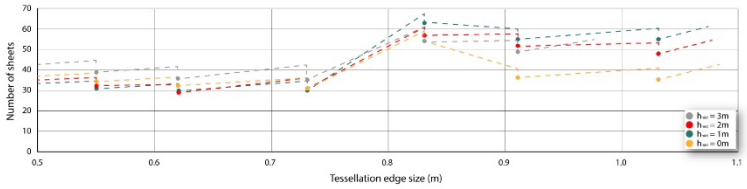


Figure 4: Influence of tessellation edge size on number of sheets required (combined)

Sheet thickness

Table 5: Raw material required to create reciprocal frame for different sheet thicknesses

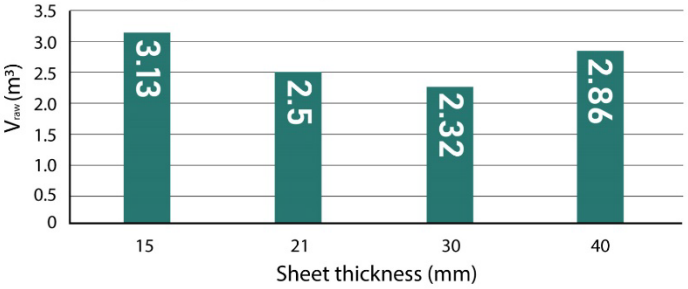
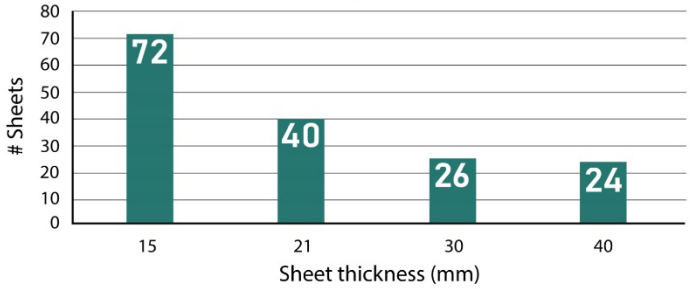
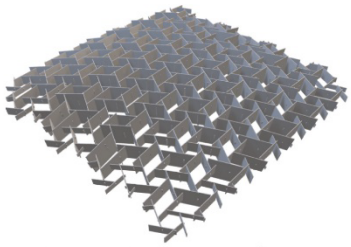


Table 6: Number of sheets required to create reciprocal frame for different sheet thicknesses



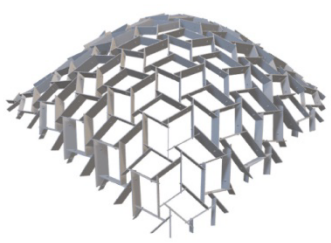
Most optimal reciprocal frame shape for sheet thicknesses (note: there may be multiple layouts with the same amount of sheets)

15mm



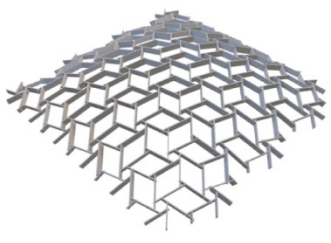
Eccentricity:	4.2mm
Edge size:	0.62m
Scale factor:	0.5
Density gradient:	0

21mm



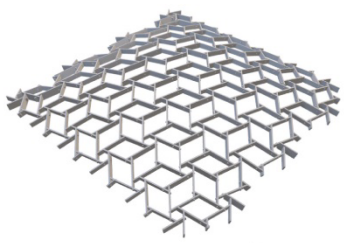
Eccentricity:	17.6mm
Edge size:	0.73m
Scale factor:	0.31
Density gradient:	-0.08

30mm



Eccentricity:	8.5mm
Edge size:	0.73m
Scale factor:	0.30
Density gradient:	0

40mm



Eccentricity:	6.2mm
Edge size:	0.73m
Scale factor:	0.32
Density gradient:	-0.07

Annex 1: Calculation reports

The reciprocal frame designer automatically generates calculations reports based on the export settings. The user can choose to generate a summary report which only shows the values of the unity checks or a full calculation report with the steps of the calculations. In this annex, a snippet of the following example calculation reports are shown:

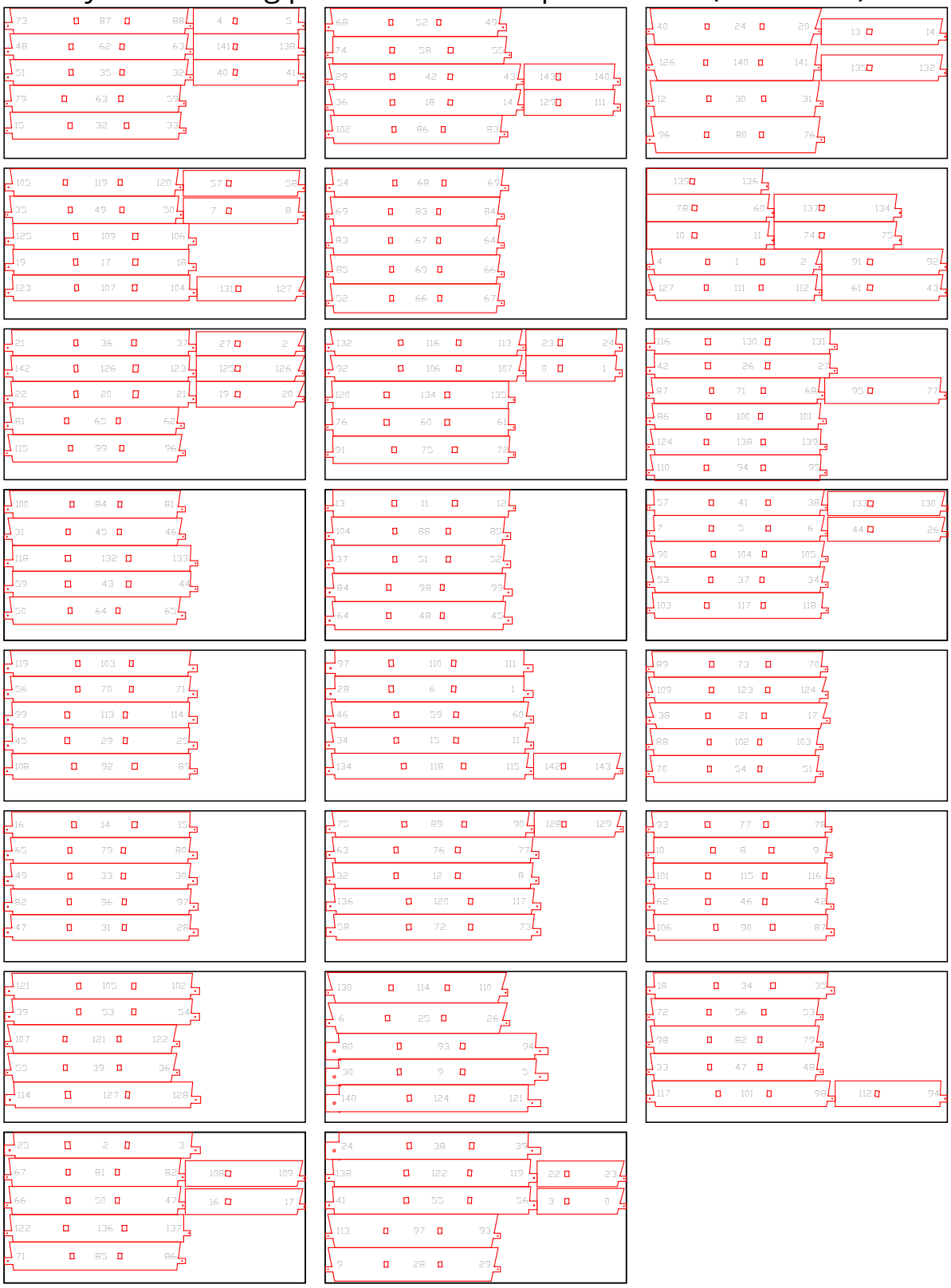
- Annex 1.1: Summary calculation report
- Annex 1.2: Full calculation report (including internal force diagrams)

These calculation reports are generated for a reciprocal frame structure with the following properties:

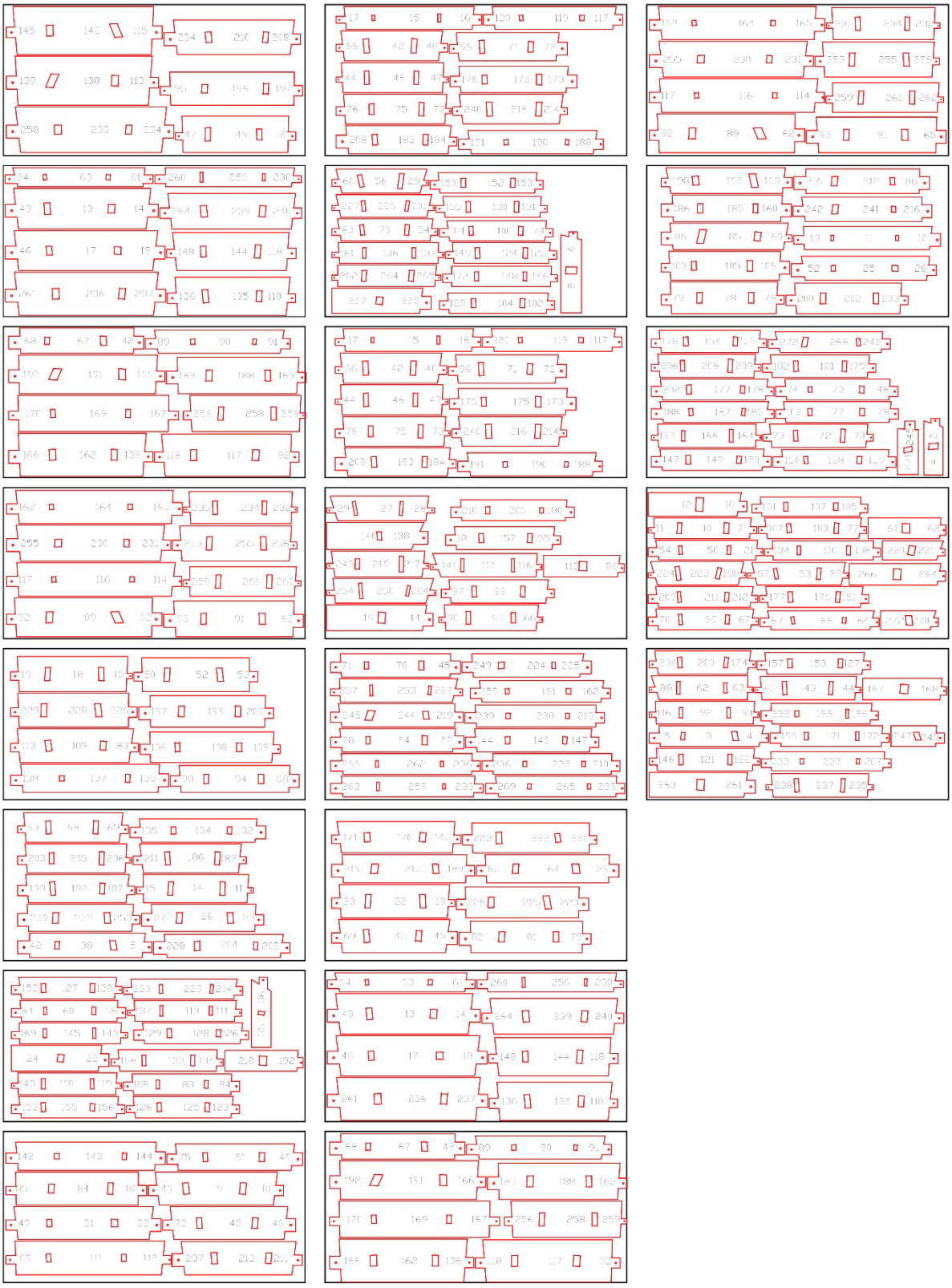
- Reciprocal frame dimensions: 8x8m
- Tessellation pattern: Square
- Edge size: 1m
- Tessellation density gradient: 0
- Scale factor: 0.5
- Eccentricity: 40mm
- Plywood sheet thickness: 30mm
- Maximum allowed UC: 0.8
- Base height z 3m
- Wind area: II (Unbuilt)
- Consequence class: CC2
- Cladding density: 0.2 kN/m^2

Annex 2: Plywood cutting patterns

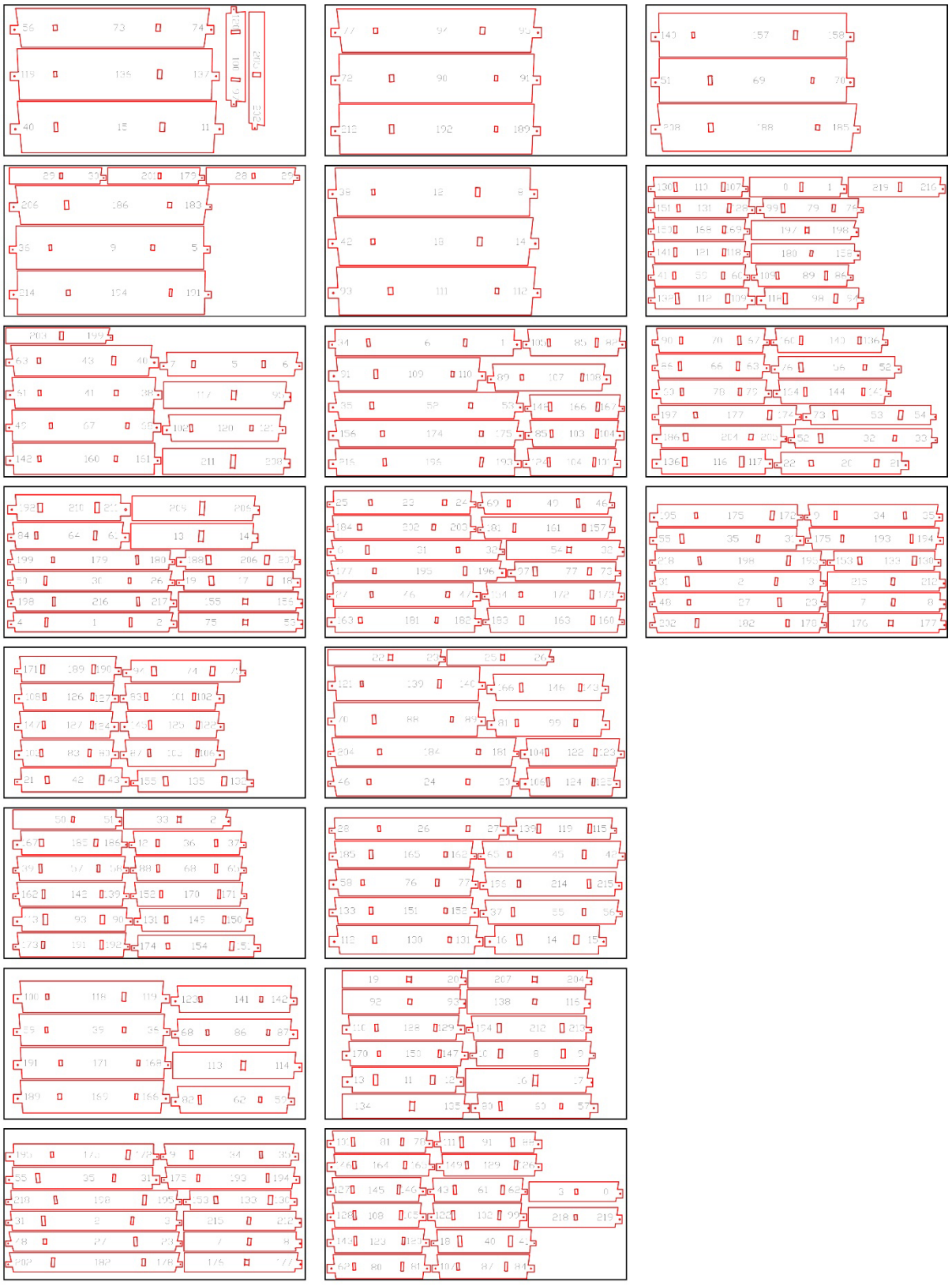
2.1: Plywood cutting pattern of a non-optimized RF (T = 30mm)



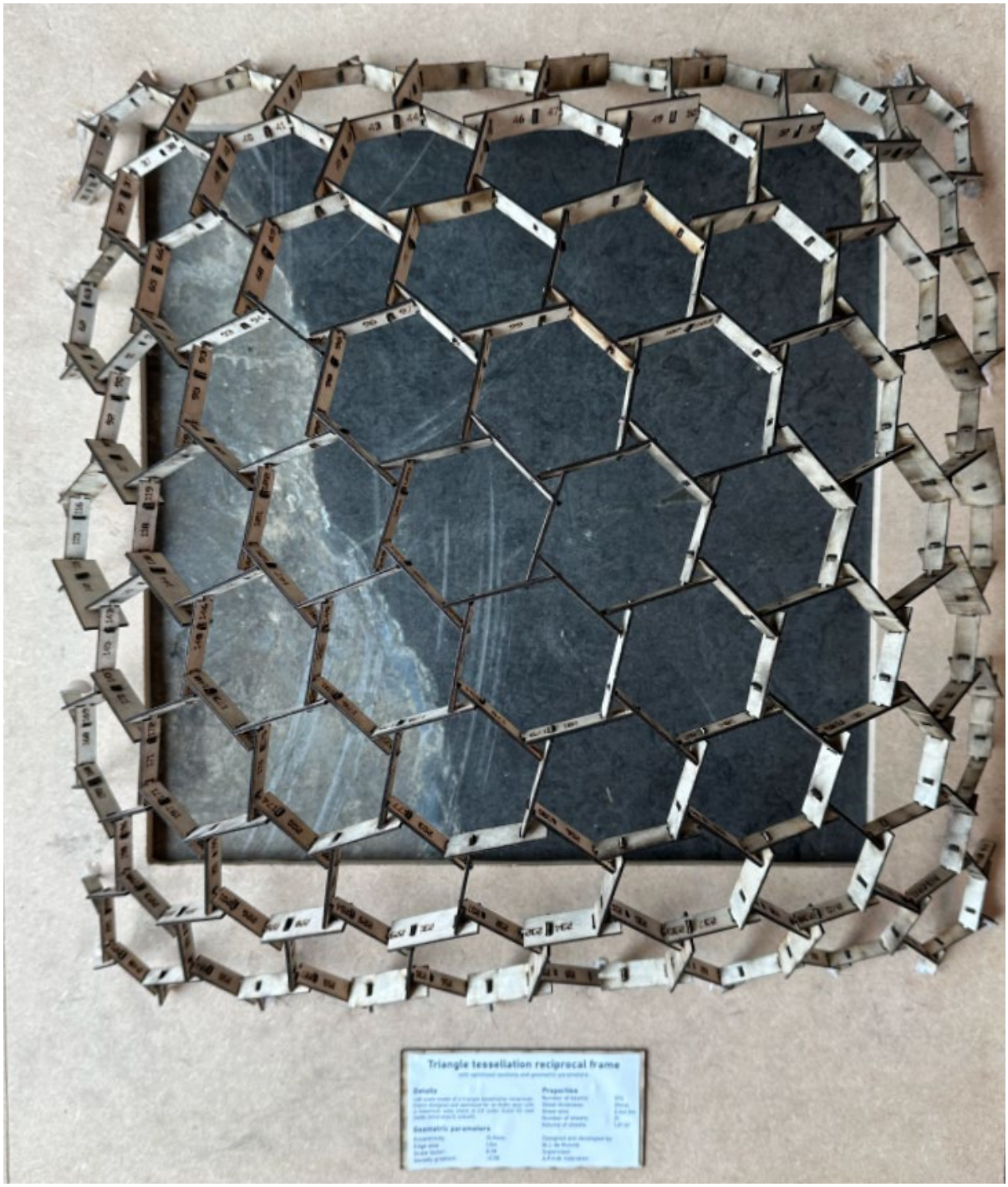
2.2: Plywood cutting pattern after optimization: Triangle (T =21mm)



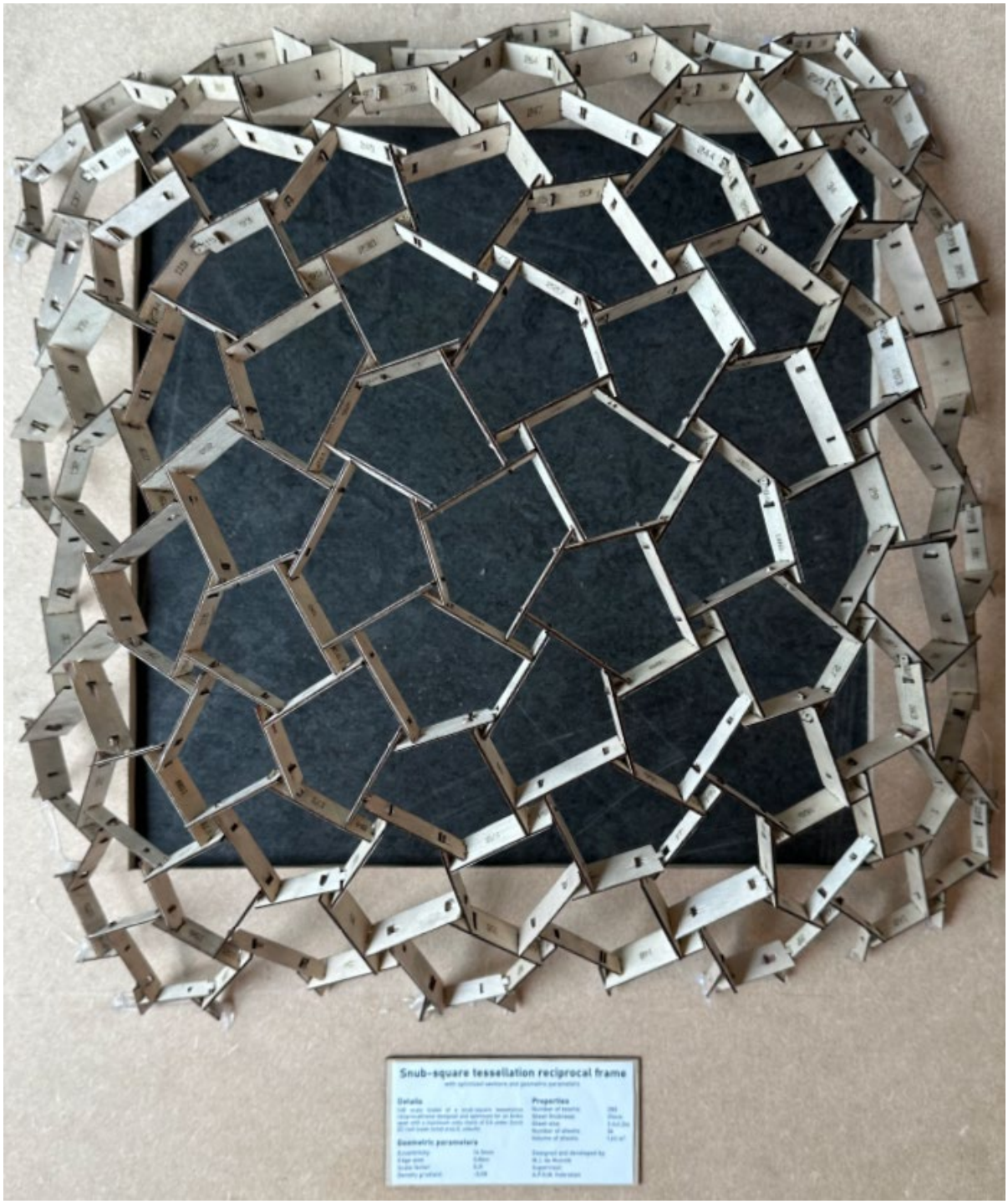
2.3: Plywood cutting pattern for example case: Square



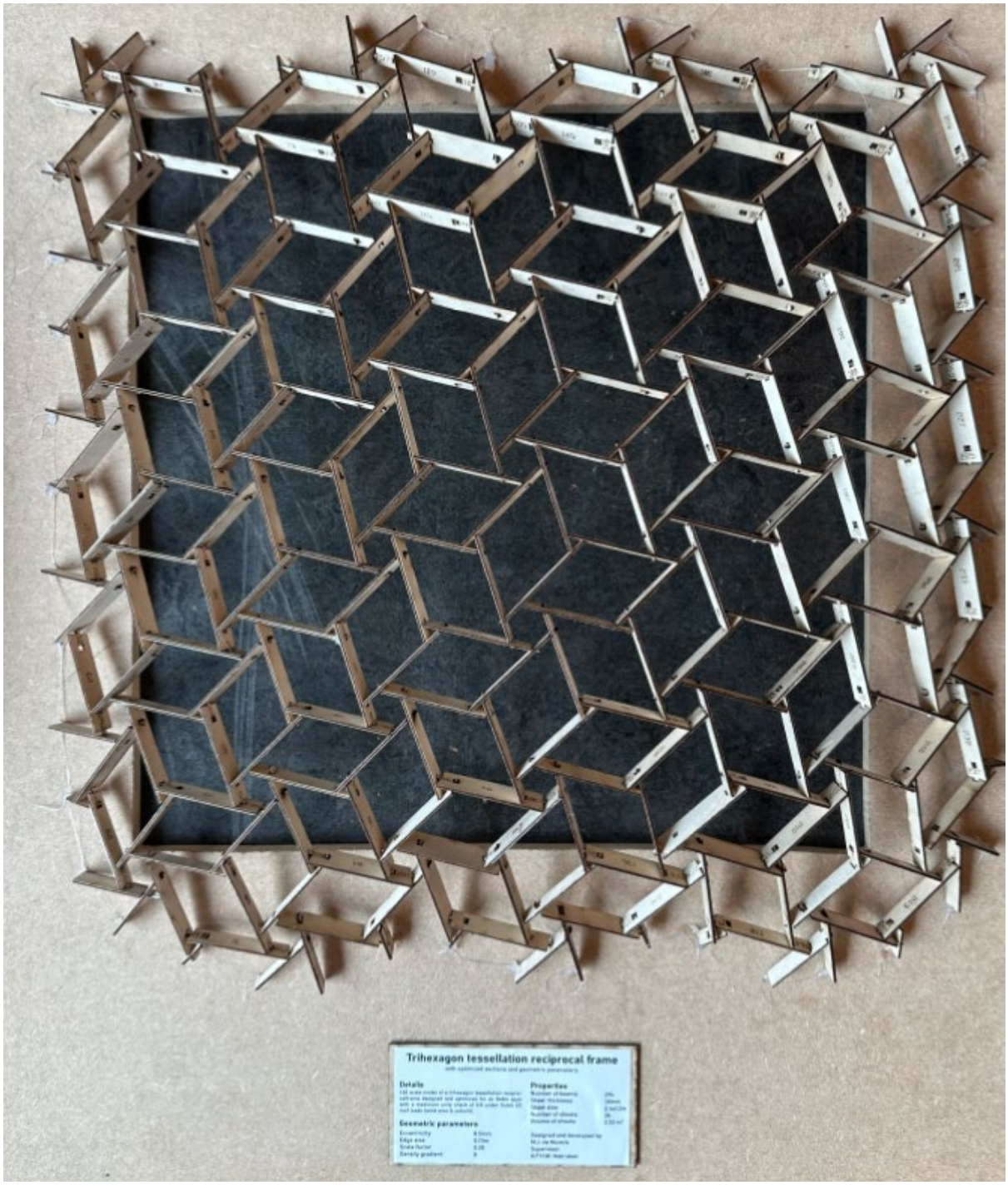
Annex 3: Scale model pictures




Square tessellation reciprocal frame
Details
Properties
Geometric parameters


Snub-square tessellation reciprocal frame
Details
Properties
Geometric parameters


Honeycomb tessellation reciprocal frame
with optimized sections and geometric parameters
Details
Properties
Geometric parameters


Trihexagon tessellation reciprocal frame
Details
Geometric parameters
Properties